FIGURES

ÁBRAGYŰJTEMÉNY

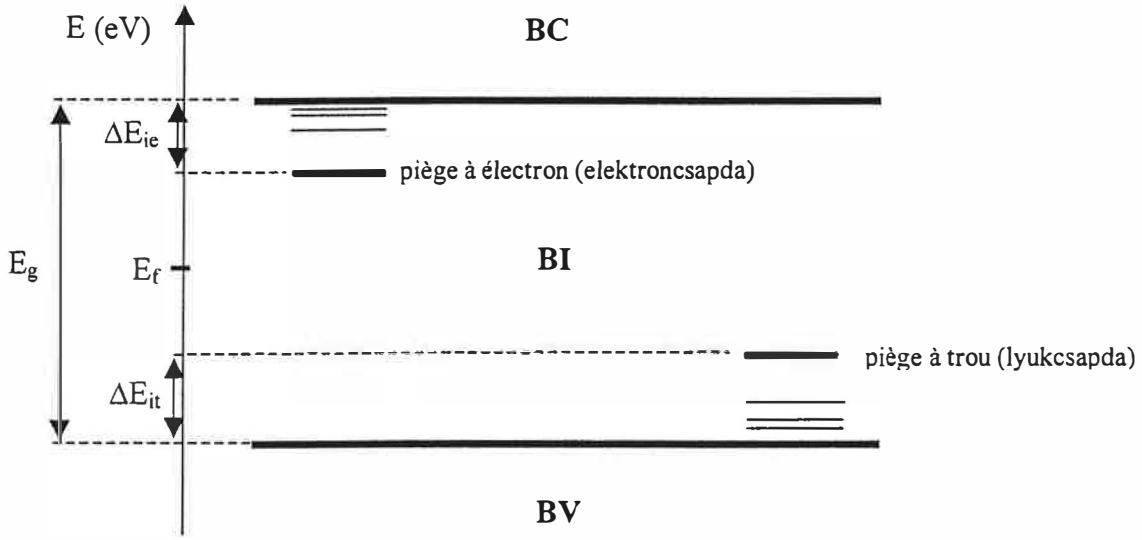

Figure I.1 : Schéma des bandes d'un matériau isolant imparfait (symboles dans le texte)

I.1. ábra: A szigetelők sávszerkezetének ábrázolása kristályhibákkal

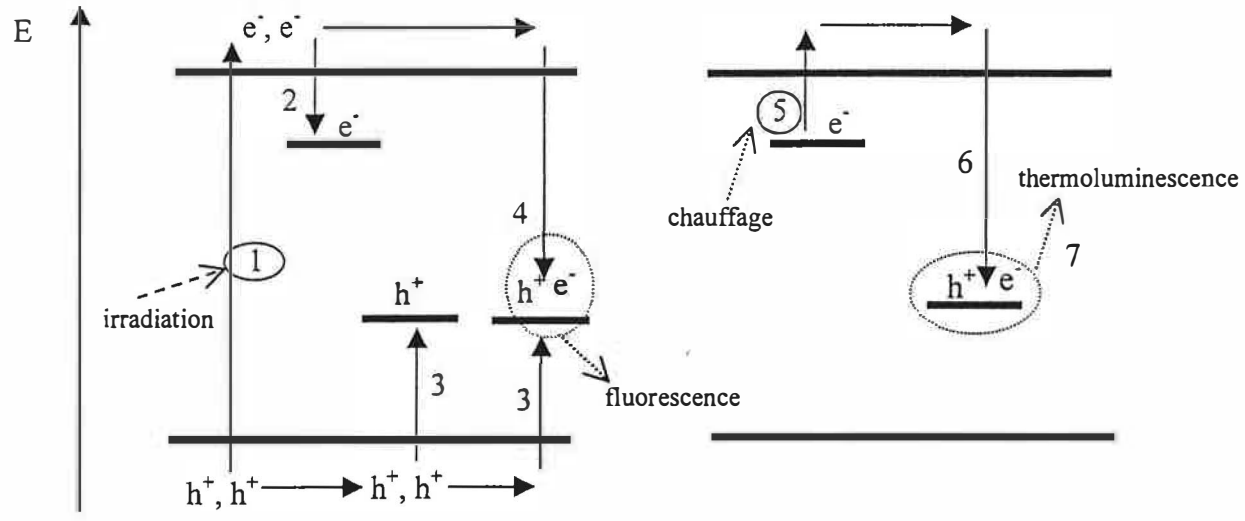

phase 1 : irradiation
1: besugárzás

phase 2 : chauffage
2: kifűtés

Figure I.2: Interprétation de la TL dans le cas d'un modèle simplifié. (symboles dans le texte)

I.2. ábra: A termolumineszcencia jelenségének egyszerűsített sávszerkezeti modellje

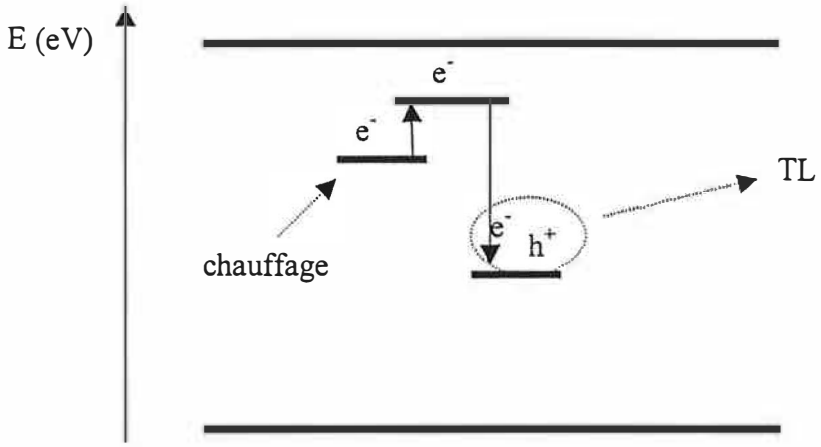

phase II : chauffage

Figure I.3 : Interprétation de la TL dans le cas du modèle de centre luminogène isolé

I.3. ábra: TL mechanizmus csapda és emissziós centrum közti közvetlen átmenettel

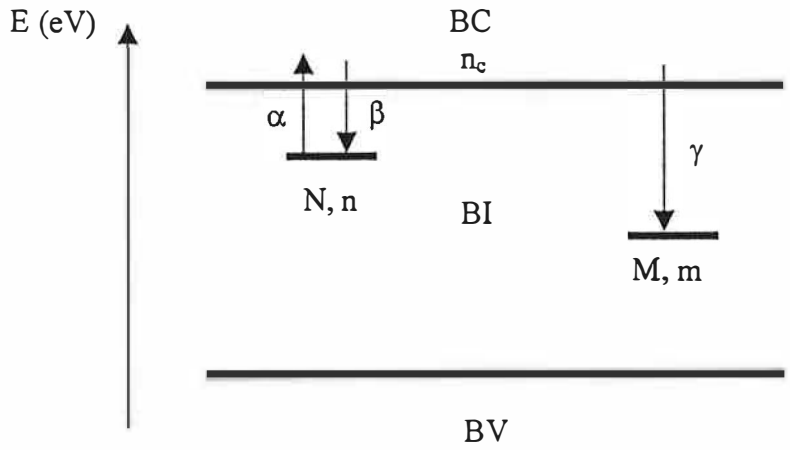

Figure I.4 : Modèle cinétique simplifié de la TL

I.4. ábra: A termolumineszcencia jelenségének egyszerűsített kinetikai modellje

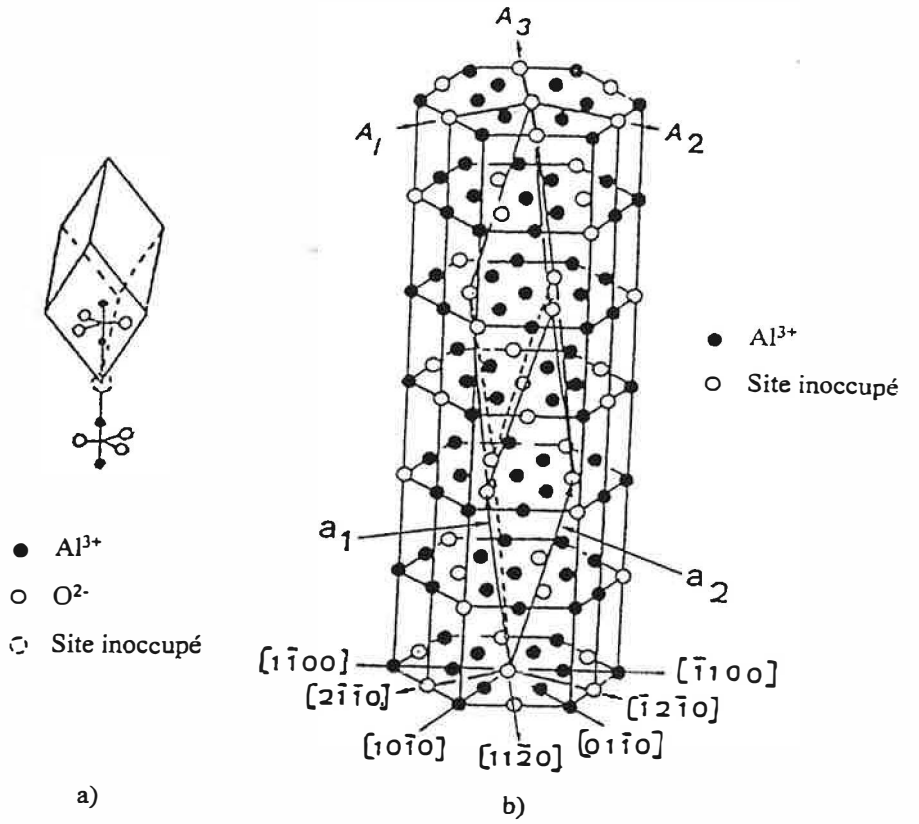

Figure I.5 : Représentations de l'alumine α : maille rhomboédrique (a) et hexagonale (b) [VAL99]

I.5. ábra: A korund kristályszerkezete: romboéderes (a) és hexagonális (b) ábrázolás [VAL99]

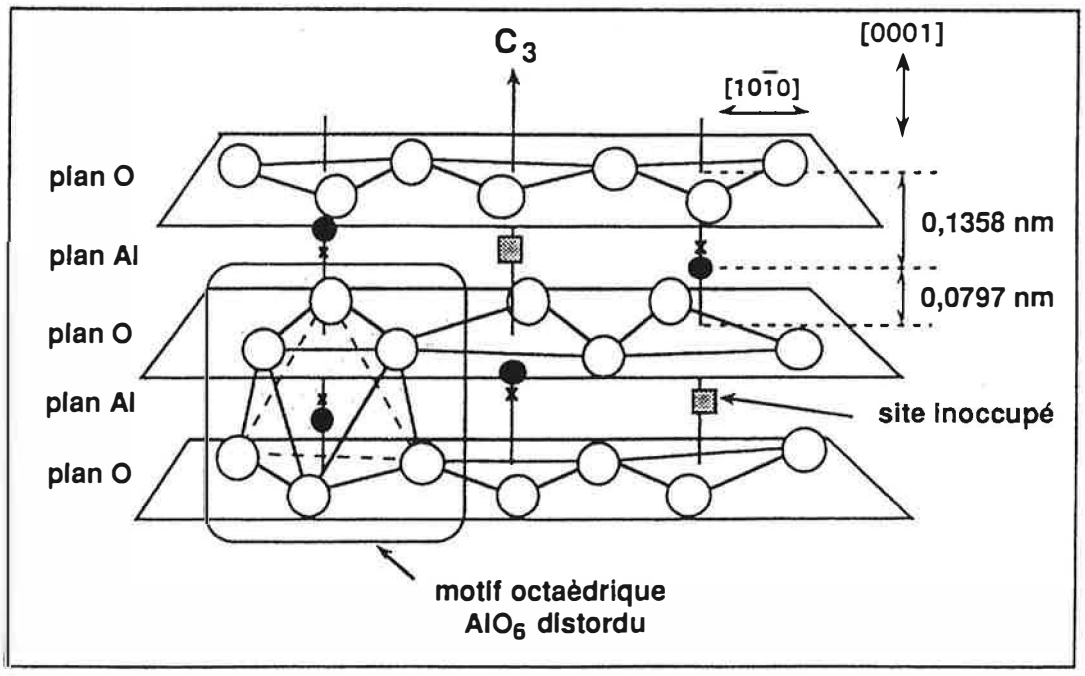

Figure I.6 : Représentation de la structure corindon [BIG96]

I.6. ábra: A korund kristályszerkezetének vázlata [BIG96]

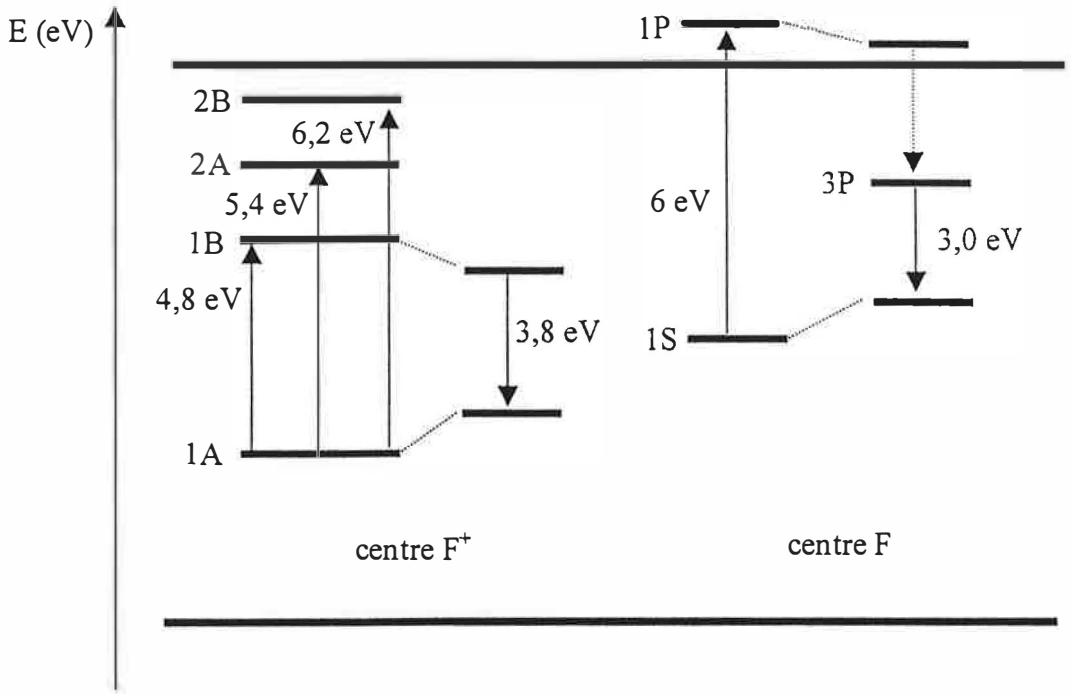

Figure I.7 : Structure électronique des centres F et F^+ [LEE79, STA94]

I.7. ábra: Az F és F^+ centrumok elektronszerkezete [LEE79, STA94]

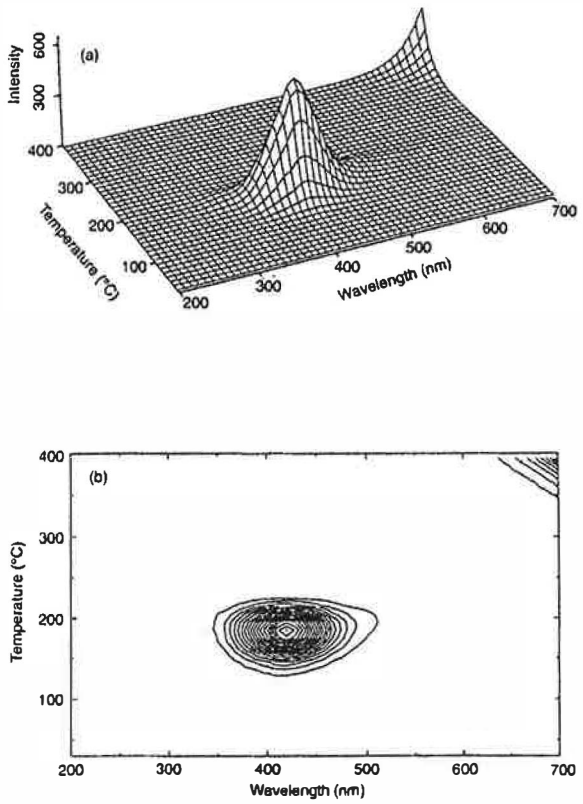

Figure I.8 : Le pic dosimétrique du TLD-500 [MCK95]

I.8. ábra: A dózismérésre használt TL csúcs a TLD-500 doziméter esetében [MCK95]

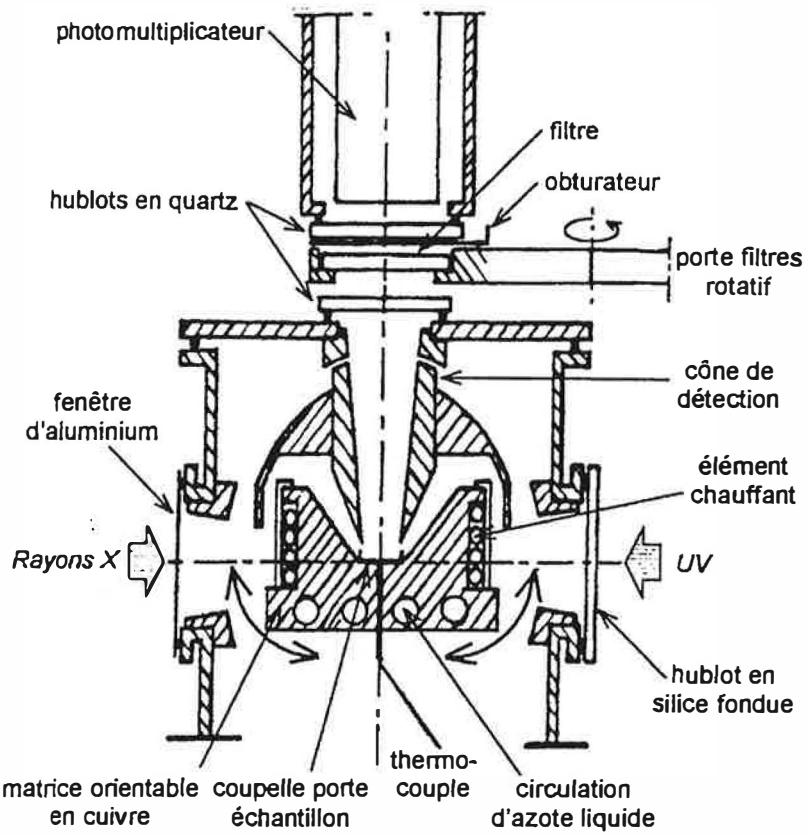

Figure II.1 : Schéma de principe du dispositif de TLBT

II.1.ábra: Az alacsony hőmérsékletű TL készülék felépítése

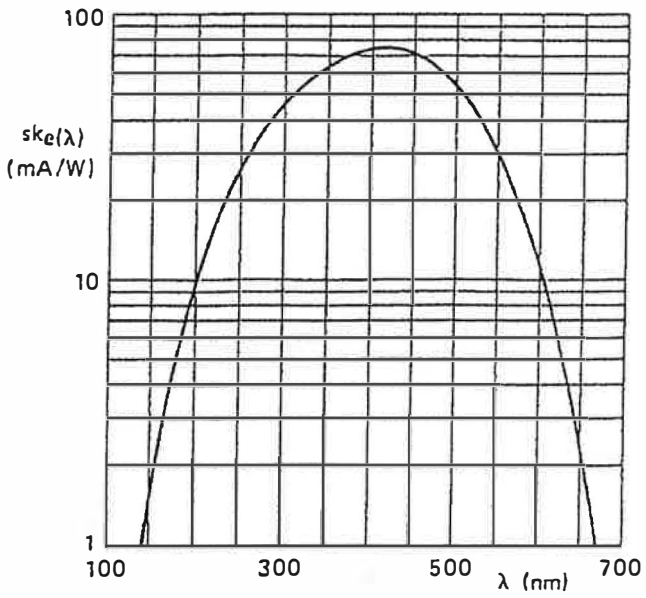

Figure II.2 : Réponse spectrale du photomultiplicateur XP-2018B

II.2.ábra: Az XP-2018B fotoelektronsokszorozó spektrális érzékenysége

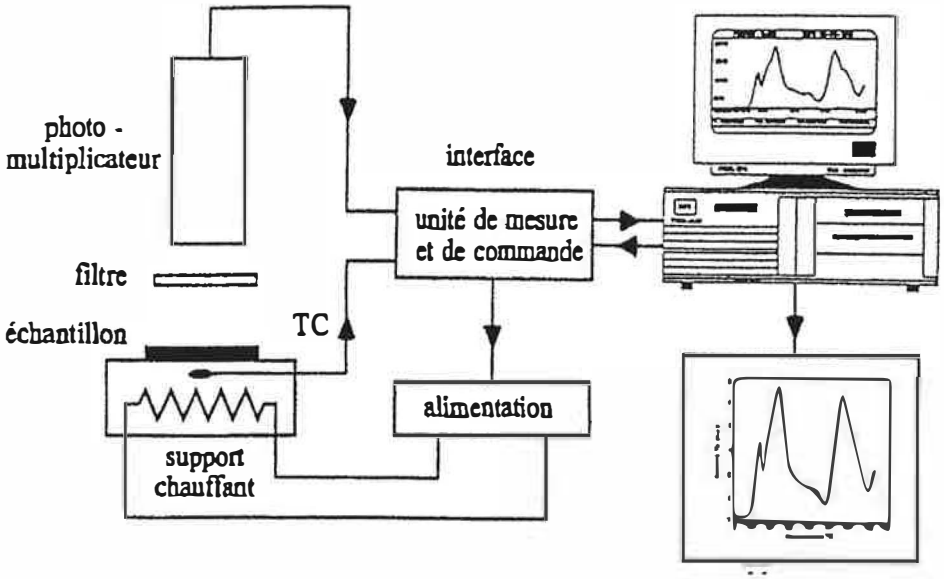

Figure II.3 : Schéma de principe du dispositif de TLHT

II.3.ábra: A magas hőmérsékletű TL készülék felépítése

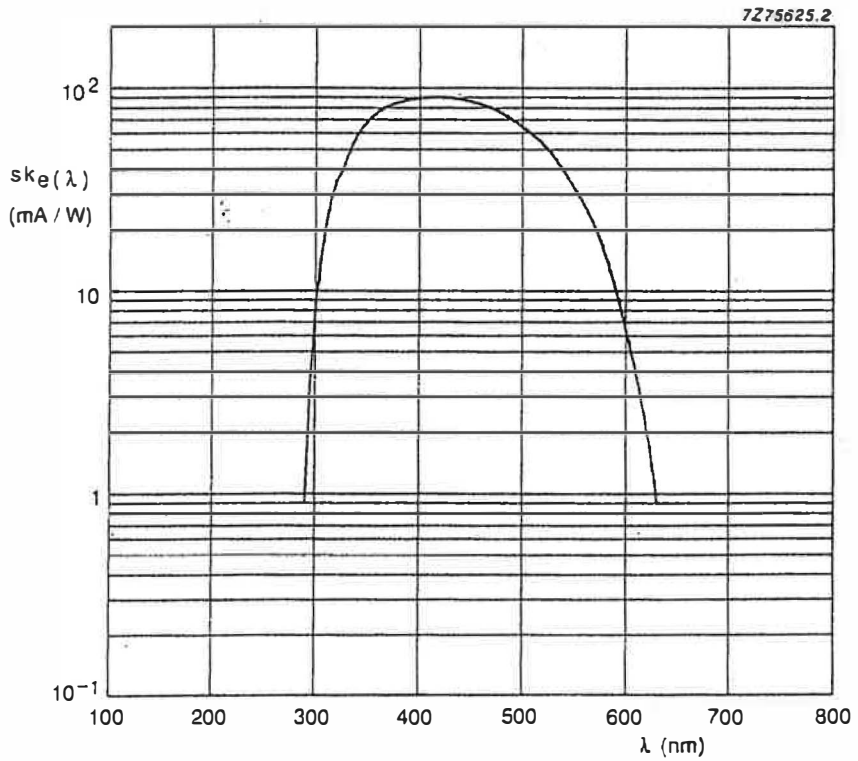

Figure II.4 : Réponse spectrale du photomultiplicateur XP-2262B

II.4.ábra: Az XP-2262B fotoelektronsokszorozó spektrális érzékenysége

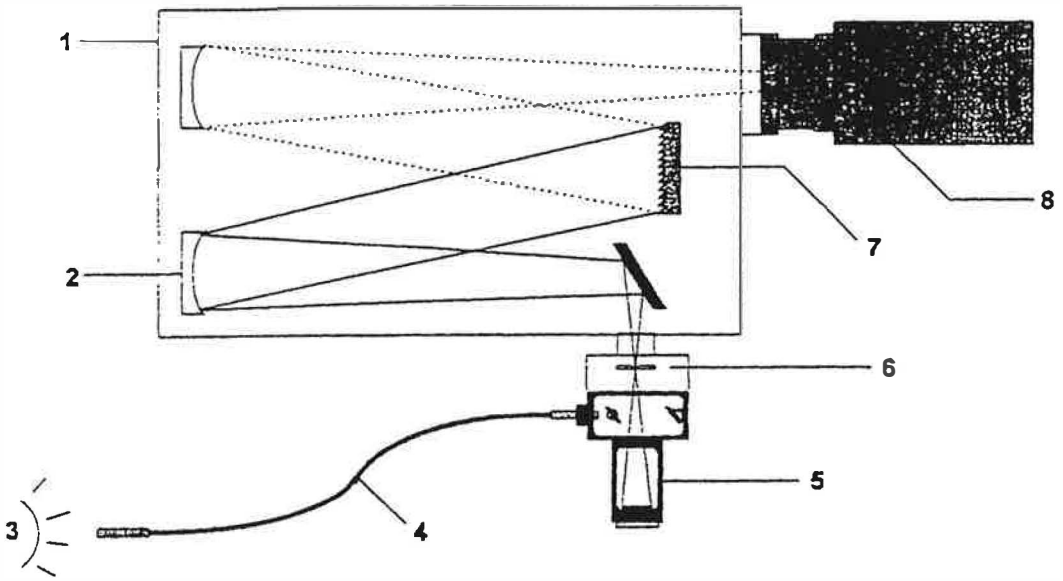

Figure II.5 : Schéma de principe de l'analyse spectrale de la TL
(1 : spectrographe, 2 : miroir, 3 : échantillon, 4 : faisceau de fibres optiques, 5 : dispositif de focalisation sur la fente, 6 : fente d'entrée, 7 : réseau, 8 : matrice CCD)

II.5.ábra: A TL emissziós spektrum mérésére használt spektrográf elvi vázlata

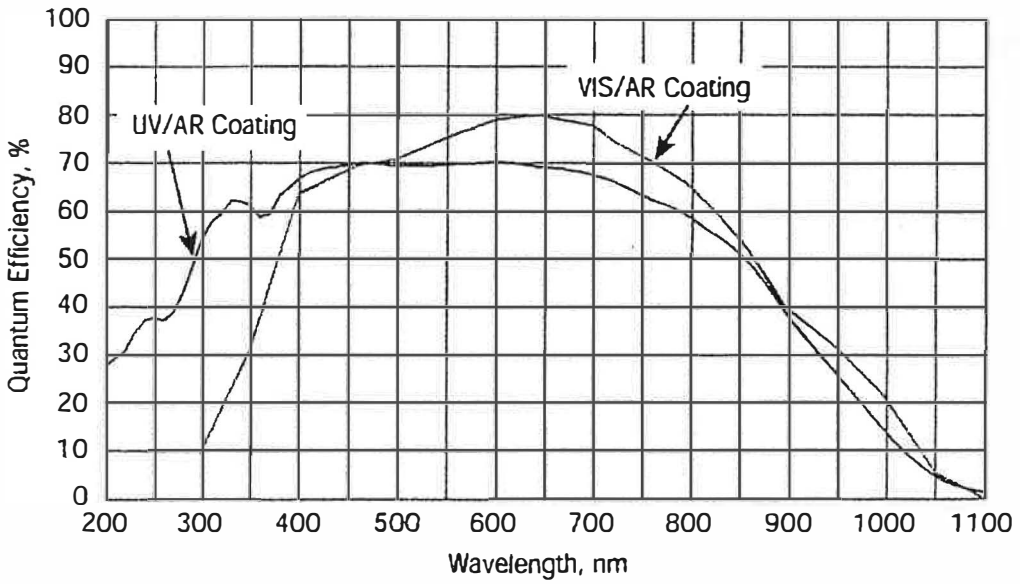

Figure II.6 : Réponse spectrale du CCD-1100PB-**UV/AR** (notre système)

II.6.ábra: A 1100PB-**UV/AR** CCD kamera spektrális érzékenysége

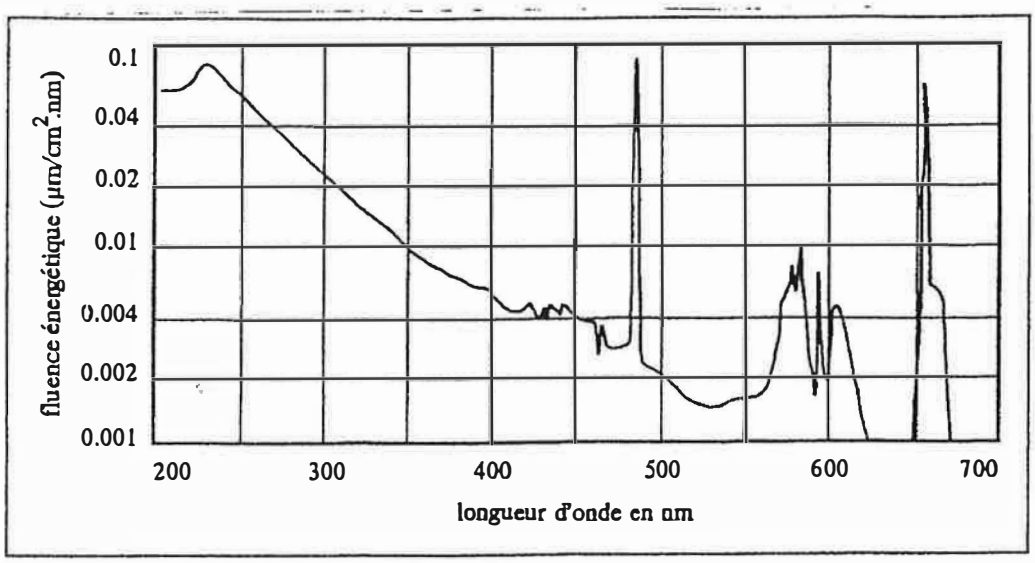

Figure II.7 : Spectral irradiance de la lampe à deutérium (Oriel-6316)

II.7.ábra: Az Oriel-6316 deutérium lámpa fényének spektruma

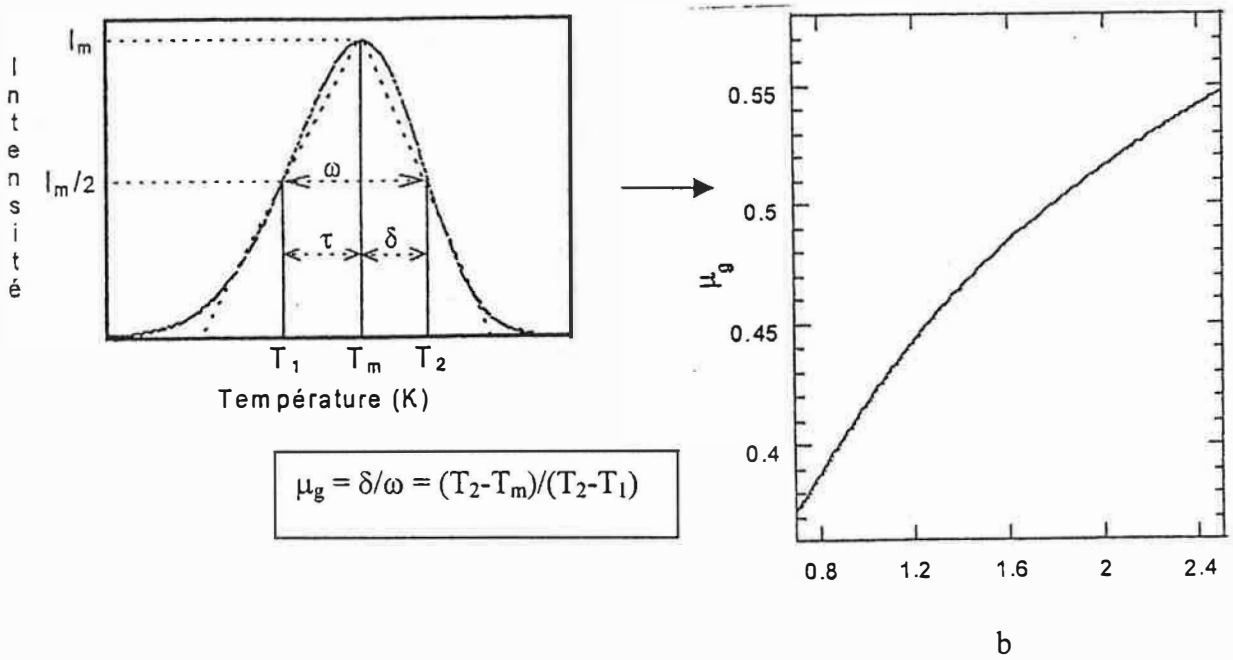

Figure II.8 : Détermination de l'ordre de cinétique (b) à partir d'un pic isolé de TL

II.8. ábra: A kinetikai rend meghatározására használt módszer egy izolált TL csúcs esetében

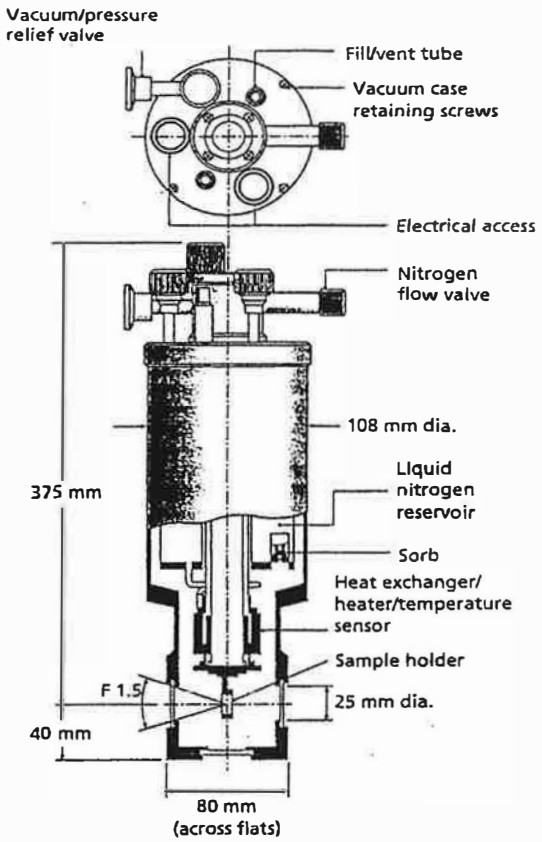

Figure II.9 : Schéma du cryostat DN-1754

II.9.ábra: A DN-1754 kriosztát felépítése

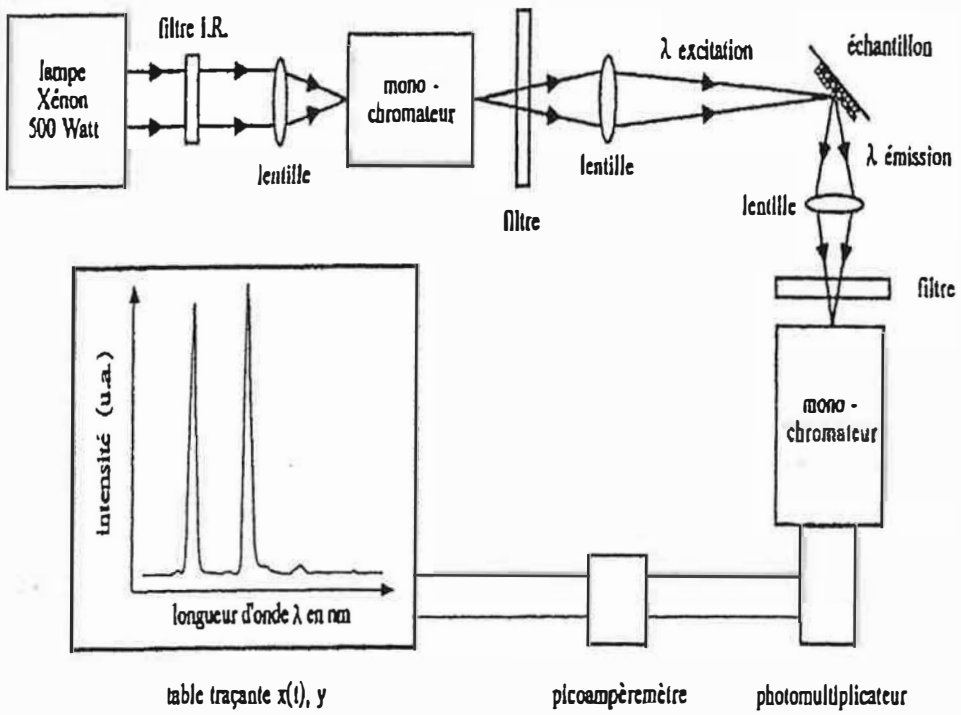

Figure II.10 : Schéma du dispositif d'étude de la photoluminescence (excitation et émission)

II.10.ábra: A fluoreszcens spektrométer felépítésének elvi vázlata

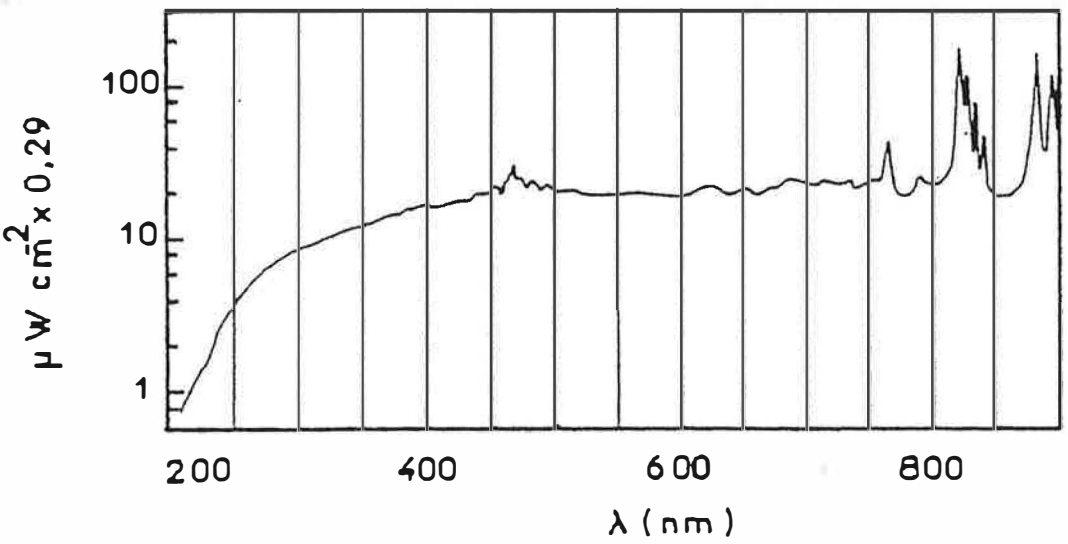

Figure II.11 : Répartition spectrale de l'émission de la lampe à xénon (Oriel-6261)

II.11.ábra: Az Oriel-6261 xenon lámpa fényének spektruma

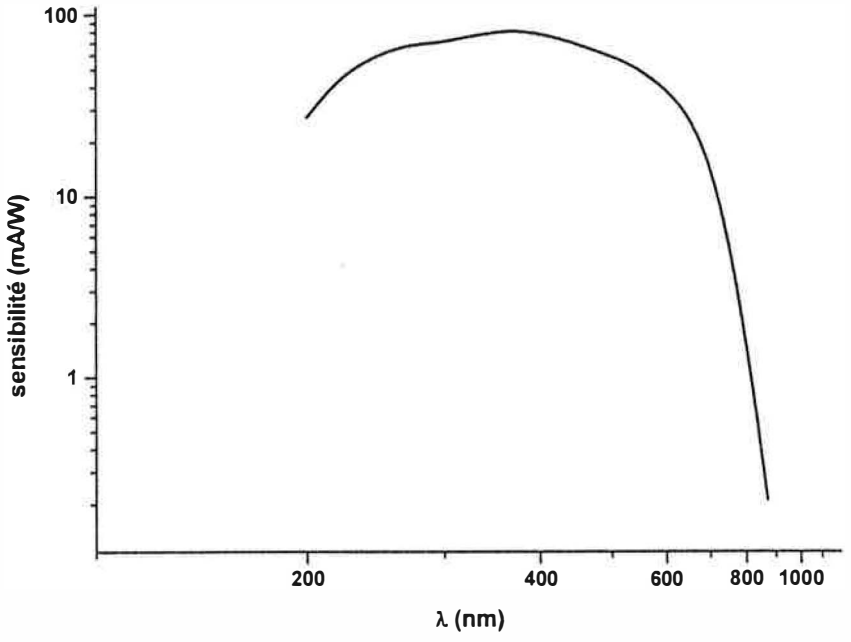

Figure II.12 : Réponse spectrale du photomultiplicateur R928

II.12.ábra: Az R928 fotoelektronsokszorozó spektrális érzékenysége

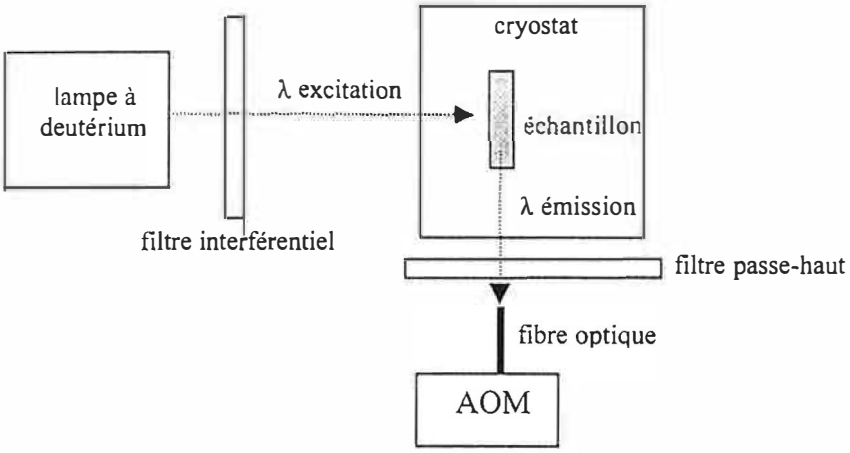

Figure II.13 : Schéma du dispositif d'étude de la photoluminescence en fonction de la température

II.13.ábra: Spektrométer a fluoreszcencia hőmérsékletfüggésének vizsgálatára

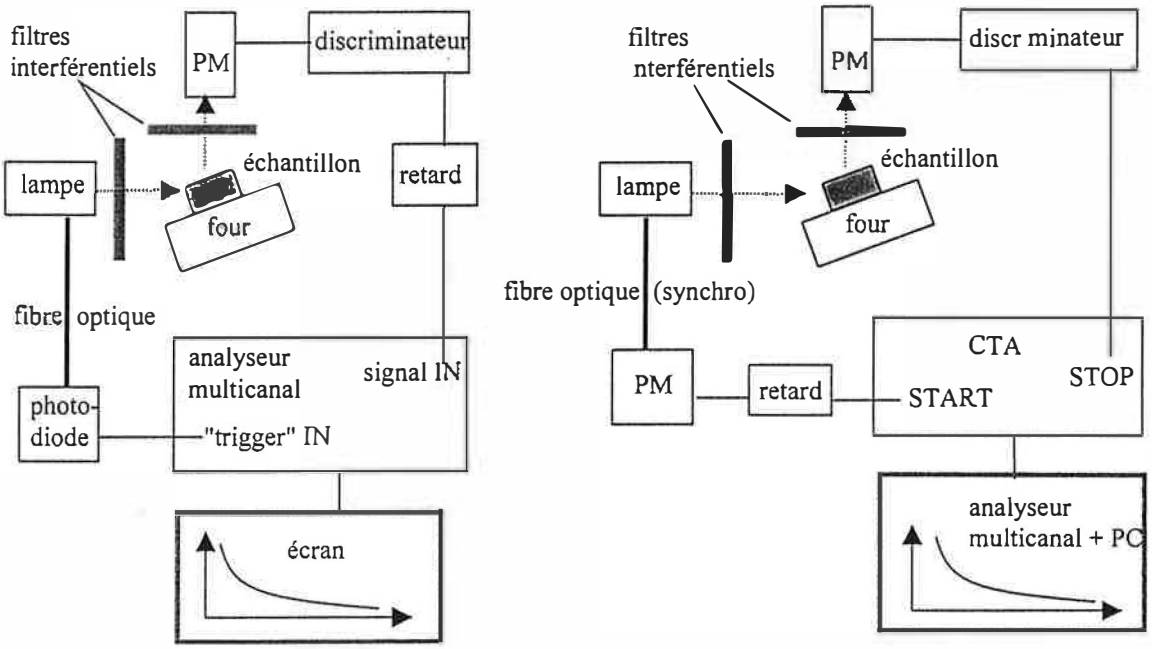

dispositif "lent" *dispositif "rapide"*

Figure II.14 : Dispositifs pour mesurer les déclins de la luminescence

II.14.ábra: A fluoreszcencia élettartam meghatározására használt készülék elvi vázlata

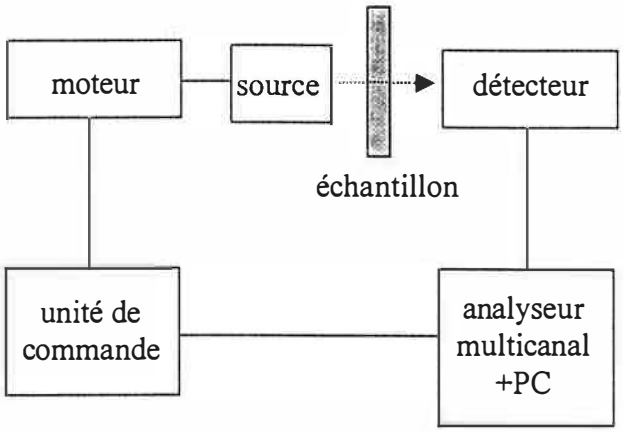

Figure II.15 : Schéma de principe du spectromètre Mössbauer

II.15.ábra: A Mössbauer spektrométer felépítésének elvi vázlata

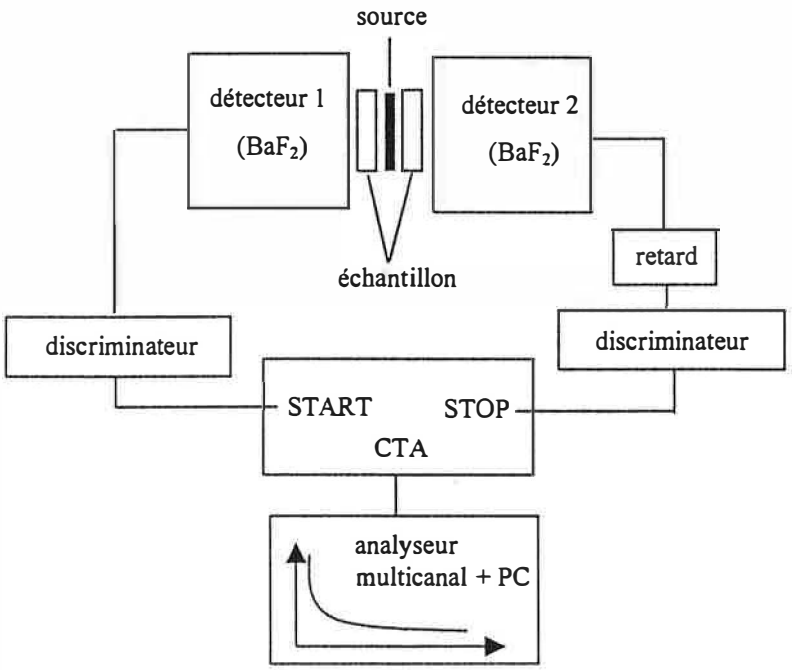

Figure II.16 : Dispositif de mesure du déclin des positrons

II.16.ábra: A pozitron élettartam meghatározására használt készülék elvi vázlata

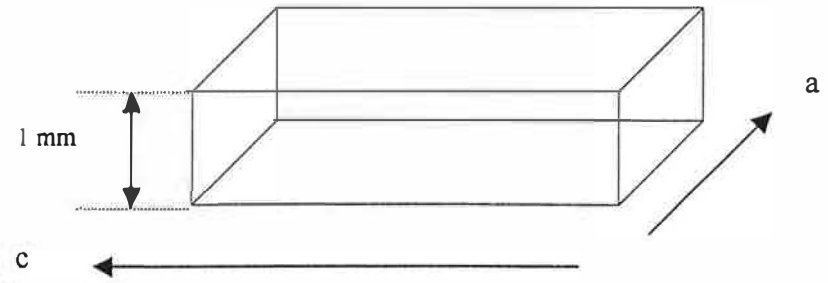

Figure III.1 : Orientation cristallographique des cristaux étudiés

III.1. ábra: A vizsgált kristályok krisztallográfiai orientációja

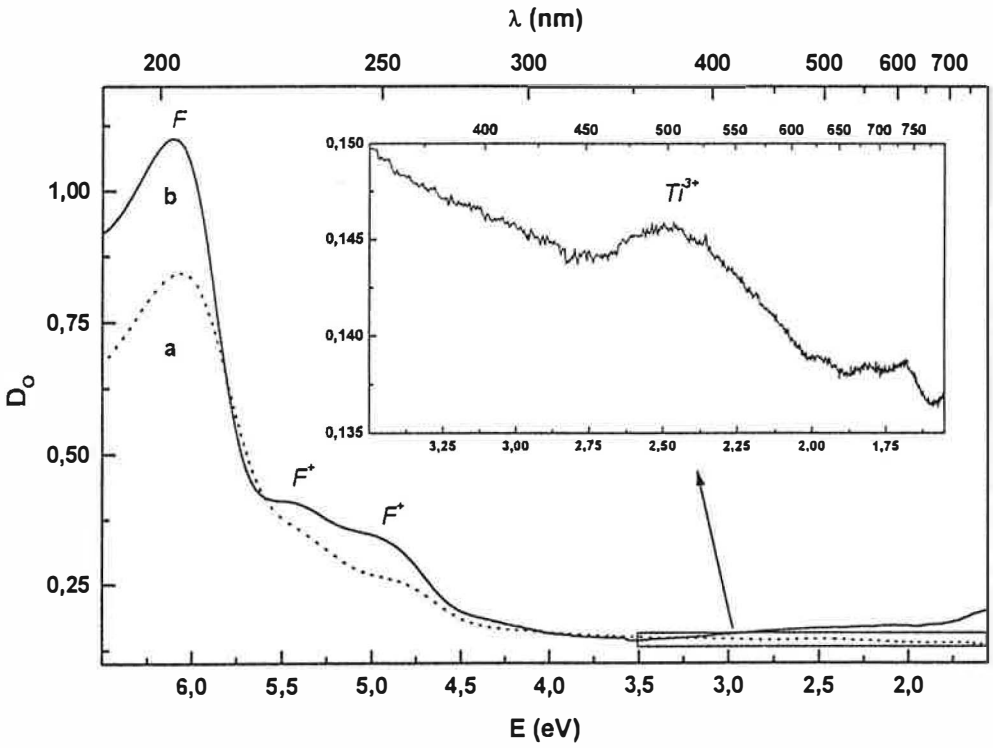

Figure III.2 : Courbes d'absorption optique d'un cristal initial, a : à 300 K, b : à 77 K

III.2. ábra: Egy kiindulási kristály abszorpciós spektruma, 300 (a) és 77 (b) K-en

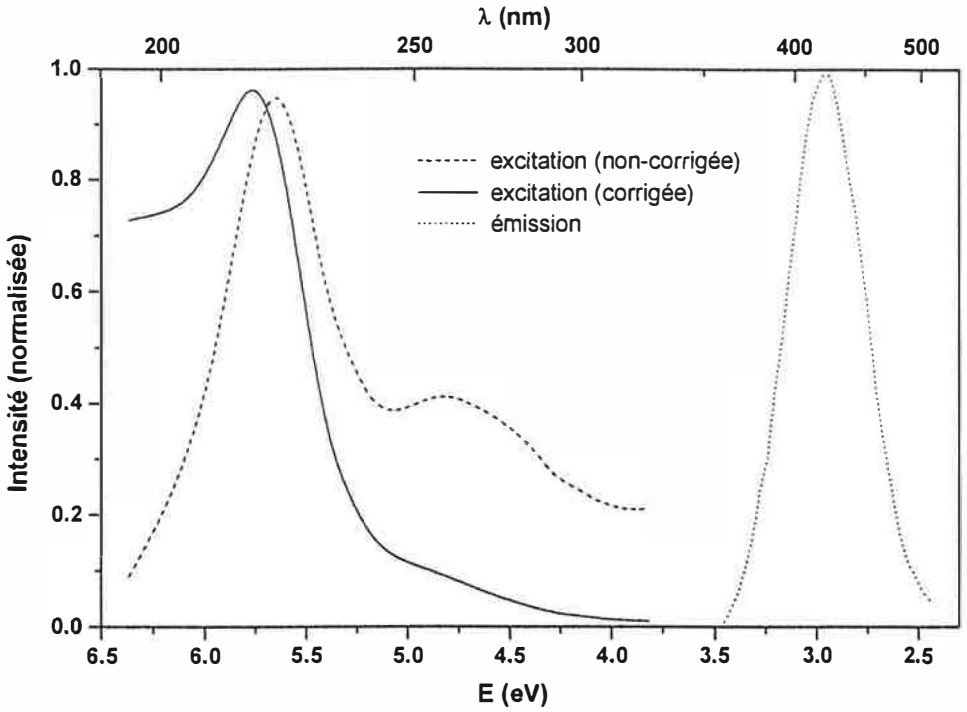

Figure III.3 : Spectres d'excitation et d'émission des centres F (obtenus à 300 K)

III.3. ábra: Az F centrumok gerjesztési és emissziós spektruma (300 K-en)

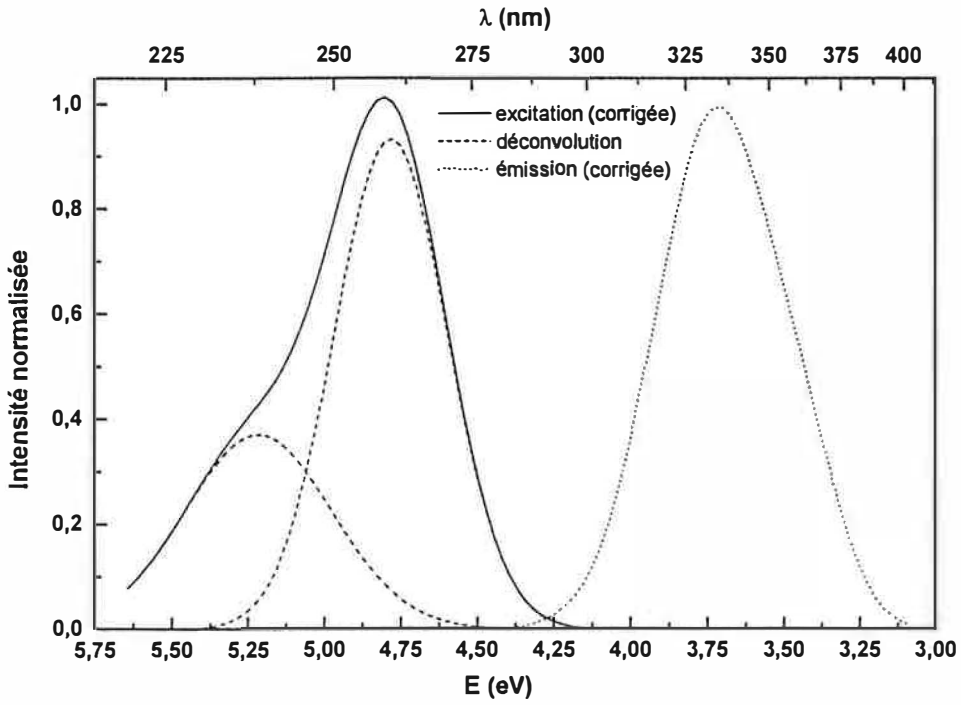

Figure III.4 : Spectres d'excitation et d'émission des centres F^+ (obtenus à 300 K)

III.4. ábra: Az F^+ centrumok gerjesztési és emissziós spektruma (300 K-en)

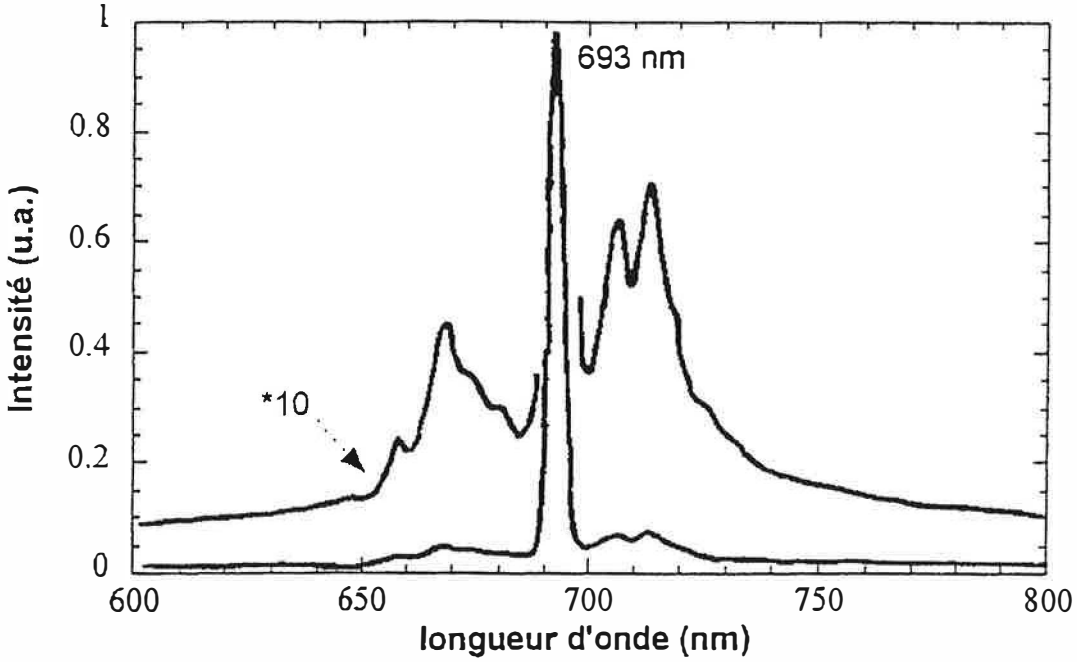

Figure III.5 : Spectre d'émission des ions Cr^{3+} (obtenus à 300 K)

III.5. ábra: A Cr^{3+} ionok emissziós spektruma (300 K-en)

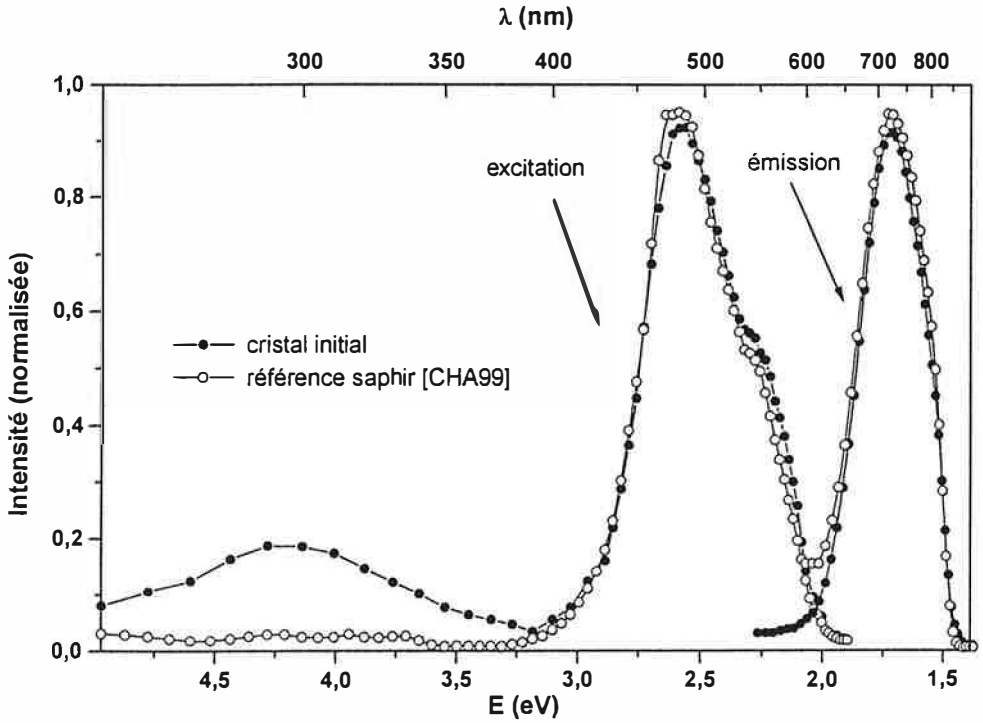

Figure III.6 : Spectres d'excitation et d'émission des ions Ti^{3+} (obtenus à 300 K)

III.6. ábra: A Ti^{3+} ionok gerjesztési és emissziós spektruma (300 K-en)

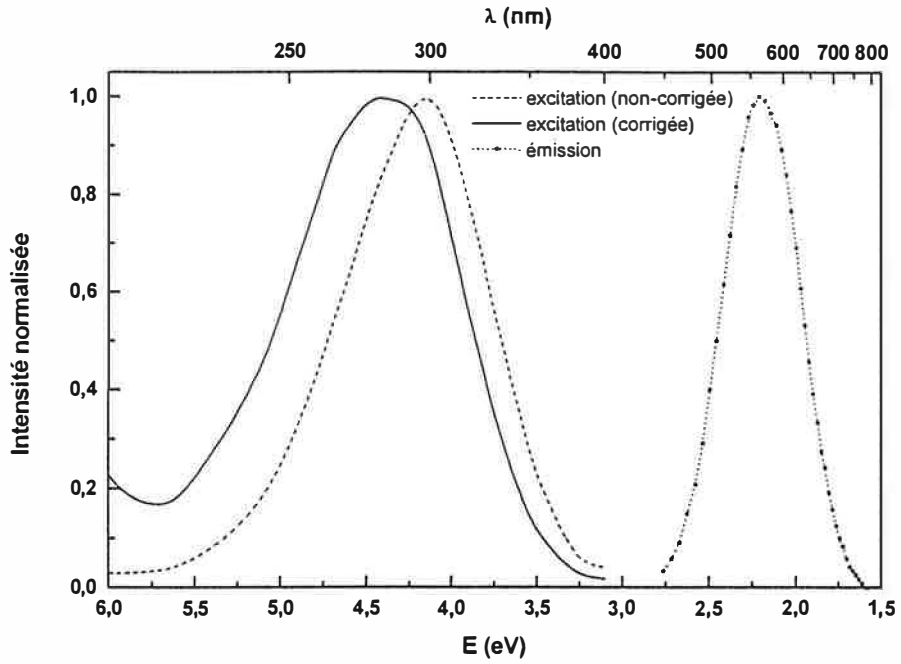

Figure III.7 : Bande d'émission à 565 nm et son spectre d'excitation (obtenus à 300 K)

III.7. ábra: Az 565 nm-es emissziós sáv és gerjesztési spektruma (300 K-en)

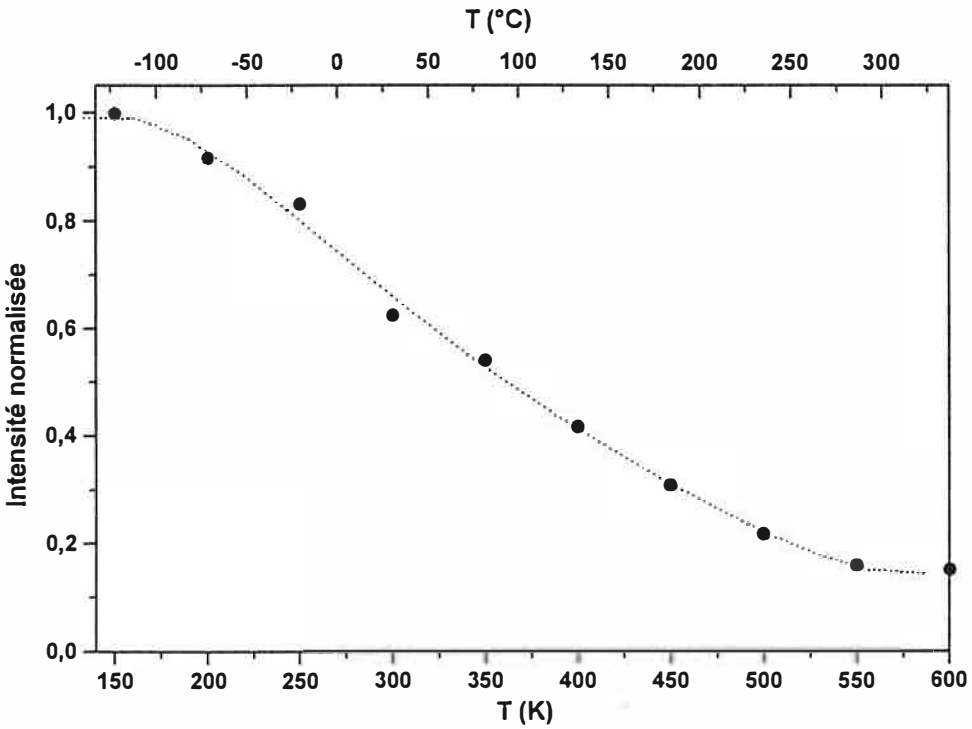

Figure III.8 : Evolution de l'intensité de l'émission à 565 nm en fonction de la température

III.8. ábra: Az 565 nm-es emissziós sáv intenzitása a hőmérséklet függvényében

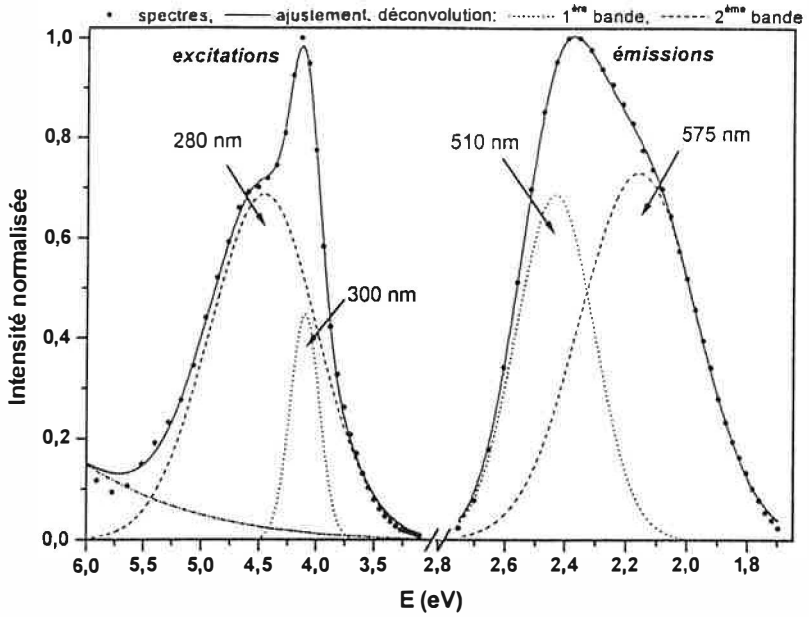

Figure III.9 : Déconvolution des bandes d'émission entre 500-600 nm et de leurs spectres d'excitation

III.9. ábra: Az 500-600 nm közti emissziós sávok és az ezeknek megfelelő gerjesztási spektrumok

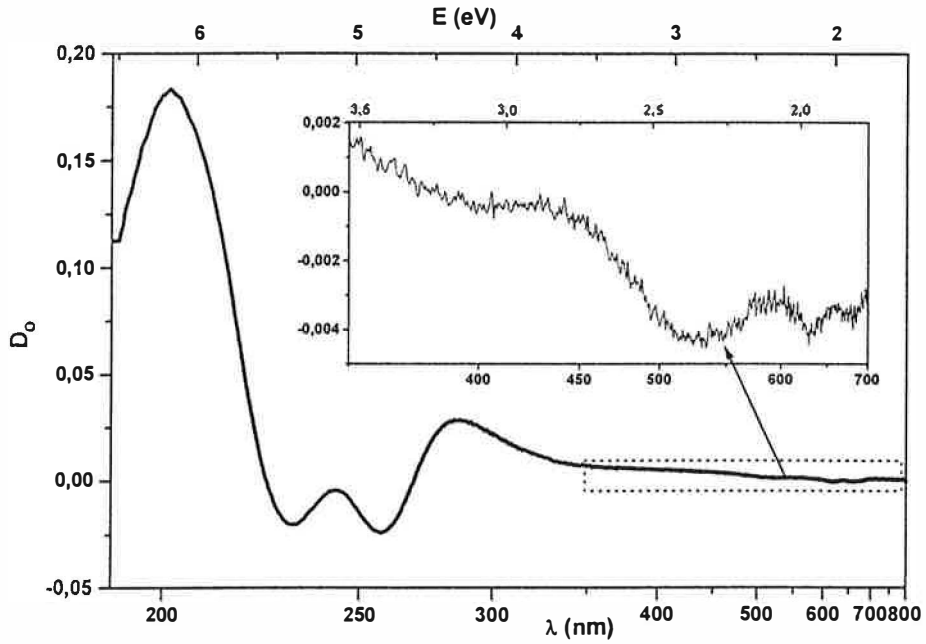

Figure III.10 a : Spectre d'absorption induite par irradiation X (3 kGy) à 300 K dans un cristal initial (absorption induite = absorption du cristal irradié - absorption du même cristal non irradié)

III.10.a ábra: Az optikai abszorpciós spektrum változása röntgensugárzás (3 kGy, 300 K-en) hatására egy kiindulási kristályban (abszorpciós referencia: a kristály besugárzás előtt)

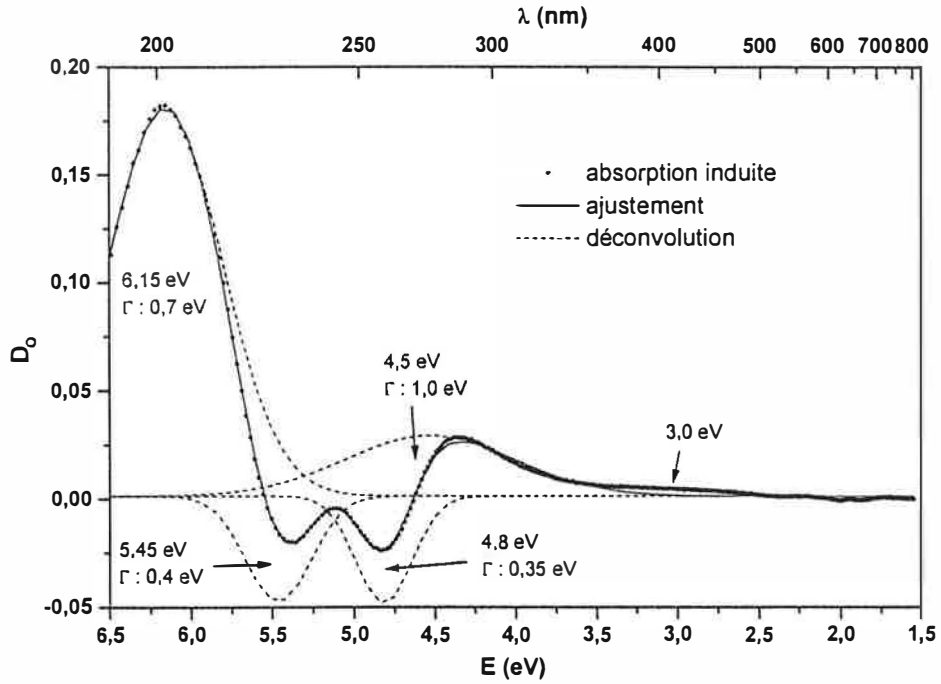

Figure III.10 b : Déconvolution des bandes d'absorption induites par irradiation X (3 kGy à 300 K)

III.10.b ábra: A *III.10.a* spektrum dekonvolúciója

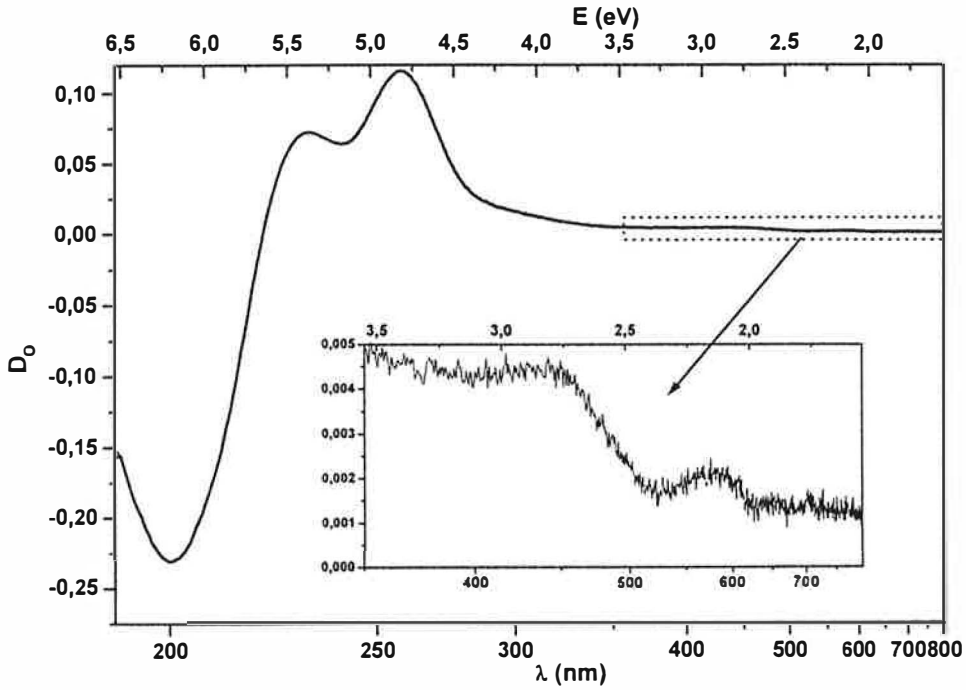

Figure III.11 a : Spectre d'absorption induite par excitation UV à 300 K dans un cristal initial (absorption induite = absorption du cristal irradié - absorption du même cristal non-irradié)

III.11.a ábra: Az optikai abszorpciós spektrum változása UV sugárzás (deutérium lámpa, 300 K-en) hatására egy kiindulási kristályban (abszorpciós referencia: a kristály besugárzás előtt)

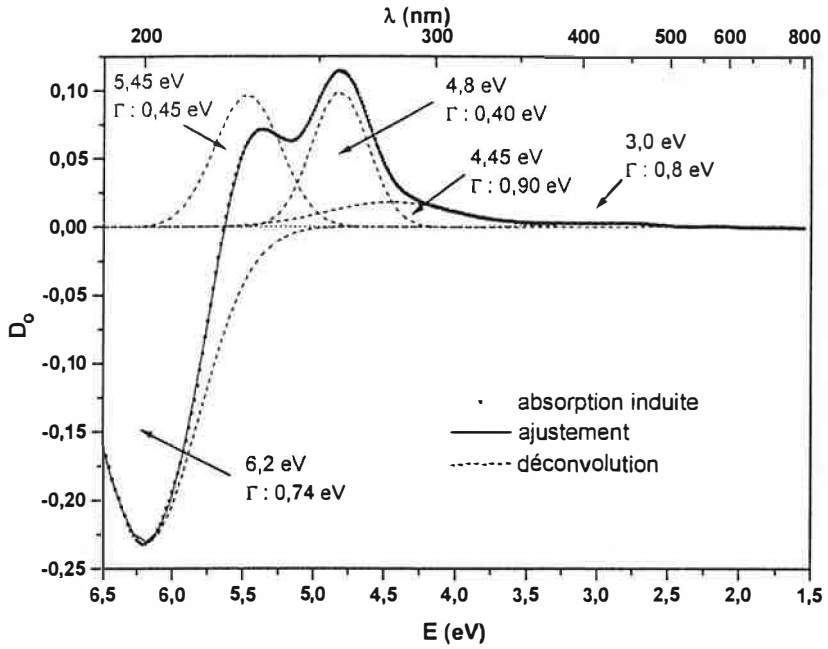

Figure III.11 b : Déconvolution des bandes d'absorption induites par excitation UV à 300 K

III.11.b ábra: A *III.11.a* spektrum dekonvolúciója

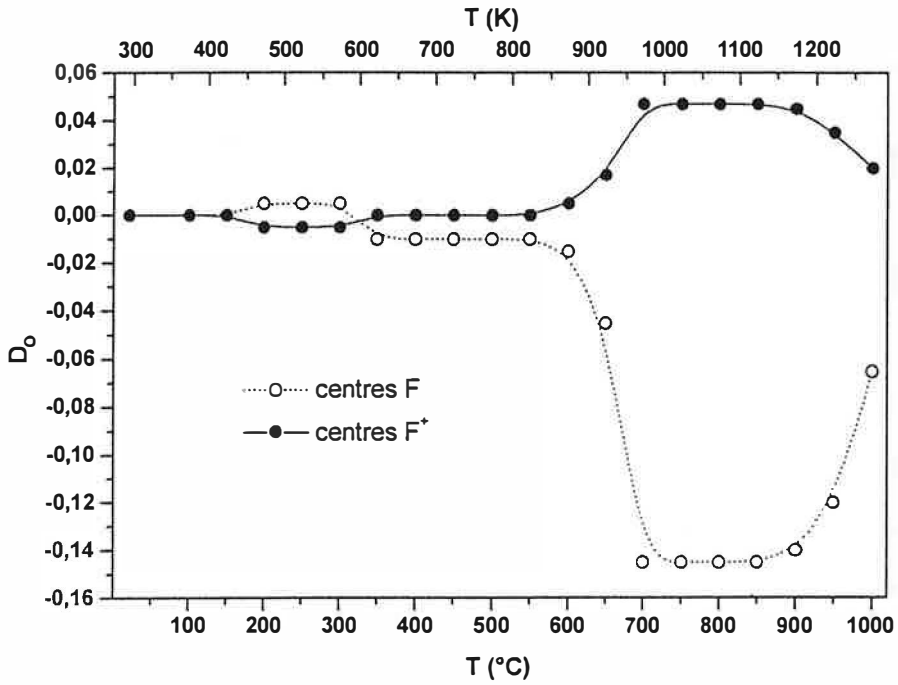

Figure III.12 a : Evolution de la densité optique (concentration) des centres F et F^+ en fonction de la température par référence à leur concentration après irradiation X de 3 kGy à 300 K

III.12.a ábra: Az F és F^+ centrumok koncentrációjának (optikai abszorpció) változása hevítés hatására egy kiindulási kristályban röntgen besugárzás után (3 kGy, 300 K-en)

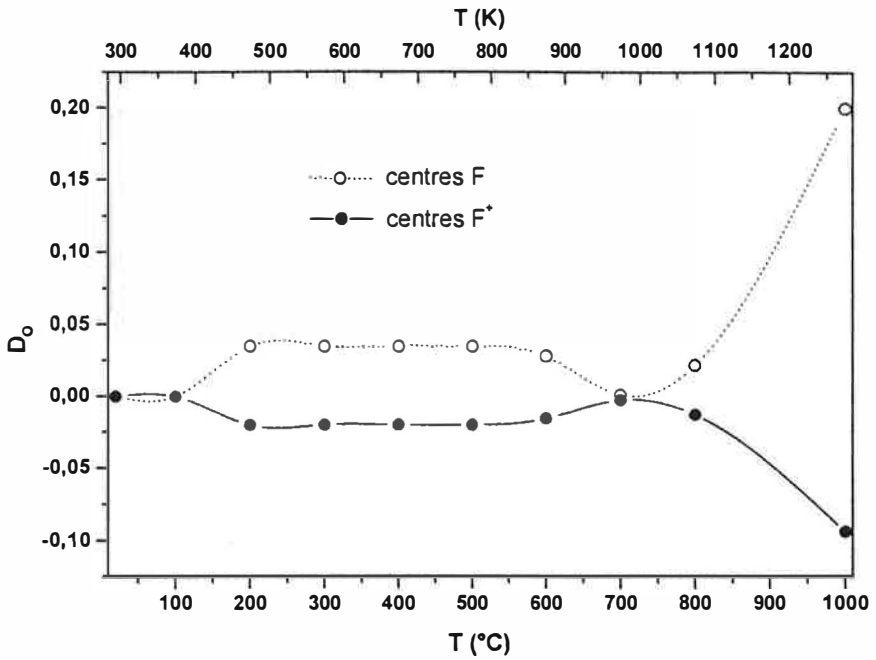

Figure III.12.b : Evolution de la densité optique (concentration) des centres F et F^+ en fonction de la température par référence à leur concentration après excitation UV à 300 K

III.12.b ábra: Az F és F^+ centrum abszorpciójának változása hevítés hatására egy kiindulási kristályban UV besugárzás után

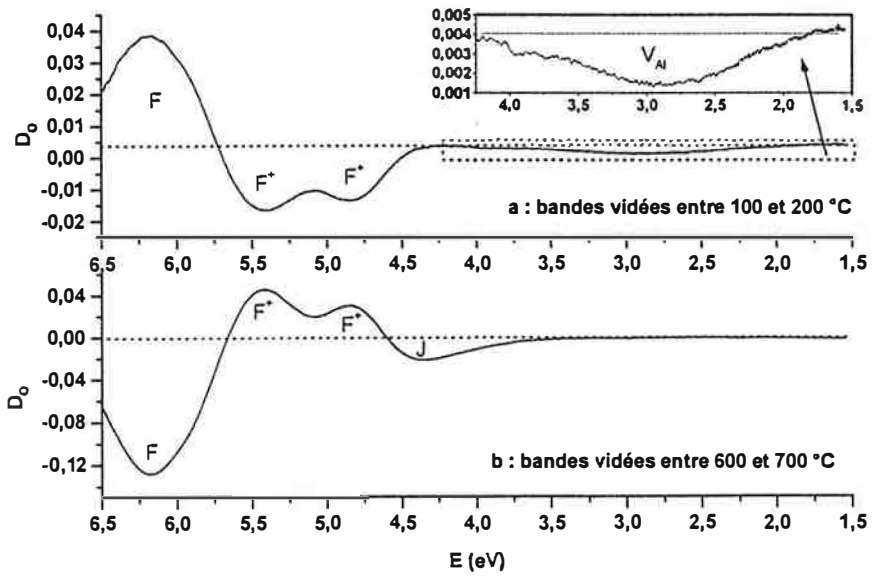

Figure III.13 : Vidage thermique des bandes d'absorption induites par irradiation X (6 kGy à 25 °C) dans un cristal initial

III.13. ábra: Az optikai abszorpciós spektrum változása hevítés hatására egy kiindulási kristályban röntgen besugárzás után (6 kGy, 25 °C-on)

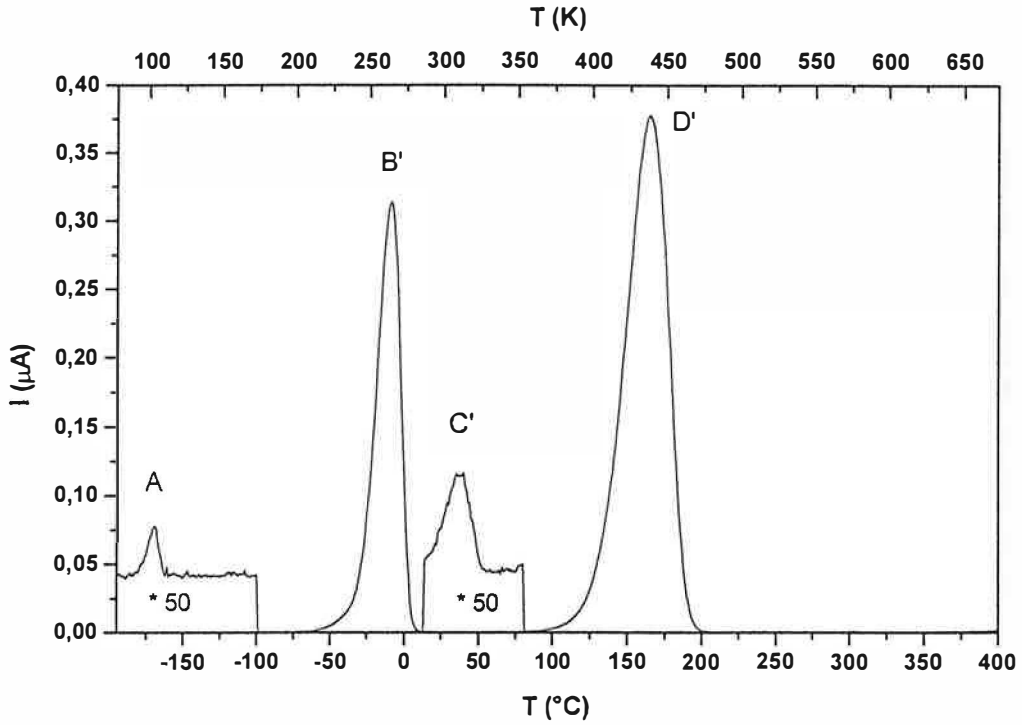

Figure III.14 : Courbe de TL d'un cristal initial après irradiation X à 77 K (3 Gy)

III.14 ábra: TL görbe egy kiindulási kristályban röntgen besugárzás után (3 Gy, 77 K-en)

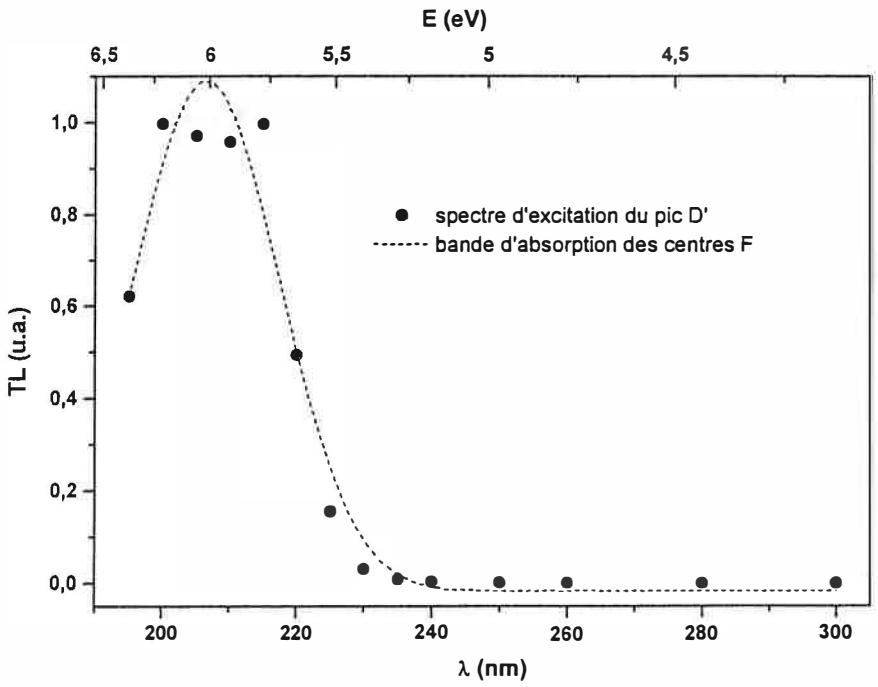

Figure III.15 : Spectre d'excitation (pour un flux constant de photons) du pic D'

III.15 ábra: A D' TL csúcs gerjesztési spektruma

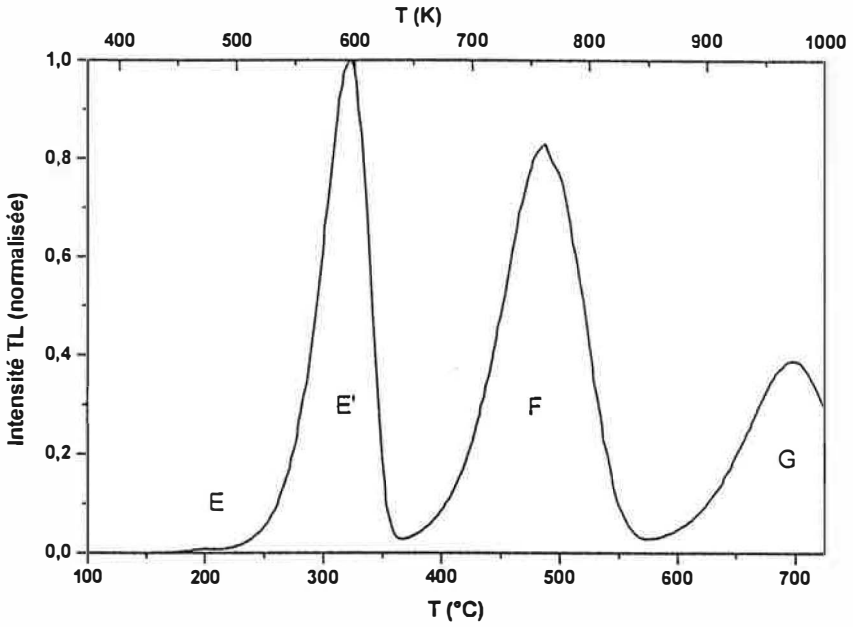

Figure III.16 : Courbe de TL enregistrée à 340 nm d'un cristal initial après excitation UV (206 nm) à 500 K

III.16 ábra: TL görbe 340 nm-en regisztrálva egy kiindulási kristályban UV besugárzás után (206 nm, 500 K-en)

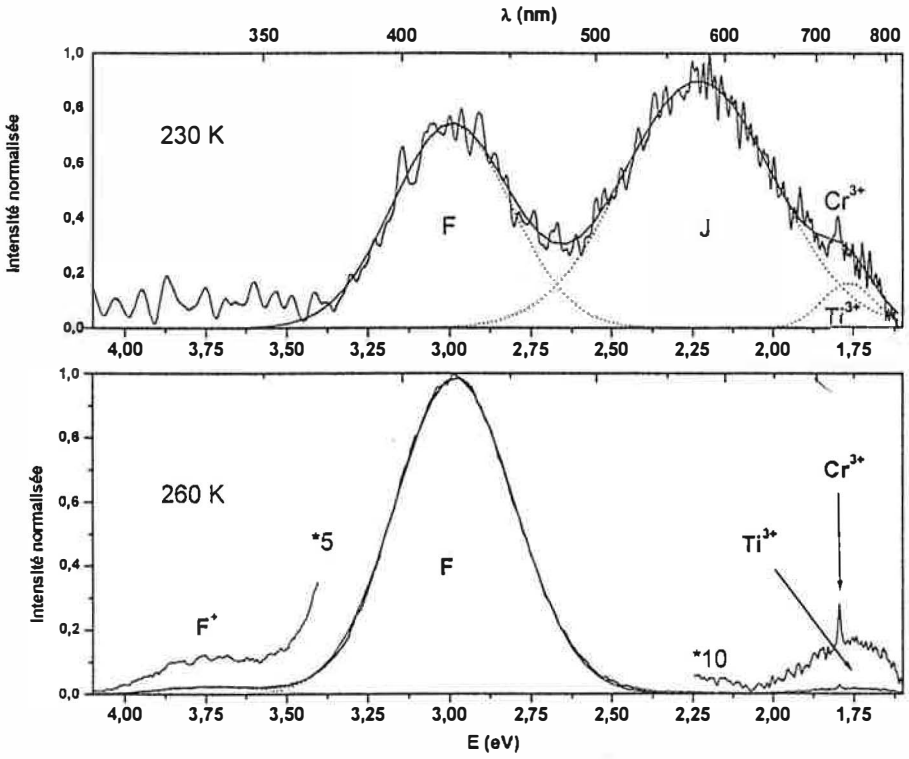

Figure III.17 : Analyse spectrale de la TL à 230 K (pics B et B') et à 260 K (pic B') d'un cristal initial après irradiation X à 77 K (12 Gy)

III.17 ábra: TL emissziós spektrum 230 és 260 K-en röntgen besugárzás után (12 Gy, 77 K)

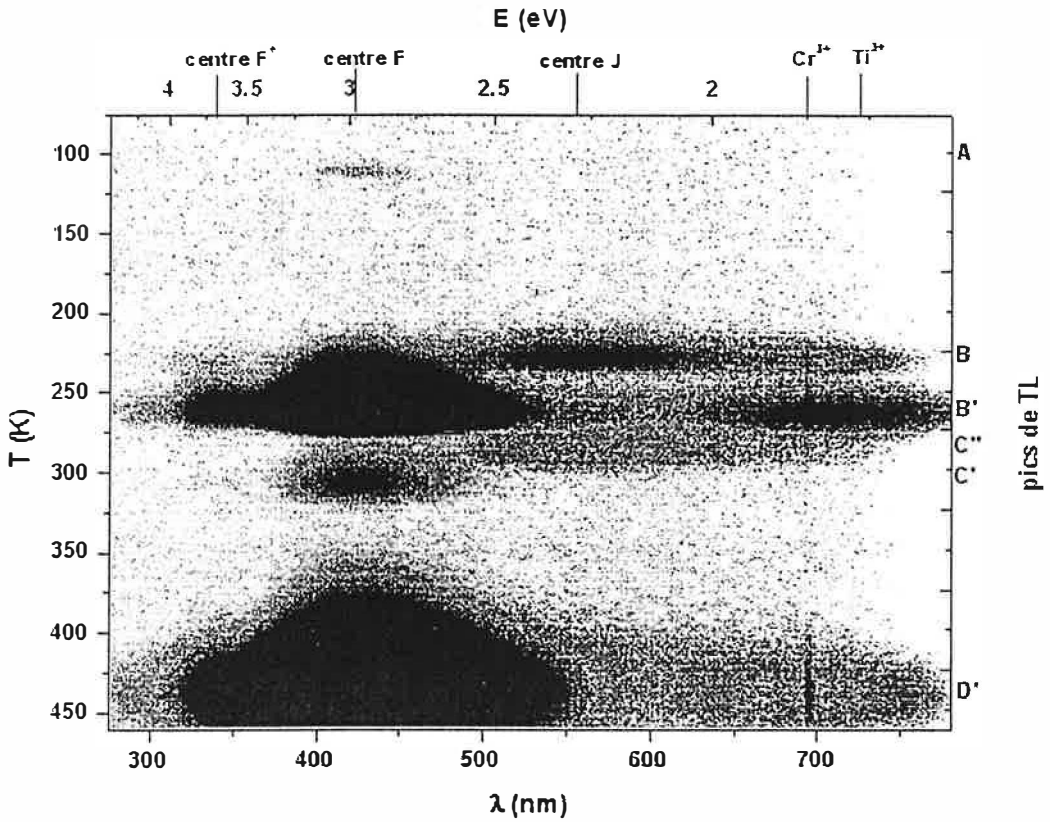

Figure III.18 : Image d'analyse spectrale « 3D » de la TL après irradiation X de 12 Gy à 77 K
III.18 ábra: 3D-TL egy kindulási kristályról röntgen besugárzás után (12 Gy, 77 K)

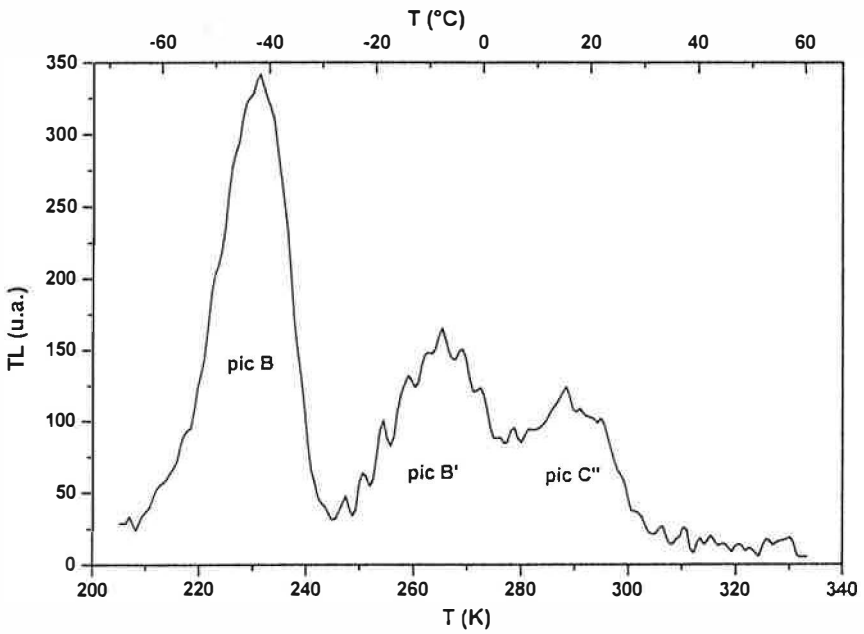

Figure III.19: Courbe de TL d'un cristal initial enregistrée à 565 nm après irradiation X (12 Gy à 77 K)

III.19 ábra: TL görbe 340 nm-en regisztrálva egy kiindulási kristályban
röntgen besugárzás után (12 Gy, 77 K)

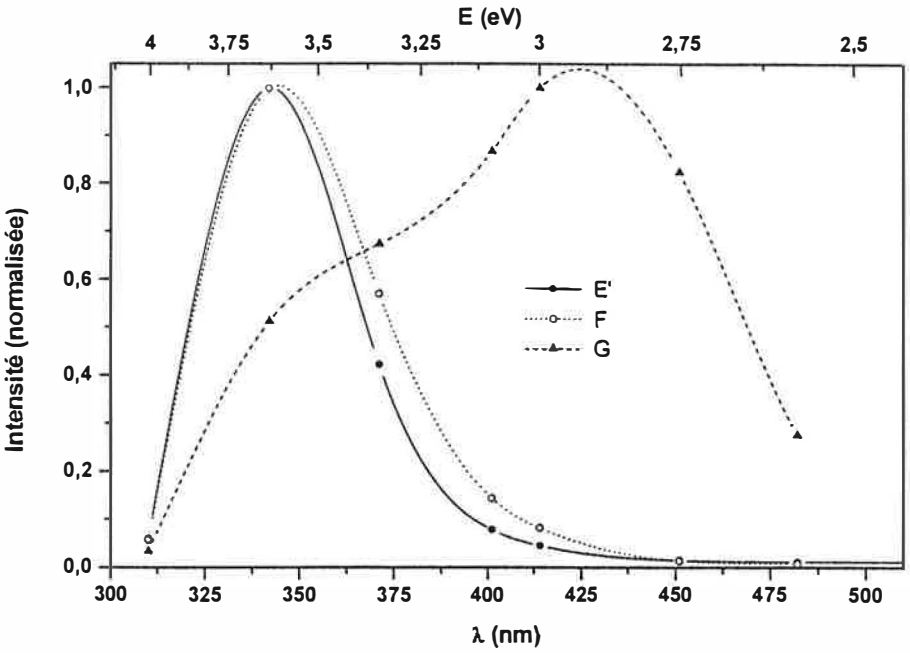

Figure III.20 : Analyse spectrale des pics de TL à 580 K (E'), à 750 K (F) et à 950 K (G) d'un cristal initial après irradiation UV (206 nm) à 500 K

III.20 ábra: TL emissziós spektrum 580, 750 és 950 K-en UV besugárzás (206 nm, 500 K) után egy kiindulási kristályban

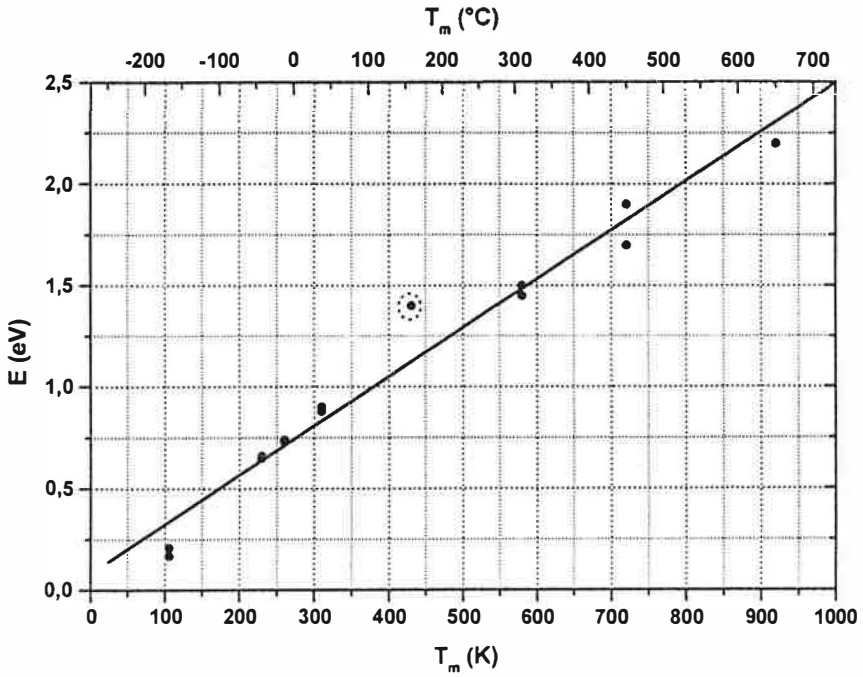

Figure III.21 : Variation de la profondeur des pièges en fonction de la température des pics

III.21. ábra: A töltéscsapdák aktivációs energája ("mélysége") a TL csúcsok hőmérsékletének függvényében

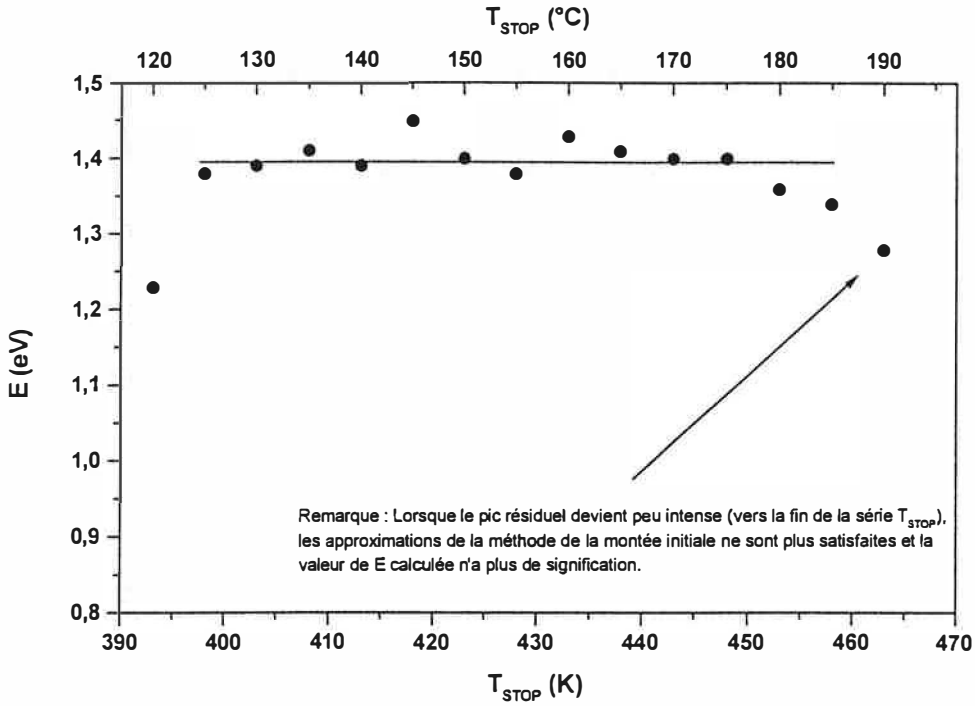

Figure III.22 : Application de la méthode T_{STOP} au pic D'

III.22. ábra: A T_{STOP} módszer alkalmazása a D' TL csúcs vizsgálatára

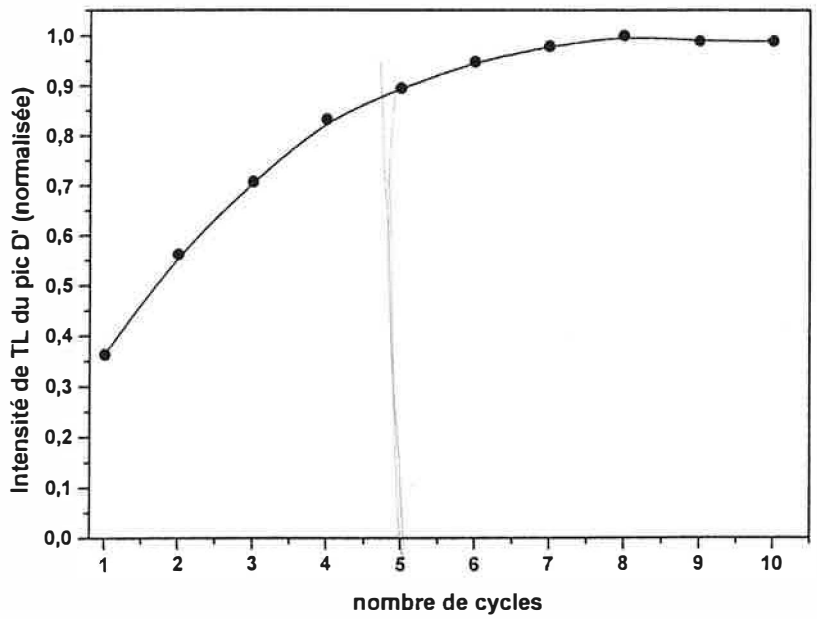

Figure III.23 : Variation de l'intensité de TL du pic D' en fonction du nombre de mesures, à dose d'irradiation constante (UV-206 nm, 1 min)

III.23. ábra: A D' TL csúcs intenzitása a mérések számának függvényében állandó besugárzási dózis mellet (UV-206 nm, 1 min)

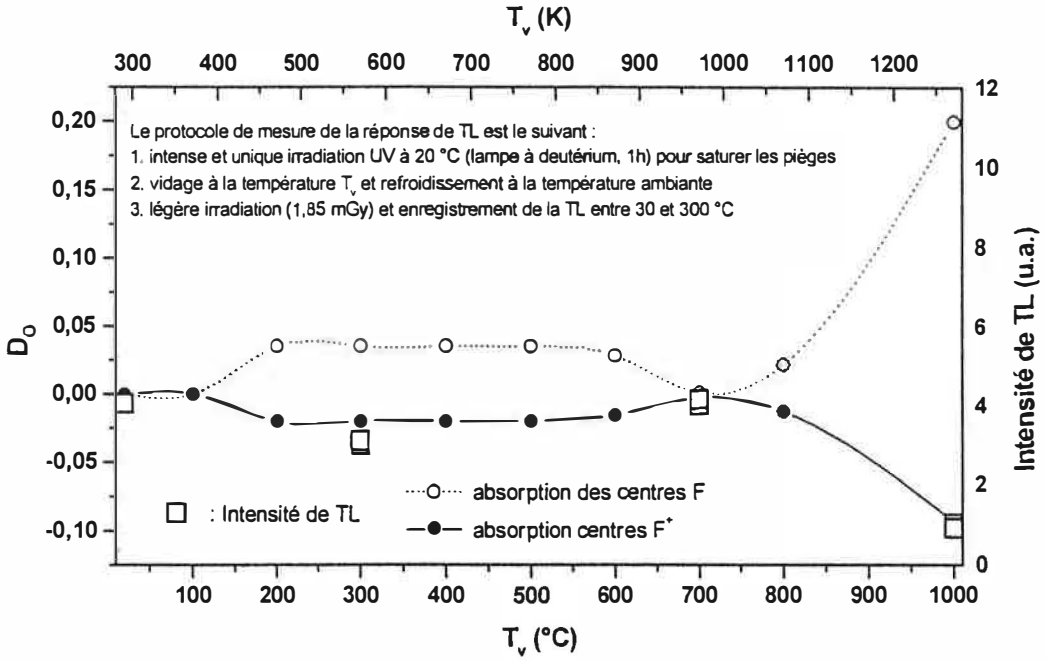

Figure III. 24 : Effet de la température de vidage T_v sur la sensibilité du pic D'. Comparaison avec les variations de concentration des centres F et F^+ telles que reportées sur la figure III.12.

III.24 ábra: A D' TL csúcs intenzitása a kifűtési hőmérséklet (T_v) függvényében. Összehasonlítás az F és F^+ centrumok koncentrációjának változásával (III.12 ábra).

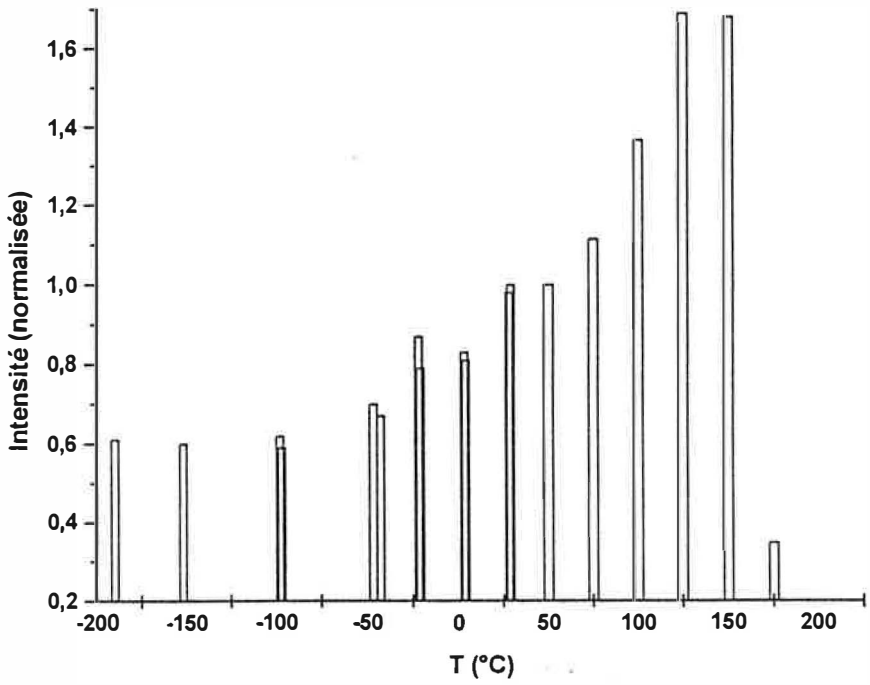

Figure III.25 : Evolution de l'intensité du pic D'
en fonction de la température d'irradiation (UV, 206 nm, 20 s)

III.25 ábra: A D' TL csúcs intenzitása a besugárzási hőmérséklet függvényében (UV, 20 s)

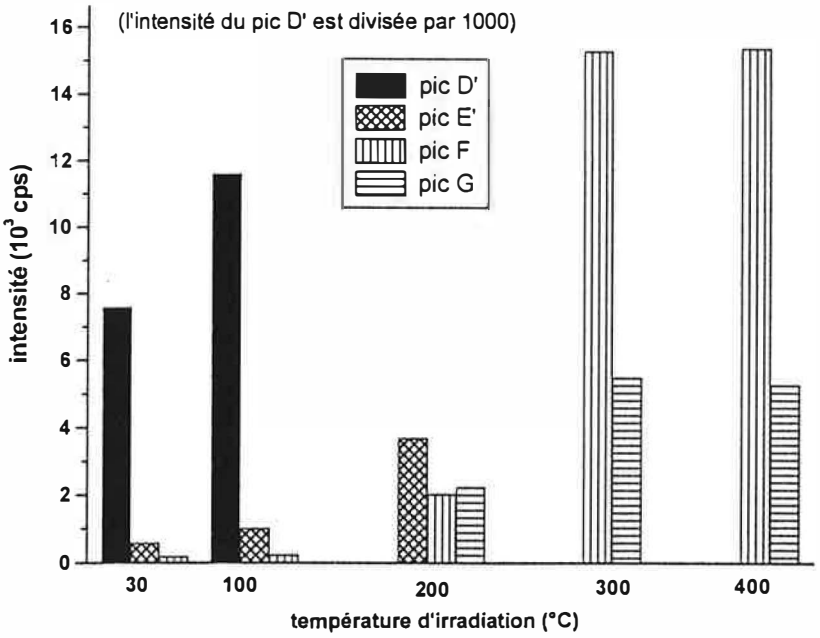

Figure III.26 : Evolution de l'intensité des pics de TL
en fonction de la température d'irradiation (irradiation UV 206 nm, 10 min)

III.26. ábra: A TL csúcsok intenzitása a besugárzási hõmérséklet függvényében (UV, 10 min)

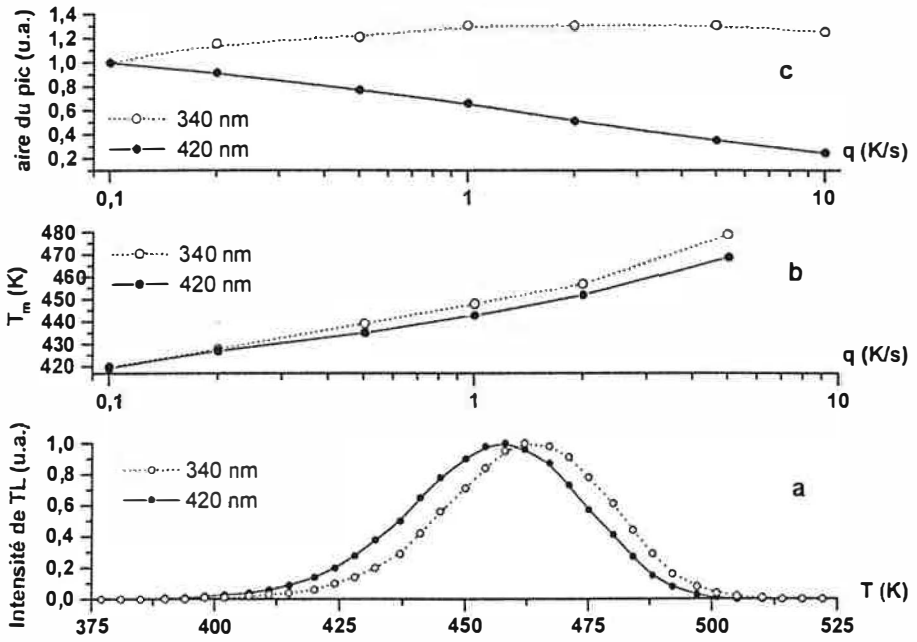

Figure III.27 a : Observation du pic D' à deux longueurs d'onde (q = 2 K/s)
Evolution de la position (b) et de la surface (c) du pic D' en fonction de la vitesse de chauffe

III.27. ábra, a: A D' TL csúcs két különböző hullámhosszon mérve (q = 2 K/s)
A csúcs pozíciójának (b) és területének (c) változása a kifűtési sebesség függvényében

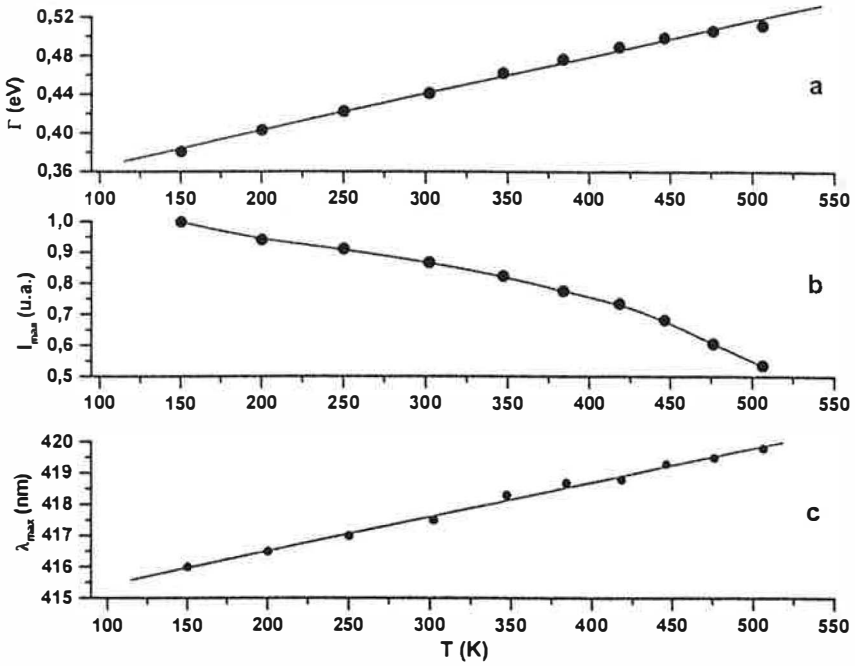

Figure III.28. Evolution de la largeur à mi-hauteur (a), l'intensité (b) et la position (c) de la bande d'émission des centres F en fonction de la température

III.28. ábra: Az F centrum fluoreszcencia sávszélesség (a), intenzitás (b) és hullámhossz a hőmérséklet függvényében

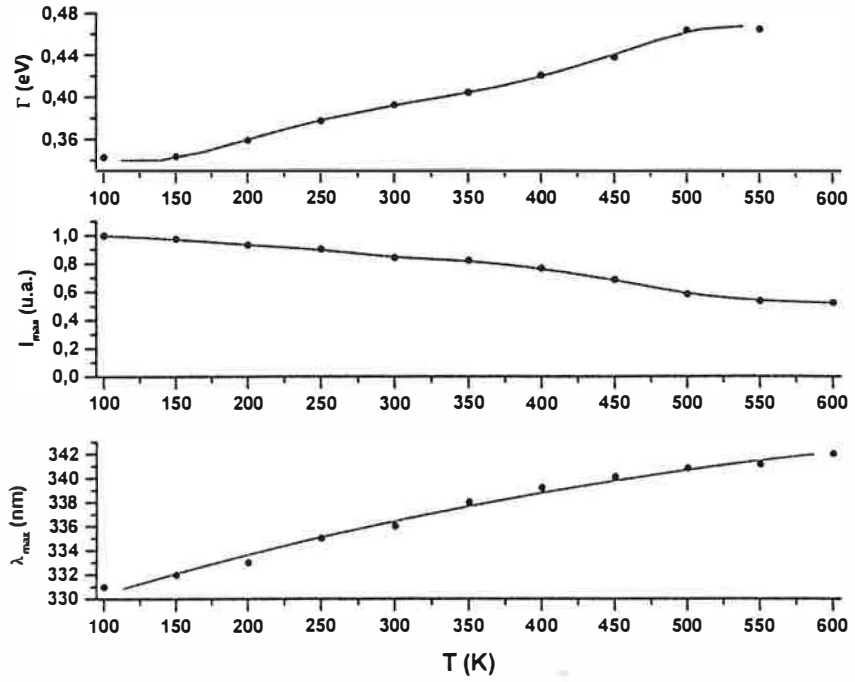

Figure III.29. Evolution de la largeur à mi-hauteur (a), l'intensité (b) et la position (c) de la bande d'émission des centres F^+ en fonction de la température

III.29. ábra: Az F^+ centrum fluoreszcencia sávszélesség (a), intenzitás (b) és hullámhossz a hőmérséklet függvényében

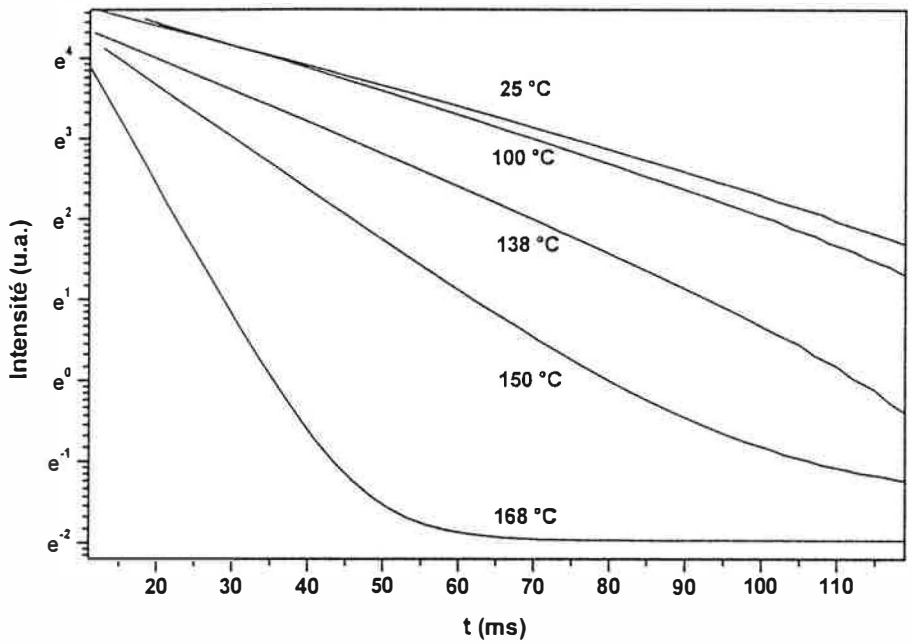

Figure III.30 : Déclins de fluorescence des centres F à différentes températures

III.30. ábra: Az F centrum fluoreszcencia "lecsengése" a hőmérséklet függvényében

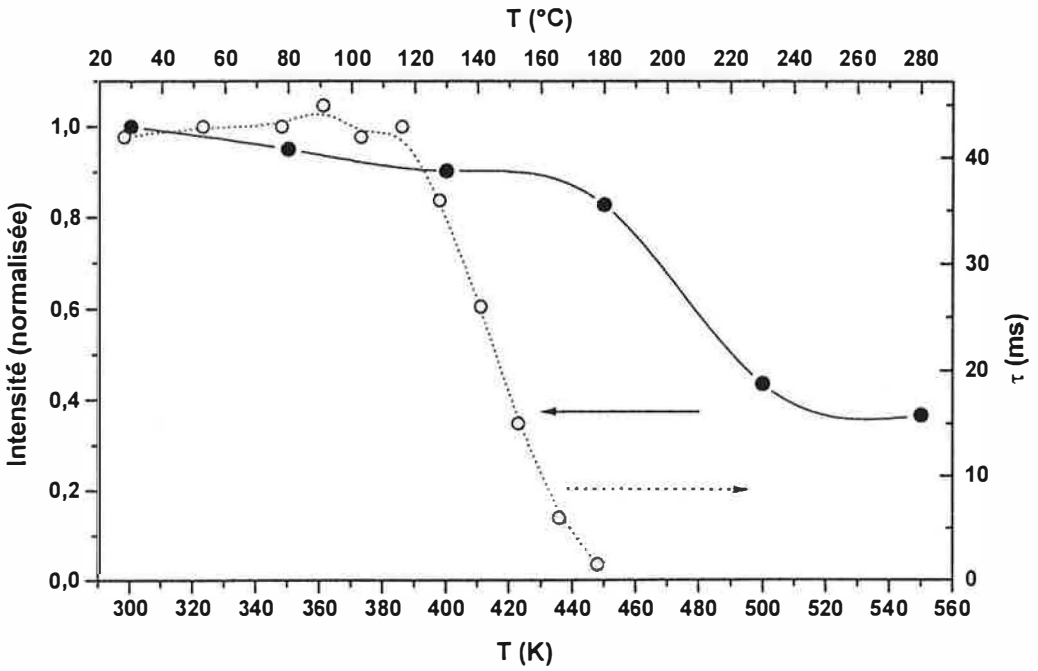

Figure III.31 : Evolution de l'intensité et de la durée de vie de la photoluminescence des centres F en fonction de la température

III.31. ábra: Az F centrum fluoreszcencia intenzitás és élettartam a hőmérséklet függvényében

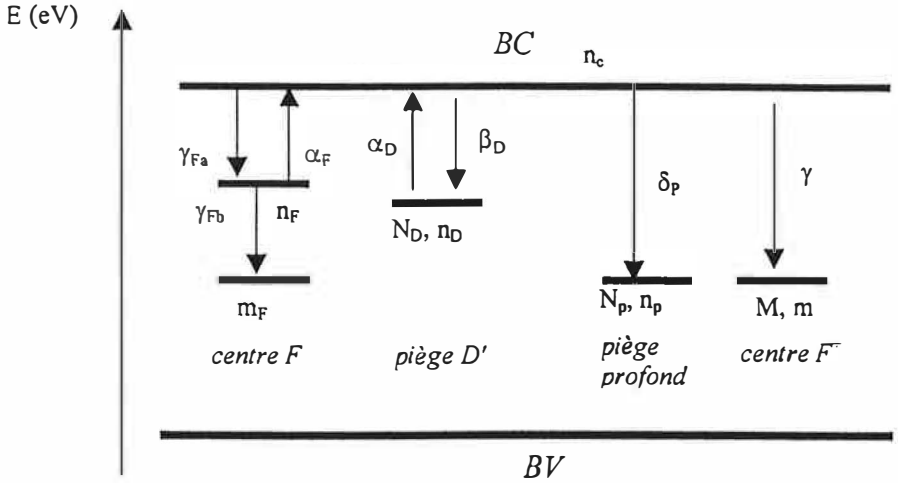

n_c : densité d'électrons dans la bande de conduction (cm^{-3}) (elektronkoncentráció a vezetési savban)

n_D : densité d'électrons dans les pièges D' (cm^{-3}) (elektronkoncentráció a D'-csapdákban)

N_D : densité de pièges D' (cm^{-3}) (a D'-csapdák koncentrációja)

α_D : probabilité de dépiégeage des pièges D' (s^{-1}) (a csapdából való kiszabadulás valószínűsége) $\alpha_D = \alpha_{D0} \exp(-E_D/kT)$

β_D : coefficient de repiégeage aux pièges D' (cm^3s^{-1}) (újrabefogási együttható a D'-csapdákban)

M : densité de centres F^+ (cm^{-3}) (az F^+ centrumok koncentrációja)

m : densité des trous dans les centres F^+ (cm^{-3}) (töltéskoncentráció az F^+ centrumokban)

γ : coefficient de recombinaison dans les centres F^+ (cm^3s^{-1}) (rekombinációs együttható az F^+ centrumokban)

m_F : densité des trous dans les centres F (cm^{-3}) ("lyuk"-koncentráció az F centrumokban)

n_F : densité d'électrons à l'état excité des centres F (cm^{-3}) (elektronkoncentráció az F centrumok gerjesztett állapotában)

γ_{Fa} : coefficient de recombinaison dans les centres F (cm^3s^{-1}) (rekombinációs együttható az F^+ centrumokban)

γ_{Fb} : coeff. de relaxation radiative dans les centres F (cm^3s^{-1}) (a sugárzásos átmenet együtthatója az F centrumokban)

α_F : probabilité de retour dans la bande de conduction (s^{-1}) (a vezetési sávba visszajutás valószínűsége) $\alpha_F = \alpha_{F0} \exp(-E_F/kT)$

n_P : densité d'électrons dans les pièges profonds (cm^{-3}) (elektronkoncentráció a mély csapdákban)

N_P : densité des pièges profonds (cm^{-3}) (a mély csapdák koncentrációja)

δ_P : coefficient de piégeage dans les pièges profonds (cm^3s^{-1}) (befogási együttható a a mély csapdákban)

Figure III.32 : Modèle "interactif" du pic D'

III.32. ábra: A D' TL csúcs sávelméleti modellje

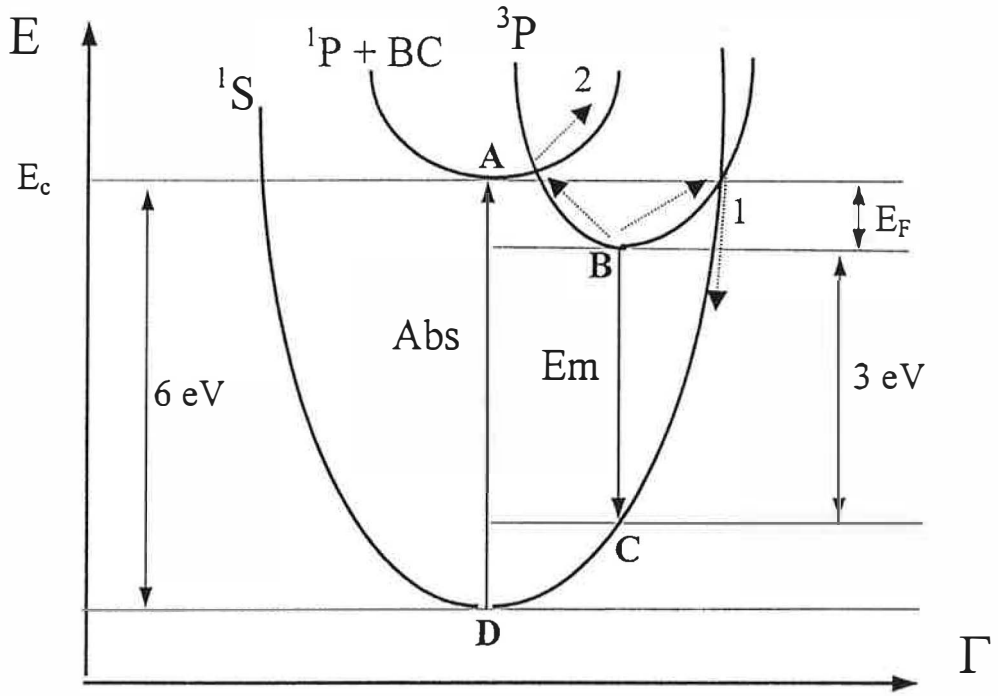

Figure III.33 : Courbe de configuration des centres F, (Abs : absorption, Em : émission)
Les flechès représentent les chemins de relaxation non radiative :
1- Mott-Seitz, 2- modèle interactif,

III.33. ábra: Az F centrum abszorpciójának (Abs), emissziójának (Em) és a sugárzásmentes átmenetek értelmezése a konfigurációs koordináta diagram segítségével
sugárzásmentes átmenetek: 1- Mott-Seitz modell, 2- az általunk javasolt mechanizmus

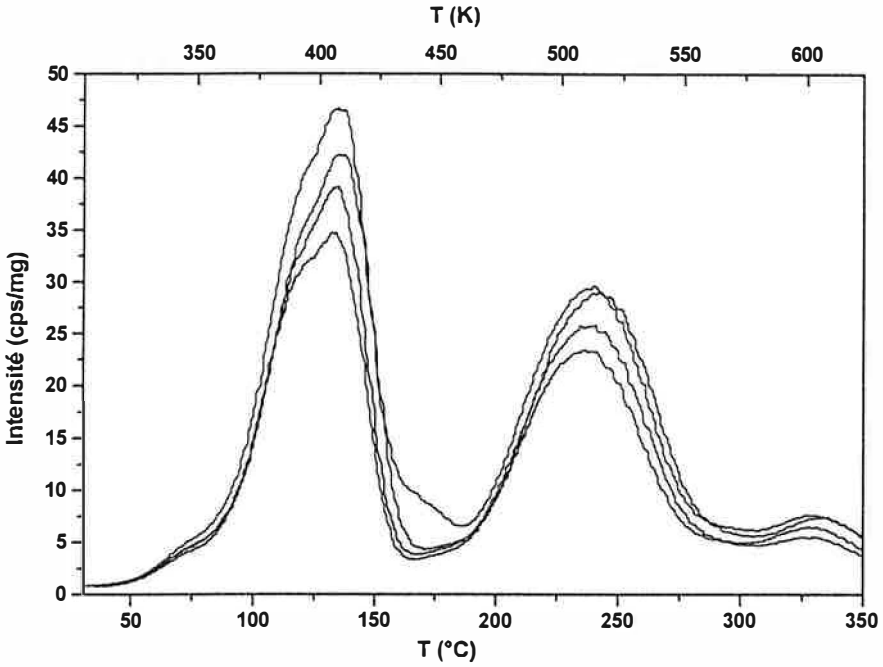

Figure IV.1 : Réponse de TL (par unité de masse) de quatre cristaux traités sous oxygène (échantillons de type 100ox) après irradiation X à 300 K (20 Gy)

IV.1. ábra: Reprodukálhatósági vizsgálat: oxigénben, azonos körülmények között kezelt kristályok TL görbéi (egységnyi tömegre) 20 Gy röntgenbesugárzás után (300 K-en)

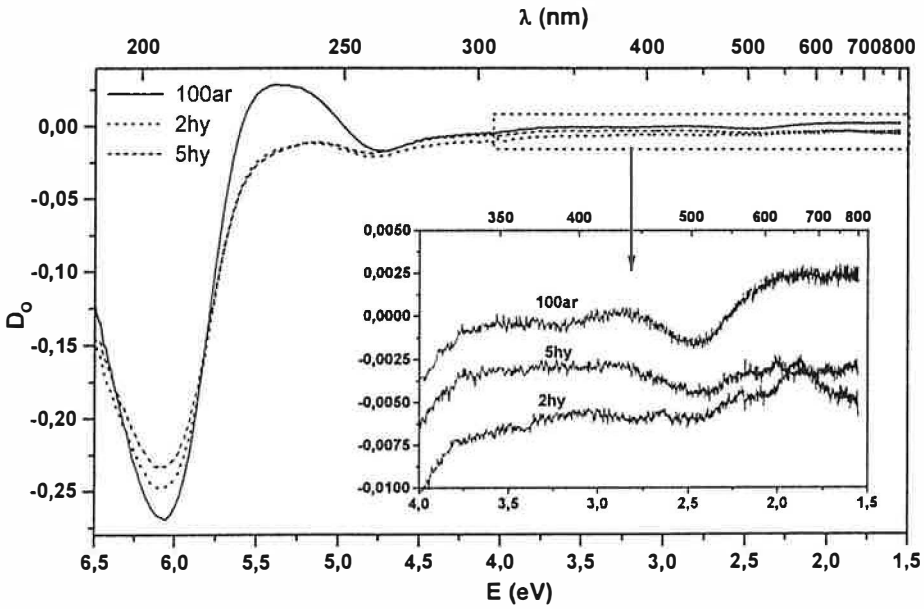

Figure IV.2 : Spectres d'absorption induite par les différents traitements réducteurs. (absorption induite = absorption d'un cristal traité - absorption du même cristal initial)

IV.2. ábra: A reduktív hőkezelések okozta változások a kristályok abszorpciójában (abszorpciós referencia: ugyanaz a kristály hőkezelés előtt)

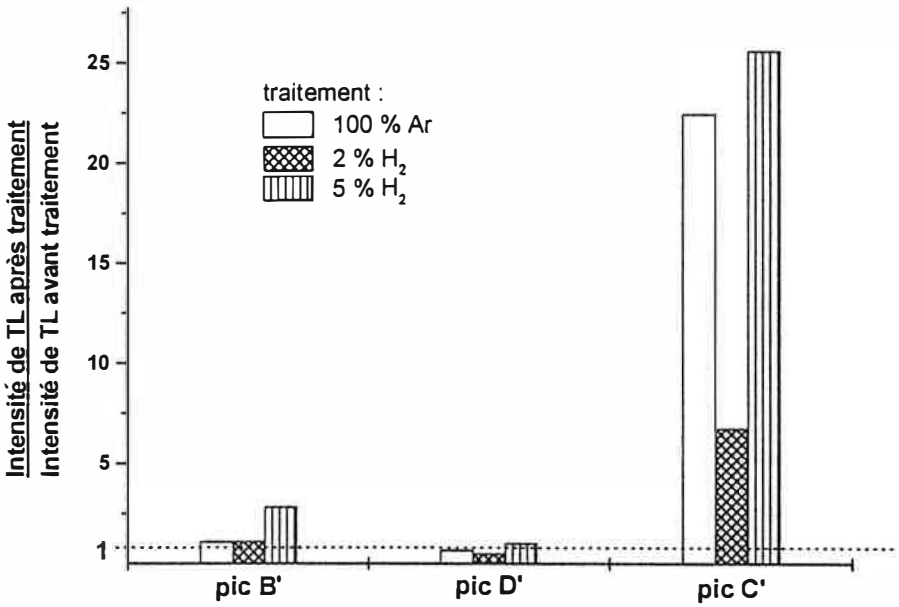

Figure IV.3 : Rapport des intensités des pics de TL avant et après les différents traitements réducteurs (TL enregistrée après irradiation X de 3 Gy à 77 K)

IV.3. ábra: A különböző TL csúcsok intenzitásának aránya a reduktív hőkezelések után és előtt (A TL-t 3 Gy 77 K-en adott röntgendózis után regisztráltuk.)

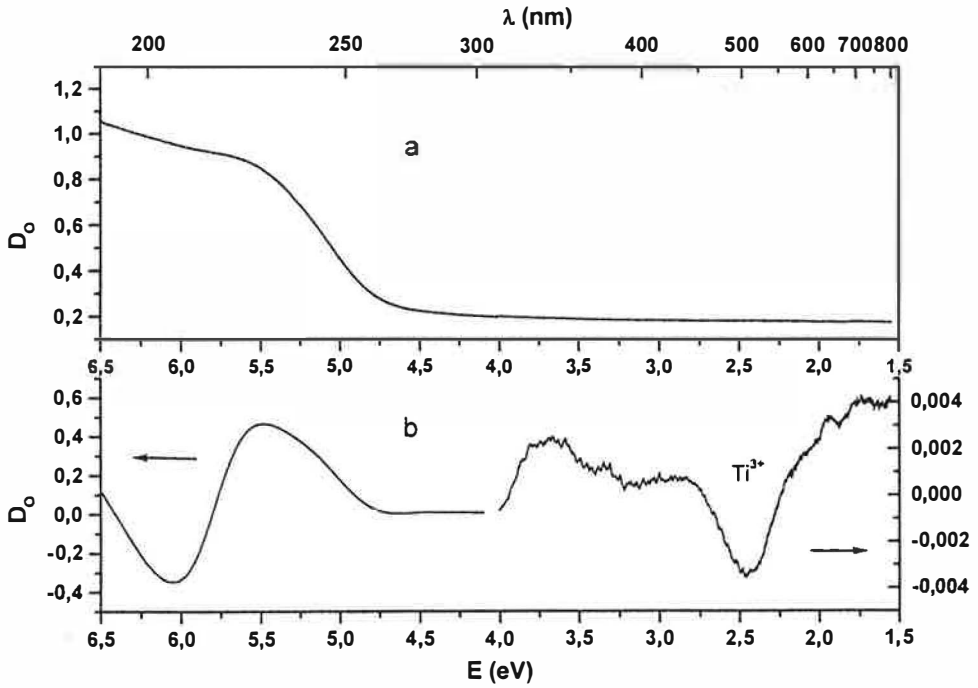

Figure IV.4 : Spectre d'absorption optique d'un cristal après un traitement oxydant, a : par rapport à l'absorption de l'air, b : par rapport à l'absorption du même cristal avant oxydation

IV.4. ábra: Az oxidáció okozta változások a kristályok abszorpciójában (abszorpciós referencia: levegő (a) vagy ugyanaz a kristály hőkezelés előtt (b))

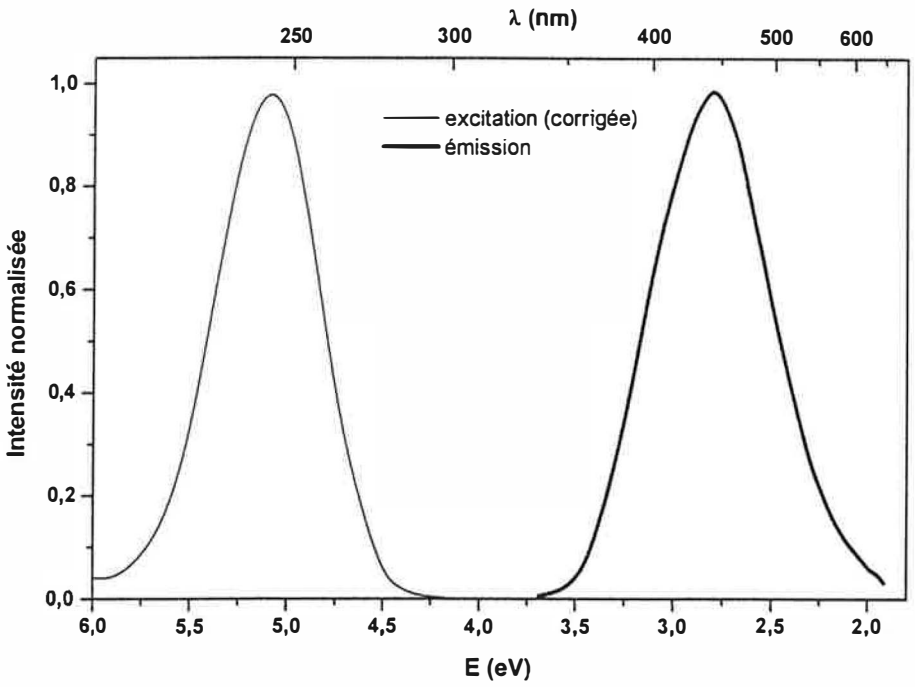

Figure IV.5 : Spectres d'excitation et d'émission attribués au Ti^{4+} dans un cristal "100ox"

IV.5. ábra: A Ti^{4+} ionok gerjesztési és emissziós spektruma egy oxidált kristályban

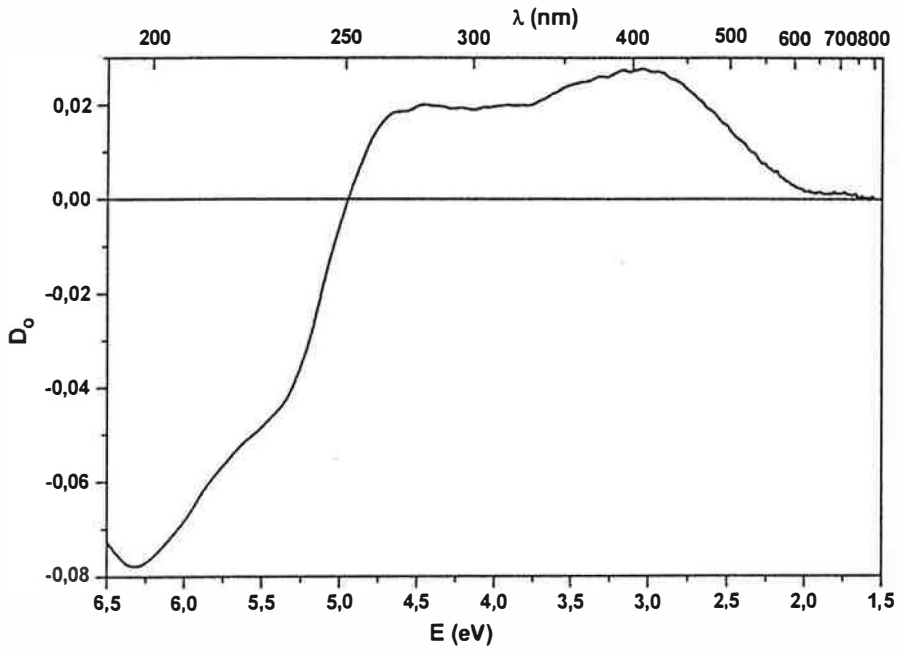

Figure IV.6 : Spectre d'absorption induite par rayons X (800 Gy) à 300 K dans un cristal "100ox" (absorption induite = absorption du cristal irradié - absorption du même cristal non-irradié)

IV.6. ábra: Röntgensugarak (800 Gy, 300 K-en) okozta változások egy oxidált kristály abszorpciójában (abszorpciós referencia: ugyanaz a kristály besugárzás előtt)

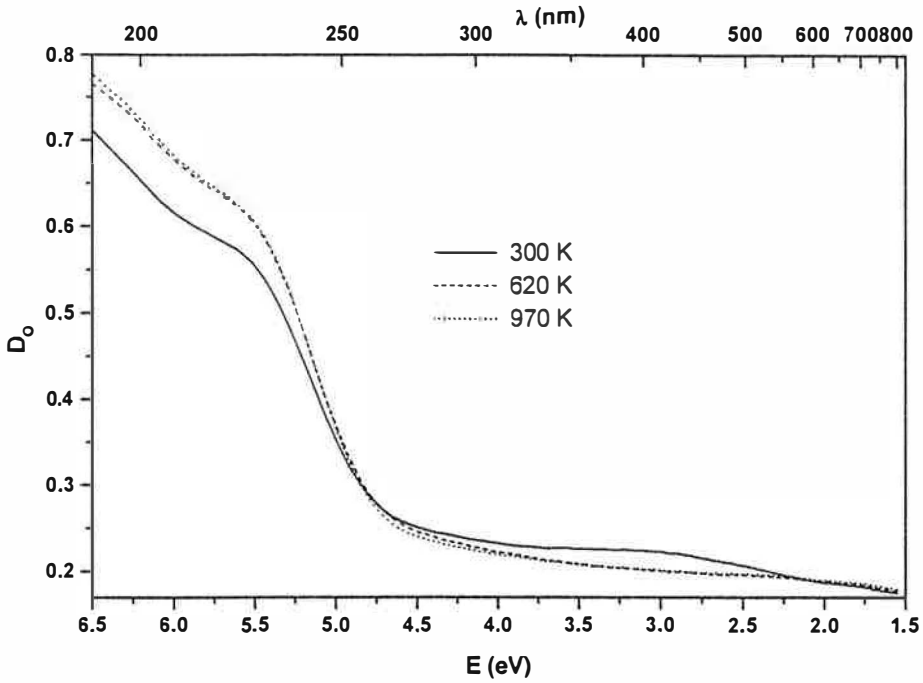

Figure IV.7 : Spectre d'absorption (référence : l'air) d'un cristal "100ox" irradié aux rayons X (800 Gy) à 300 K puis recuit à différentes températures (300, 620 et 970 K)

IV.7. ábra: Az abszorpciós spektrum változása hevítés hatására egy oxidált kristályban Az első spektrum 25 Gy röntgen besugárzás (300 K-en) után lett regisztrálva.

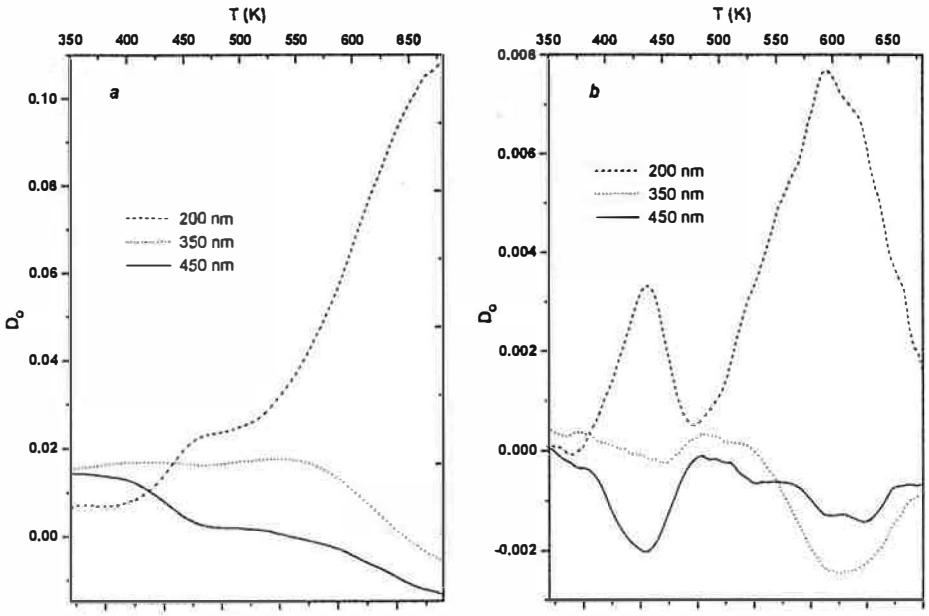

Figure IV.8 a : Evolution de l'absorption d'un cristal "100ox" irradié aux rayons X (800 Gy) à 300 K en fonction de la température, b : dérivée des "courbes a"

IV.8. ábra a: Az abszorpciós spektrum változása hevítés hatására egy oxidált kristályban 25 Gy röntgen besugárzás (300 K-en) után, b: az "a-görbe" deriváltja

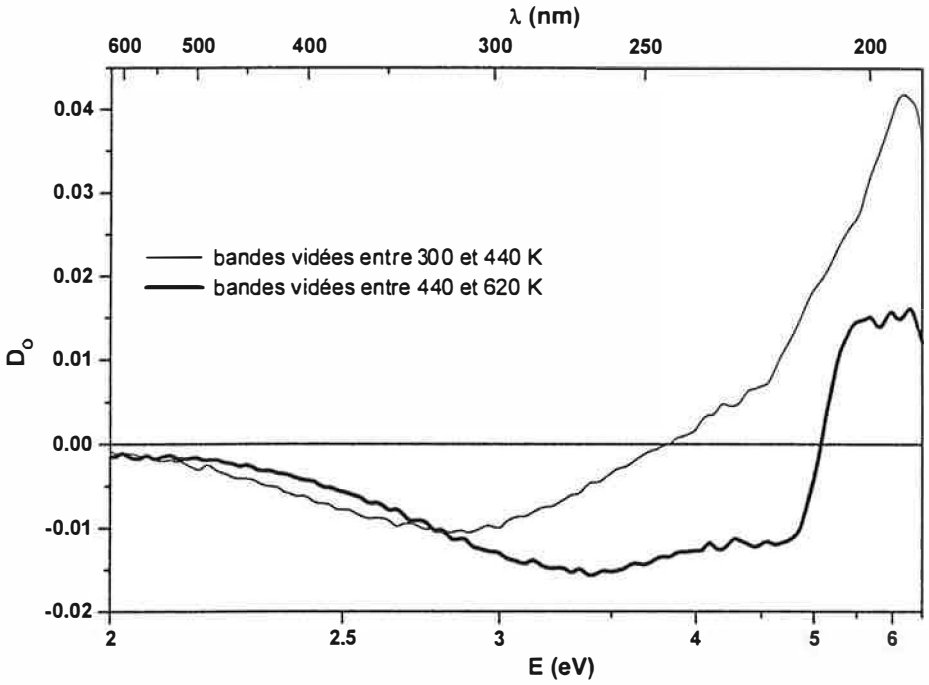

Figure IV.9 : Vidage thermique des bandes d'absorption induites par rayons X (800 Gy) à 300 K dans un cristal "100ox"

IV.9. ábra: Az optikai abszorpciós spektrum változása hevítés hatására egy oxidált kristályban 25 Gy röntgen besugárzás (300 K-en) után

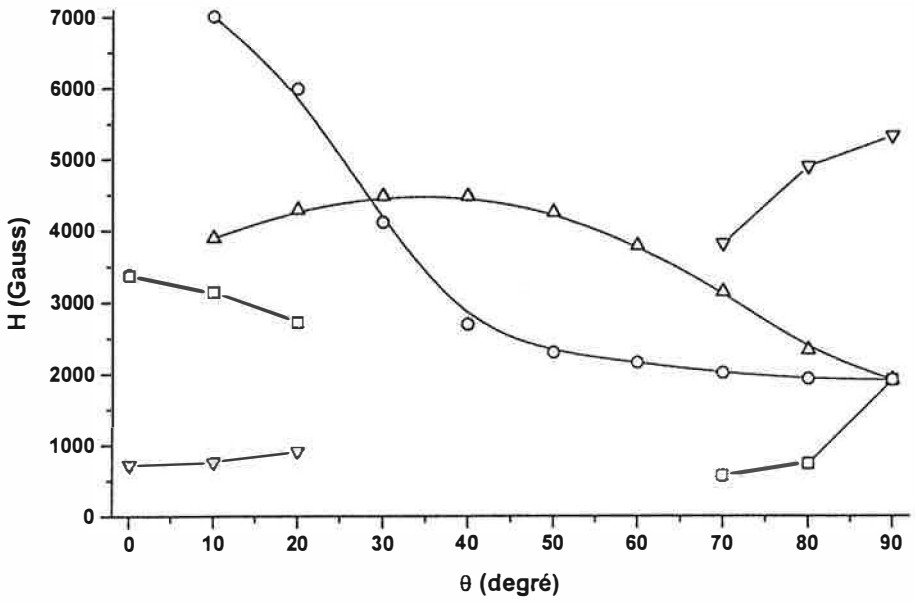

Figure IV.10 : Positions des raies RPE du Cr^{3+} en fonction de l'angle polaire θ (cristal : 5hy)

IV.10. ábra: A Cr^{3+} ESR vonalainak pozíciója a forgatási szög (θ) függvényében egy redukált kristályban

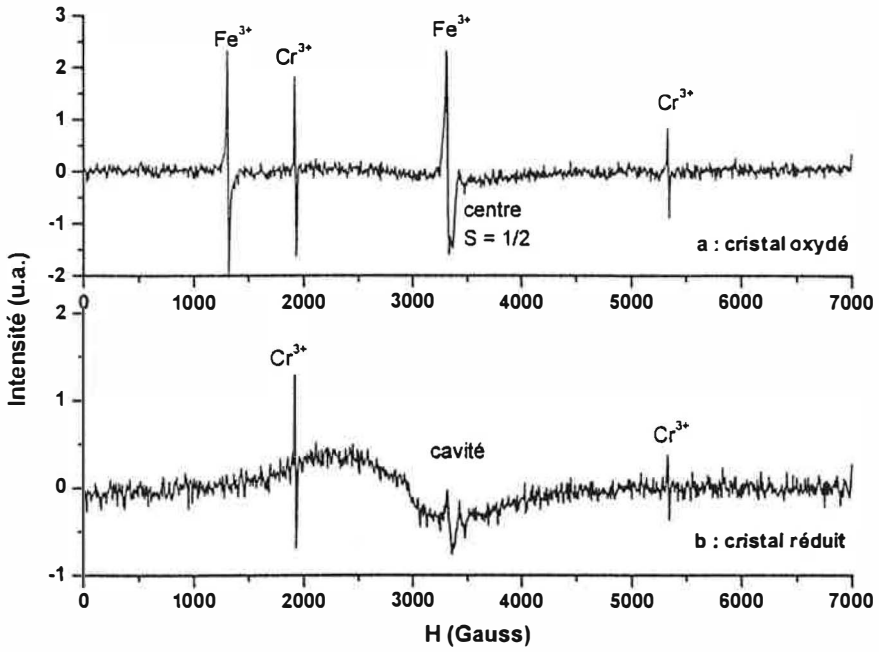

Figure IV.11 : Spectres RPE enregistrés à 20 °C et à θ = 90° (H⊥c)

IV.11. ábra: ESR spektrumok 20 °C-on és θ = 90° -nál (H⊥c) regisztrálva egy oxidált (a) és egy redukált (b) kristályban

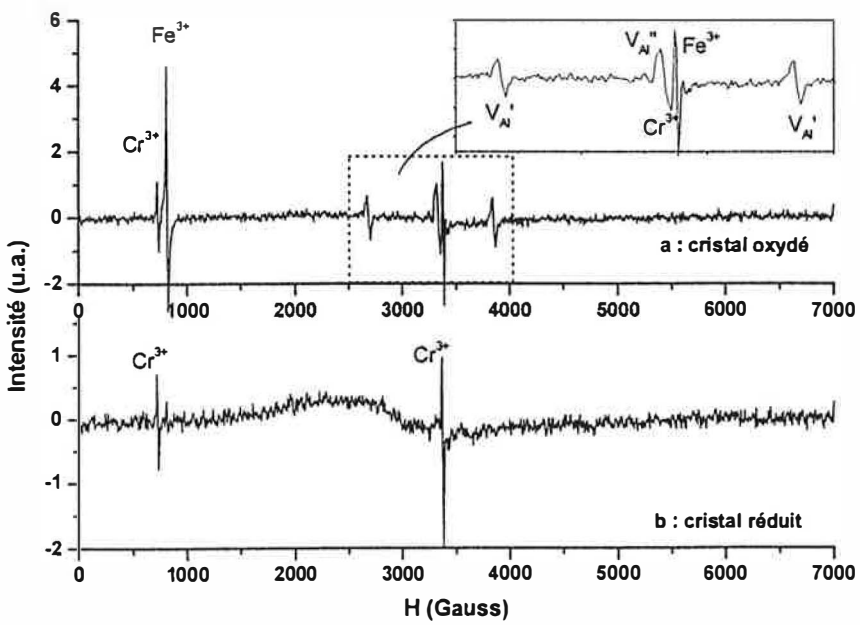

Figure IV.12 : Spectres RPE enregistrés à 20 °C et à θ = 0° (H//c)

IV.12. ábra: ESR spektrumok 20 °C-on és θ = 0° -nál (H//c) regisztrálva egy oxidált (a) és egy redukált (b) kristályban

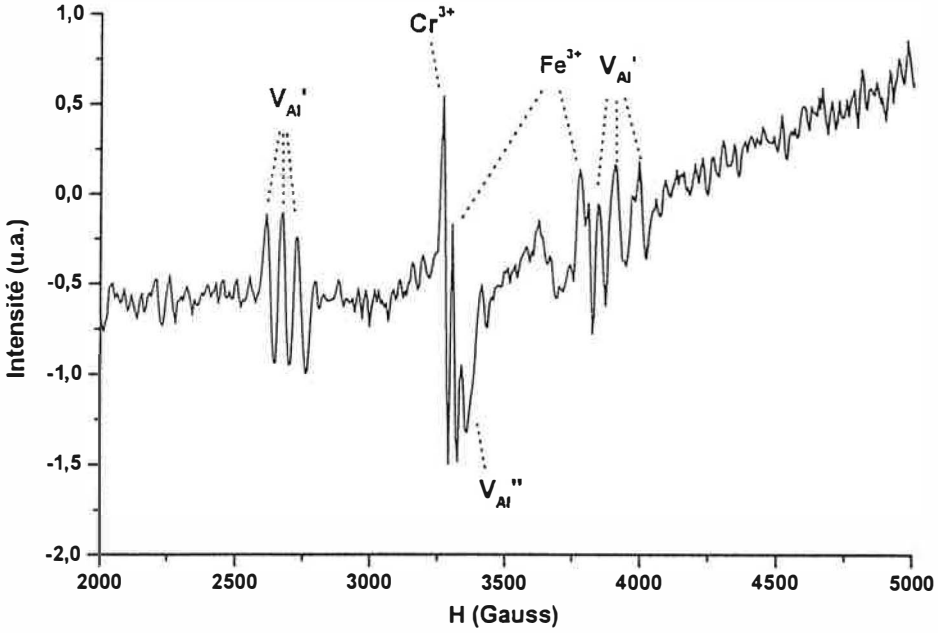

Figure IV.13 : Spectre RPE d'un cristal oxydé enregistré à -175 °C et à θ = 1°

IV.13. ábra: ESR spektrum -175 °C-on és θ = 1°-nál egy oxidált kristályban

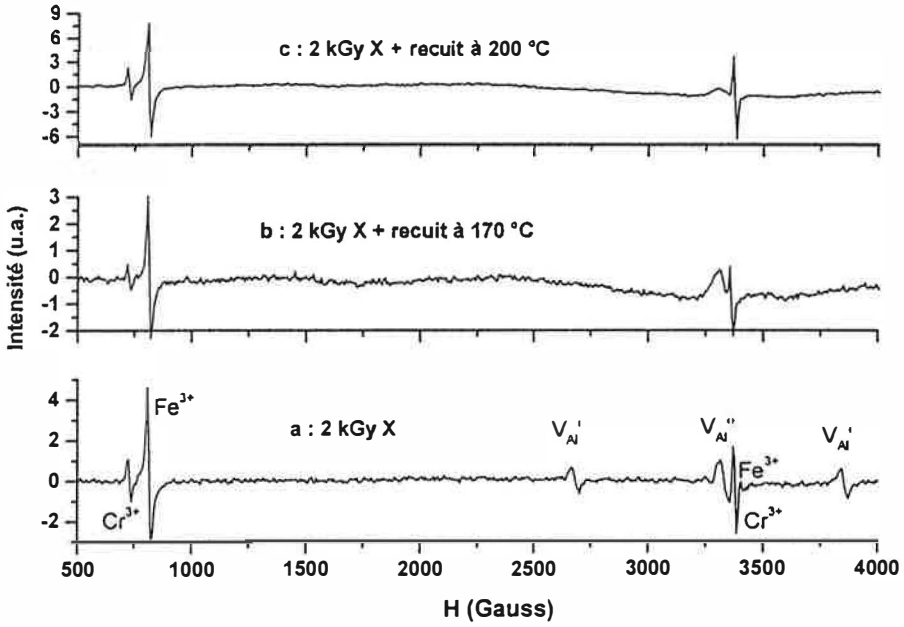

Figure IV.14 : Spectres RPE d'un cristal oxydé enregistré à 20 °C et à θ = 0°
a : après irradiation X, b : cristal irradié et recuit à 170 °C, c : cristal irradié et recuit à 200 °C

IV.14. ábra: ESR spektrumok 20 °C-on és θ = 0° -nál (H//c) regisztrálva
a: röntgen besugárzás után, majd 170 °C-ra (b) ill. 200 °C-ra (c) kifűtve

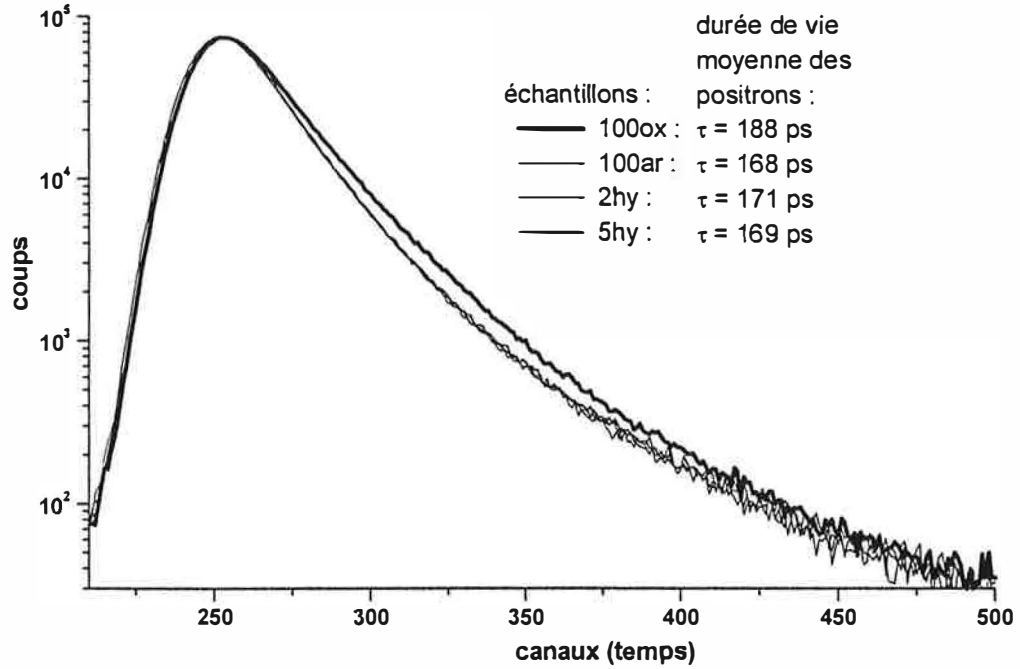

Figure IV.15 : Spectres de temps de vie des positrons dans des différents cristaux

IV.15. ábra: Pozitron élettartam spektrumok különböző mintákban
és a megfelelő átlagos élettartam adatok

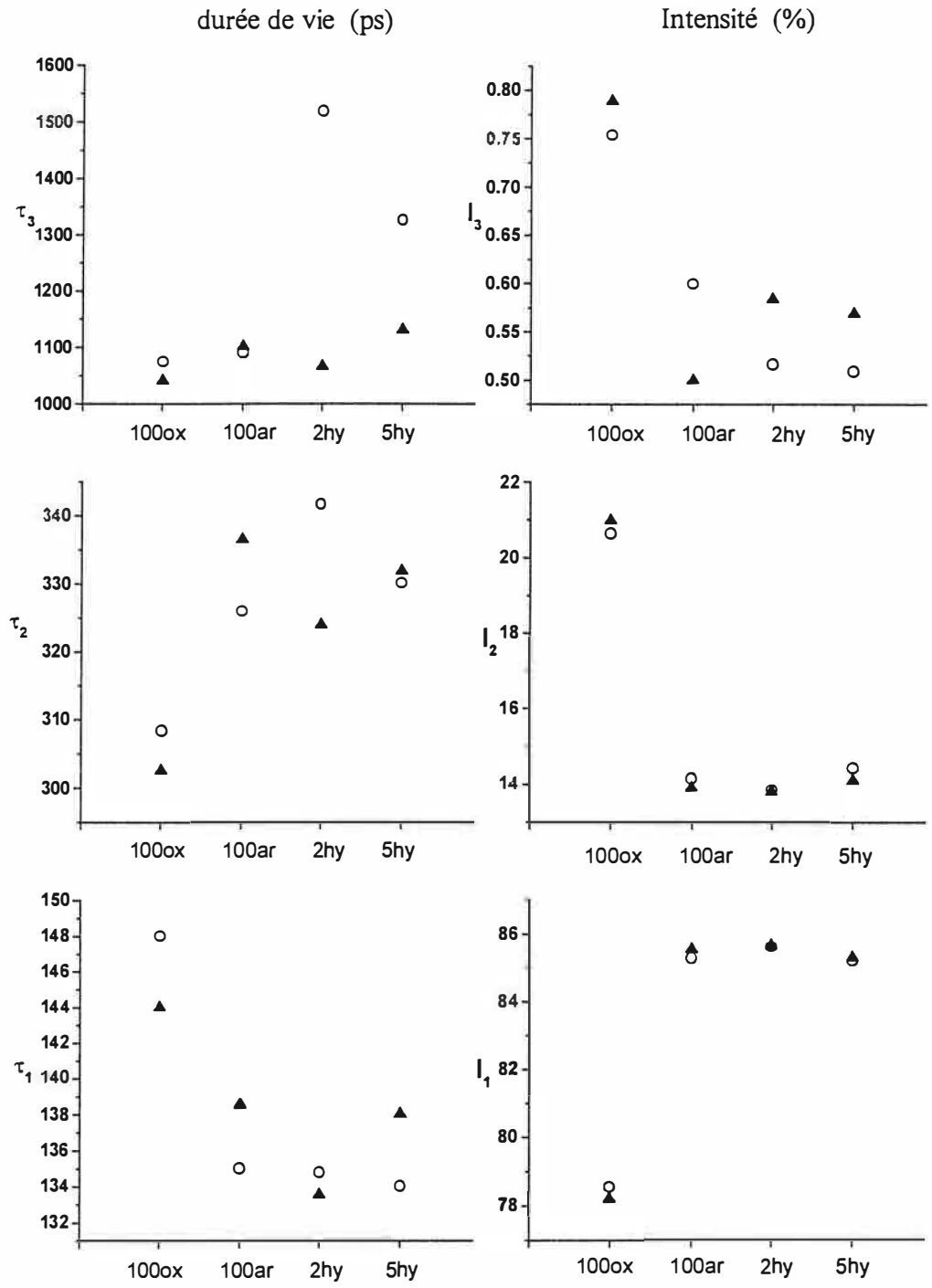

Figure IV.16 : Composantes de durée de vie des positrons et des intensités correspondantes dans des cristaux traités sous différentes conditions (avant (o) et après (▲) irradiation γ)

IV.16. ábra: Különböző pozitron élettartamok és a nekik megfelelő intenzitások a hőkezelt mintákban γ besugárzás előtt (o) és után (▲)

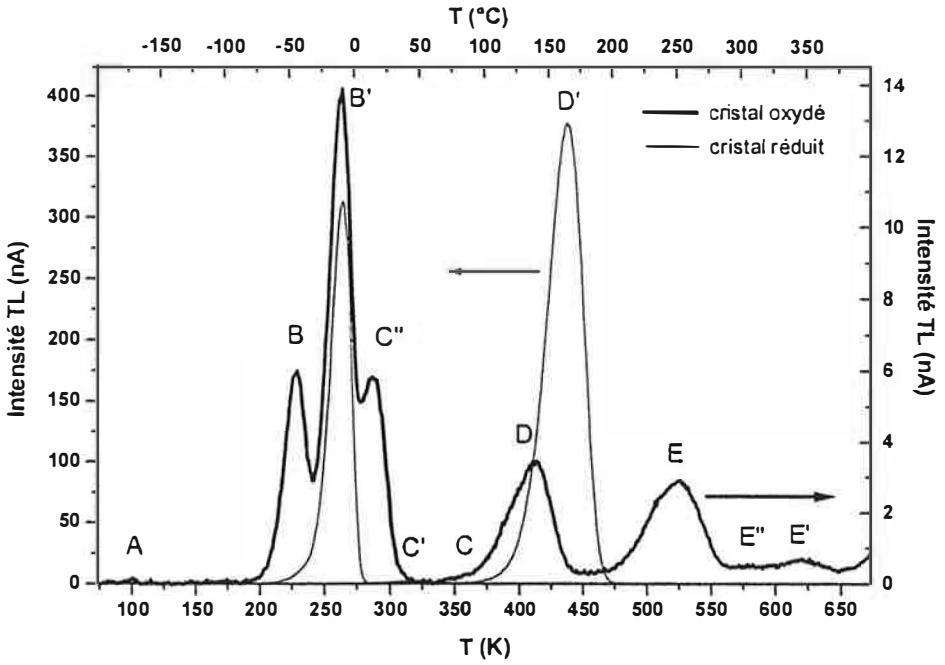

Figure IV.17 : Courbes de TL d'un cristal avant et après un traitement oxydant TL enregistrée après irradiation X à 77 K (3 Gy)

IV.17. ábra: Alumínium-oxid egykristály TL görbéje oxidáció előtt és után (A mérés előtt a kristályok 77 K-en 3 Gy röntgen dózist kaptak)

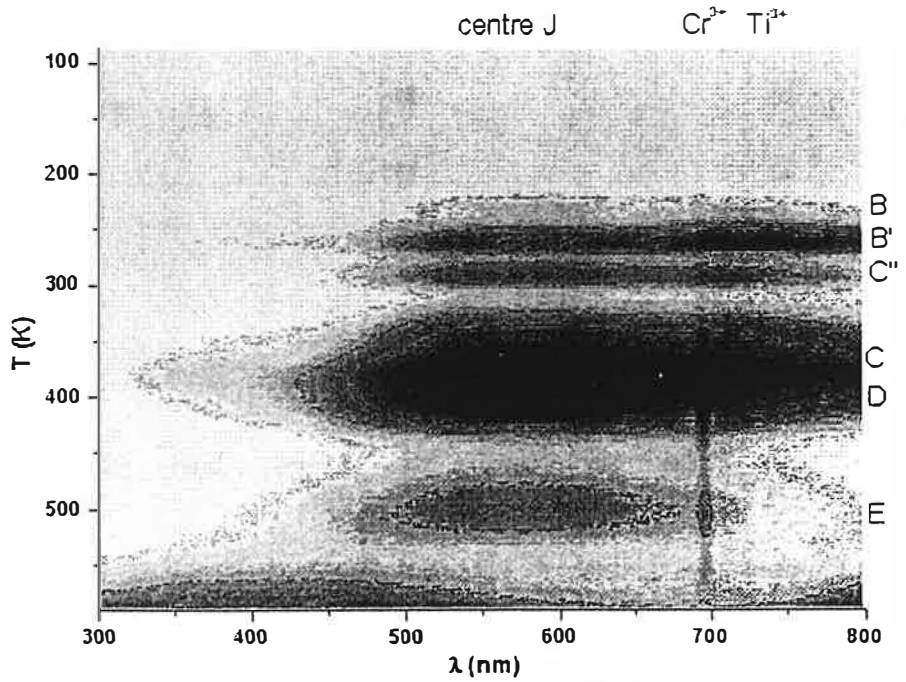

Figure IV.18 : Image de l'analyse spectrale de la TL d'un échantillon « 100ox » après irradiation X de 12 Gy à 77 K et de 1 kGy à 300 K

IV.18. ábra: Egy oxidált kristály 3D-TL vizsgálata 12 Gy (77 K-en) és 1 kGy (300 K-en) röntgen besugárzás után

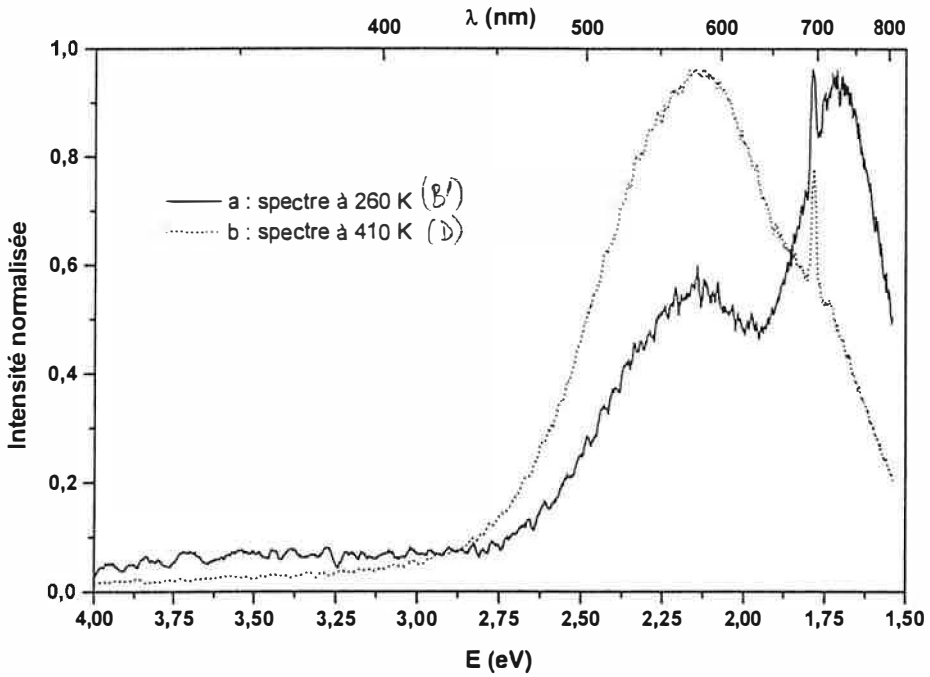

Figure IV.19 a : Spectre d'émission de la TL d'un échantillon "100ox" à 260 K (irradiation X de 12 Gy à 77 K)
b : Spectre d'émission de la TL d'un échantillon "100ox" à 410 K (irradiation X de 1000 Gy à 300 K)

IV.19. ábra: Egy oxidált kristály TL emissziója 260 (a) és 410 (b) K-en (12 ill. 100 Gy besugárzás után)

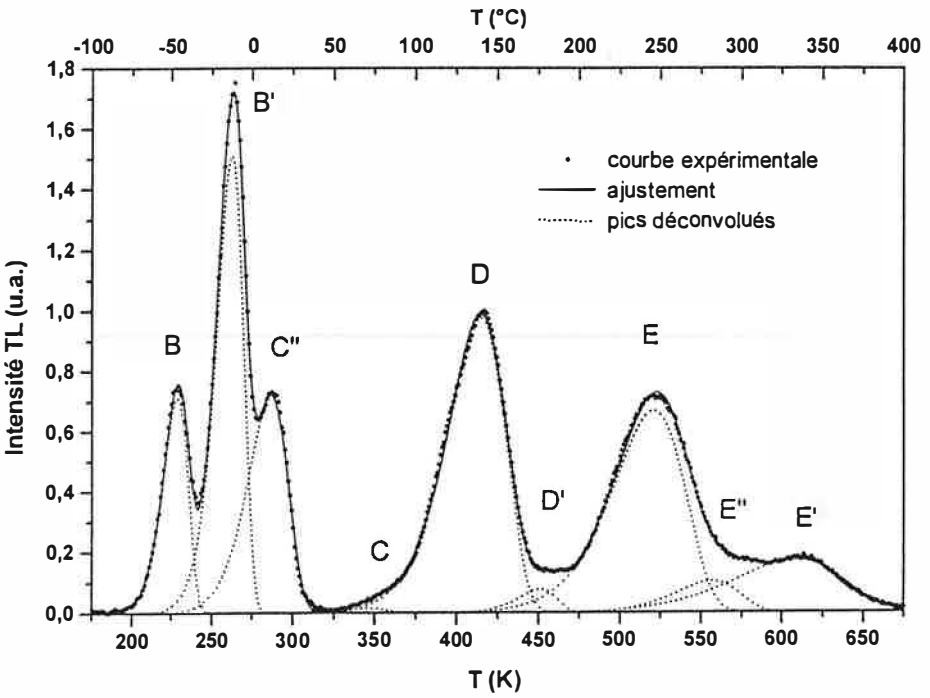

Figure IV.20 : Déconvolution des pics de TL d'un échantillon "100ox"

IV.20. ábra: Egy oxidált kristály TL görbéjének dekonvolúciója

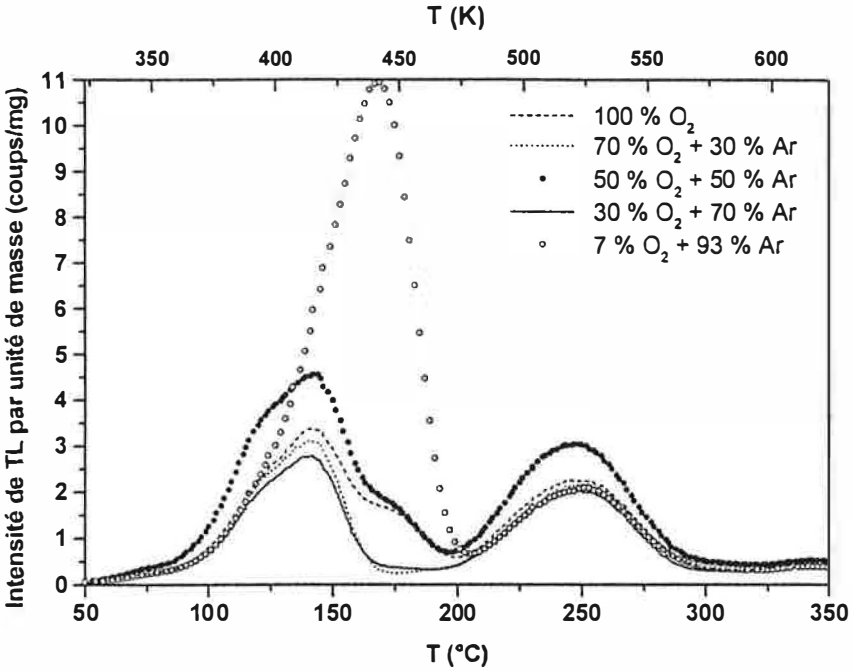

Figure IV.21 : Courbes de TL (après irradiation X de 20 Gy à 30 °C) des cristaux traités à différentes pressions partielles d'oxygène

IV.21. ábra: Különböző oxigén parciális nyomás alatt hőkezelt kristályok TL görbéi 20 Gy (30 °C-on) röntgen besugárzás után

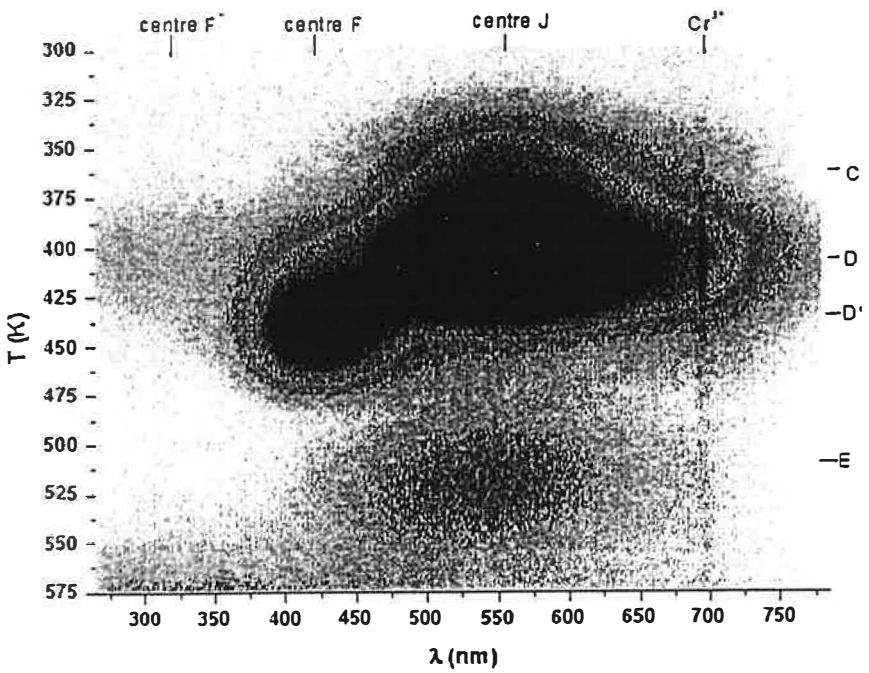

Figure IV.22 : Image de l'analyse spectrale de la TL d'un échantillon « 7ox » après irradiation X à 300 K (1 kGy)

IV.22. ábra: Egy "7ox" kristály 3D-TL vizsgálata 1 kGy (300 K-en) röntgen besugárzás után

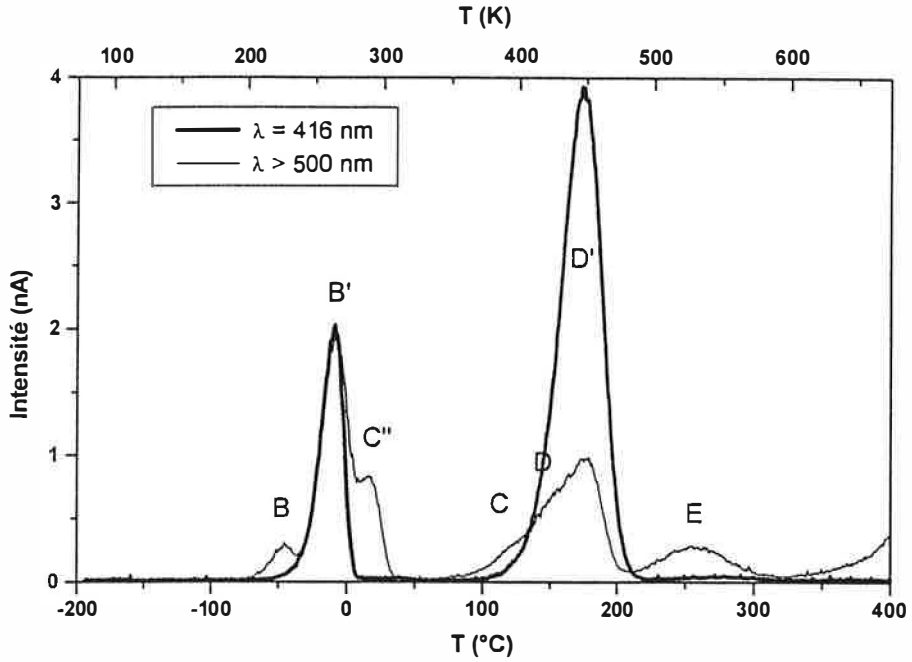

Figure IV.23 : Courbes de TL d'un cristal "7ox" enregistrées à différentes longueurs d'onde après irradiation X à -196 °C (9 Gy)

IV.23. ábra: Egy "7ox" kristály TL görbéje különböző hullámhosszakon 9Gy (-196 °C-on) röntgen besugárzás után

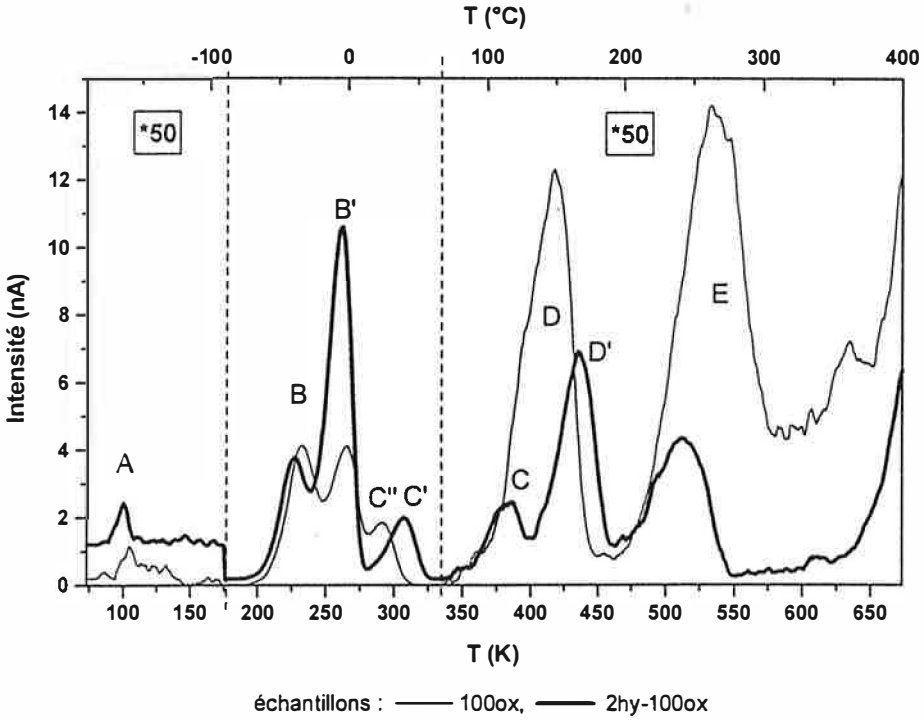

Figure IV. 24 : Courbe de TL d'un cristal oxydé avant (100ox) et après (2hy-100ox) un recuit réducteur (TL enregistrée après irradiation X de 12 Gy à 77 K)

IV.24.ábra: Egy oxidált kristály TL görbéje reduktív kezelés előtt (100ox) és után (2hy100ox) (A mérés előtt a kristályok 77 K-en 3 Gy röntgen dózist kaptak)

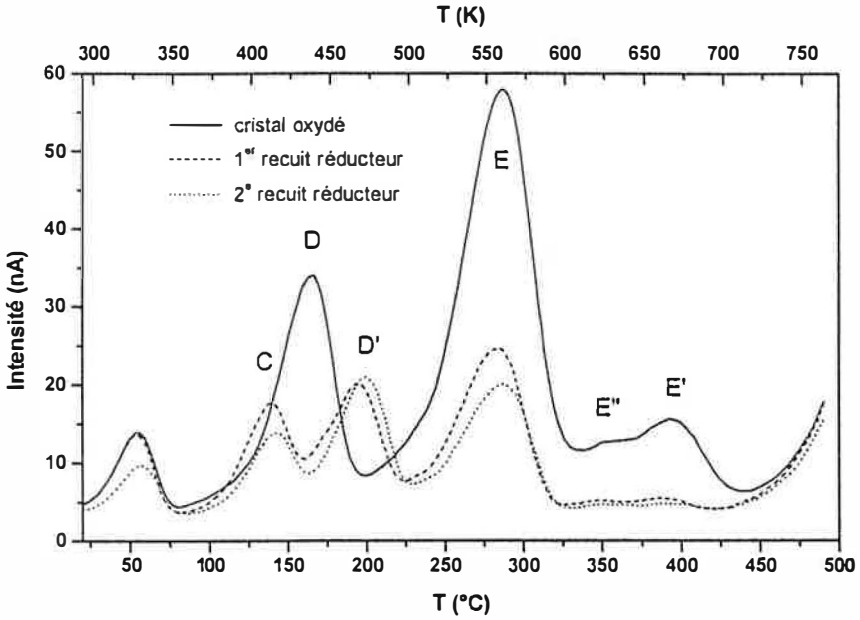

Figure IV.25 : Courbes de TL d'un cristal oxydé après un ou deux recuits réducteurs (TL enregistrée après irradiation X de 18 Gy à 30 °C)

IV.25.ábra: Egy oxidált kristály TL görbéje egy ill. két reduktív kezelés után (A mérés előtt a kristályok 30 °C -on 18 Gy röntgen dózist kaptak)

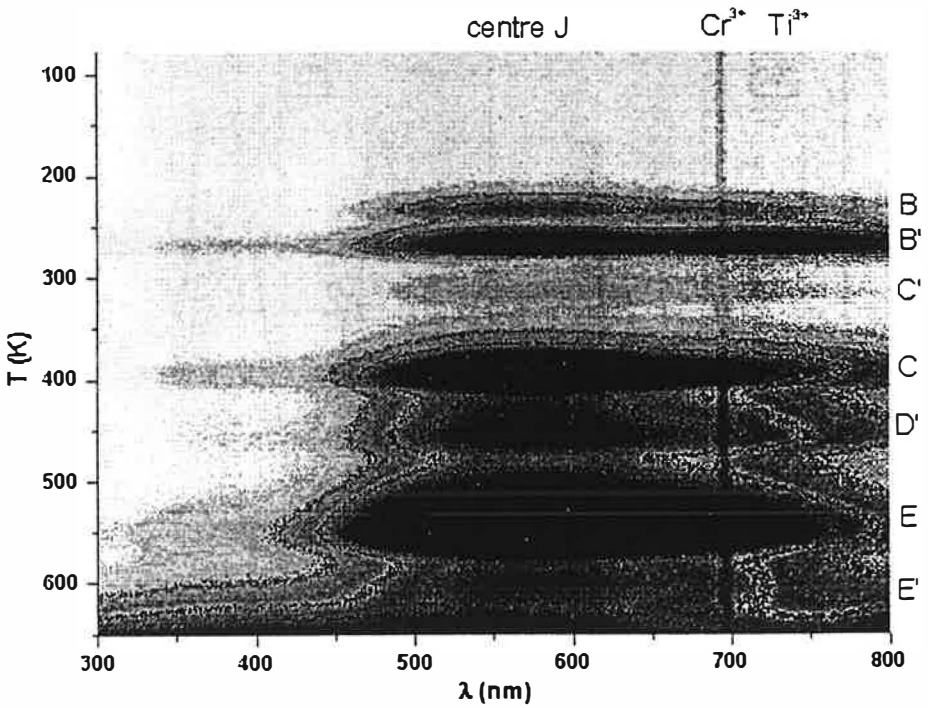

Figure IV.26 : Image de l'analyse spectrale de la TL d'un échantillon « 5hy-100ox » après irradiation X de 12 Gy à 80 K et de 1 kGy à 300 K

IV.26. ábra: Egy « 5hy-100ox » kristály 3D-TL vizsgálata 12 Gy (77 K-en) és 1 kGy (300 K-en) röntgen besugárzás után

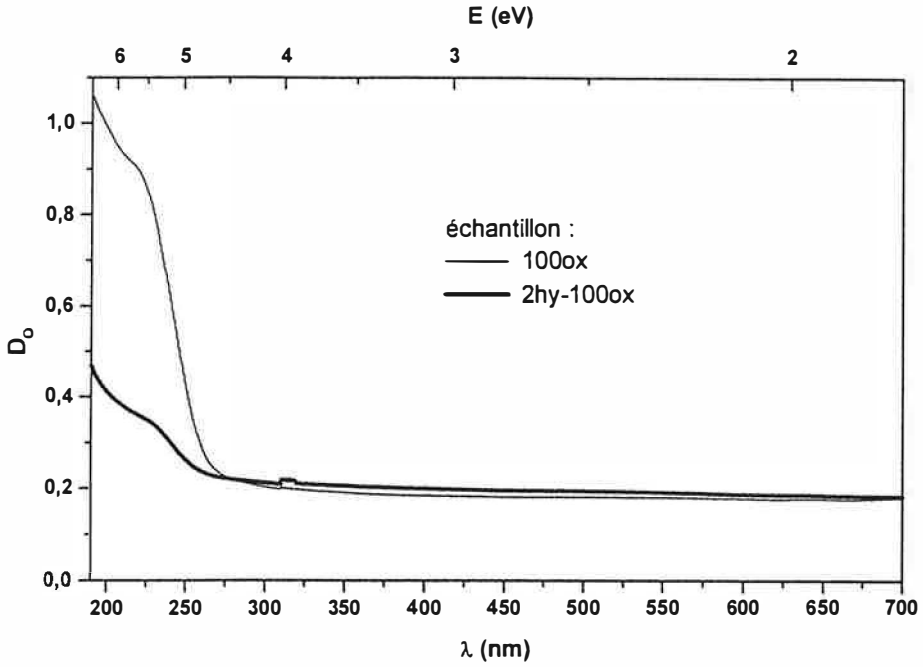

Figure IV.27 : Courbes d'absorption optique d'un cristal oxydé avant et après un recuit réducteur

IV.27. ábra: Egy oxidált kristály abszorpciós spektruma redukció előtt (100ox) és után (2hy-100ox)

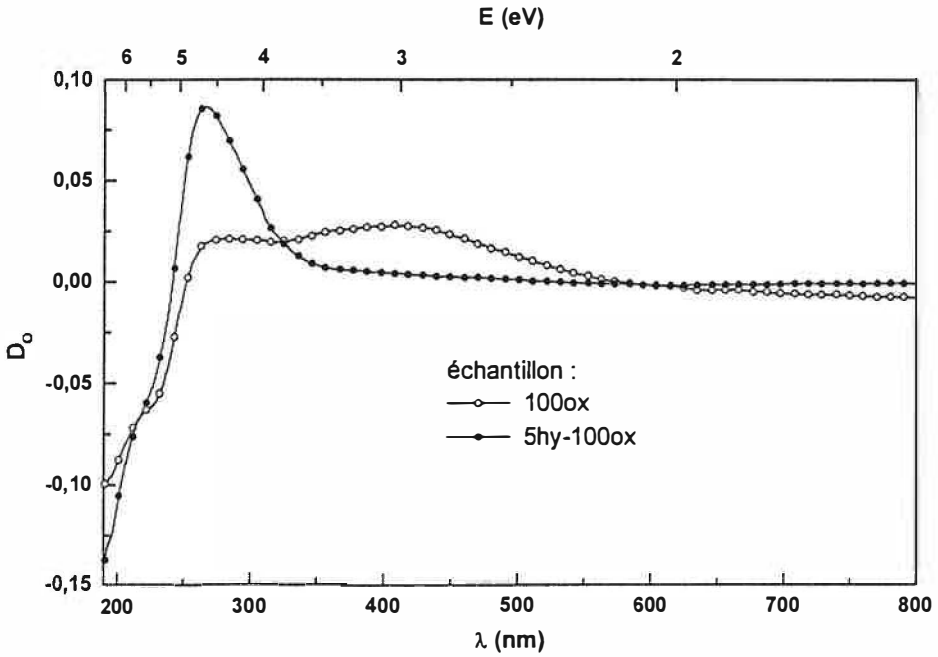

Figure IV.28 : Spectres d'absorption induite par irradiation X à 25 °C (800 Gy)
(Absorption induite = absorption du cristal irradié - absorption du cristal non irradié)

IV.28. ábra: Röntgensugarak (800 Gy, 25 °C -on) okozta változások különböző kristályok abszorpciós spektrumában (abszorpciós referencia: ugyanaz a kristály besugárzás előtt)

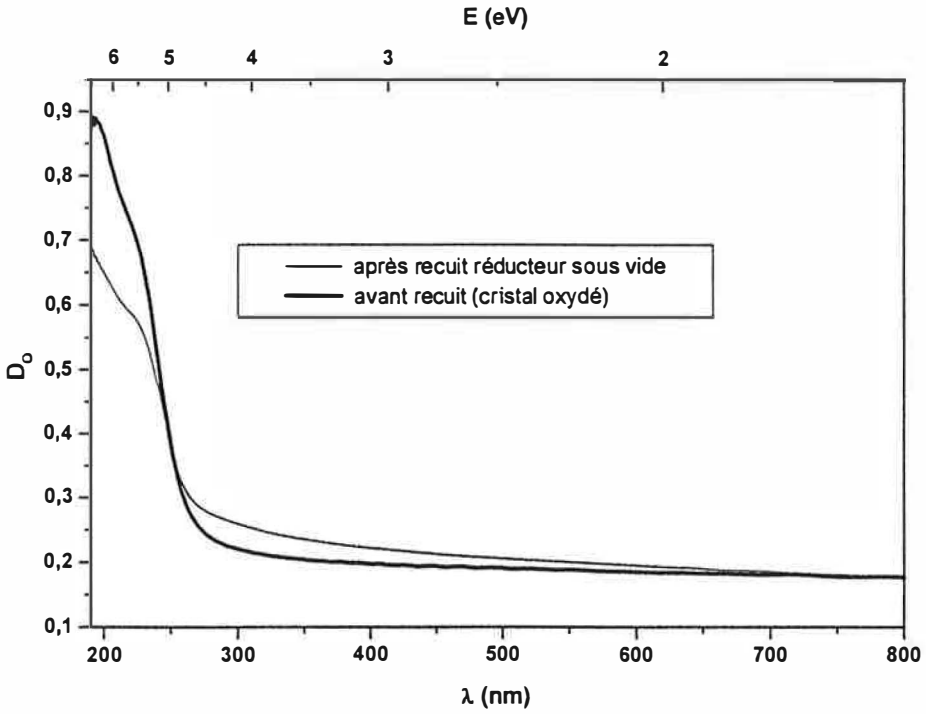

Figure IV.29 : Spectres d'absorption optique d'un cristal oxydé
avant et après un recuit réducteur sous vide

IV.29. ábra: Egy oxidált kristály abszorpciós spektruma redukció (vákuumban) előtt és után

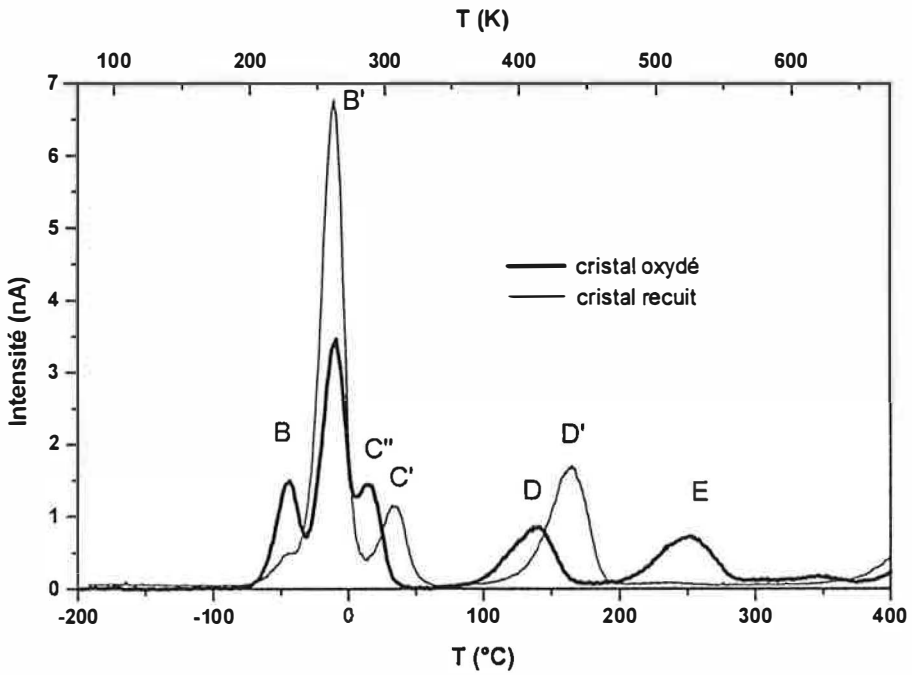

Figure IV.30 : Courbes de TL d'un cristal oxydé avant et après un recuit réducteur sous vide
(TL enregistrée après irradiation X de 3Gy à -195 °C)

IV.30.ábra: Egy oxidált kristály TL görbéje reduktiv kezelés (vàkuumban) előtt és után
(A mérés előtt a kristályok -195 °C -on 3 Gy röntgen dózist kaptak)

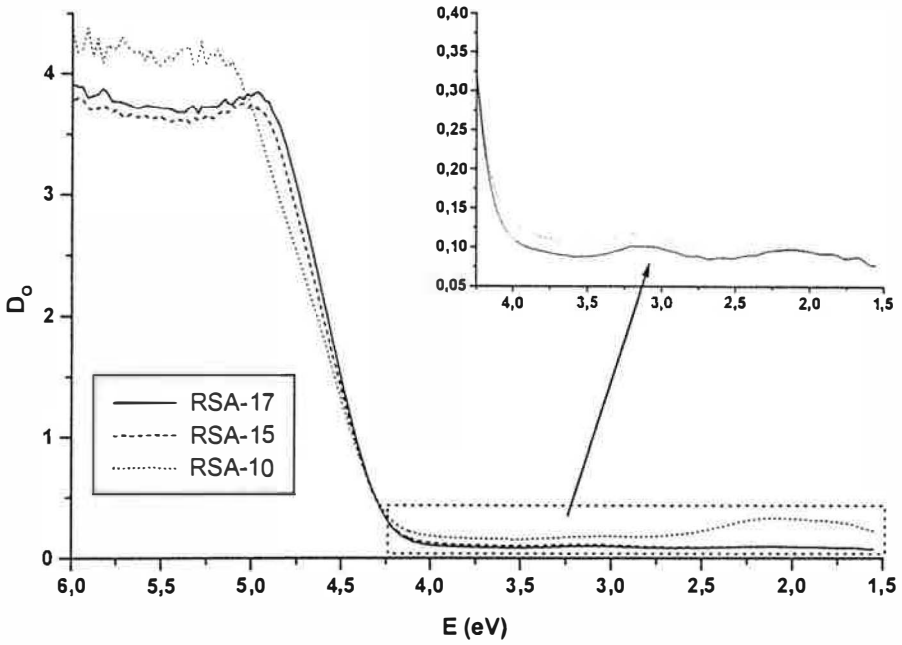

Figure V.1 : Courbes d'absorption optique des cristaux RSA

V.1. ábra: Az RSA kristályok abszorpciós spektruma

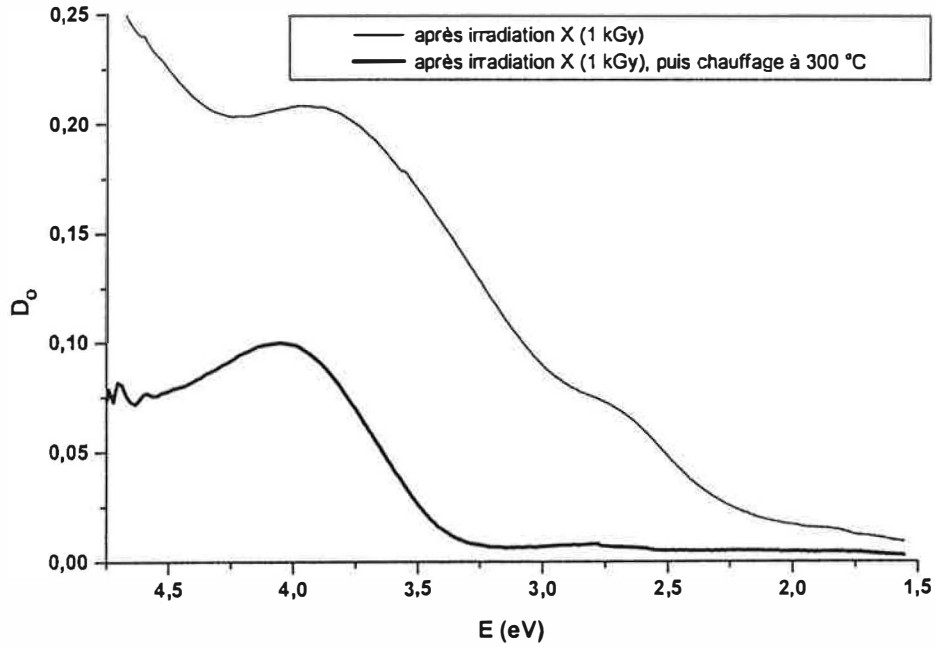

Figure V.2 : Evolution de l'absorption du cristal RSA-17 après irradiation X puis chauffage à 300 °C

V.2. ábra: Röntgensugárzás majd hevítés (300 °C-ig) okozta változások az RSA-17 kristály abszorpciós spektrumában (abszorpciós referencia: ugyanaz a kristály besugárzás előtt)

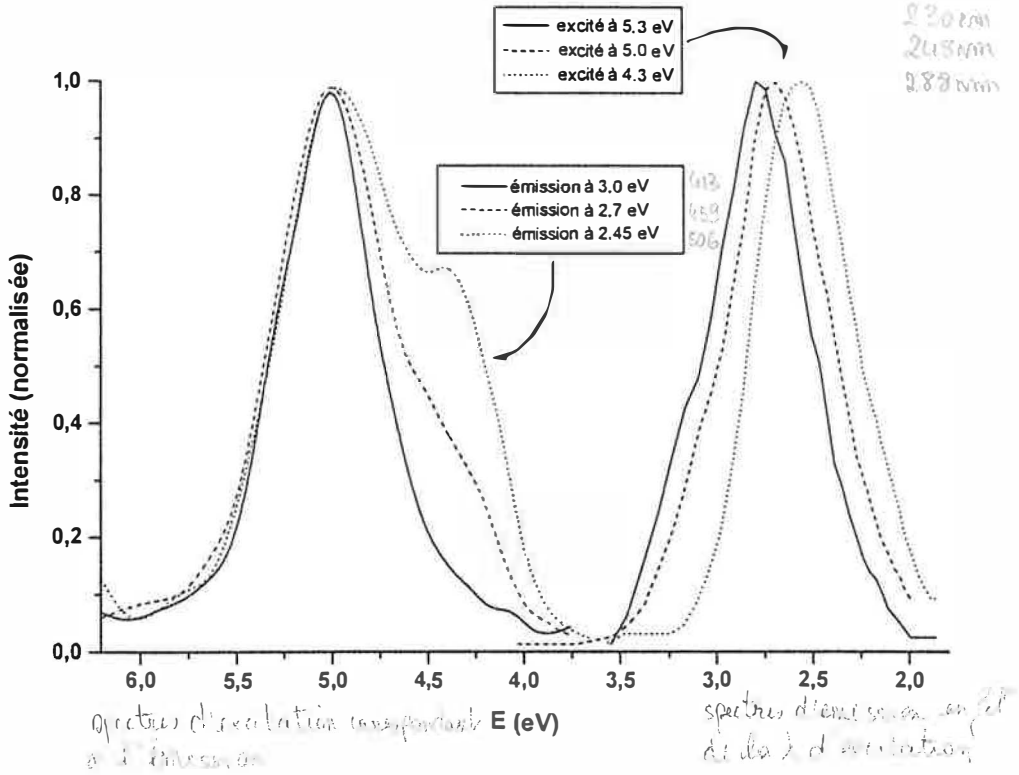

Figure V.3 : Spectres d'excitation et d'émission attribués au divers types de Ti^{4+} dans un cristal RSA-17

V.3. ábra: Különböző Ti^{4+} specieszek gerjesztési és emissziós spektruma az RSA-17 mintában

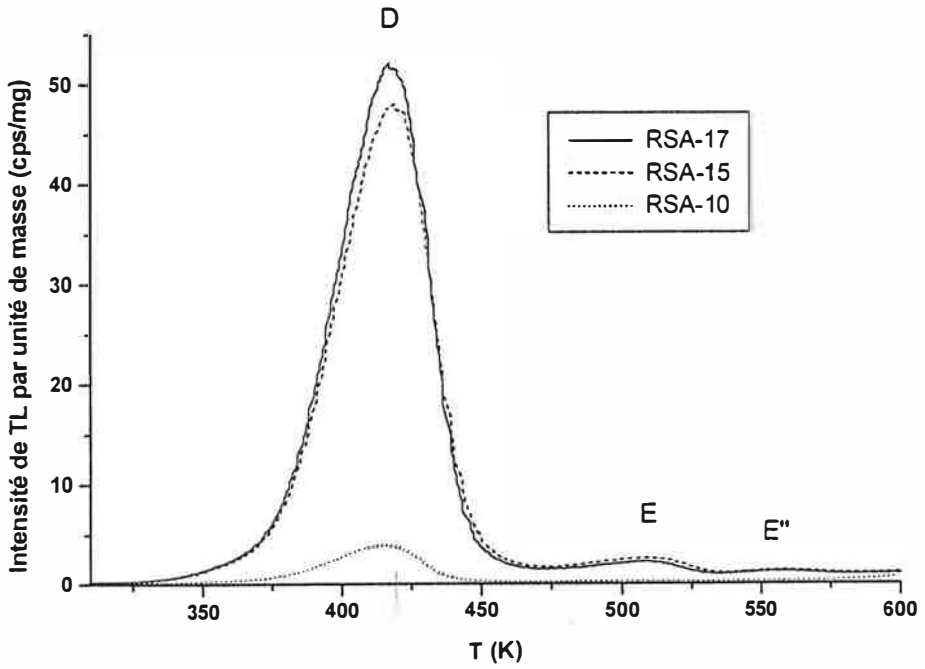

Figure V.4 : Courbes de TL des cristaux RSA après irradiation X à 300 K (20 Gy)

V.4. ábra: Az RSA kristályok TL görbéi 20 Gy röntgenbesugárzás után (300 K-en)

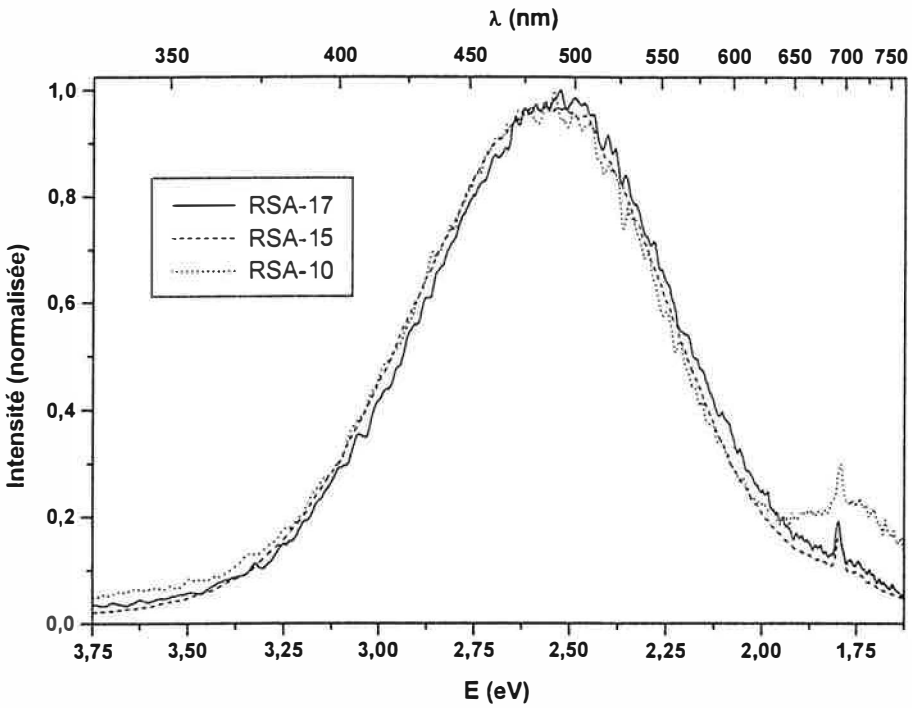

Figure V.5 : Spectres d'émission du pic D dans les cristaux RSA
(TL enregistrée après irradiation X de 1 kGy à 300 K)

V.5. ábra: A D jelu TL csùcs emissziós spektruma az RSA kristályokban
(1 kGy röntgenbesugárzás után (300 K-en))

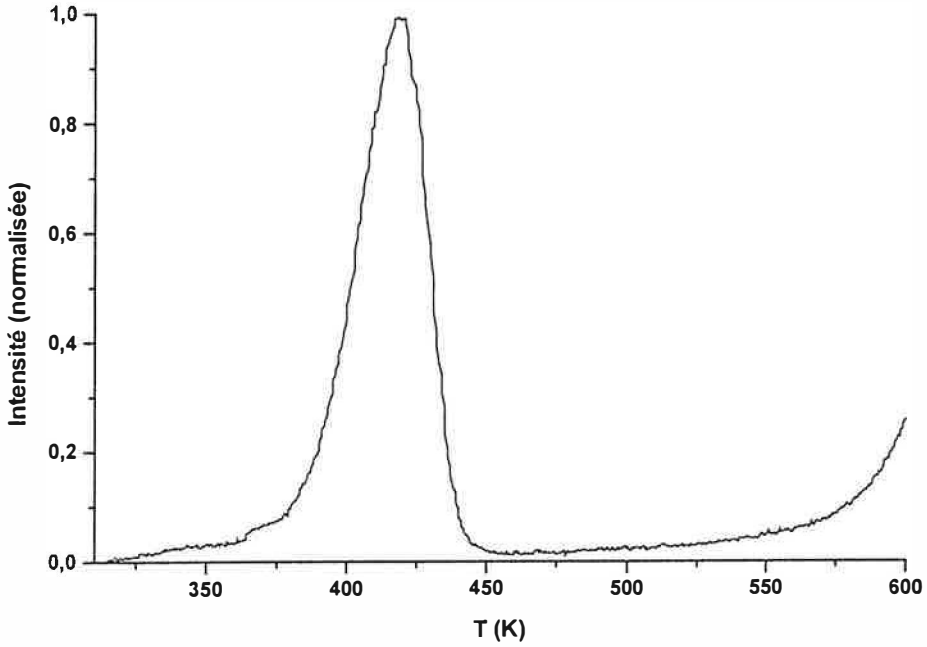

Figure V.6 : Courbe de TL de l'échantillon BDX-1 après irradiation X à 300 K (20 Gy)

V.6. ábra: A BDX-1 minta TL görbéje 20 Gy röntgenbesugárzás után (300 K-en)

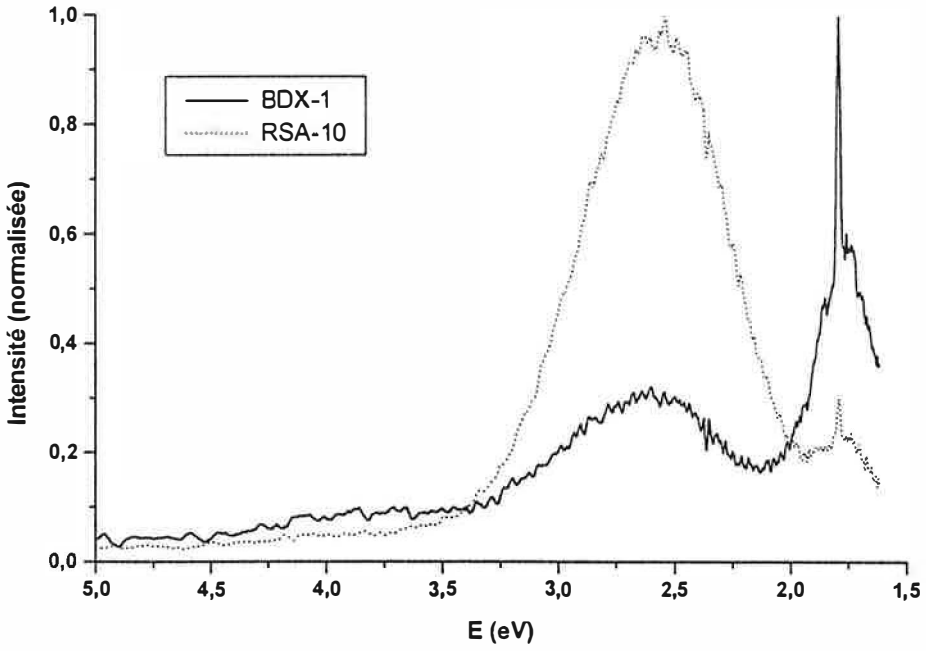

Figure V.7 : Spectres d'émission du pic D dans un cristal RSA et dans la poudre BDX-1 (TL enregistrée après irradiation X de 1 kGy à 300 K)

V.7. ábra: A D jelu TL csùcs emissziós spektruma egy RSA kristályban és a BDX-1 mintában (1 kGy röntgenbesugárzás után (300 K-en))

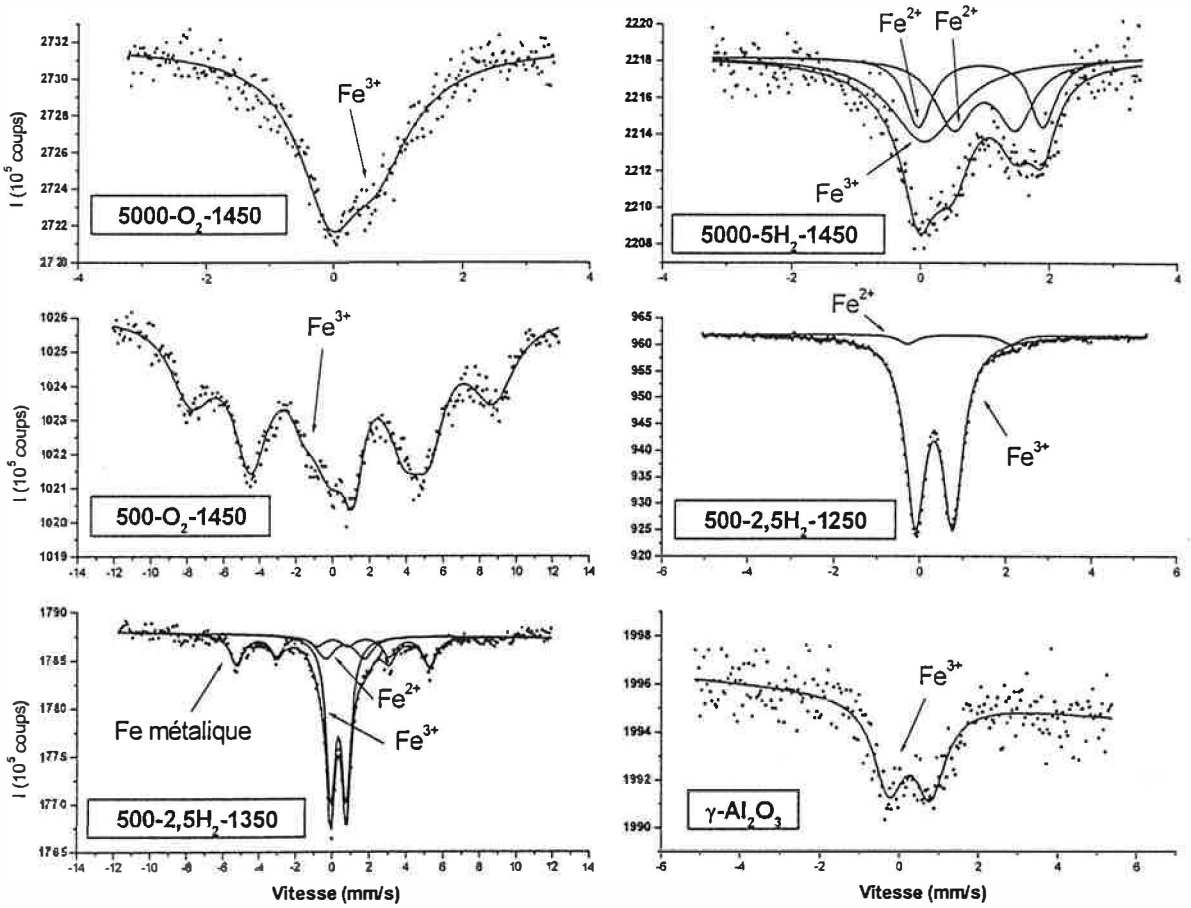

Figure V.8 : Spectres de Mössbauer des poudres d'alumine dopées au fer

V.8. ábra: Vassal szennyezett alumínium-oxid porok Mössbauer spektrumai

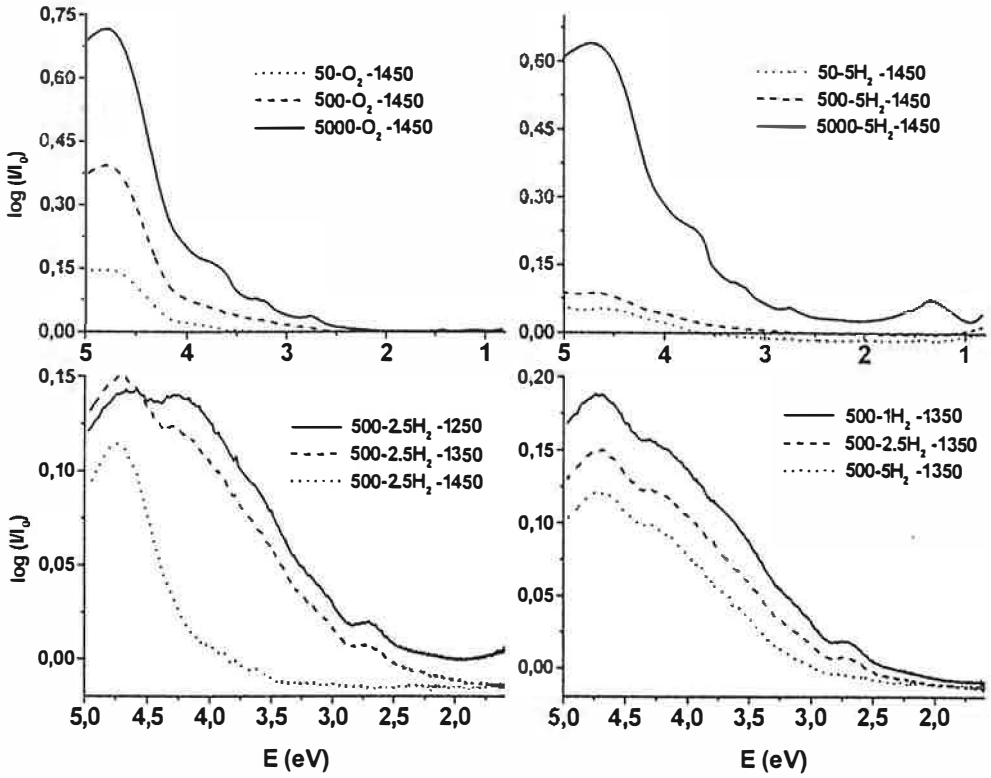

Figure V.9 : Spectres de réflexion diffuse des poudres d'alumine dopées au fer

V.9. ábra: Vassal szennyezett alumínium-oxid porok diffúz reflexiós spektrumai

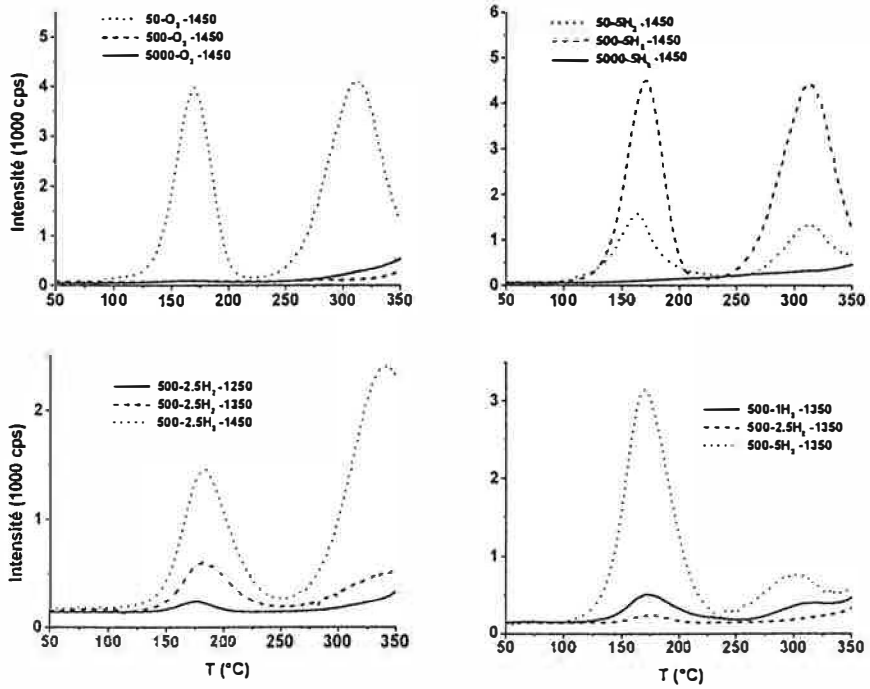

Figure V.10 : Courbes de TL des poudres d'alumine dopées au fer
après irradiation X à 25 °C (20 Gy)

V.10. ábra: Vassal szennyezett alumínium-oxid porok TL görbéi 20 Gy röntgenbesugárzás után (300 K-en)

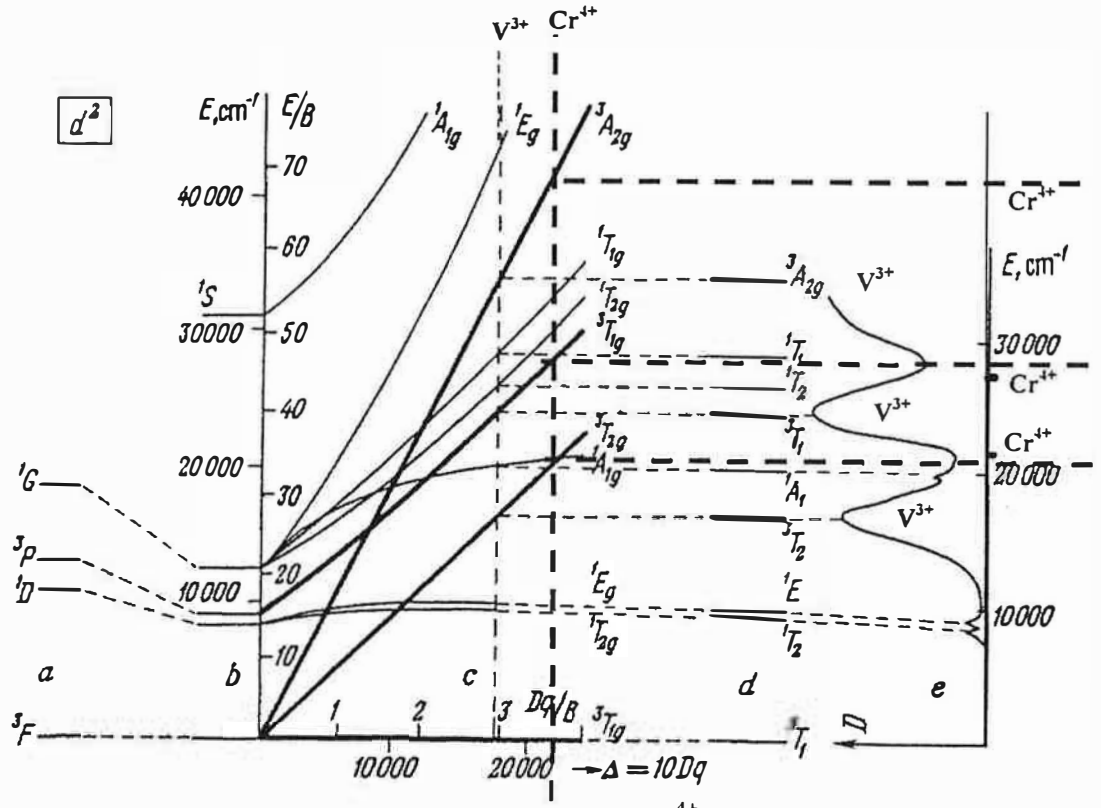

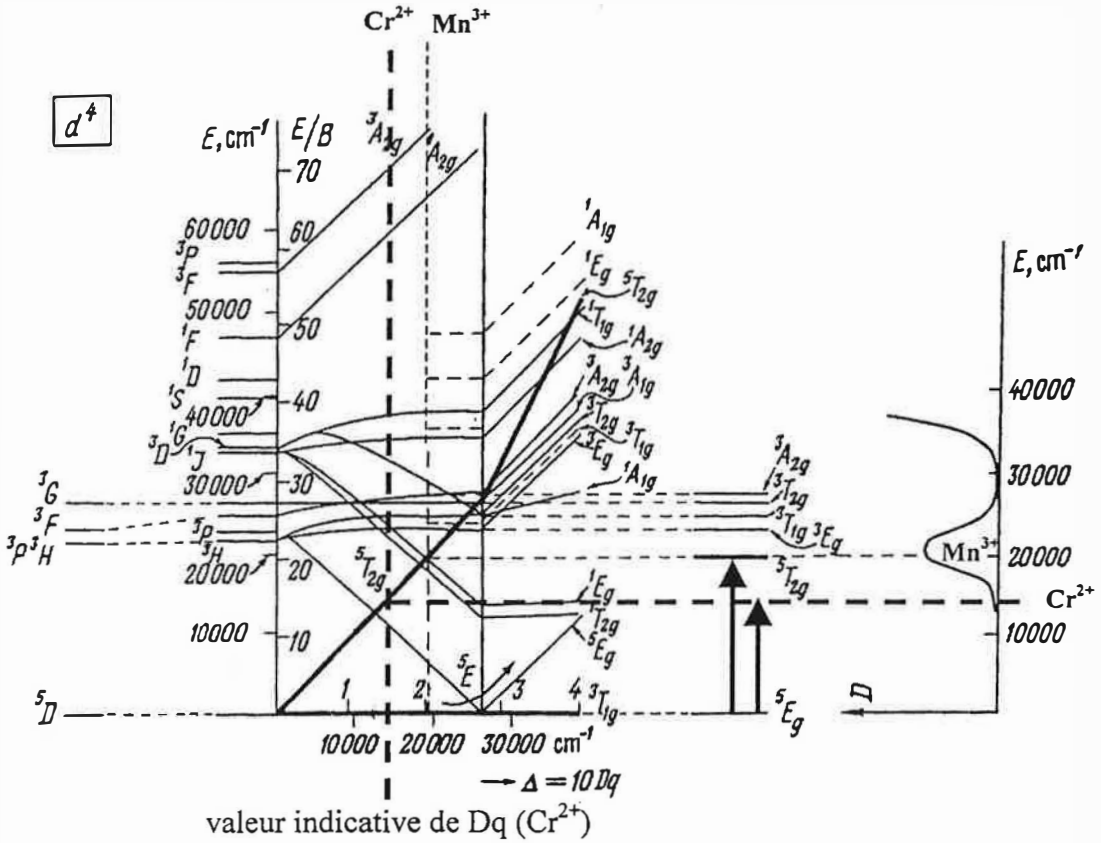

Figure V.11 : Schéma des niveaux d'énergie et spectres des ions d^2 et d^4 dans α-Al_2O_3 [MAR79]

V.11. ábra: A d^2 és d^4 ionok elektronszerkezete és spektruma α-Al_2O_3-ban [MAR79]

PUBLICATIONS

KÖZLEMÉNYEK

PUBLICATIONS / KÖZLEMÉNYEK

1. G. Molnár, J. Borossay, Zs.Varga, M. Ballók, A.Bartha: *Microwave digestion of thermoluminescent α-Al_2O_3 powders and determination of trace impurities by inductively coupled plasma atomic emission spectroscopy,* **Mikrochim. Acta, Vol. 134 (3/4), 193-197 (2000)**
2. G.Molnár, E.Papin, P.Grosseau, B.Guilhot, J.Borossay, M.Benabdesselam, P.Iacconi, D.Lapraz: *Thermally stimulated luminescence and exoelectron emission mechanism of the 430 K (D') peak of α-Al_2O_3,* **Radiat. Prot. Dosim., Vol. 84 (1-4), 253-256 (1999)**
3. G. Molnar, M. Benabdesselam, J. Borossay, P. Iacconi, D. Lapraz, M. Akselrod: *Influence of the irradiation temperature on charge trapping in Al_2O_3:C,* **Radiat. Meas. (submitted)**
4. G. Molnar, M. Benabdesselam, P. Iacconi, D. Lapraz, J. Borossay: *Thermal quenching of the 430 K (D') TL peak in α-Al_2O_3,* **proceedings of the IRPA Regional Conference on Radiation Protection in Central Europe**, Budapest, Hungary (1999)
5. G.Molnár, J.Borossay, M.Benabdesselam, P.Iacconi, D.Lapraz, K.Süvegh, A.Vértes: *Oxidation/reduction effects on the thermoluminescence of α-Al_2O_3 crystals,* **Phys. Stat. Solidi (a), Vol. 179, 249-260 (2000),**
6. Molnar, M. Benabdesselam, J. Borossay, P. Iacconi, D. Lapraz, V. Kortov, A. Surdo: *Photoluminescence and thermoluminescenceof titanium ions in sapphire crystals,* **Radiat. Meas. (submitted)**
7. G. Molnár, Z. Homonnay, A. Vértes, J. Borossay, B. Serrano, P. Iacconi: *Mössbauer spectroscopic and optical study of iron incorporation into termoluminescent alumina powders,* **J. Phys. Chem. Solids, in press (2000)**

COMMUNICATIONS / ELŐADÁSOK

12th International Conference on Solid State Dosimetry, Burgos, Spain, 1998 (poster)

G.Molnár, E.Papin, P.Grosseau, B.Guilhot, J.Borossay, M.Benabdesselem, P.Iacconi, D.Lapraz: *Thermally stimulated luminescence and exoemission mechanism of the 430 K (D') peak of α-Al_2O_3*

9th „Tihany" Symposium on Radiation Chemistry, Tata, Hungary, 1998 (oral)

G.Molnár, J.Borossay, M.Benabdesselam, P.Iacconi, D.Lapraz, K.Süvegh, A.Vértes: *Oxidation/reduction effects on sapphire TL dosimeters*

8th Solid Sampling Spectrometry Colloquium, Budapest, Hungary, 1998 (poster)

G.Molnár, A.Varga, Zs.Varga, B.Nagy, J.Borossay, Gy.Záray: *Analytical investigation of alumina TLD powders by spectrochemical methods*

IRPA Regional Congress on Radiation Protection in Central Europe, Budapest, Hungary, 1999 (poster)

G. Molnár, M.Benabdesselam, P.Iacconi, D.Lapraz, J.Borossay: *Thermal quenching of the 430 K (D') TL peak in α-Al_2O_3*

16e Journées des Laboratoires Associés de Radiophysique et de Dosimétrie, Besançon, France, 1999 (oral)

G. Molnár, M.Benabdesselam, P.Iacconi, D.Lapraz: *Influence de l'extinction thermique sur l'aire et la forme du pic dosimétrique dans TLD-500*

4th European Conference on Luminescent Detectors and Transformers of Ionizing Radiation, Riga, Latvia, 2000 (poster)

G. Molnar, M. Benabdesselam, J. Borossay, P. Iacconi, D. Lapraz, V. Kortov, A. Surdo: *Photoluminescence and thermoluminescenceof titanium ions in sapphire crystals*

4th European Conference on Luminescent Detectors and Transformers of Ionizing Radiation, Riga, Latvia, 2000 (oral)

G. Molnar, M. Benabdesselam, J. Borossay, P. Iacconi, D. Lapraz, M. Akselrod: *Influence of the irradiation temperature on charge trapping in Al_2O_3:C*

1. MICROWAVE DIGESTION OF THERMOLUMINESCENT ALUMINIUM-OXIDE POWDERS AND DETERMINATION OF TRACE IMPURITIES BY INDUCTIVELY COUPLED PLASMA ATOMIC EMISSION SPECTROSCOPY

Abstract. Five commercial and three laboratory prepared thermoluminescent aluminium-oxide powders as well as three reference samples were digested by a microwave digestion system and the impurities were analyzed by ICP-AES method. The physico-chemical properties of the different samples were found to influence highly the decomposition efficiency. Optimized decomposition parameters were developed for the samples with different physico-chemical properties (phase composition, grain size). The detection limits of the impurities of interest are presented, the analysis results of the aluminium-oxide dosimetric samples and the standards are given as well.

Key words: aluminium-oxide, thermoluminescence, microwave assisted acid digestion, ICP-AES

Introduction

Recently, specially prepared aluminium-oxide ceramics (and single crystals as well) have been increasingly applied in the field of thermoluminescence (TL) dosimetry [1]. Since impurities can be directly involved in TL mechanism, they can determine basic TL properties such as sensitivity and emission spectra. Therefore, the analysis of impurities in these materials is very important. When elaborating the analysis procedure, it must be considered that the role of the different impurities is not well known, consequently, a general purity test must be performed. Detection limits should be around 5-10 μg/g. However, for some selected trace elements (e.g. Cr, Mg), detection limits should be around 1 μg/g.

Analysis of aluminium-oxide powders used for the production of TL dosemeters can be achieved either by solid sampling or solution based methods. Solid sampling methods like slurry [2-5], electrothermal vaporisation (ETV) [2-7] and direct sample insertion (DSID) [4-6] sampling coupled with ICP-AES or atomic absorption spectroscopy (AAS) proved to be useful only in some special case. Neutron activation analysis (INAA) is a highly sensitive method for many elements but cannot be easily used [2,9]. The most wide-spread techniques are DC-arc atomic emission spectrography [10] and X-ray fluorescence (XRF) spectroscopy [2,4,9]. DC-arc AES is fairly sensitive for many elements but its analytical precision is low (around 5-10 μg/g) and solid reference materials must be used for calibration [10]. XRF technique with melt technology sampling can be applied to eliminate morphologic effects, i.e. the use of solid reference materials, but this method is not sufficiently sensitive for testing light elements (esp. Mg, Si). Total reflection x-ray fluorescence (TRXRF) technique provides higher sensitivity but this can be used only for powders which have small grain size (< 1-5 μm) [2].

For solution based methods like ICP-AES or AAS, the complete dissolution of the samples must be performed. This can be achieved either by fusion [2,11] or by acid digestion [2-5,8,11-14] techniques. In the former case one can use lithium carbonate / boric acid or alkali hydroxide fusion systems. The use of fusion techniques is advantageous for the analysis of the major and minor components in the sample. However, the determination of trace elements, especially alkali or alkali earth elements, is limited because of the high blank values of the flux. Moreover, memory effects can arise in case of those elements (esp. Fe) which can form alloys with platinum [11].

Acid digestion techniques are known to be more reliable but they are more time consuming and their efficiency depends strongly on different physico-chemical parameters of the sample [12, 13] such as grain size, specific surface area, phase composition etc. α-Al_2O_3 used for dosimetric purposes is the most resistant form of aluminium-oxide with high melting point (2050 °C), hardness (9 on Mohs' scale) and chemical inertness [1]. As it was shown by Matusiewicz [14], the analytical performance of "conventional" and microwave digestion methods is very similar, however, the former technique requires much more time. For this reason the use of microwave power for acid digestion can be especially helpful in our case.

The aim of this work was to optimize microwave digestion of different aluminium-oxide powders, to determine parameters which influence the digestion process and to analyze dosimetric powders by ICP-AES technique following sample digestion.

Experimental

ICP emission spectrometer and microwave digestion system. Digestions were realized by a Milestone (Sorisole, Italy) MLS 1200 MEGA microwave digestion unit equipped with 6 TFM digestion vessels. Different

acids and microwave programs were tested in order to find the most efficient method. The following reagents were used: cc H_3PO_4 (Fluka, for trace analysis), H_2SO_4 (96 %), HCl (37 %), HNO_3 (65 %), HF (48 %) (BDH, Dorset, England) and deionised water (> 18 MΩ/cm). From each analyzed sample 4 analogous digestions were made.

A Jobin Yvon (Longjumeau, France) 70 spectrometer with an ICP source was used. Sample solution was introduced into a crossflow nebulizer with a peristaltic pump. Table 1 summarizes the operating conditions and analytical lines used.

Physico-chemical properties of the powders. X-ray diffraction studies were performed with a Philips (Eindhoven, Holland) system using a PW1730 Cu tube (40 kV, 30 mA). Particle size distribution was determined by an Analysette 22 laser particle sizer (Fritsch, Idar-Oberstein, Germany). Electron microscopic images of the samples were obtained with the aid of an Amray 1830 I/T6 (KLA-Tencor, San José, CA., USA) scanning electron microscope. A preliminary chemical analysis of the samples (mixed with graphite) was achieved by a PGS-2 spectrograph (Carl Zeiss, Jena, Germany) with a dc-arc source (220 V, 10 A, 264 s) and by an Extra IIA (Atomika, Munich, Germany) TRXRF spectrometer (Mo-tube, 50 kV, 38 mA, 300 sec) using the slurry method for sample preparation.

Samples. Five commercial aluminium-oxide samples, namely CA-600, CA-320 (Desmarquest, Evreux, France), 2600-80 (Victoreen, Cleveland, OH., USA), 93/C (Hungalu, Budapest, Hungary) and W (Motim, Mosonmagyaróvár, Hungary), and three aluminium-oxide reference materials TSAL-2, TSAL-3 and Al53-2-TMI2 (Spex, Edison, NJ., USA) were investigated. Moreover we have also studied three powders prepared in our laboratory. Preparation of these samples was achieved using an ultra-pure γ-Al_2O_3 powder (CR-140, Baikowski Chimie, Annecy, France) that we heated to 1450 °C for 2 hours in order to obtain the alpha-phase that can be used for dosimetry. In this way, a nominally pure (Pure-0223) and two doped samples were obtained with a nominal concentration of 840 μg/g cerium (Ce-0225) and 920 μg/g gadolinium (Gd-0317) respectively. The physico-chemical properties of the samples are summarized in Table 2.

Results and Discussion

Decomposition

Table 3 shows the digestion parameters and the effectiveness of the microwave decomposition. For all the decomposition programs the same amount of sample (50 mg) was weighed into the digestion vessels. After decomposition, the concentration of the sample solutions was always adjusted to 1 g /dm^3.

Since we did not have enough experience in the digestion of Al_2O_3 and because our microwave unit is not equipped with pressure or temperature control accessories we started with sample-A which is a relatively easily decomposable (γ-Al_2O_3) sample. The first method, a Milestone application (table 3) was not effective enough - there was some residue after the decomposition procedure. When changing the acid composition to pure H_2SO_4 (method 2 of table 3), there was still some residue and the microwave vessels have been damaged. Finally, the mixture of HNO_3 and HCl (method 3 of table 3) proved to be good, but only for γ-Al_2O_3.

Diluted (1:1) H_2SO_4, used by Tatár et al. [13], was still not effective enough for the digestion of α-Al_2O_3 samples (method 4 of table 3). Using stronger acids [12] and changing the decomposition parameters (methods 5, 6 of table 3) about half of our samples, those which have relatively small grain size (F, G and H), could have been decomposed without residue but at the end some gray rings appeared on the vessels.

Concentrated H_3PO_4 proved to be the best for decomposing our samples. Using this acid (method 7 of table 3), all the samples, even the most refractory sample-C, which was prepared by grinding corundum single crystals, could have been decomposed without residue.

Analysis

The solutions after the microwave decompositions (method 7 of table 3) were analyzed by ICP-AES method. It is known that both phosphoric acid and aluminium ions decrease the emission intensity of impurities since they reduce the nebulization efficiency [11]. For this reason, calibration was performed with solutions containing the same amount of acids and aluminium ions as the sample solutions. The effect of matrix components on the background had to be considered also. This was done by the selection of appropriate analytical lines (table 1).

Detection limits, defined as the concentration which gives a net signal equal three times the standard deviation of the background signal, and the results for the SPEX standards can be seen in table 4. For some elements (Na, K, Fe, Mn, Mg) which are normally in the major concentration range in our laboratory, the

detection limits and reproducibility are a bit poorer than they supposed to be according to their ICP-AES sensitivity. This is certainly a contamination problem. Also for this reason, we failed to achieve a reliable analysis for Si.

The detailed analytical results of 4 independent decompositions of sample-D, which is a rather refractory sample are shown in table 5. The results for all the examined samples are summarized in table 6. The F, G and H samples - which were prepared in the same laboratory - are very similar to each other. They are highly pure, the only difference is the high Ce and Gd value for the F and G samples respectively, which are close to the nominal values. The D and E samples show similar contaminations probably because of their same origin. The sample-C contains some Mo impurity due to the molybdenum crucible used for the preparation technology. The iron contamination in samples B, C, D and E can be originated from the iron balls used at the grinding procedure. The Na concentration can change in a wide concentration range depending on the preparation method. Ga is a common impurity in Al_2O_3 (B, D and E samples). The Cu, Zn, Ca and Mg contaminations indicate the different origin of the samples.

Conclusions

Optimized microwave decomposition parameters were developed for γ- and α-aluminium-oxide powders. Large grain sized α-Al_2O_3 samples could have been digested only by concentrated phosphoric acid. Samples were then analyzed by ICP-AES with acceptable detection limits. However, as with all kind of solution based methods, there is a risk to contaminate the samples. Moreover, phosphoric acid - used for the decomposition - is troublesome for ICP-AES analysis. Therefore, the use of some parallel - preferably solid sampling (e.g. INAA or TRXRF) - methods might be advantageous.

Acknowledgments. The authors gratefully acknowledge Mr. P. Kovács and Ms. I. Baráth (Geological Institute of Hungary) for the X-ray diffraction measurements. We thank Ms. M.Gál, Ms. Sz. A. Baross, Ms. B. Nagy (Dep. of Petrology and Geochemistry, Eötvös Loránd University) for the electron microscopic images and for the particle size distribution and spectrographic measurements and Ms. A. Varga and Mr. Gy. Záray (Dep. of Chemical Technology and Environmental Chemistry, Eötvös Loránd University) for discussions and TRXRF measurements. Ms. P. Fodor (Cemkut Ltd.) is acknowledged for the gracious loan of reference materials.

References

[1] S.W.S. McKeever, M. Moscovitch, P.D. Townsend, *Thermoluminescence Dosimetry Materials: Properties and Uses*, Nuclear Technology Publishing, Ashford, 1995, p. 117-159.
[2] T. Graule, A. von Bohlen, J.A.C. Broekaert, E. Grallath, R. Klockenkämper, P. Tschöpel, G. Tölg, *Fresenius' Z. Anal. Chem.* **1989,** *335,* 637.
[3] J.A.C. Broekaert, T. Graule, H. Jenett, *Fresenius' Z. Anal. Chem.* **1989,** *332,* 825.
[4] J.A.C. Broekaert, G. Tölg, *Mikrochim. Acta* **1990,** *II,* 173
[5] Gy. Záray, Thesis, Eötvös Loránd University, Hungary, 1994.
[6] T.Kántor, Gy. Záray, *Fresenius J. Anal. Chem.* **1992,** *342,* 927.
[7] Z. Slovák, B. Docekal, *Anal. Chim. Acta* **1981,** *129,* 263.
[8] Gy. Záray, G. Konya, J.A.C. Broekaert, F. Leis, *Chem. Analit.* [Warsaw] **1990,** *35,* 311.
[9] H. Rausch, S. Török, A. Simonits, *Isotopenpraxis* **1985,** *21,* 229.
[10] W. Schrön, M. Krieg, D. Wienke, M. Wagner, K. Danzer, *Spectrochim. Acta B* **1992,** *47,* 189.
[11] T. Ishizuka, Y. Uwamino, A. Tsuge, T. Kamiyanagi, *Anal. Chim. Acta* **1984,** *161,* 285.
[12] M.T. Larrea, I. Gómez-Pinilla, J.C. Fariñas, *J. Anal. At. Spec.* **1997,** *12,* 1323.
[13] E. Tatár, I. Varga, Gy. Záray, *Mikrochim. Acta* **1993,** *111,* 45.
[14] H. Matusiewicz, *Mikrochim. Acta* **1993,** *111,* 71.

R.f. power:	1000 W
Argon gas flow rates:	carrier 0.4 l /min, plasma 12 l /min, sheath 0,2 l /min
Slit widths:	entrance 30 μm, exit 35 μm
Observation height:	5 mm
Sample uptake rate:	1,5 ml /min
Analytical lines [nm]:	
B: 208.959, Be: 313.042, Na: 589.592, Mg: 279.55, K: 769.896, Ca: 317.933, Ti: 334.941, V: 311.071, Cr: 205.552, Mn: 257.610, Fe: 259.940, Co: 228.616, Ni: 231.604, Cu: 324.754, Zn: 213.856, Ga: 294.364, Mo: 202.030, Ce: 413.765, Gd: 342.247	

Table 1. ICP-AES operating conditions and analytical lines.

sample	reference	impurities [1]	α-phase [%]	β-phase [%]	other phase [%]	grain size [2] [μm]
A	MOTIM	Cu	0	0	γ : 100	< 0.5
B	93C	Na, Fe, Ga	92	8	0	-
C	2600-80	Mo, Fe, Cu	100	0	0	20
D	CA-600	Fe, Na, Ga, Zn	88	12	0	11
E	CA-320	Fe, Na, Ga, Zn	83	17	0	44
F	Ce-0225	Ce, Fe, Ga	100	0	0	0.6
G	Gd-0317	Gd, Fe, Ga	100	0	0	0.6
H	Pure-0223	Fe, Ga	100	0	0	0.6
SPEX-2	TMI-2	2 μg/g altogether				
SPEX-10	TSAL-3	10 μg/g each [3]				
SPEX-100	TSAL-2	100 μg/g each [3]				

Table 2. Physico-chemical properties of the investigated aluminium-oxide samples.
[1] Impurities were determined by dc-arc-OES and TRXFS or given by the manufacturer in case of the SPEX standards.
[2] 50 % sample cut-off diameter. [3] except Gd

Method	Reagents	Time [min]	Performance [Watt]	Sample (50 mg)	Notes
1.		10	250		
	2 cm^3 HNO_3	10	400		
	+ 2 cm^3 H_2SO_4	6	600	A	some residue
		2	750		
2.		10	250		
	4 cm^3 H_2SO_4	10	400	A	some residue
		6	600		vessels damaged
		2	750		
3.		8	250		A:
	2 cm^3 HNO_3	6	400	A, B, C,	total decomposition
	+ 2 cm^3 HCl	6	500	D, E	B, C, D, E:
					residue
4.		13	250		
	10 cm^3 diluted (1:1) H_2SO_4	10	400	B, C, D, E, H	residue
		4	600		
5.	6 cm^3 H_3PO_4				F, G, H:
	+ 1 cm^3 HF	7	600	C, D, E,	total decomposition
	+ 10 cm^3 H_3BO_3	15	350	F, G, H	C, D, E:
	(saturated)				residue
6.					F, G, H:
	3 cm^3 H_2SO_4	7	600	C, D, E,	total decomposition
	+ 3 cm^3 H_3PO_4	15	350	F, G, H	C, D, E:
					some residue
7.		15	250		
	4 cm^3 H_3PO_4	7	550	B, C, D, E,	all samples :
		7	550	F, G, H	total decomposition

Table 3. Parameters and results of the different microwave decomposition methods.

	Detection limit [μg/g]	SPEX-10 [μg/g]	SPEX-100 [μg/g]
Mo	5	12 ± 2	107 ± 0.5
Cr	10	<10	106 ± 1
B	25	<25	99 ± 8
Zn	10	<10	108 ± 7
Co	10	<10	123 ± 14
Ni	10	<10	107 ± 0.5
Mn	5	11 ± 5	113 ± 13
Fe	5	12 ± 5	101 ± 1
Mg	5	11 ± 9	105 ± 3
Ga	15	<15	109 ± 2
V	5	<5	99 ± 2
Be	2	6 ± 0.5	100 ± 0.5
Ca	10	<10	95 ± 4
Cu	2	8 ± 3	107
Ti	2	6 ± 0.5	135 ± 2
Ce	20	<20	92 ± 9
Gd	10	<10	<10
Na	50	<50	145 ± 2
K	100	<100	<100

Table 4. Detection limits (3σ criterion) obtained for selected impurities in aluminium-oxide and the analysis results (mean ± standard deviation) of the mixed SPEX standards.

measurement:	1	2	3	4	mean ± s.d. [μg/g]
Zn	92	92	85	70	85 ± 10
Ni	14	15	11	< 10	13 ± 2
Fe	126	129	113	110	120 ± 9
Mg	15	13	23	25	19 ± 6
Ga	53	65	64	65	62 ± 6
Be	2	3	2	< 2	2 ± 0.6
Ca	126	126	126	120	123 ± 3
Cu	2	2	< 2	< 2	< 2
Ti	2	4	< 2	3	3 ± 1
Na	1190	1170	1110	1300	1190 ± 80

Table 5. Analysis results of sample 'D' after 4 independent decompositions by "method-8" (see table 3). (concentration of Mo, Cr, B, Co, V, Mn, Ce, Gd and K was below detection limit)

sample:	A [μg/g]	B [μg/g]	C [μg/g]	D [μg/g]	E [μg/g]	F [μg/g]	G [μg/g]
Mo	<5	<5	16 ± 3	<5	<5	6 ± 2	<5
Zn	<10	12 ± 2	<10	85 ±10	42 ± 8	<10	<10
Ni	<10	<10	<10	12 ± 2,5	<10	<10	<10
Fe	<5	65 ± 7	66 ± 22	120 ± 9	365 ± 24	6 ± 1.5	<5
Mg	<5	30 ± 9	11 ± 2,5	19 ± 6	<5	<5	<5
Ga	<15	75 ± 8	<15	62 ± 6	66 ±9	<15	<15
Be	<2	<2	<2	2 ± 0.6	4 ± 0	<2	<2
Ca	<10	350 ± 10	11 ± 3	123 ± 3	13 ± 2.5	<10	<10
Cu	2 ± 0,5	<2	29 ± 2	< 2	<2	<2	<2
Ti	<2	<2	<2	3 ± 1	12 ± 1.5	<2	<2
Ce	<20	<20	<20	<20	<20	867 ± 23	<20
Gd	<10	<10	<10	<10	<10	<10	936 ±17
Na	<50	1200±80	<50	1190±80	3100±200	<50	<50

Table 6. Analysis results (mean ± standard deviation) of aluminium-oxide samples (concentration of Cr, B, Co, Mn, V, and K was below the detection limit). In sample H, concentration of all impurities was found to be below the detection limit.

2. THERMALLY STIMULATED LUMINESCENCE AND EXOELECTRON EMISSION MECHANISM OF THE 430 K (D') DOSIMETRIC PEAK OF α- Al_2O_3

Abstract - Several α-Al_2O_3 samples were studied in order to determine the mechanism of electron-hole processes of the 430 K (D') thermoluminescence (TL) and thermally stimulated exoelectron emission (TSEE) dosimetric peak. Single crystals prepared in highly reducing conditions were treated in different atmospheres (reducing / oxidising) and their optical absorption (after isochronous annealing), fluorescence and TL properties were investigated. From these results an electron trap is suggested for the 430 K peak which is in contradiction with some data taken from the literature: this problem is discussed then. Pure and Th^{4+} doped α-Al_2O_3 powders were studied by TL method in function of doping concentration and preparation conditions. The role of aluminum vacancies is proved this way. Considering these new results, literature data and different hypotheses, the possible nature of the trap is discussed.

INTRODUCTION

The thermoluminescence (TSL) and thermally stimulated exoemission (TSEE) properties of Al_2O_3 has been extensively studied during the past 40 years [1]. It has been suggested as a dosemeter for both ultraviolet light and ionizing radiation [1-3]. The challenge is to optimize the properties which influence the dosimetric applications: sensitivity, stability, fading etc. More recently, interest has centered on the anion-deficient oxides when high sensitivity TL/TSEE radiation detectors were achieved, based on Al_2O_3:C [3]. These detectors are characterized by a very intensive TL/TSEE peak - often called peak D' - at around 430 K which can be used for low level dose measurements.

It has been ascertained that this D' peak appears mostly in samples prepared in highly reducing conditions that can be explained in terms of recombination processes as follows. The emission spectra of the 430 K peak usually consists of 420 and 695 nm luminescence with the first being much stronger [2, 3]. These emissions are due to radiative decay of F centres (420 nm) and Cr^{3+} ions (695 nm) [1]. Another emission has also been observed [3] at 320 nm (F^+ centres). It is well known that reduction of alumina leads to formation of oxygen-vacancies (F-type centres) [1] which will act then as emission centres so they will enhance the D' TL peak intensity.

On the other hand, the trap responsible for this peak has not yet been identified, even its nature (electron-hole) is debated [3,4].

For this reason, the aim of this work is to study the mechanism of electron - hole processes responsible for TL/TSEE peak at 430 K. This would be also necessary in order to improve further the dosimetric properties of these detectors.

SAMPLES AND EXPERIMENTAL PROCEDURE

Two series of experiences were carried on:

Nominally pure α-Al_2O_3 single crystal discs (commercialised by Inmas ltd., Hungary) were used to test optical properties, and atmosphere effects. Four crystals were treated at 1450 °C for 2 hours under different atmospheres: O_2, Ar, Ar + 2% H_2, Ar + 5% H_2. TL curves of single crystals were recorded by means of a photomultiplier (Philips 2018B) between 77 and 700 K (heating rate: 0,3 K/s) after X-ray (W/Cu anode, 45 kV, 2 mA, 0.6 Gy/min) irradiation. The TL emission spectra were measured by a Chromex 250IS optical multi-chanel analyser (Princeton Instruments) between 300 and 800 nm. Optical absorption measurements were made by a Cary 5 spectrophotometer in the 190 - 800 nm range at ambient temperature. Isochronal annealing was accomplished in an air oven by steps of 100 K. Fluorescence emission and excitation spectra were detected also at ambient temperature by a spectrometer mounted in our laboratory [5].

Undoped and Th^{4+} doped alumina powders were prepared by calcination of ultrapure γ-Al_2O_3 powders (CR140, Baikowski Chimie, France). The preparation and doping method was described elsewhere [6]. TL response of the powders was measured by a photomultiplier (EMI 6094S) from room temperature to 780 K with a heating rate of 1 K/s. Spectra of TL emission was detected by the same instrument used to investigate single crystals.

RESULTS

Single-crystals

TL curve (Figure 1) of the original crystals showed two prominent glow peaks at 260 K (B') and 430 K (D') and two additional small peaks at 105 K (A) and 310 K (C'). The emission spectrum of the prominent peaks consists of two large bands around 420 nm (F centre) and 740 nm (Ti^{3+}) and a sharp ray at 695 nm (Cr^{3+}), the F-centre band being the most intense. Identification of these emissions was achieved by taking into account their luminescence excitation spectra.

In the original samples we have observed four absorption bands at around 205 nm (F centre), 230 nm (F^+ centre), 260 nm (F^+ centre) and 520 nm (Ti^{3+}), the latest being very weak and diffuse.

Following X-ray exposure, the absorption bands at 230, 260 (F^+) and 520 nm (Ti^{3+}) were reduced while the 205 nm (F) band increased and a new, unidentified band appeared around 280 nm. UV exposure (deuterium lamp, continuous spectra from 200 to 400 nm) of the crystals enhanced the bands at 230 and 260 nm while the 205 nm band decreased.

Isochroneal annealing of the irradiation induced absorption bands revealed the existence of three charge traps between 370 and 1300 K (Figure 2). The first (*trap I or trap D'*) anneals between 370 and 470 K which corresponds to the thermostimulated peak D'. The emptying of this trap reduce the intensity of the F^+ centre absorption bands while enhance the intensity of the F centre absorption. The second trap (*trap II*) anneals between 770 and 970 K. In this temperature region we observed the augmentation of F^+ centre and Ti^{3+} bands while the F centre and 280 nm bands diminished. The deepest trap (*trap III*) anneals between 970 and 1270 K. While annealing this trap we found that the concentration of F centres rise and that of F^+ centres falls.

Oxidation of the crystals changed completely the TL characteristics (Figure 1): peaks B' and D' diminished by two orders of magnitude, meanwhile new peaks appeared at 225 K (B), 410 K (D) and 525 K (E). The emission spectra of these peaks consists of two bands at around 570 nm (unknown origin) and 740 nm (Ti^{3+}) and the rays of Cr^{3+}. The reduction of the crystals caused only slight changes in the TL intensities - neither the position nor the emission spectra of the peaks changed.

Powders

Thermoluminescence of undoped, ultrapure powders prepared under different conditions (O_2 or Ar + 2% H_2) is shown in Figure 3. Two prominent glow curves occur at 470 K (D') and 620 K (E'). We have showed and verified thoroughly (by comparing with our single crystals and TLD-800 detectors) that the 470 K peak is in fact the 430 K (D') peak and the temperature shift (~ 40 K) is caused by incorrect calibration of our TL instrument. TL emission spectra of undoped powders consists of the emission of Cr^{3+} only.

We studied the intensity of D' peak in function of Th^{4+} concentration (Figures 4,5) for powders prepared both in oxidising (O_2) and in reducing conditions (Ar + 2% H_2). We found that for 500 ppm Th^{4+} the intensity of peak D' is multiplied by 30 (O_2) or 100 (Ar/H_2) when comparing to the reference undoped sample. By introducing more than 500 ppm Th^{4+} into the lattice, the TL intensity will not change anymore what we explain by the low solubility of Th^{4+} in alumina. The TL emission spectra of Th-doped samples consists of the same Cr^{3+} rays than that of undoped powders.

DISCUSSION

Trap nature

The emission spectra of TL peak D' consists of F centre, Cr^{3+} and Ti^{3+} emissions. Furthermore, in the literature F^+ centre emission was also reported [3]. In the framework of an electron trap model one can easily describe these emissions [1].

In the framework of a hole trap model, it is much more difficult to consider the emission of F centres. Kortov et al. [3] established a two stage Auger-model in which F centre emission results from energy transfer between F^+ and F centres as follows (see footnote):

$$V_O^X + h^o \rightarrow (V_O^o)^* \qquad (1)$$

$$(V_O^o)^* + V_O^X \rightarrow V_O^o + (V_O^X)^* \rightarrow V_O^o + V_O^X + h\nu\,(420\ nm) \qquad (2)$$

Although these processes do occur in alumina, they cannot be responsible for D' peak emission for the following reasons:

- according to this Auger-like model, while emptying the D' trap F band absorption should decrease and F^+ band absorption should increase which is in contradiction with our isochronal annealing experiments
- F^+ centre emission (3.75 eV) does not coincide with F centre absorption (6.05 eV) so such an energy transfer has low possibility which means that F centre emission should accompany F^+ emission only as a less intense sideband which is not the case.

There is another possibility to explain F centre emission in the case of a hole trap:

$$V_O' + h^o \rightarrow (V_O^x)^* \rightarrow V_O^x + h\nu\,(420\ nm) \qquad (3)$$

So as such a process could happen we must suppose that F^- centres are stable at 430 K what is not supported by theoretical calculations [7]. Moreover equation 3 still does not explain the isochronal annealing experiments.

Another argument that supports the electron trap model is the very intense exoelectron emission that is generally observed at 430 K.

Although there still remains some questions, we believe that the 430 K thermostimulated peak is due to thermal release of an electron since this model is more consistent with experimental and theoretical data.

Defect model

In order to study the defect structure of the trap D' we introduced cations of valence different to 3+ into the lattice of alumina. The case of Th^{4+} is particularly interesting. We suppose that Th^{4+} ions substitute Al^{3+} ions. Formation of an interstitial Th^{4+}_i is not a probable event because of its large ionic radius (0.1 nm). Substitution of Al^{3+} by Th^{4+} needs charge compensation which can be assured by the formation of aluminium vacancies (V_{Al}'''):

$$3\,ThO_2 \rightarrow 3\,Th_{Al}^{\circ} + 6\,O_O^{x} + V_{Al}''' \qquad (4)$$

Now we should discuss the possible effects of Th^{4+} on the thermoluminescence.

- Th doping doesn't influence the morphology of alumina so it must have an effect on point defects.
- One can assume that Th acts as a recombination center or it will create new recombination centers but it is not the case because we haven't observed new emissions neither luminescence quenching at high Th^{4+} concentrations.
- Th^{4+} is certainly not the charge trap which gives rise the 430 K peak because it is an intentionally introduced impurity that cannot be found in the starting material even in traces, meanwhile this peak is quite intense in the undoped material.
- We think that Th^{4+} doping has an indirect effect. It enhances the formation of aluminium vacancies which will participate in the defect structure responsible for the 430 K peak (equation 4).

The problem which arise then is that aluminium vacancies are known to be hole traps and that is probably not the case of trap D'. For this reason we assume the hypothesis that aluminium vacancies are associated with another type of defect (for example with oxygen vacancies - which can assure local electroneutrality as well) such a way that this complex defect should be an electron trap.

By this trap model we can as well explain the observed atmosphere effects. In case of our single crystals a treatment under oxidising atmosphere completely eliminated the peak D'. On the other hand oxidising atmosphere enhanced this peak in the case of our undoped powders. For single crystals we can easily explain the atmosphere effect: a treatment under oxygen (equation 5) reduces the oxygen-vacancy concentration so there remains less recombination centers.

$$V_O^{oo} + 1/2\,O_2 \rightarrow O_O^{x} + 2\,h^{\circ} \qquad (5)$$

In case of the powders the emission centres are not oxygen-vacancies but Cr^{3+} ions. We suppose that oxidising atmosphere enhance the formation of aluminium-vacancies (equation 6) which - at least in our estimation - participate in the complex trap responsible for this peak.

$$1/2\,O_2 \rightarrow O_O^{x} + 2/3\,V_{Al}''' + 2\,h^{\circ} \qquad (6)$$

CONCLUSION

By analysing experimental and theoretical data we concluded that the trap responsible for the 430 K TL/TSEE/TSC peak in α-Al_2O_3 must be an electron trap. Doping of alumina by Th^{4+} revealed that this trap is related to aluminium vacancies. We suggested a complex defect structure (association of aluminium vacancies with some charge compensators - probably with oxygen vacancies) to explain all these characteristics. Contradictory atmosphere effects were succesfully described by this model.

REFERENCES

1. Summers, G.P. *Thermoluminescence in single crystal α-Al_2O_3.* Radiat. Prot. Dosim. **8** (1/2), 69-80 (1984).

2. Cooke, D.W., Roberts, H.E., Alexander, Jr. C. *Thermoluminescence and emission spectra of UV-grade Al_2O_3 from 90 to 500 K.* J. Appl. Phys. **49** (6), 3451-3457 (1978).

3. Akselrod, M.S., Kortov, V.S. *Thermoluminescent and exoemission properties of new high-sensitivity TLD α-Al_2O_3:C crystals* Radiat. Prot. Dosim. **33** (1/4), 123-126 (1990).

4. Bindi, R., Iacconi, P., Lapraz, D., Petel, F. *The effective electron affinity estimation from the simultaneous detection of thermally stimulated luminescence and exoelectron emission: Application to an α-alumina single crystal.* J. Phys. D : Appl. Phys. **30**, 137-148 (1997).

5. Lapraz, D., Iacconi, P., Daviller, D., Guilhot, B. *Thermostimulated luminescence and fluorescence of α-Al_2O_3:Cr^{3+} samples (ruby).* Phys. Stat. Solidi (a) **126**, 521 (1991).

6. Papin, E., Grosseau, P., Guilhot, B., Benabdesselam, M., Iacconi, P., Lapraz, D. *Influence of the calcining conditions on the thermoluminescence of pure and doped α-alumina powders.* Radiat. Prot. Dosim. **65**, 243-246 (1996).

7. Kotomin E.A., Stashans A., Kantorovitch L.N., Lifshitz A.I., Popov A.I., Tale I.A.: *Calculations of the geometry and optical properties of F_{Mg} centers and dimer (F_2-type) centers in corundum crystals,* Phys. Rev. B **51(14)**, 8770-8778 (1995).

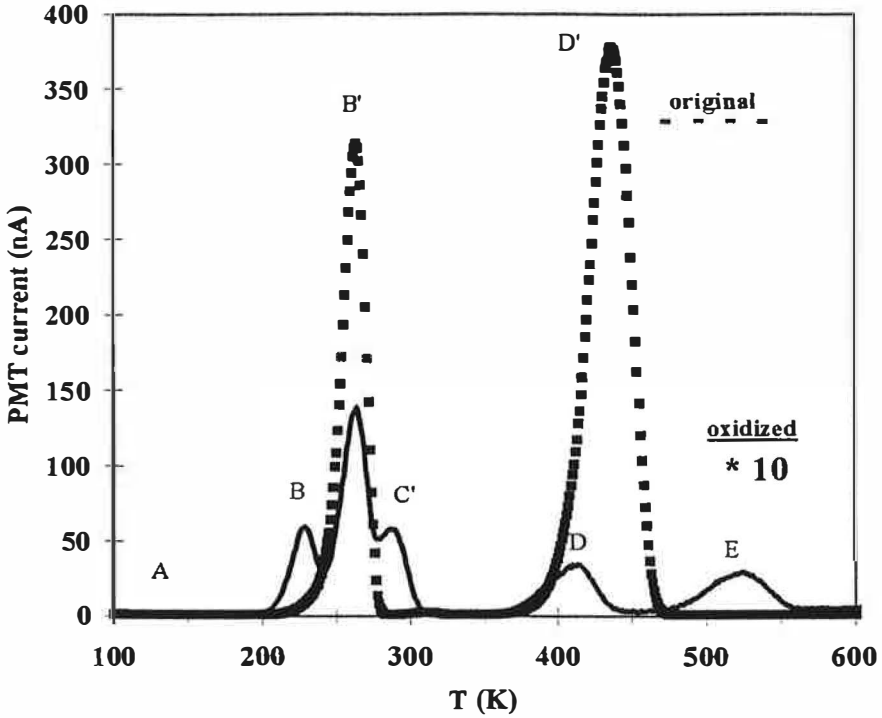

Figure 1: TL glow curves of original (- - -) and oxidised (—) Al_2O_3 single crystals following 3 Gy X ray exposure

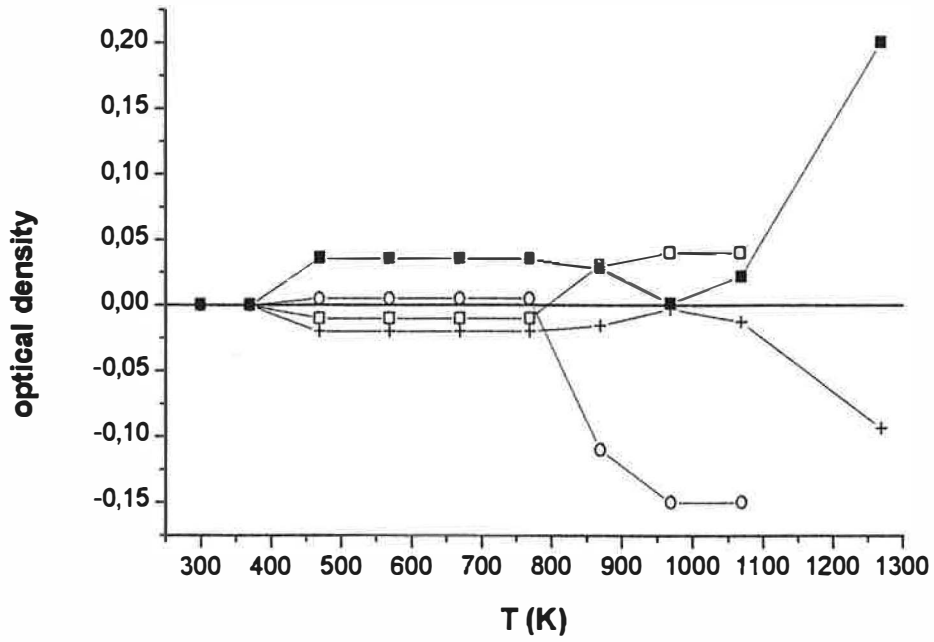

Figure 2: Isochroneal annealing of X-ray induced F (o) and F^+ (□) center and UV induced F (■) and F^+ (+) center absorption bands

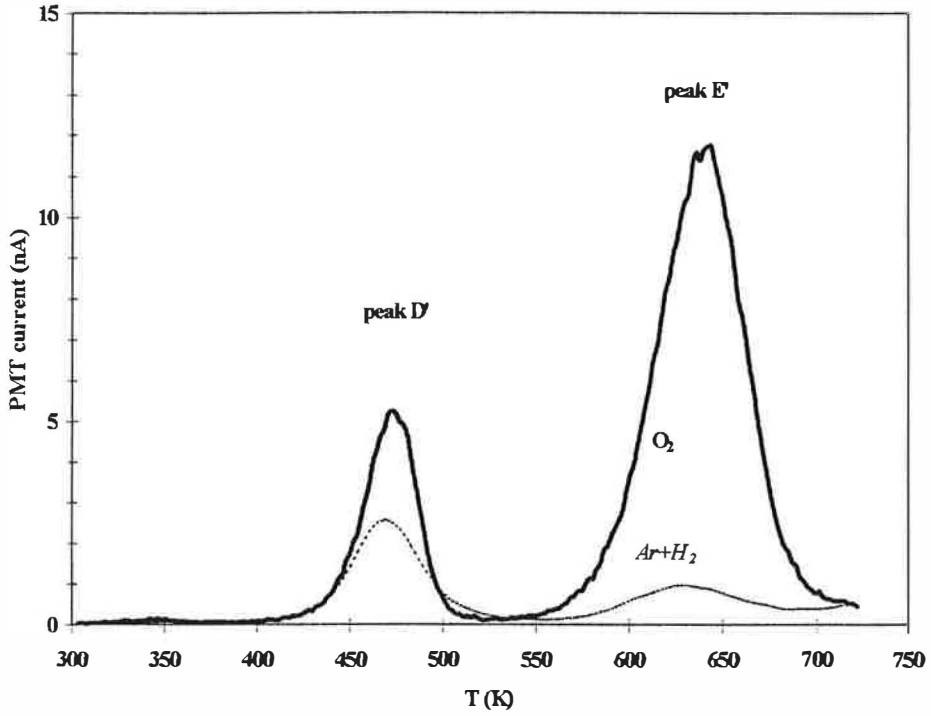

Figure 3: TL glow curves of non-doped Al_2O_3 powders (3 mg) calcined under different atmospheres

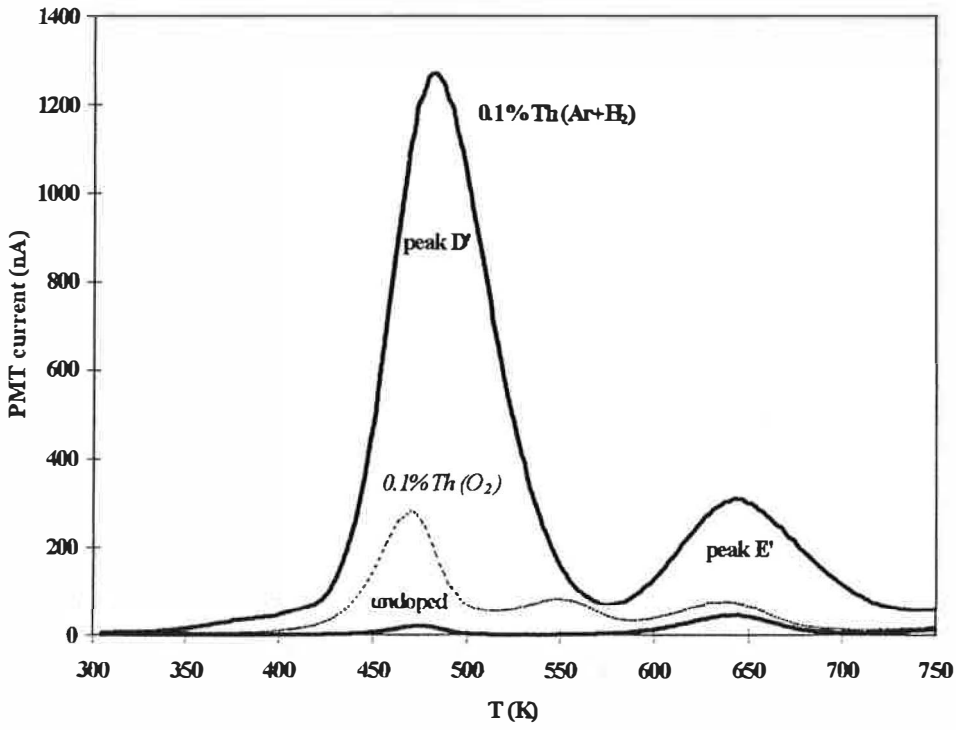

Figure 4: TL glow curves of Th^{4+} -doped Al_2O_3 powders (3 mg) calcined under different atmospheres

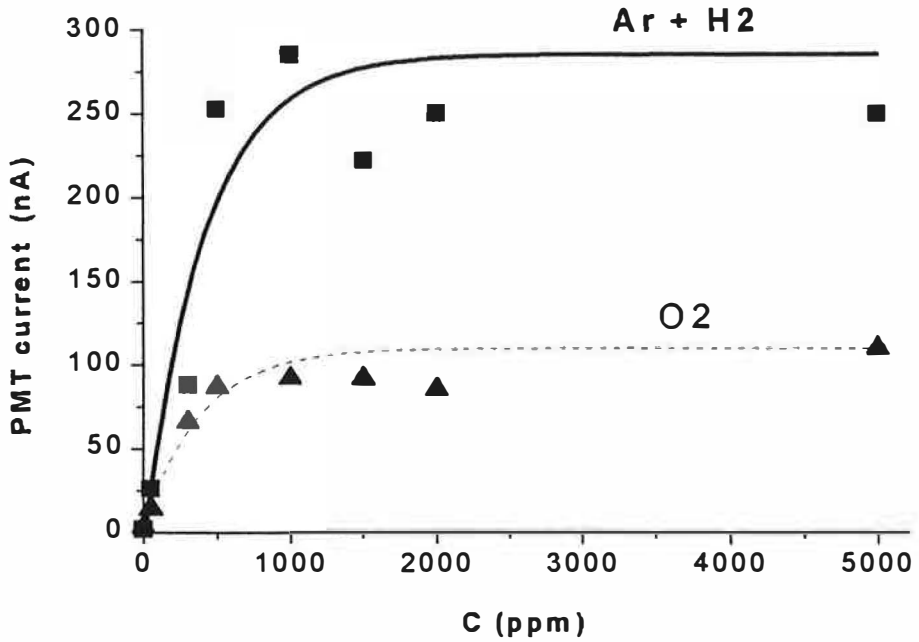

Figure 5: Intensity of the 430 K TL peak in function of Th^{4+} concentration (for 1 mg powders, prepared under O_2 or under Ar + 2% H_2)

3. Influence of the irradiation temperature on charge trapping phenomena in Al_2O_3 :C

Abstract – Al_2O_3:C TL/OSL dosemeters were irradiated at different temperatures. TL sensitivity was found to decrease by about 40 % with decreasing irradiation temperature between +30 and -100 °C. High temperature TL peaks were shown to appear only if the irradiation temperature is higher than 200 °C. Recombination of holes with electrons in the dosimetric traps was proposed as a mechanism to explain these phenomena.

Keywords - Al_2O_3:C, irradiation temperature, thermoluminescence

1. INTRODUCTION

Irradiation of thermoluminescent (TL) or optically stimulated luminescent (OSL) dosemeters is generally preformed at room temperature. Relatively extreme temperatures occur only in restricted areas, e.g. in reactor and space research. However, temperature can vary in a rather large scale during environmental monitoring as well. In environmental measurements, dosemeters are freely exposed in air up to monitoring periods of one year. During this time, the influence of sunshine may cause relatively high temperature but often low temperatures have to be considered as well (Piesch E., 1981). This variation of the ambient temperature may give rise to two phenomena which perturb the accuracy of dose measurements. First of all, temperature dependent fading may lead to a significant loss of signal during exposure and storage before read-out. Furthermore, TL sensitivity may also depend on irradiation temperature. For example, this phenomenon was observed in case of LiF:Mg,Ti dosemeters (Regula, 1981).

In this study, we are interested in Al_2O_3 :C dosemeter which is one of the modern ultrasensitive TL (as well as OSL) dosimetry materials. It has been shown (Akselrod et al., 1990) that, using Al_2O_3 :C, dose measurements below 1 μGy are possible making this material a good choice for low dose applications, particularly for environmental monitoring. Moreover, we note that high dose and high temperature applications of alumina were also proposed earlier (Portal et al., 1980) although this possibility was not yet studied in case of Al_2O_3 :C. For both of these applications (environmental or high temperature dosimetry), the influence of thermal fading on the stability of the TL signal and the effect of the irradiation temperature on the sensitivity of the dosimeter must be well known. Since thermal fading has already been investigated by several authors (see for example Akselrod et al., 1990), we propose to study the effects of irradiation temperature.

2. SAMPLES AND EXPERIMENTAL METHODS

TLD quality Al_2O_3:C single crystal samples were obtained from Inmas Ltd. (Hungary). These samples were described in a recent paper (Molnar et al., 2000). POSL and DOSL quality single crystals were grown specially for this work at Landauer Inc. and have similar features than those described by McKeever et al. in 1999.

X-ray irradiations were performed with a W/Cu tube (45 kV, 2 mA). For UV exposures, an Oriel 6316 deuterium lamp fitted with a narrow band 206 nm interference filter (MTO) was used. TL measurements were carried out using two different setups which allow to perform irradiations at low or high temperatures, respectively. The "high temperature (HT) setup" consists of a heating element, a photomultiplier (PM) tube (Philips XP2262B) and a data acquisition and control unit. Between the sample and the PM tube, a 340 or 420 nm narrow band interference filter (Oriel) is introduced. Samples are irradiated in air at different temperatures between 20 and 400 °C and then heated in air from room temperature to 700 °C at a heating rate of 1 °C/s. The "low temperature (LT) setup" is different because the sample is irradiated and heated in a vacuum chamber (10^{-5} Torr) and luminescence is detected by a Philips 2018B PM tube through a narrow band interference filter (MTO) centered at 416 nm. The sample can be irradiated from –196 °C up to +50 °C, then it is heated to 450 °C at a heating rate of 0.5 °C/s. In all cases, storage time between irradiation and readout was short (~1 min). No special annealing was applied between the readout cycles. Deep traps which are not annealed by the heating cycles were kept filled during the measurements. Filling of deep traps was achieved by a long (1 hour) UV exposure followed by heating to 700 °C (HT setup) or to 450 °C (LT setup) before the first TL measurement.

3. RESULTS

Irradiation at "low temperatures"

All samples are characterized by the well known dosimetric TL peak around 195 (± 20) °C at a heating rate of 0.5 °C/s. The emission spectra of this peak results mainly from F center emission near 420 nm.

To clarify the effect of temperature during exposure on TL sensitivity of the dosimetric peak, Al_2O_3:C detectors were irradiated at different temperatures. Because of technical reasons, these measurements were realized following UV exposure. However, we note that similar results, though with less precision, were obtained after X-ray irradiation. In case of TLD quality samples, the measurements revealed (figure 1) that at –150 °C TL sensitivity decreases to about 60 % when normalized to the TL sensitivity at 30 °C. This drop of sensitivity seems to occur in two steps between 30 and 0 °C as well as between –20 and –50 °C. For irradiation between 30 and 50 °C, TL sensitivity remained approximately constant. From 50 °C, however, TL sensitivity increases to about 170 % until 125 °C. Further increasing of the irradiation temperature leads to the diminution of the sensitivity and above 175 °C the dosimetric peak can not be induced.

Although the increase of TL sensitivity above 75 °C is an interesting phenomenon, from a dosimetric point of view it is not really disturbing. However, we note that this behavior is quite similar to that of observed in case of LiF:Mg,Ti dosemeters (Regula, 1981).

On the other hand, the variation of the temperature between +30 and –50 °C may be important in environmental applications. In fact, around these temperatures, TL peaks due to shallow traps are often detected. These traps may influence the charge distribution among different defect levels. For this reason, we have grown different single crystal samples which exhibit a similar dosimetric peak but which possess different amounts of shallow traps. In particular, DOSL samples show a relatively high concentration of shallow -15 °C traps and low concentration of 40 °C traps while POSL samples are characterized by relatively weak TL peaks around –15 and 40 °C (figure 2). The difference among these two types of samples was also shown by phosphorescence measurements (McKeever et al., 1999). In DOSL samples, two decay components can be seen at room temperature: 36 ms decay of F center luminescence as well as phosphorescence (up to 600 ms), caused by shallow traps. On the other hand, in POSL samples, the luminescence signal decays exponentially with a time constant of ~36 ms and no phosphorescence is detected.

Figure 3 represents the TL sensitivity versus temperature curves of these samples. If we compare figures 2 and 3, we can not, however, find any correlation between the intensity of the low temperature peaks and the drop of TL sensitivity. Consequently, a simple model based on the competition of traps for the localization of charges can not be used in this case. Nevertheless, we believe that there must be a connection between shallow traps and the decrease of TL sensitivity.

Irradiation at "high temperatures"

We have also investigated the correlation between the dosimetric and the high temperature TL peaks which appear around 300, 450 and 675 °C. The point of interest is that these high temperature peaks can hardly be observed when irradiating the dosemeters below 200 °C, even if the irradiation dose is very high. However, if we increase the irradiation temperature, these peaks appear clearly (figure 4). The influence of the dosimetric traps is obvious in this case. In fact, increasing the irradiation temperature from 100 to 200 °C, which corresponds to the temperature region when the dosimetric peak vanishes, results in 5-20 times intense high temperature peaks. As a further proof, we note that high temperature peaks around 450 and 630 °C can easily be introduced at room temperature in alumina samples which do not contain dosimetric traps (Portal et al., 1980).

In a first time, we thought that the detrimental effect of the dosimetric peak is connected to its emptying. To verify this possibility, we have compared the intensity of the high temperature peaks after a unique irradiation at 230 °C (5 min UV) and after two irradiations at 40 then at 230 °C (both 5 min). However, the high temperature peaks had the same intensity in both cases. A second possibility is that the dosimetric traps have such a large electron capture cross section (relative to that of the deep traps) that trapping in deep traps would be negligible at room temperature. If this possibility were true, at high doses (i.e. above the saturation dose of the dosimetric peak) the high temperature peaks should appear. Again, this hypothesis appears to be false since even for irradiations 50 times of the saturation dose the high temperature peaks remain hardly observable.

On the basis of the nature of these TL peaks, one can speculate on another possibility. In fact, the dosimetric peak was shown to be due to an electron trap (Molnar et al., 1999). As for the high temperature

peaks, we believe that they are due to hole traps because the emission spectra of these peaks consist mainly of F^+ center emission which is characteristic to hole traps. Now, a possible explanation of the deleterious effect of the dosimetric peak can be given. For this, we suppose that electrons in the dosimetric traps can recombine with free holes. If the probability of this recombination process is high, hole trapping at other centers will not occur. Although this mechanism (i.e. hole capture by electrons in the dosimetric traps) is only a speculation, we note that it may also explain the low temperature sensitivity drop. However, to address this question, we should first identify the electron-hole nature of each low temperature peak.

4. CONCLUSION

TL sensitivity of Al_2O_3:C dosemeters was found to decrease with decreasing irradiation temperature between +30 and -100 °C. This means that temperature profile during field exposure must be measured when using this dosemeter. However, some of the investigated samples do not change sensitivity until about -25 °C. These samples should be preferentially used for environmental monitoring. Although this drop of sensitivity is probably connected to low temperature TL peaks, we found no clear correlation with the intensity of these peaks. On the other hand, high temperature TL peaks show a very strong correlation with the dosimetric peak since they can be observed only if the irradiation temperature is higher than 200 °C, i.e. the temperature of the dosimetric peak.

Acknowledgements - One of the authors (G.M.) gratefully acknowledges financial support received from the Ministry of Foreign Affairs of the French Republic in the form of a Graduate Research Fellowship.

REFERENCES

Akselrod M.S., Kortov V.S., Kravetsky D.J., Gotlib V.I., (1990) Highly sensitive thermoluminescence anion-defective α-Al_2O_3:C single crystal detectors, *Radiat. Prot. Dosim.* vol 32, 15-20.

McKeever S.W.S., Akselrod M.S., Colyott L.E., Agersnap Larsen N, Whitley V., (1999) Characterization of Al_2O_3 for use in thermally and optically stimulated luminescence dosimetry, *Radiat. Prot. Dosim.* vol 84, 163-168.

Molnár G, Papin E., Grosseau P., Guilhot B., Borossay J., Benabdesselam M., Iacconi P., Lapraz D., (1999) Thermally stimulated luminescence and exoelectron emission mechanism of the 430 K (D') dosimetric peak of α-Al_2O_3, *Radiat. Prot. Dosim.* vol 84, 253-256.

Molnár G, Borossay J., Benabdesselam M., Iacconi P., Lapraz D., Süvegh K., Vértes A., (2000) Oxidation/reduction effects on the thermoluminescence of α-Al_2O_3 single crystals, *Phys. Stat. Sol. (a)* vol 179, 249-260.

Piesch E., (1981) application of TLD systems for environmental monitoring in: Applied Thermoluminescence Dosimetry, ed. M. Oberhofer and A. Scharmann (A. Hilger, Bristol) 197-228.

Portal G., Lorrain S., Valladas G., (1980) Very deep traps in Al_2O_3 and $CaSO_4$:Dy, *Nucl. Instr. & Methods* vol 175, 12-14.

Regula D.F., (1981) TLD operational aspects in: Applied Thermoluminescence Dosimetry, ed. M. Oberhofer and A. Scharmann (A. Hilger, Bristol) 123-141.

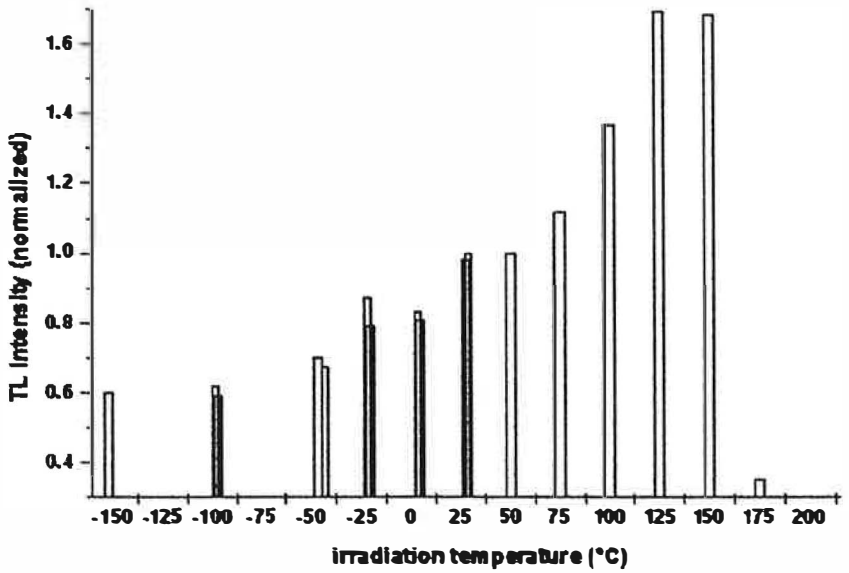

Figure 1. Intensity of the dosimetric TL peak in function of the irradiation temperature for a constant irradiation exposure (20 sec UV)

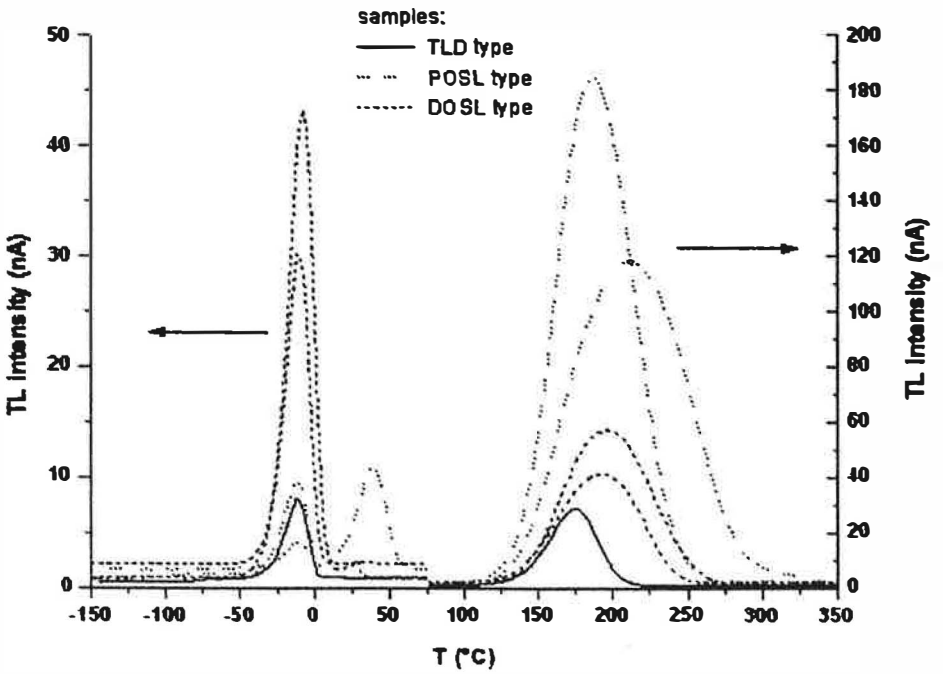

Figure 2. TL glow curves of various samples obtained following irradiation at -150 °C (20 sec UV)

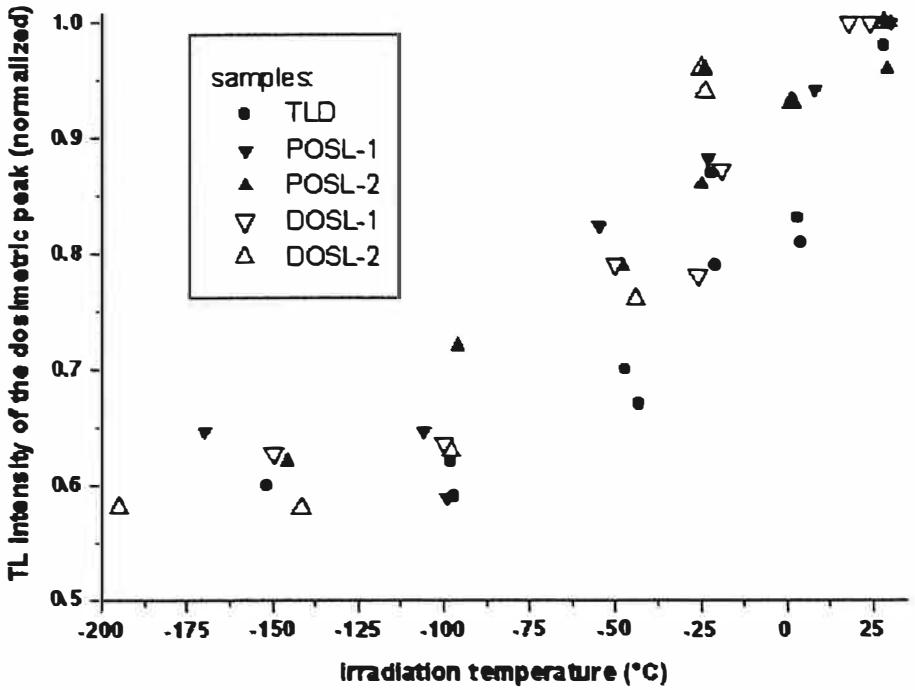

Figure 3. Intensity of the dosimetric TL peak in function of the irradiation temperature for a constant irradiation exposure (20 sec UV)

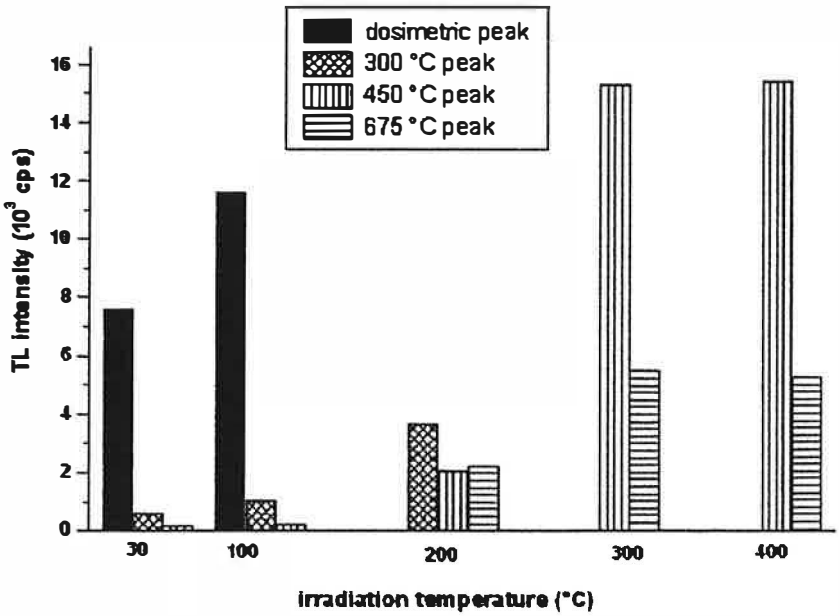

Figure 4. Intensity of the dosimetric and the high temperature TL peaks in function of the irradiation temperature for a constant irradiation exposure (300 sec UV)

4. THERMAL QUENCHING OF THE 430 K (D') TL PEAK IN α-Al_2O_3

Abstract. Anion deficient aluminium-oxide is one of the latest ultrasensitive thermoluminescent (TL) dosimetric materials. It is well known that the response of its dosimetric peak diminish with increasing heating rates which leads to lower sensitivity and reproducibility at high heating rates applied in routine dosimetry. Heating rate dependence is generally explained by thermal quenching of the luminescent F-centres. However, there is a debate in the literature on the actual mechanism of the luminescence quenching. In this work, we present some new experimental results which suggest that two different channels of quenching can be effective at the same time.

Introduction

Anion deficient alumina single crystal TL detector (α-Al_2O_3:C), developed first at the Urals Polytechnical Institute [1] is one of the most sensitive TL materials that can be used advantageously for many dosimetric purposes especially for environmental monitoring. These crystals exhibit a well-separated dosimetric peak (also called peak D') around 430 K whose emission spectra consists of mainly blue F-centre emission [1,2].

A specific feature of the dosimetric peak of α-Al_2O_3:C is that the integrated TL signal decreases drastically with increasing heating rate [1]. This observation is inconsistent with classical TL theory that predicts that the TL light sum (integral) is independent of the heating rate. Taking into account that commercial TL readers use high heating rates, the consequence of this phenomena is that high TL sensitivity of the material can not be really exploited for routine dosimetric applications. Moreover, this phenomena can be an important source of measurement error if the heating cycle is not sufficiently reproducible.

The first explication of the heating rate dependence of TL light sum of peak D' were based on the Mott-Seitz theory of luminescence quenching. Kortov et al. [3,4] studied the temperature dependence of radioluminescence and photoluminescence of F-centres and they found that strong quenching occurs between 400 and 530 K, i.e. in the temperature range of the dosimetric TL peak. The consequence of the quenching is that TL intensity will be decreased at higher heating rate since with increasing heating rate the TL peak shifts to higher temperature. Akselrod et al. [5] investigated the simultaneous TL-TSC (thermally stimulated current) signal of this peak and realised that the TSC signal does not depend on the heating rate. Since TSC is not affected by the thermal quenching process this would be another argument in favour of the Mott-Seitz model.

On the other hand, in a recent study Kortov et al. [6] proposed an interactive process of F-centre thermal quenching. According to this interactive or "external" thermal quenching model, a temperature dependent competition occurs between the emission centres and some deep electron traps for the localisation of electrons during the TL readout. They suggested that this temperature dependence is a consequence of the fact that the excited level of F-centres is close to the conduction band, so the electrons captured at this level could return to the conduction band and they can be localised at other centres such as deep electron traps. The return to the conduction band (thermoionisation) is a thermally activated process that can be described by similar parameters than that of used in the theory of Mott and Seitz.

From the review of the literature it can be concluded that different theoretical models are proposed to explain the heating rate dependence of Al_2O_3:C TL output, but the published experimental and theoretical works do not allow for deciding between these models. In this work we present some new results in order to elucidate this problem.

Samples and experimental methods

Anion deficient alumina single crystal discs used in this work were provided by INMAS Ltd. Hungary. Sample properties were described in details earlier [7].

TL curves were recorded from 300 to 970 K at a constant heating rate. TL was detected by a photomultiplier (Philips, XP2262B) through different interference filters (Oriel, centred at 416 nm or at 340 nm). Before heating, the samples were irradiated by a deuterium lamp (Oriel, 50 W) through an interference filter (M.T.O., centred at 206 nm). The spectral distribution of the TL was studied by an optical multichannel analyser (Chromex, 250IS) in the 300-750 nm spectral range.

To study the temperature dependence of the F- and F^+-centre photoluminescence, a crystal was mounted in a cryostat (Oxford Instruments) and irradiated by a deuterium lamp (Oriel, 50 W) through appropriate interference filters (M.T.O., centred at 206 nm or 250 nm). The photoluminescence emission signal

was detected by an optical multichannel analyser (Chromex, 250IS) in the 300-750 nm spectral range while cooling the sample from 600 to 300 K by steps of 50 K.

Results and discussion

The main idea of our experimental approach was to monitor the heating rate dependence of the TL at different wavelength. This idea came from the observation of the emission spectra of the dosimetric peak that revealed for us that this spectra consist of different emission bands. Thus, if the heating rate dependence occurs as a result of F-centre thermal quenching we should not observe this dependence at any other wavelength but in the F-centre emission band.

3.1. F- and F^+-centre quenching

The investigated samples show a well-separated TL peak at around 435 K at a heating rate of 0,5 K/s (figure 1). The emission spectra of this dosimetric (D') peak is dominated by an emission band at 416 nm (F-centres). However, one can observe a fairly intense emission band at 335 nm (F^+-centres), a weak band around 740 nm (Ti^{3+}) and the emission line of Cr^{3+} ions at 695 nm (figure 1).

Because of the low sensitivity of the PM of our TL instrument at around 700 nm and of other experimental complications (superposition of Cr^{3+} and Ti^{3+} emissions), we restricted our work to the study of F- and F^+-centre emission behaviour.

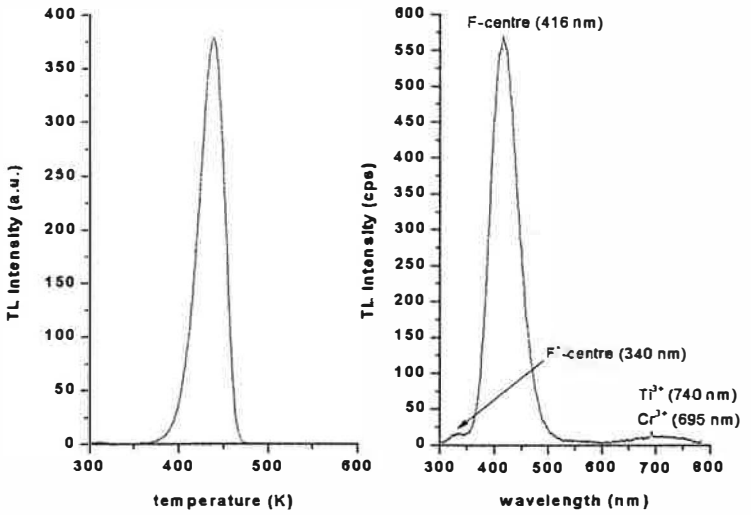

Figure 1 (left): TL of α-Al_2O_3 at a heating rate of 0,5 K/s following UV (206 nm) exposure. (right): TL emission spectra of the dosimetric peak.

The evolution of TL light sum in function of the heating rate was then investigated at different wavelength using interference filters centred at 416 or 340 nm. In doing so, we could separate F and F^+ centre emissions, respectively. As shown in figure 2, if detected at 416 nm the area of the dosimetric peak decreases with increasing heating rate in the well known manner. On the other hand, TL output when detected at 340 nm is even slightly increasing at higher heating rates. This result demonstrate that the anomalous heating rate dependence occurs due to the F-centres.

An additional observation is that the TL peak when it is detected at 340 nm appears at higher temperatures comparing to the case when it is detected at 416 nm and this temperature shift becomes larger at higher heating rates (figure 3). This suggest again that the F-centre emission is being quenched when the temperature increases and this is why the peak appears at lower temperature at 416 nm.

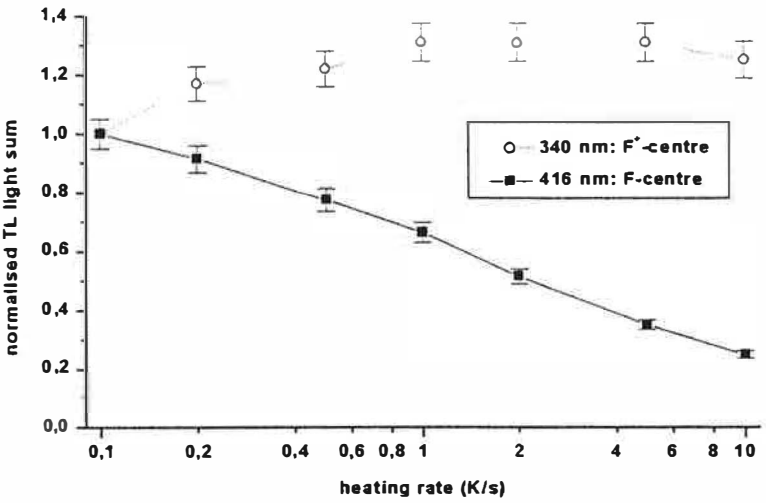

Figure 2: Normalised area of the dosimetric TL peak as a function of the heating rate. TL was detected through a 340 nm or a 416 nm interference filter following 15 s UV (206 nm) exposure.

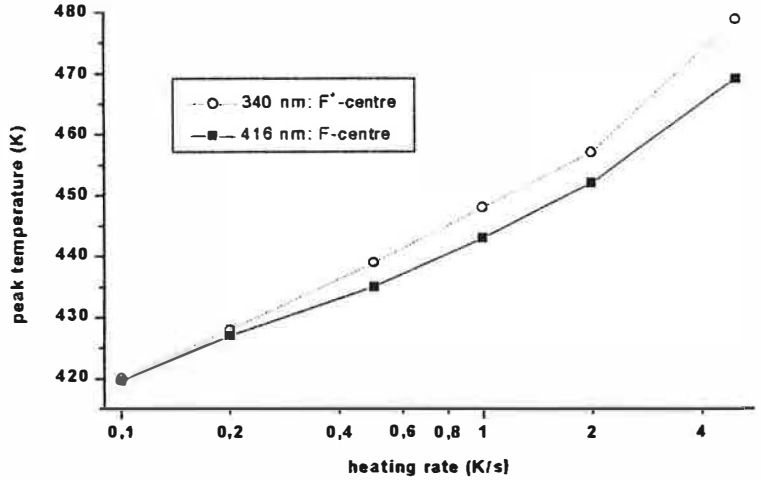

Figure 3: Temperature of the dosimetric TL peak in function of the heating rate. TL was detected through a 340 nm or a 416 nm interference filter following 15 s UV (206 nm) exposure.

The temperature dependence of the photoluminescence of F- and F^+-centres was also measured in order to compare this with the thermoluminescence quenching. To avoid the interference with trapping and detrapping processes these measurements were done during the cooling cycle. We found that F-centre photoluminescence quenching occurs around the temperature range of the dosimetric peak (figure 4). F^+-centre photoluminescence intensity also decrease somewhat with increasing temperature but not so abruptly.

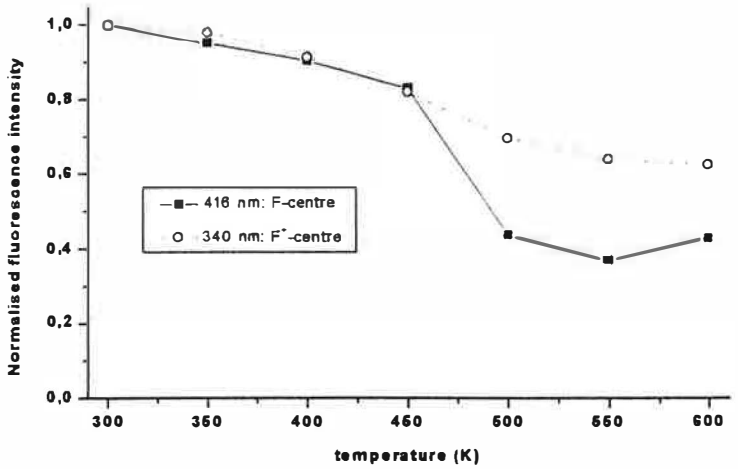

Figure 4: Fluorescence intensity of F and F^+- centres emission as a function of temperature. The wavelength of the excitation band (206 and 250 nm for F- and F^+-centres, respectively) was selected by interference filters.

Effect of deep traps on the quenching process

Following the suggestion of Kortov et al. [6] deep traps may have an important effect on the heating rate dependence. In our samples deep traps were detected by means of high temperature TL measurements. In order to eliminate the radiation of the heating strip, we had to use interference filters. By using filters with different transmission characteristics, we got some indications on the TL emission spectral distribution as well. Similarly to the results of Kortov et al. [6], our samples present 3 TL peaks between 500 and 1000 K (figure 5). At a heating rate of 2 K/s they appear at 570 K, at 720 K and at 930 K. It is difficult to detect emission spectra at such high temperatures, however, TL measurements using different filters and optical absorption annealing measurements suggest that holes are liberated from these traps giving rise to F^+-centre emission. From optical absorption annealing data [7] we can suggest as well that deep electron traps are emptied between 1000 and 1200 K. These assignments show fairly good agreement with those of Akselrod and Gorelova [8].

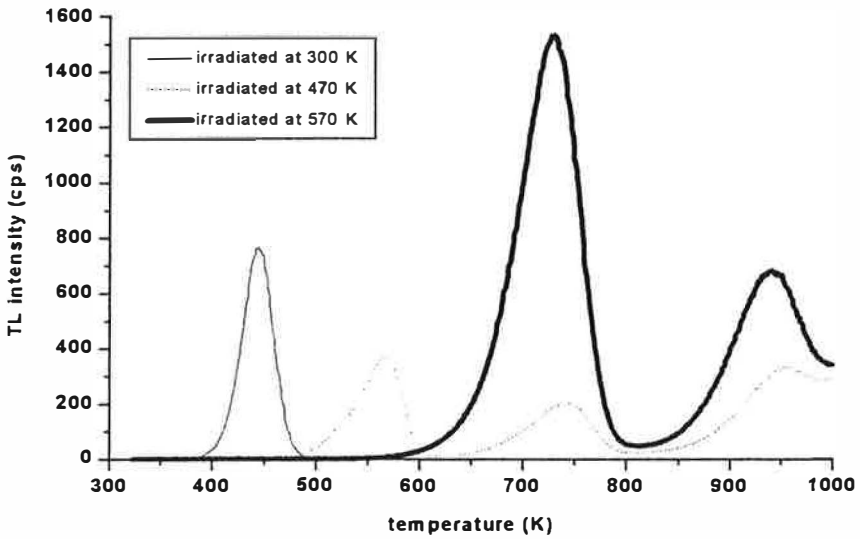

Figure 5: TL of α-Al_2O_3 at a heating rate of 1 K/s following 300 s UV (206 nm) exposure. TL was detected through a 340 nm interference filter.

The effect of deep traps on the quenching phenomena was then investigated. For this, we repeated the heating rate dependence measurements shown on figure 2 using exactly the same experimental set-up, but before each

measurement deep traps were filled by irradiating the sample at 570 K by 206 nm UV-light. As demonstrated in figure 6, the filling of the deep traps results in an increased heating rate dependence of the TL output at 416 nm. This is somewhat surprising since Kortov et al. [6] found an inverse trend, i.e. the heating rate dependence decreased when they filled the deep traps. However, we note here that if we use the trap interaction model developed by Kortov et al. [6], the electron or hole nature of the deep traps must be considered as well. If the deep traps are mostly electron traps, the filling of the deep traps will reduce the heating rate dependence while in case of hole traps one have to observe an increased dependence.

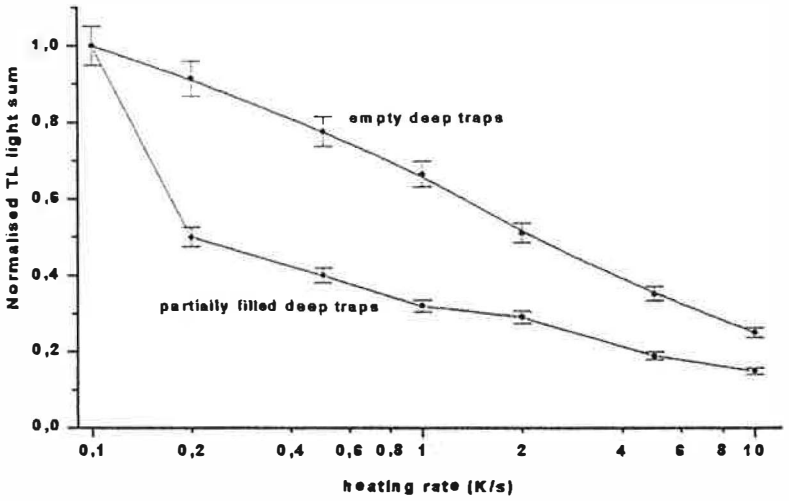

Figure 6: Normalised area of the dosimetric peak as a function of the heating rate. TL was detected through a 420 nm interference filter following 15 s UV (206 nm) exposure. Deep traps were filled by a UV (206 nm) pre-exposure at 570 K for 600 s.

Conclusion

Investigation of the dosimetric TL peak at different wavelength (i.e. in different emission bands) revealed that the heating rate dependence is connected to the thermal quenching of F-centres since this dependence does not exist in case of the F^+-centre emission. However, another quenching mechanism may be effective at the same time if we take into account that the quenching phenomena was found to depend also on the degree of filling of deep traps. A possible explanation of this observation is that there exist an interaction between the active and deep traps via the "external quenching» mechanism proposed by Kortov et al. [6].

REFERENCES

1. Akselrod, M.S., Kortov, V.S., Kravetsky, D.J. and Gotlib V.I. *Highly sensitive thermoluminescent anion-defective α-Al_2O_3:C single crystal detectors,* Radiat. Prot. Dosim. **32(1)** 15-20 (1990).
2. Akselrod, M.S., Kortov, V.S. and Gorelova, E.A. *Preparation and properties of α-Al_2O_3:C,* Radiat. Prot. Dosim. **47(1/4)** 159-164 (1993).
3. Kortov, V.S., Milman, I.I., Kirpa, V.I. and Lesz, Ja. *Some features of α-Al_2O_3 dosimetric thermoluminescent crystals,* Radiat. Prot. Dosim. **55(4)** 279-283 (1994).
4. Kortov, V.S., Milman, I.I., Kirpa, V.I. and Lesz, Ja. *Thermal quenching of TL in dosimetric crystals,* Radiat. Prot. Dosim. **65(1-4)** 255-258 (1996).
5. Akselrod, M.S., Agersnap Larsen, N., Whitley, V. and McKeever, S.W.S. *Thermal quenching of F centre luminescence in Al_2O_3:C,* Radiat. Prot. Dosim. **84(1-4)** 39-42 (1999).
6. Kortov, V.S., Milman, I.I. and Nikiforov, S.V. *The effect of deep traps on the main features of thermoluminescence in dosimetric α-Al_2O_3 crystals,* Radiat. Prot. Dosim. **84(1-4)** 35-38 (1999).
7. Molnár, G., Papin, E., Grosseau, P. Guilhot, B., Borossay, J., Benabdesselam, M., Iacconi, P. and Lapraz, D. *Thermally stimulated luminescence and exoelectron emission mechanism of the 430 K (D') dosimetric peak of α-Al_2O_3,* Radiat. Prot. Dosim. **84(1-4)** 253-256 (1999).
8. Akselrod, M.S. and Gorelova, E.A. *Deep traps in highly sensitive α-Al_2O_3:C TLD crystals,* Nucl. Tracks Radiat. Meas. **21(1)** 143-146 (1993).

5. OXIDATION / REDUCTION EFFECTS ON THE HERMOLUMINESCENCE OF α-Al_2O_3 SINGLE CRYSTALS

Abstract - α-Al_2O_3 crystals were treated in different atmospheres (reducing/oxidising) at high temperature and their optical, positron-annihilation and thermoluminescent (TL) properties were investigated. From optical absorption and positron-annihilation spectra we concluded that aluminium-vacancies were created while oxygen-vacancies were destroyed in oxidised samples indicating a Schottky-type disorder. Structural changes were correlated with TL glow curves and the origin of some TL peaks was explained.

1. Introduction

Aluminium-oxide has been proposed as a TL dosemeter many times since the 1950's [1]. However, interest for the use of this material has been multiplied since the development of highly sensitive anion deficient α-Al_2O_3 TLD crystals at the Urals Polytechnical Institute [2, 3].

Despite many works on this field [4-6], TL mechanisms as well as defect formation reactions are not clearly understood in alumina. Mainly for this reason, it is still not unambiguously established how preparation conditions (dopants, oxidising-reducing atmospheres) influence point defects and thus TL properties of this material, although this knowledge would be necessary in order to improve the dosimetric characteristics.

Overwhelming evidence has shown that under highly reducing conditions oxygen-vacancies (also called F and F^+-centres) are created in alumina [2, 7]. These samples are generally characterised by two intense TL peaks at around 270 K (peak B') and 430 K (peak D'). The emission spectra of these glow peaks are dominated by F-centre emission. On the other hand, trap nature of peaks B' and D' is unknown but they are generally thought to be of electron traps [4, 8].

Lee et al. [9, 10] studied oxidation effects on Al_2O_3 single crystals by ESR spectroscopy and presented results indicating that the oxidised crystals contained several hole traps. These traps were identified as various kinds of aluminium-vacancies and they were correlated with TL peaks at 370 K and 500 K.

The influence of synthesis conditions (atmosphere, temperature, dopants) on the TL of alumina powders was systematically studied by Papin et al. [11, 12]. Their thermodynamical model allowed them to show that oxidisation or doping with Th^{4+} leads to aluminium-vacancy formation which can act as charge traps resulting in two TL peaks: D' and E'. It also turned out that the same thermal treatment can have completely different effects on the TL. These effects depend on many factors such as impurities and the thermal history of the solid.

Oxidation and reduction mechanisms of alumina were extensively studied by the group of Krōger [13]. They suggested that Frenkel cation disorder is dominant especially at low dopant concentration. According to this assumption, oxidation of alumina occurs mainly through the creation of aluminium vacancies and the destruction of aluminium-interstitials.

In an attempt to understand more about defect formation mechanisms, we studied high temperature oxidation and reduction effects on α-Al_2O_3 single crystals by means of optical and positron annihilation spectroscopies. The obtained results were then used to explain TL behaviour.

2. Experimental

Nominally pure α-Al_2O_3 single crystals, cut from crystal rods grown from the melt, were purchased from Inmas-Mechatronica Ltd. (Hungary) in the form of plates (approximately 10*10*1 mm^3 in dimensions) whose faces are parallel to the C_3 axis. They were polished to optical grade by diamond suspension then cleaned and annealed at 1300 K in pure argon for 2 hours.

Specimens sliced from the same crystal were then submitted to thermal treatments in different gases (O_2, Ar, Ar + 2% H_2 or Ar + 5% H_2) at 1720 K for 2 hours in a horizontal tube furnace under continuous gas flow. For each atmosphere, at least two crystals were treated. This allowed us to test the reproducibility of the treatments.

TL measurements were carried out from 77 to 650 K at a heating rate of 0.5 K/s in a vacuum chamber (10^{-3} Pa). Prior to heating, samples were irradiated by X-rays (W/Cu anode, 45 kV, 2 mA, 0.6 Gy/min) at 77 K. TL glow peaks were detected either by a photomultiplier tube (Philips 2018B) or by an optical multi-channel analyser (Chromex 250 IS, Princeton Instruments, spectral range: 300-800 nm, spectral response not corrected). After each TL reading (as well as after each kind of measurement which involved the irradiation of the sample), the crystals were annealed simply by heating them to 970 K in air.

Optical absorption spectra were taken using a CARY 500 spectrophotometer in the 190-800 nm range in air at room temperature (RT). Fluorescence excitation and emission spectra were measured in the 200-800 nm range in air at RT [14]. The spectra were not corrected for the spectral response of the whole system.

Positron lifetime spectra were recorded at room temperature using a fast-fast coincidence system consisting of BaF_2 based detectors and standard electronics. The time resolution of the system was around 200 ps. The positron source was prepared of about $5x10^5$ Bq activity carrier free $^{22}NaCl$ sealing it between two kapton foils. The measured spectra were evaluated by the "RESOLUTION" computer code [15].

For each kind of method, the same α-Al_2O_3 specimen was applied. The only problem raised in case of positron lifetime measurements where two pieces of the same sample must be put because of geometric reasons. This was achieved by using two specimens cut from the same crystal and treated exactly in the same conditions.

3. Results

3.1 As-received crystals

In the as-received crystals, we identified four kinds of point defects: F-centres (or according to the Krõger-Vink notation [18]: V_O^X-centres), F^+-centres (V_O°), Ti^{3+} (Ti_{Al}^X) and Cr^{3+} ions (Cr_{Al}^X) from optical absorption, luminescence excitation and emission spectra (table 1, figure 1). Furthermore, we have observed an unidentified emission band at around 565 nm.

We also investigated the changes of the optical spectra following X-ray exposure of the crystals. It was found that the absorption (concentration) of F-centres increased while that of F^+-centres and Ti^{3+} ions decreased when X-ray exposure increased (figure 2). In case of Cr^{3+} ions and of the unidentified emission centre (at 565 nm), we could only follow changes of emission band intensities after X-ray irradiation and we found that both emissions decreased.

A representative TL glow curve of the as-received crystals is shown in figure 3. Two prominent glow peaks occur at 260 K (peak B') and at 435 K (peak D'). At higher dose, other low intensity peaks appear clearly at 105 K (peak A), 225 K (peak B), 285 K (peak C'') and 310 K (peak C').

TL emission spectra (figure 4) of peaks B' and D' are very similar. They consist of three large bands at around 335 nm (F^+-centre), 420 nm (F-centre) and 740 nm (Ti^{3+} ions), the F-centre emission being the most intense. We could also recognise the weak emission of Cr^{3+} ions at 693 nm. In case of the peaks A and C', we could only observe the F-centre emission probably because of the weak intensity of these peaks. On the other hand, peaks B and show an orange glow at around 565 nm (figure 5) and the weak Cr^{3+} emission as well.

3.2 Influence of oxidising and reducing treatments

3.2.1. Reducing treatments

We noticed that reducing treatments (Ar or Ar + H_2) did not affect markedly TL and optical properties of the crystals. This is probably due to the fact that the crystals were initially anion deficient that is to say „reduced".

3.2.2 Oxidising treatments

TL glow curve (figure 3) of Al_2O_3 treated in oxygen is rather different to that of the original crystals. The major peaks (B' and D') were diminished by two orders of magnitude while some other peaks appeared clearly at around 380 K (peak C), 410 K (peak D) and 530 K (peak E).

TL emission spectra (figure 4) of peak B' in oxidised crystals consists of two large emission bands at around 565 nm and 740 nm (Ti^{3+}) and we could also observe the weak emission of Cr^{3+} ions at 693 nm. These emissions are also observed for the other peaks (B, C, D and E); however, the relative intensity of the Ti^{3+} emission decreases comparing to the 565 nm emission. The most important feature of this TL emission spectra is that no luminescence of oxygen-vacancies could be detected, suggesting that oxygen-vacancy concentration decreased significantly. This hypothesis was supported by fluorescence measurements since we could not detect any F or F^+ centre emissions in oxidised crystals by means of this technique.

Oxidised crystals absorb light in the 190-260 nm region (figure 1) but this absorption can not be explained in terms of F and F^+ centre absorption for the lack of corresponding luminescence emissions (420 nm and 335 nm). However, in fluorescence we observed a new emission band at around 455 nm. We believe that this new emission and the associated excitation band at 230 nm are due to impurity related charge-transfer transitions. A possible candidate is Ti^{4+} ion since Ti^{3+} ion absorption decreased following the oxidation. The assignment of different Ti emissions was supported by a comparison with a synthetic sapphire sample studied earlier by Chapoulie et al. [19]. Their sample (Djeva Co. Ltd., Switzerland) - doped by approx. 400-400 ppm Ti

and Fe ions - exhibited the same emissions (figure 6) as our samples at around 455 nm and 720 nm which they could identify as transitions of Ti^{4+} and Ti^{3+} ions, respectively.

After X-ray exposure, the oxidised crystals turn to yellow. This colour results from a large radiation induced absorption band with maximum at 410 nm (figure 2). From literature data [20], hole trapping at aluminium-vacancies may be considered as the origin of this absorption band. On the other hand, the UV absorption bands in the 190-260 nm region decrease after X-ray exposure that might be due to electron trapping at impurities.

The radiation induced absorption can be correlated with TL glow curves of oxidised crystals. As illustrated in figures 7a and 7b, an absorption band with maximum at 450 nm vanishes when thermal release of trapped charges from traps corresponding to peak D occurs. The emptying of traps related to peak E is accompanied by the vanishing of an absorption band with maximum at 370 nm. On the other hand, absorption in the 190 – 260 nm range increase continuously while heating the crystals from 300 to 600 K.

3.2.3 Reducing treatments of oxidised crystals

In an attempt to study the reversibility of oxidation effects, oxidised crystals were submitted to a reducing treatment (Ar + 5% H_2, 1450 °C, 2h). Following this second treatment, TL peaks B' and D' were slightly enhanced while peaks D and E were diminished (figure 3). TL emission spectra was similar to that of the oxidised crystals (565, 695 and 740 nm emissions). Oxygen-vacancy related emissions were not observed neither in TL nor in photoluminescence. This fact may seem surprising but one have to consider that oxygen vacancy formation was reported earlier [2,7] in case of more reducing conditions and higher temperature than used in this study.

Optical absorption of these crystals (figure 1) is similar to that of oxidised crystals although absorption bands between 190 and 260 nm were decreased. Following this second treatment the crystals do not exhibit irradiation induced absorption at around 410 nm (figure 2), i.e. they do not get yellow colour after X-ray irradiation.

3.2 Positron annihilation spectroscopy (PAS)

Positron is the antiparticle of electron and - in vacuum - it is as stable as electrons. On the other hand, it annihilates in normal matter and its lifetime depends on the local electron density. After their thermalization, positrons "diffuse" in the material screening the bulk electron density and providing a very short lifetime. During this diffusion positrons can be trapped by crystal defects (vacancies or voids) having a negative charge relative to the perfect crystal. In our case these defects are Al-vacancies and macroscopic voids.

As a result of trapping, positron lifetimes longer than „bulk lifetime" can be measured. In our case, positron annihilation spectra were fitted by three lifetime components (figure 8). The shortest lifetime component (τ_1) and its intensity (I_1) are due to the annihilation of positrons in the bulk material. Those of the second, intermediate, component (τ_2) and its intensity (I_2) are assumed to be associated with the annihilation of positrons trapped in aluminium-vacancies. The longest component with $\tau_3 \approx 1.1$ ns and $I_3 \approx 0.6$ % belongs to positronium formation and annihilation phenomena in macroscopic defects.

As shown in fig.8, aluminium-vacancy content, estimated by I_2, is significantly higher for oxidised crystals. For the twofold treated crystal, I_2 is an intermediate value between that of oxidised and reduced crystals, indicating that, as a result of the second (reducing) treatment, aluminium-vacancy concentration decreased. It is also observed that the positron lifetime values (τ_2) are lower in oxidised samples than those measured in the other samples. Therefore, we can suggest that there are different kinds of aluminium-vacancies in these samples. Bulk lifetime values (τ_1) show an inverse trend than τ_2 but at present it is difficult to explain this behaviour.

4. Discussion

4.1 As-received crystals

As-received sapphire single crystals exhibited two important TL peaks at 260 (B') and 435 K (D') with emissions at 335, 420, 695 and 740 nm. We could interpret these emissions as luminescence of F^+-centres, F-centres, Cr^{3+} and Ti^{3+} ions, respectively. It is interesting to note that the emission spectra of some other peaks (B and C'') are completely different: they have an orange glow.

Since it is well established that peak B occurs due to hole detrapping from Mg_{Al}^{X} centres [4], we suggest that peaks with an orange glow (B and C'') correspond to hole traps. On the other hand, peak B' is known to be due to an electron trap [4], so we suggest that peaks with similar blue glow (A, B', C', D') correspond to

electron traps. However, in case of the high temperature peaks this simple rule must be used carefully because of the thermal quenching phenomena which appears above RT.

4.2 Influence of oxidising and reducing treatments

Defect structure and TL properties of these crystals were not influenced much by treatments under reducing conditions since the crystals were initially anion deficient (i.e. "reduced").

On the other hand, all oxygen-vacancy related optical absorption and emission bands disappeared following thermal treatment of the crystals in oxygen which means that oxygen-vacancies were destroyed. Furthermore, as it was shown by positron annihilation experiments, aluminium-vacancies were created while incorporating oxygen. Moreover, Ti^{3+} ions were partly oxidised to Ti^{4+} ions.

$$\tfrac{1}{2}\, O_2 + 2\, Ti_{Al}{}^{X} = O_O{}^{X} + 2/3\, V_{Al}''' + 2\, Ti_{Al}{}^{\circ}$$

$$\tfrac{1}{2}\, O_2 + V_O{}^{\circ\circ} + 2\, Ti_{Al}{}^{X} = O_O{}^{X} + 2\, Ti_{Al}{}^{\circ}$$

The increasing aluminium-vacancy and the decreasing oxygen-vacancy concentration suggest that Schottky-type disorder is dominant in α-Al_2O_3.

As a result of changes in defect-structure, TL features has also been changed after oxidation. Predominant TL peaks B' and D' decreased significantly that can be explained in terms of recombination processes. Since in oxidised crystals the oxygen-vacancies are destroyed, the recombination of released electrons can not take place at F^+ centres, so they must be replaced by other recombination centres that leads to a reduced TL yield.

On the other hand, TL glow curve of oxidised crystals exhibit some other peaks that appeared at 360, 410 and 520 K. Taking into consideration that the annealing temperature of absorption bands associated with aluminium-vacancies corresponds well to the annealing temperature of traps responsible for peaks D (410 K) and E (520 K) one can assume that these traps are aluminium-vacancies or some kind of aluminium-vacancy clusters. By ESR spectrometry, Lee et al. [9, 10] found one- and two-hole centres in oxidised Al_2O_3 which annealed around 370 and 500 K. They described these annealing processes as follows:

$$V_{Al}' \rightarrow V_{Al}'' + h^{\circ}\ (370\ K)$$

$$V_{Al}'' \rightarrow V_{Al}''' + h^{\circ}\ (500\ K)$$

In our case, this model can not give account on peaks D and E since, according to this model, annealing of peak D (V_{Al}' centres) should lead to the formation of V_{Al}'' centres and consequently to an increase of the 370 nm absorption band that has not been observed (figure 7). Now, a possible explanation of this discrepancy is that our samples contain a small amount of Ti^{3+} impurity ions that may have been partly oxidised to Ti^{4+} ions which must be charge compensated. The most obvious compensation mode is clustering with aluminium-vacancies because it reduces defect formation energies. As a result of clustering, aluminium-vacancies perturbed by Ti^{4+} ions will, in effect, be observed in thermoluminescence besides the isolated vacancies. One can speculate that this kind of clustering processes might be responsible for different τ_2 value in oxidised crystals measured by PAS.

Following the treatment of oxidised crystals under reducing conditions, the aluminium-vacancy correlated irradiation induced absorption bands (around 410 nm) do not appear anymore. The decrease of aluminium-vacancy concentration was also confirmed by PAS. TL peaks D and E were also decreased confirming the hypothesis that they are related to some kind of aluminium-vacancies. The decrease of aluminium-vacancy concentration was not followed by the formation of oxygen-vacancies that might be an indication of a Frenkel-type cationic disorder.

5. Conclusion

This work has concentrated first on defect formation mechanism following oxidising and reducing treatments of α-Al_2O_3 single crystals. With the aid of positron annihilation spectroscopy, we presented direct evidence for aluminium-vacancy formation under oxidising conditions which was accompanied by the destruction of oxygen-vacancies and the oxidation of Ti^{3+}. Furthermore, our results indicate that Schottky as well as cation Frenkel disorders may be of importance in α-Al_2O_3. Changes in defect structure were correlated with TL properties. Glow peaks at 260 K (B') and 435 K (D') were related to electron traps and oxygen-vacancies which act as emission centres. TL peaks at 410 (D) and 520 K (E) emerge after oxidising treatment. They are related

to aluminium-vacancies which probably act as hole traps although these traps can not be described by a simple isolated vacancy model.

Acknowledgements: We would like to thank Mr. B. Guilhot and Mr. E. Papin (Centre SPIN, Ecole des Mines de St-Etienne, France) for providing facilities for the thermal treatments, Mr. R. Chapoulie (CRPAA, Université Michel de Montaigne-Bordeaux 3, France) for the loan of sapphire reference samples. One of the authors (G.M.) gratefully acknowledges financial support received from the Ministry of Foreign Affairs of the French Republic in the form of a Graduate Research Fellowship.

REFERENCES

[1] S.W.S. McKeever, M. Moscovitch and P.D. Townsend, Thermoluminescence dosimetry materials: properties and uses, Nuclear Technology Publishing, Ashford 1995.
[2] M.S. Akselrod and V.S. Kortov, Radiat. Prot. Dosim. **33(1/4)**, 123 (1990).
[3] M.S. Akselrod, V.S. Kortov and E.A. Gorelova, Radiat. Prot. Dosim. **47 (1/4)**, 159 (1993).
[4] G.P. Summers, Radiat. Prot. Dosim. **8(1/2)**, 69 (1984).
[5] V.S. Kortov, T.S. Bessonova, M.S. Akselrod and I.I. Milman, phys. stat. sol. (a) **87**, 629 (1985).
[6] P. Iacconi, F. Petel, D. Lapraz and R. Bindi, phys. stat. sol. (a) **139**, 489 (1993).
[7] K.H. Lee and J.H.Jr. Crawford, Phys. Rev. B **19(6)**, 3217 (1979).
[8] G. Molnár, E. Papin, P. Grosseau, B. Guilhot, J. Borossay, M. Benabdesselam, P. Iacconi and D. Lapraz, Radiat. Prot. Dosim. **84(1-4)**, 253 (1999)
[9] K.H. Lee, G.E. Holmberg and J.H. Crawford, Solid State Commun. **20**, 183 (1976).
[10] K.H. Lee, G.E. Holmberg and J.H.Jr. Crawford, phys. stat. sol. (a) **39**, 669 (1977).
[11] E. Papin, P. Grosseau, B. Guilhot, M. Benabdesselam, P. Iacconi and D. Lapraz, Radiat. Prot. Dosim. **65(1-4)**, 243 (1996).
[12] E. Papin, Thesis, Ecole des Mines de St-Etienne, France (1997).
[13] F.A. Kröger, Solid State Ionics **12**, 189 (1984).
[14] D. Lapraz, P. Iacconi, D. Daviller and B. Guilhot, phys. stat. sol. (a) **126**, 521 (1991).
[15] P. Kirkegaard, M. Eldrup, O.E. Mogensen and N.J. Pedersen, Comput. Phys. Commun. **23**, 307 (1981).
[16] B.D. Evans and M. Stapelbroek, Phys. Rev. B **18(12)**, 7089 (1978).
[17] M. Yamaga, T. Yosida, S. Hara, N. Kodama and B. Henderson, J. Appl. Phys. **75(2)**, 1111 (1994).
[18] F.A. Kröger, The Chemistry of Imperfect Crystals, North Holland Publishing, Amsterdam 1974.
[19] R. Chapoulie, C. Capdupuy, M. Schvoerer and F. Bechtel, phys. stat. sol. (a) **171**, 613 (1999).
[20] T.J. Turner and J.H. Crawford, Solid State Commun. (a) **17**, 167 (1975).

optical absorption (nm)		luminescence excitation (nm)		luminescence emission (nm)		point defect	reference
measured	literature	measured	literature	measured	literature		
205	205	220	205	420	415	V_O^x	[7]
230, 260	230, 255	235, 260	230, 255	335	330	V_O°	[16]
520 (diffuse)	485, 550	475, 545	485, 550	720	720	Ti_{Al}^x	[17]
-	400, 550	400, 550	400, 550	693	693	Cr_{Al}^x	[14]
-	-	295	-	565	-	?	-

Table 1: Optical absorption and luminescence bands of the as-received α-Al_2O_3 crystals.

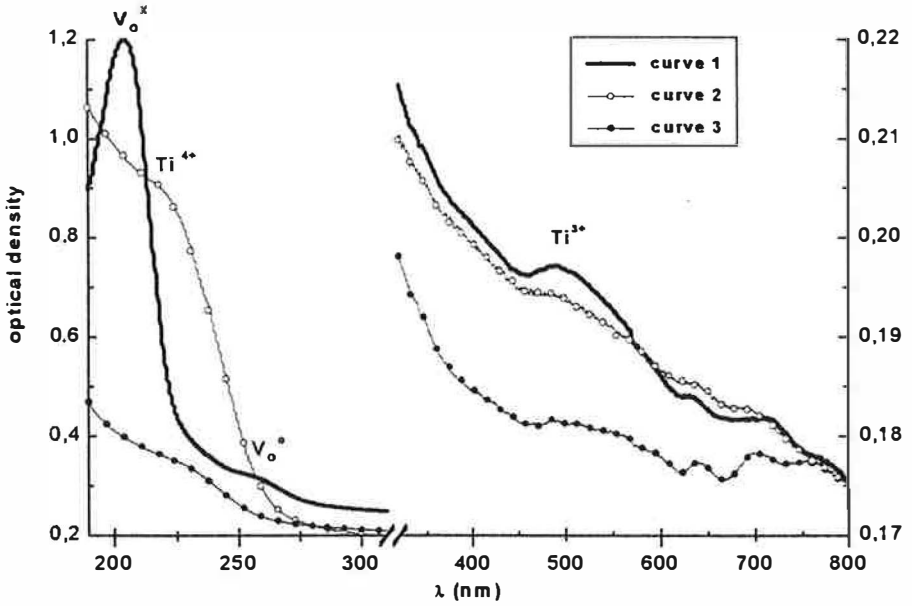

Figure 1: Optical absorption of an α-Al_2O_3 crystal. The absorption reference is air. (curve 1: as-received sample, curve 2: sample treated in O_2 at 1720 K for 2 hours, curve 3: sample treated first in O_2 then in Ar+5 % H_2 at 1720 K for 2 hours in both atmospheres.)

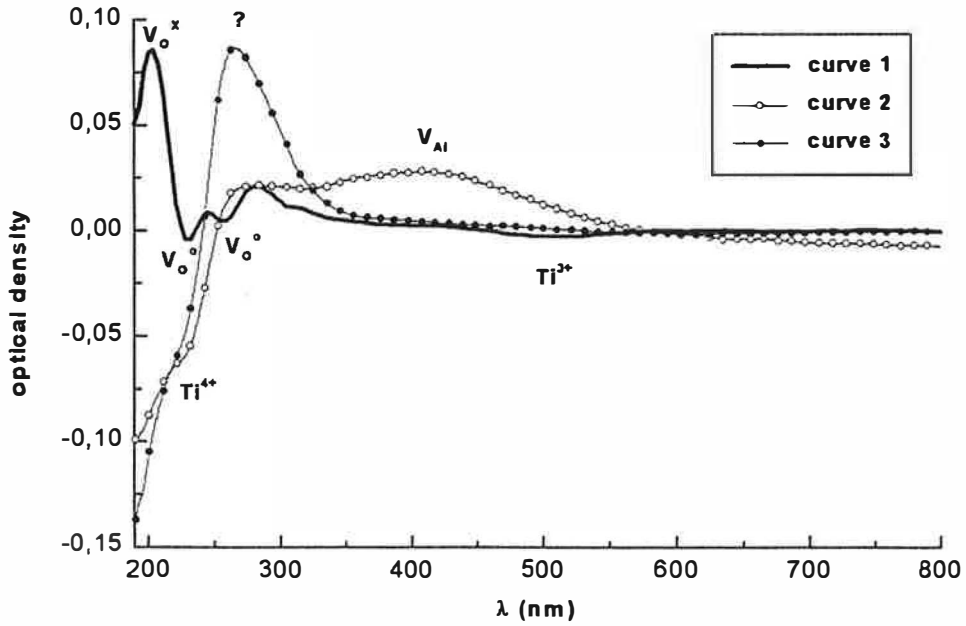

Figure 2: Optical absorption of an α-Al_2O_3 crystal following 800 Gy X-ray air kerma at RT. The absorption reference is the same crystal before irradiation. (see the legend of fig.1, the designations are the same)

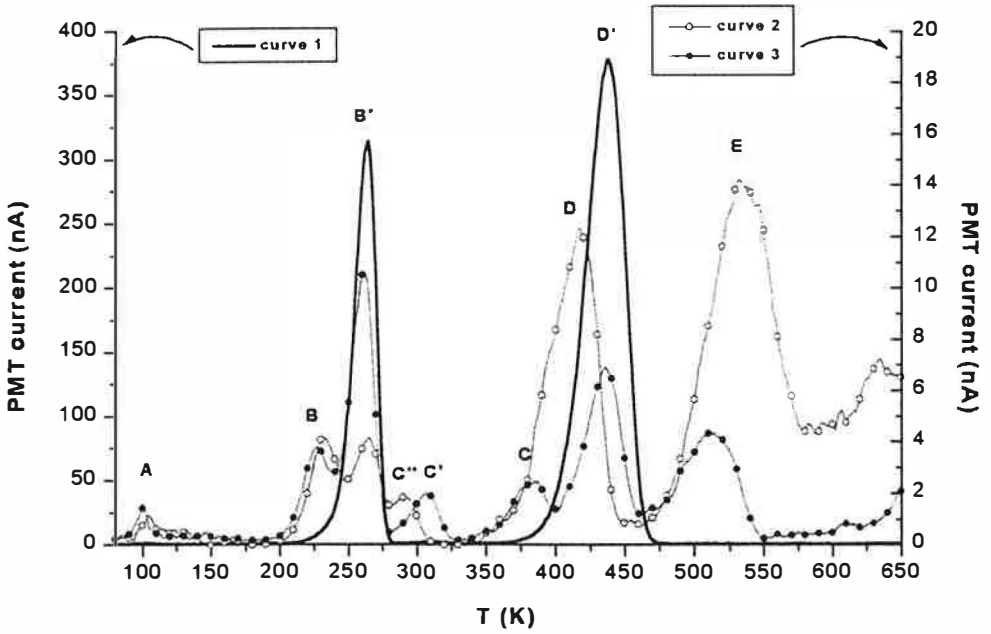

Figure 3: TL glow curve of an as-received α-Al_2O_3 crystal following 3 Gy X-ray air kerma at 77 K. (see the legend of fig. 1, the designations are the same)

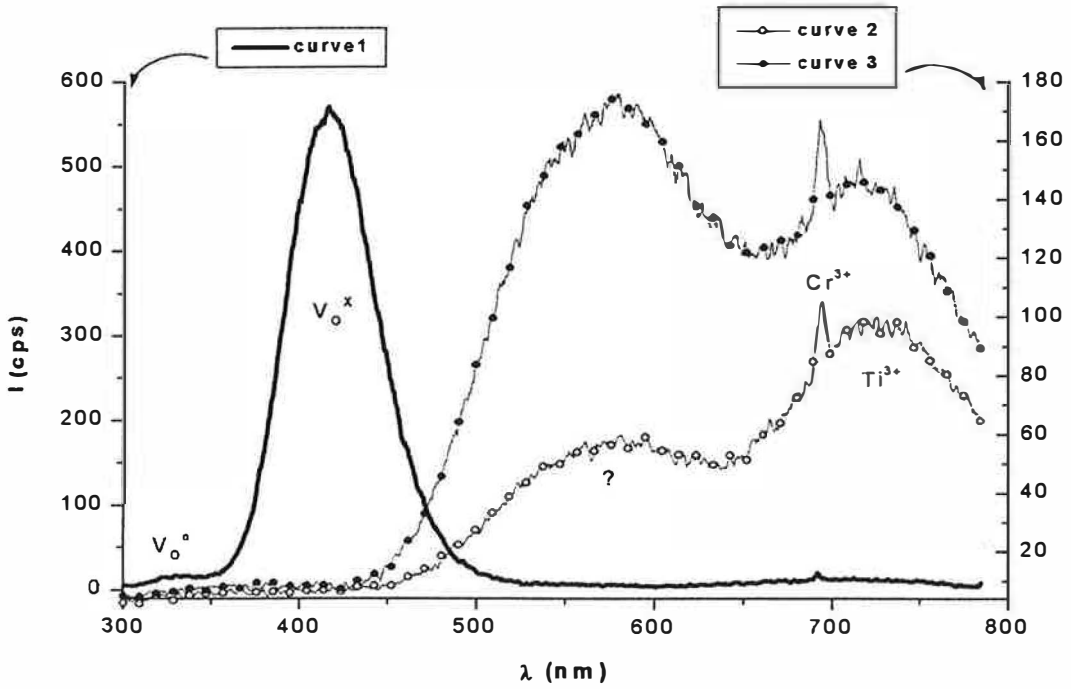

Figure 4: TL emission spectra at 260 K (peak B') of an α-Al_2O_3 crystal following 12 Gy X-ray air kerma at 77 K (see the legend of fig.1, the designations are the same).

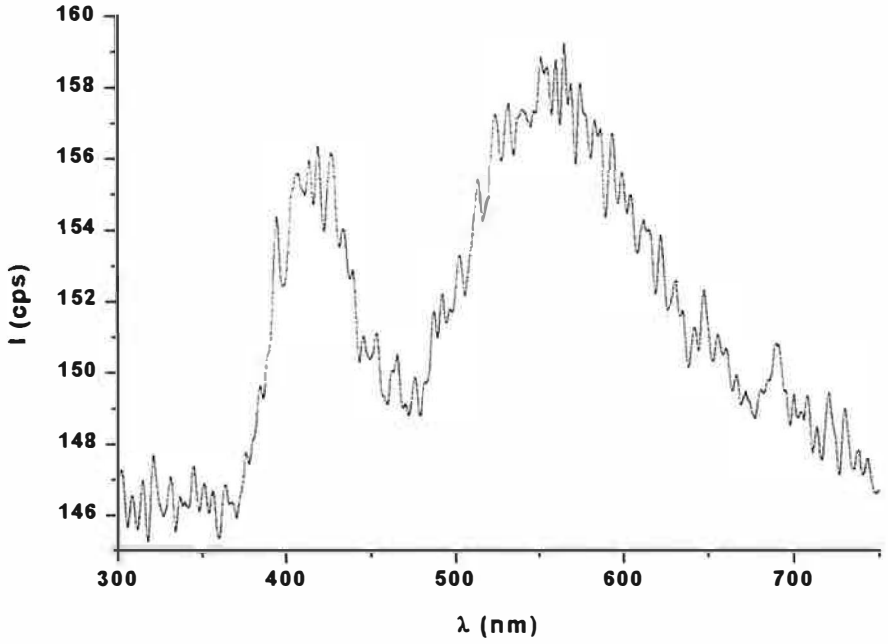

Figure 5: TL emission spectra at 225 K (peak B) of an as-received α-Al_2O_3 crystal following 12 Gy X-ray air kerma at 77 K. (The emission band at 420 nm occurs due to the rising part of the peak B'.)

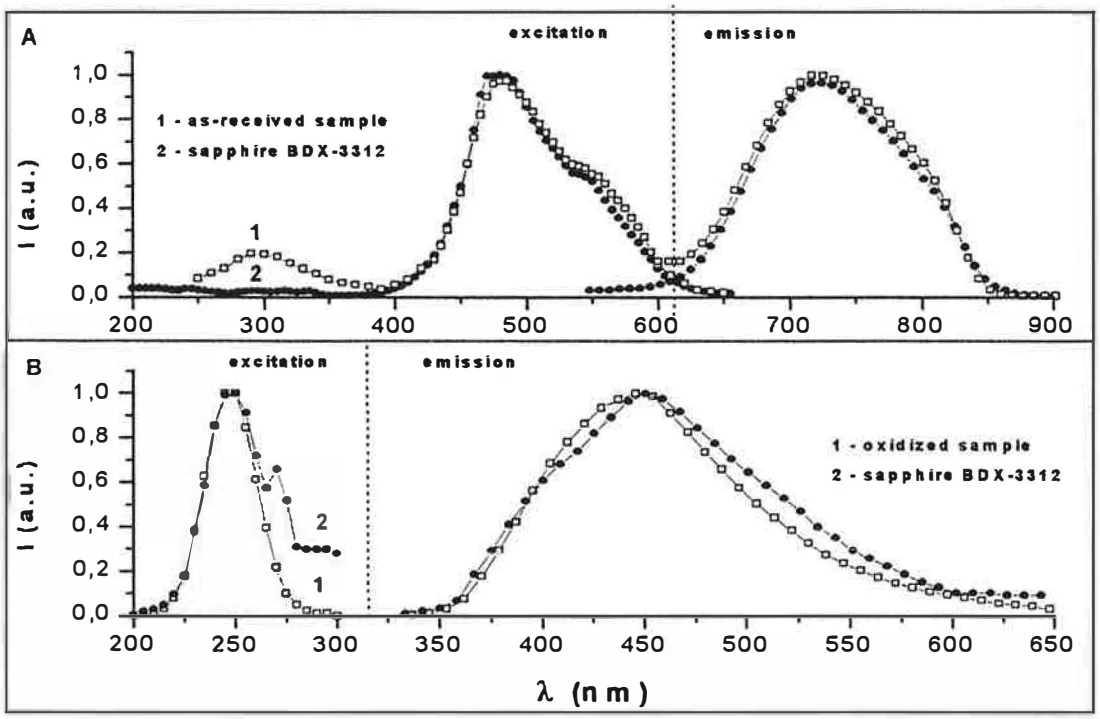

Figure 6: Titanium impurity related fluorescence excitation and emission spectra of an as-received α-Al_2O_3 crystal and of a sapphire reference sample. A: Ti^{3+}, B: Ti^{4+}

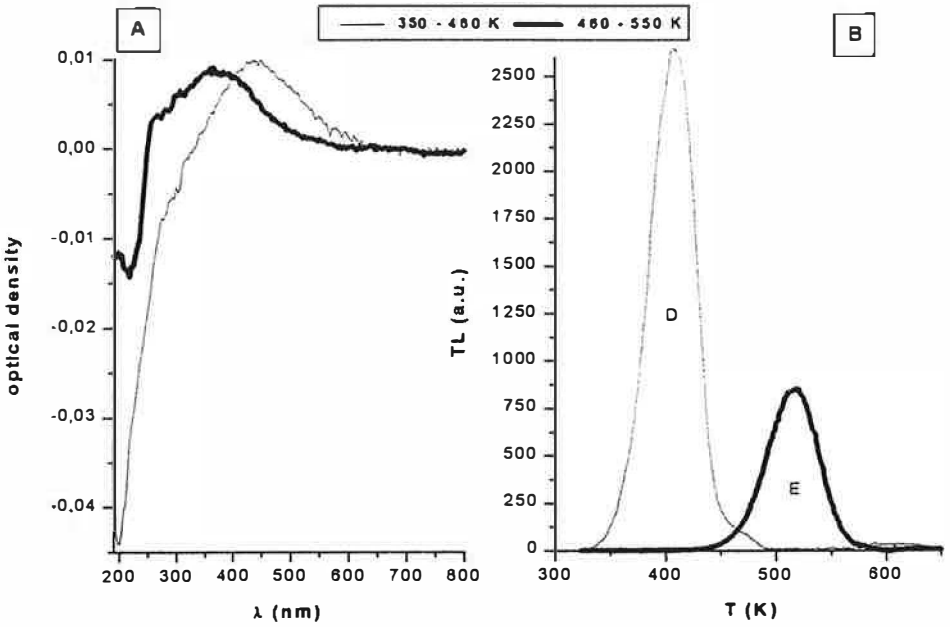

Figure 7:
A: Stepwise annealing of X-ray (800 Gy at 300 K) induced absorption bands of an α-Al_2O_3 crystal treated in O_2 at 1720 K. Each curve is a part of the composite irradiation induced absorption that vanishes in the indicated temperature range.
B: Stepwise annealing of X-ray (800 Gy at 300 K) induced TL glow peaks D and E of an α-Al_2O_3 crystal treated in O_2 at 1720 K. Each curve is a part of the entire TL glow curve that vanishes in the indicated temperature range.

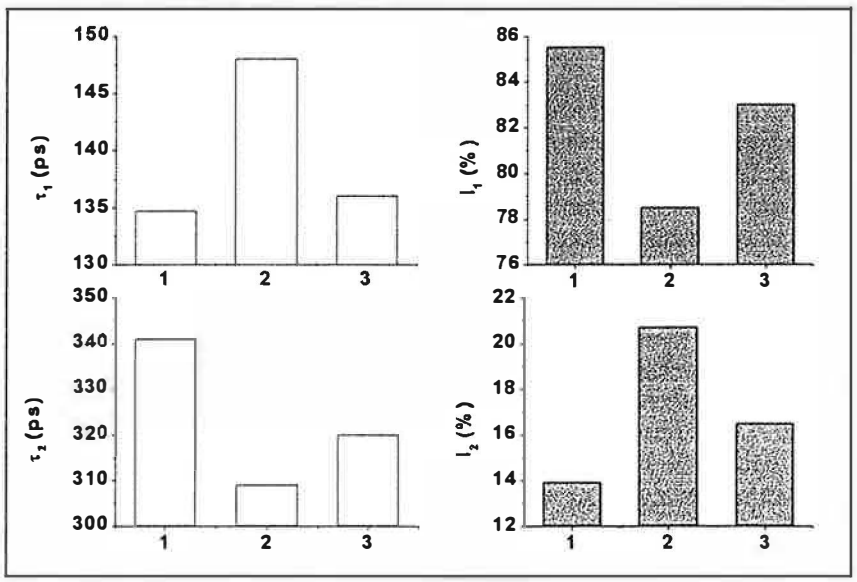

Figure 8: Positron lifetime components (τ_1 and τ_2) and corresponding intensities (I_1 and I_2) in different α-Al_2O_3 crystals: 1 – as-received, 2 – oxidised, 3 – oxidised and reduced.

6. Photoluminescence and thermoluminescence of titanium ions in sapphire crystals

Abstract - Several titanium species (Ti^{3+}, Ti^{4+}, Ti^{4+}-V_{Al} clusters) were identified in sapphire samples from their optical spectra. In highly reduced samples, we observed only Ti^{3+} centres while oxidized samples contain Ti^{3+} and Ti^{4+} ions as well. The formation of Ti^{4+} ions occurs simultaneously with the formation of aluminium-vacancies which are charge compensators for Ti^{4+} ions and act as hole traps in charge exchange process. We could observe locally and non-locally compensated Ti^{4+} as well. It is shown that Ti^{3+} is a deep hole trap while Ti^{4+} is a deep electron trap. In the TL process they act as recombination centers for electrons and holes, respectively. However, in TL we observed only the emission of locally compensated Ti^{4+}, probably because of spatial correlation.

Keywords - sapphire, titanium, thermoluminescence, photoluminescence

1. INTRODUCTION

Optical transitions and defect chemistry of titanium in α-Al_2O_3 host crystal have been extensively studied in the past (see for example Evans, 1994) because of its application as a tunable laser material and also of its role in the optical properties of sapphire gem stones. Thermoluminescence (TL) properties of some Ti doped alumina samples were also investigated (Mehta et al., 1976, Portal et al., 1980). Recently, it was proposed that titanium impurity has an influence on the dosimetric properties of anion deficient α-Al_2O_3 TL detectors as well (Surdo et al., 1999). Although some studies are available (Wong et al., 1995), a discussion of the role of Ti in the charge trapping and recombination mechanism is missing. The present work specifically addresses this question. In particular, Ti containing α-Al_2O_3 crystal samples were annealed out and the consequences of these treatments were assessed using optical absorption (OA), photoluminescence (PL) and TL methods.

2. SAMPLES AND EXPERIMENTAL CONDITIONS

We have studied two sapphire crystals provided by Inmas Ltd. (Hungary) and by RSA (France), respectively. Both crystals were cut into 1-2 mm thick slices with surface parallel (Inmas) or perpendicular (RSA) to the C_3 axis. They were given a surface polish by diamond suspension.

The Inmas sample is fairly pure with about 190 ppm Na, 50 ppm Fe, 3 ppm Ti, and 3 ppm Cr as main impurities. Being industrial secret, we ignore the preparation conditions of the as-received crystal (sample AS#IN), but it was shown earlier (Molnar et al., 2000) that it is of Al_2O_3:C (anion deficient) type, i.e. it was prepared in highly reducing conditions. A part of this crystal was annealed at 1450 °C for two hours in pure oxygen gas (sample OX#IN).

The RSA crystal was grown by the Verneuil technique. Its impurity content is rather high, with about 500 ppm Si, 250 ppm Fe, 150 ppm Ca and 50 ppm Ti as main impurities. The crystal (sample 17#RSA) used in this study was annealed in air at 1700 °C for 24 h.

OA spectra were measured at room temperature (RT) in air using a Cary-500 spectrophotometer. OA isochronal annealing was accomplished in an air oven following X-ray irradiation (Cu anode, 45 kV, 30 mA). PL excitation and emission spectra were taken at RT in air. The exciting light was obtained from a xenon arc lamp (Oriel 6261) through a Jobin-Yvon H25 monochromator. The emitted light was detected through a Jobin-Yvon H25 monochromator by a Hamamatsu R928 photomultiplier (PM). The light selection of the two monochromators was improved using appropriate narrow band interference and high pass cut-off filters (Oriel or MTO). PL spectra were corrected only for the spectral irradiance of the xenon lamp. TL measurements were carried out from RT to 350 °C at a heating rate of 0.5 °C/s. Prior to heating, samples were irradiated at RT by X-rays (Cu anode, 45 kV, 10 or 30 mA). TL glow peaks were detected either by a Philips XP-2262B PM tube or by an optical multichanel analyzer (OMA) which consists of an optical fiber (fused silica) and a Chromex 250IS spectrograph equipped with a CCD detector (LN-1100PB-UV/AR, Princeton Instruments). The TL emission spectra were not corrected for the spectral response of the OMA.

3. RESULTS

Optical absorption

Figure 1 shows the absorption spectra of the crystals. F center (6.05 eV), F^+ center (4.8 and 5.4 eV) and weak Ti^{3+} (2.5 eV) absorption bands are clearly observed in the as-received AS#IN sample. Following oxidation (OX#IN samples), these bands disappear and new bands emerge between 5 and 6.5 eV which we assign to

impurity charge transfer transitions. Among these bands we could identify Ti^{4+} ions which absorb around 5,4 eV (Molnar et al., 2000).

The RSA sample absorb all light in the UV region because of its high impurity content. This crystal have a weak blue coloration due to impurity related absorption bands in the visible range (near 2.1 and 3.1 eV).

Following X-ray irradiation, the absorption of Ti^{3+} and Ti^{4+} decreases in AS#IN and OX#IN samples, respectively (Molnar et al., 2000). Their initial (i.e. before irradiation) absorption can be restored by heating the sample to 350 °C (Ti^{4+}) and to 750 °C (Ti^{3+}). Moreover, we note that a large absorption band centered at 3.0 eV is induced in oxidized samples (OX#IN and 17#RSA) by X-ray irradiation. This composite band is due to hole trapping at aluminium vacancies (Evans et al., 1995).

Photoluminescence

All samples contain more or less Ti^{3+} ions as witnessed by the well known 1.7 eV (FWHM ~0.35 eV) $^2E \rightarrow {}^2T$ luminescence and associated excitation doublet around 2,5 eV. Moreover, in RSA and OX#IN samples, we observed a large luminescence band around 2.8 eV (FWHM ~0.7 eV) and an associated excitation band around 5,2 eV (FWHM ~0.6 eV) that we attribute to Ti^{4+} ions (figure 2). However, the form of the excitation and emission spectra suggest as if they were composed of more than one bands. Since we have no time resolution, we tried to separate these components using different excitation wavelength. These experiences allowed us to show that there exist at least three or four emitting components extending from the blue to the green region of the spectrum (figure 2).

Thermoluminescence

TL glow curve of the RSA sample consists of peaks at around 85 (appearing only as a shoulder), 145, 240 and 285 °C (figure 3). These TL peaks have similar emission spectra with a predominant large emission band near 2.55 eV (FWHM ~0.75 eV) and with a weak emission due to Cr^{3+} ions at 1.79 eV (FWHM ~0.015 eV) and Ti^{3+} ions near 1.7 eV (figure 4). The OX#IN sample exhibit similar TL glow peaks than the RSA sample (figure 3). However, the 240 and 285 °C peaks are superposed and are more intense. Moreover, the 145 °C peak is less resolved because of the apparition of two shoulders around 120 and 175 °C. TL peaks of OX#IN sample are characterized by a large emission band at around 2.15 eV (FWHM ~0.45 eV) and by emissions due to Cr^{3+} and Ti^{3+} ions near 1.79 and 1.7 eV (figure 4). To our knowledge, the origin of the 2.15 eV band is not known. On the other hand, the AS#IN sample exhibit only one but very intense TL peak around 175 °C (figure 3). The emission of this peak is composed mainly of F center emission around 3.0 eV (FWHM ~0.4 eV) but emissions due to Cr^{3+} and Ti^{3+} ions near 1.79 and 1.7 eV, respectively, are also observed (figure 4).

4. DISCUSSION

Titanium can be present in sapphire in the trivalent and the quadrivalent state. Red luminescence and corresponding absorption of Ti^{3+} ion are well known and understood. The luminescence of Ti^{4+} ion is of a more complicated nature. In 1990, Blasse and Verweij identified a blue emission band as a result of charge transfer transition involving Ti^{4+} ion. Using times resolved spectroscopy, this emission was shown to be of a complex nature (Macalik et al., 1992). The blue and green components of this complex emission were then ascribed as the luminescence of non-locally and locally compensated Ti^{4+} ions, respectively (Yamaga et al., 1994). If we adopt these results to our observations, we can reason as follows.

Oxidation of sapphire increases the ratio of Ti^{4+} over Ti^{3+} ions (figure 1). Formation of Ti^{4+} ions involves the formation of aluminium vacancies for charge compensation. The clustering of these vacancies with Ti^{4+} ions is favorable due to the high binding energy of such clusters. Different clusters [(Ti^{4+}, V_{Al}^{3-}), $(Ti^{4+}, V_{Al}^{3-}, Ti^{4+})$, etc.] are formed that will exhibit slightly different luminescence spectra (figure 2).

Following irradiation, Ti^{3+} and Ti^{4+} absorption bands decrease, i.e. charges are localized at these ions. While heating the crystals, the absorption bands are successively regained. However, we could not correlate a unique TL peak with Ti^{3+} or Ti^{4+} absorption bands. This means that Ti^{3+} and Ti^{4+} ions act as recombination centers. Since these recombination phenomena are radiative they result in TL glow.

The recombination mechanism can be established if one knows the sign of the released charge. We have shown earlier that the 175 °C glow peak results from an electron release followed by radiative recombination (Molnar et al., 1999). In this case the obvious explanation for the observation of Ti^{3+} emission is a reaction of the type $e^- + Ti^{4+} \rightarrow (Ti^{3+})^* \rightarrow Ti^{3+} + h\nu(1.7\ eV)$. This, in turn, leads to the assumption that Ti^{3+} ions are hole traps. On the other hand, Ti^{4+} emission is connected to 145 and 240 °C glow peaks. These peaks were described earlier as a result of hole delocalization from different kinds of aluminium vacancies (Molnar et al., 2000). For this reason, the emission of Ti^{4+} will be explained by a reaction of the type $h^+ + Ti^{3+} \rightarrow (Ti^{4+})^* \rightarrow Ti^{4+} + h\nu(2.55\ eV)$. Consequently, we suggest that during irradiation Ti^{4+} ions trap electrons. The point of interest

here is that we observe only the green emission (2.55 eV) of locally compensated Ti^{4+} ions in the TL glow. The blue emission (2.85 eV) of isolated Ti^{4+} ions is not visible. This phenomena is probably due to spatial correlation between traps (V_{Al}) and recombination centers (Ti^{4+}). Finally, we note that in some cases Ti^{3+} emission is also observed for the 145 and 240 °C peaks. This emission can perhaps be explained by invoking re-absorption of either the 2.15 eV (OX#IN sample) or the 2.55 eV (17#RSA sample) emissions. However, we can not rule out the possibility of the reaction $h^+ + Ti^{2+} \rightarrow (Ti^{3+})^* \rightarrow Ti^{3+} + h\nu(1.7\ eV)$, though we think that the formation of Ti^{2+} is not favorable.

5. CONCLUSION

We have seen that Ti^{3+} and Ti^{4+} ions act as emission centers in the thermoluminescence of sapphire. From the dosimetric point of view, Ti^{3+} emission is to be avoided because it interferes with the incandescence of the heating element. On the other hand, green-blue Ti^{4+} emissions are well suited to the spectral domain of commonly used PM tubes. Naturally, this emission can only be exploited in oxidized samples and one must also take care of concentration quenching phenomena.

As for the Ti^{3+}, we propose to study their effects on the dosimetric peak of Al_2O_3:C. For this, OX#IN samples were treated under highly reducing conditions in the presence of graphite. The results of these experiences should appear in another paper.

Acknowledgements - We would like to thank Mr. J. Vallayer (Ecole Central de Lyon) for providing the Verneuil crystals. One of the authors (G.M.) gratefully acknowledges financial support received from the Ministry of Foreign Affairs of the French Republic in the form of a Graduate Research Fellowship.

REFERENCES

Blasse G., Verweij J.W.M., (1990) The luminescence of titanium in sapphire laser material, *Mater. Chem. Phys.* vol. 26, 131-137.

Evans B.D., (1994) Ubiquitous blue luminescence from undoped synthetic sapphires, *J. Lumin.* vol 60/61, 620-626.

Evans B.D., Cain L.S., (1995) A cation vacancy center in crystalline Al_2O_3, *Radiat. Effects & Def. in Solids* vol 134, 329-332.

Macalik B., Bausa L.E., Garcia-Sole J., Jaque F., Munoz Santiuste J.E., Vergara I., (1992) Blue emission in Ti-sapphire laser crystals, *Appl. Phys. B* vol 55, 144-147.

Mehta S.K., Sengupta S., (1976) Gamma dosimetry with α-Al_2O_3 thermoluminescent phosphor, *Phys. Med. Biol.* vol 21, 955-964.

Molnár G, Papin E., Grosseau P., Guilhot B., Borossay J., Benabdesselam M., Iacconi P., Lapraz D., (1999) Thermally stimulated luminescence and exoelectron emission mechanism of the 430 K (D') dosimetric peak of α-Al_2O_3, *Radiat. Prot. Dosim.* vol 84, 253-256.

Molnár G, Borossay J., Benabdesselam M., Iacconi P., Lapraz D., Süvegh K., Vértes A., (2000) Oxidation/reduction effects on the thermoluminescence of α-Al_2O_3 single crystals, *Phys. Stat. Sol. (a)* vol 179, 249-260.

Portal G., Lorrain S., Valladas G., (1980) Very deep traps in Al_2O_3 and $CaSO_4$:Dy, *Nucl. Instr. & Methods* vol 175, 12-14.

Surdo A.I., Kortov V.S., Sharafutdinov F.F., (1999) Luminescence of anion-defective corundum with titanium impurity, *Radiat. Prot. Dosim.* vol 84, 261-264.

Wong W.C., McClure D.S., Basun S.A., Kokta M.R., (1995) Charge-exchange processes in titanium doped sapphire crystals. II. Charge-transfer transition states, carrier trapping and detrapping, *Phys. Rev. B* vol 51, 5693-5698.

Yamaga M., Yosida T., Hara S., Kodama N., Henderson B., (1994) Optical and electron spin resonance spectroscopy of Ti^{3+} and Ti^{4+} in Al_2O_3, *J. Appl. Phys.* vol 75, 1111-1117.

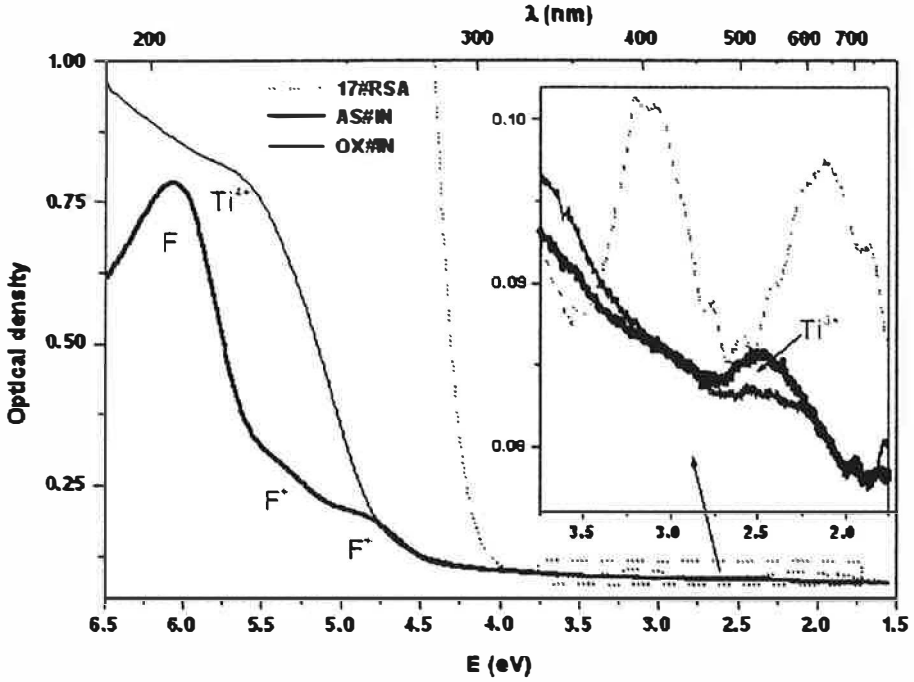

Figure 1. UV-VIS absorption of sapphire crystals (designation of the legend in the text)

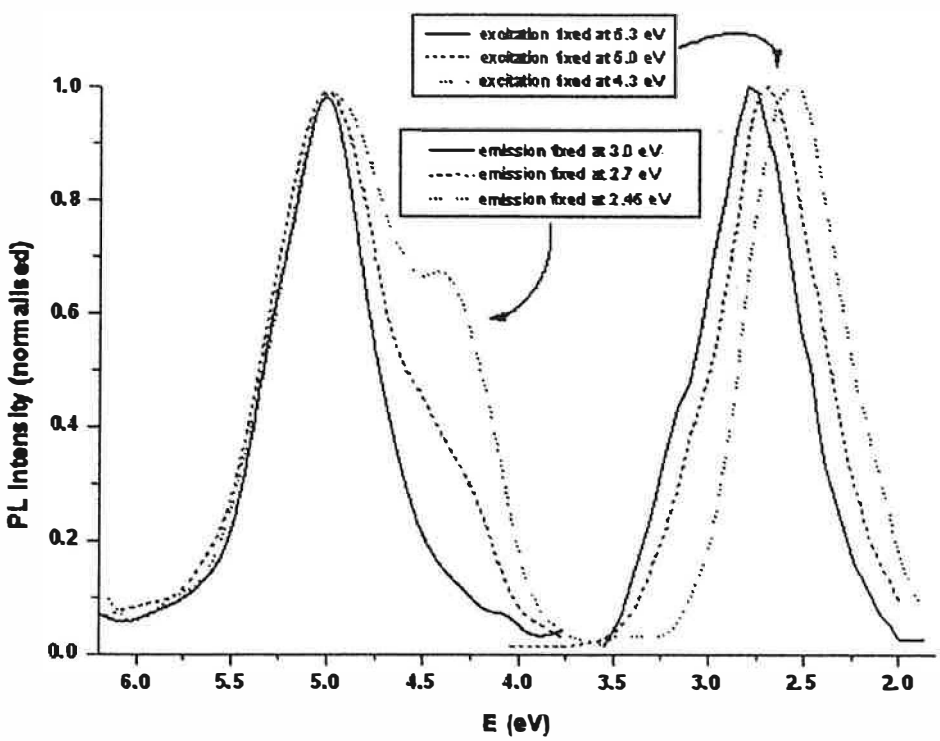

Figure 2. Excitation and emission spectra of Ti^{4+} luminescence in the 17#RSA sample (normalized)

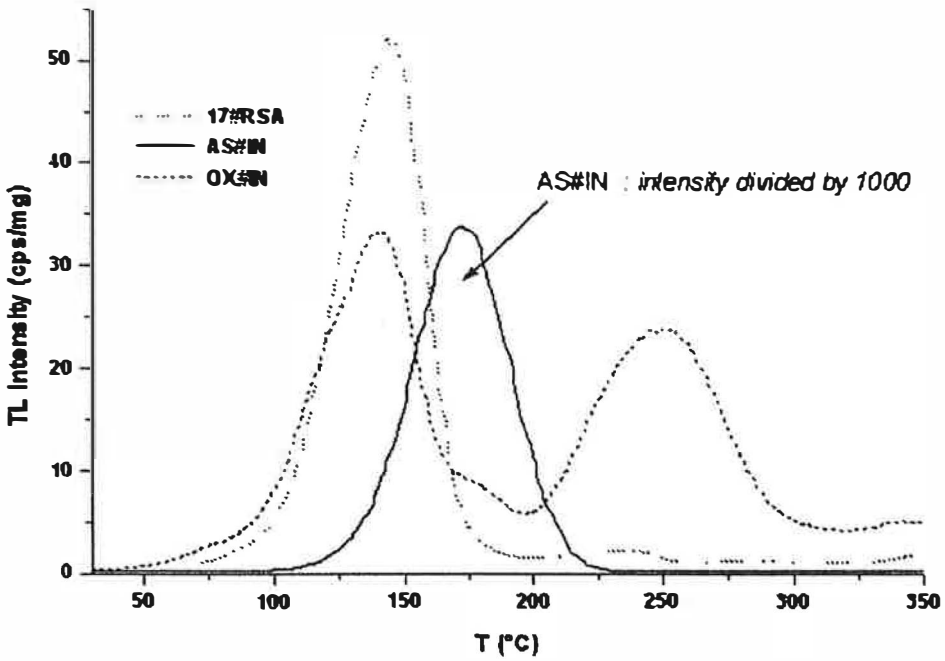

Figure 3. TL glow curves (per unity of mass) of sapphire crystals following 20 Gy X-ray irradiation (designation of the legend in the text)

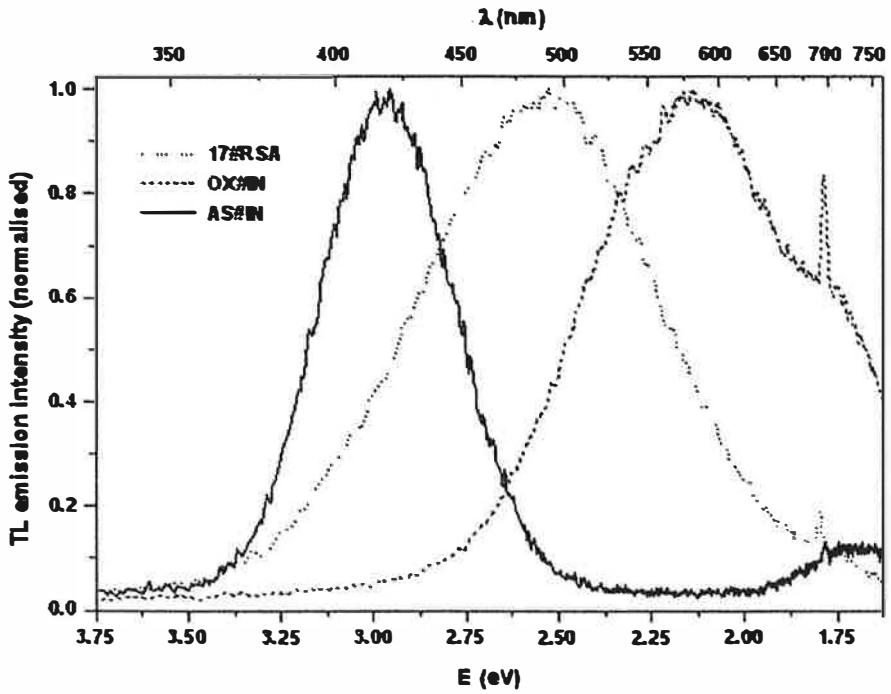

Figure 4. TL emission spectra of sapphire crystals at 125 °C following 1 kGy X-ray irradiation (designation of the legend in the text)

7. Mössbauer Spectroscopic and Optical Study of Iron Incorporation into Alumina Powders

Abstract - We used iron probe to study how doping elements are incorporated into α-alumina powders by the impregnation method. Although perturbed by relaxation phenomena, Mössbauer spectroscopy proved to be a fast and informative tool to follow the incorporation of iron. On the basis of Mössbauer data, optical absorption and thermoluminescence of the samples were also discussed.

Keywords: D. Mössbauer spectroscopy; D. defects; iron doped α-alumina

1. INTRODUCTION

Specially prepared alpha-alumina (corundum) ceramics or single crystals can be advantageously used for thermoluminescence (TL) dosimetry [1]. Alumina dosemeters, like all other TL materials, are known to be strongly influenced by different impurities. However, in case of this material, the role of impurities is not well known. Therefore, a systematic study was started on this subject [2-4]: impurities were incorporated into an ultra-pure alumina powder by the impregnation method and the TL response of these doped powders was then compared.

The impregnation method permits to obtain doped alumina powders with reproducible morphology and thermoluminescent properties. However, to understand the role of a given doping element we should also know how it is incorporated, if so, in the host lattice. The questions which arise concern homogeneity, phase composition, crystallographic site, coordination and valency of the dopant. Taking into consideration the doping levels (generally between 10 and 1000 ppm), these questions are usually difficult to answer unequivocally. This is especially true in case of powdered samples since sophisticated optical and ESR methods can be really exploited only with single crystal samples.

From the TL dosimetric point of view, iron is an undesired impurity because (at concentrations above 100-200 ppm) it quenches thermoluminescence in alumina (poison effect) [4-5]. On the other hand, iron (^{57}Fe) can be used as a tracer element because it can be studied by Mössbauer spectroscopy that gives information about hyperfine interactions between the ^{57}Fe nucleus and its environment in the crystal lattice. From this data, valency, bonding, coordination and clustering of iron can be deduced. This is the reason why we have chosen iron as a probe to study the phenomena which occur while doping elements are incorporated into alumina powders by the impregnation method.

The Mössbauer spectra and Mössbauer parameters of Fe^{3+} and Fe^{2+} ions in some α-Al_2O_3 samples have already been reported [5-9]. Spectra with dilute (less than 0.1 %) paramagnetic Fe^{3+} were complicated by spin-lattice relaxation effects [6]. On the other hand, Fe^{2+} was found to form different defect clusters with other impurities [7].

2. EXPERIMENTAL PROCEDURES

Sample preparation and characterization

Several α-Al_2O_3:Fe powders were prepared by the impregnation technique which consists of four steps. First a pure (> 99.99 %) high surface area (110 m^2/g) γ-Al_2O_3 powder is mixed with the aqueous solution of $Fe(NO_3)_3$. Then this mixture is dried at 100 °C for 24 hours. The next step is the decomposition of nitrates at 600 °C for 24 hours in an air oven. The last step is the calcination at high temperature (1250 - 1450 °C) for 2 hours when the γ-Al_2O_3 is transformed into α-Al_2O_3 and impurities are incorporated into the bulk material. The calcination is achieved in a horizontal tube furnace under continuous gas flow. Different gases (O_2 or Ar or Ar + H_2) were used to ensure oxidative or reducing preparation conditions. Such way, several samples were prepared with different Fe concentrations and under different calcination conditions (Table 1). The samples with Fe concentration less than 5000 ppm were prepared with $^{57}Fe(NO_3)_3$ (> 99 % ^{57}Fe isotopic enrichment) in order to facilitate Mössbauer measurements.

According to X-ray diffraction patterns, the powders prepared this way are of α-Al_2O_3 phase (> 95 %). Their specific surface is around 2-3 m^2/g with an average grain size of about 0.5 μm. Grain size and specific

surface slightly vary in function of the calcination temperature but not sensitive to the preparation atmosphere [4].

Spectroscopy measurements

The Mössbauer spectroscopy measurements were carried out at room temperature (RT) using a conventional Mössbauer spectrometer in constant acceleration mode (Wissel). The γ-rays were provided by a ^{57}Co(Rh) source. All isomer shift data are given relative to α-Fe throughout this paper. For spectrum evaluation we used the MössWinn 3.0 program package.

Optical absorption of the samples (~150 mg) was studied at RT in the 250 - 1500 nm range using a Carry 5 spectrophotometer equipped with a diffuse reflection sphere. The absorption reference was made of Teflon powder.

3. RESULTS AND ANALYSIS

Mössbauer spectra

The Mössbauer data obtained on samples subjected to various thermal treatments are collected in Table 2. A thermal treatment of the ^{57}Fe-impregnated (5000 ppm) γ-Al_2O_3 powder at 600 °C in air led to the formation of an amorphous iron oxide phase on the surface of γ-alumina particles as deduced from the isomer shift and the quadrupole splitting values. Such species has been observed earlier by others (e.g. [10]). The conversion of the Fe-nitrate into oxide is consistent with the IR spectroscopic observation of NO_x evolution at this stage of the preparation [4].

At 1450 °C, iron is incorporated into bulk alumina grains entirely as Fe^{3+} ions when using pure oxygen or argon for calcination (Table 2). At high iron concentration (5000 ppm), we can observe a highly distorted lineshape due to paramagnetic spin relaxation (Fig. 1). It was possible to fit the spectrum with the Blume-Tjon two state relaxation model which resulted in an isomer shift characteristic to Fe^{3+}. With decreasing iron concentration, we observed (Fig. 1) more and more resolved magnetic hyperfine structure in the oxidized (prepared in O_2 or Ar) samples which is consistent with our assumption that Fe is distributed in the lattice in monomeric form and the condition for the paramagnetic relaxation is determined by the average distance between the Fe^{3+} ions in the α-Al_2O_3 lattice. Thus we can conclude that iron does not form clusters in diluted (<500 ppm) systems under non-reductive conditions.

Samples prepared in reducing atmosphere (Ar + H_2) gave much weaker Mössbauer signals than expected from the nominal iron concentrations. We attributed this phenomenon to the reduction of iron oxide to metallic iron that can evaporate from the sample at high temperature. This loss in the iron content of the samples increased at higher calcination temperatures and at higher partial pressure of hydrogen. The remaining iron in these samples proved to be a mixture of Fe^{3+}, Fe^{2+} and metallic Fe (Fig. 1, Table 2) according to the Mössbauer data. The fraction of the reduced species in the spectra was larger when the calcination temperature and the hydrogen concentration were higher. The linewidths were anomalously high in each case (0.6-1 mm/s) indicating distribution of hyperfine parameters. This non-uniform environment for a given iron species can be due to non-homogenous doping.

From the Mössbauer parameters, it can also be deduced that Fe^{3+} is a high spin 6-coordinated species, i.e. substituting for Al^{3+} ions in the hexagonal corundum lattice [7]. However, it is interesting to note that in reduced samples we can not see magnetic hyperfine structure of Fe^{3+} but only paramagnetic doublets even at low Fe^{3+} concentrations (Fig. 1, Table 2). A possible explanation of this phenomenon is clustering of Fe^{3+} which can account for fast spin-spin relaxation and therefore paramagnetic behavior in the Mössbauer spectrum. The driving force for the clusterization, logically, is the reduction of the lattice, i.e. the increased number of oxygen vacancies. Clusterization is also supported by the Mössbauer parameters of the Fe^{2+} species found in the reduced samples. On the basis of the relatively low isomer shifts, the coordination of Fe^{2+} ions is less than 6. Fe^{2+} ions substituting for Al^{3+} ions have a net negative charge and a large ionic radius (77 pm) as compared with Al^{3+} ions (53 pm). To reduce lattice strain and ensure charge neutrality, Fe^{2+} is usually thought to form clusters with oxygen vacancies [11] which can account for the lower coordination of Fe^{2+}. Burns et al. [7] observed Fe^{2+} with parameters ($\delta \cong 1$ mm/s, $\Delta \cong 2$ mm/s) similar to ours and assigned them to Fe^{2+} ions located next to Fe^{3+} ions. In our case, this assignment is supported by the fact, that in the case of the 5000-5H_2-1450 sample, where Fe^{3+} concentration is relatively low, another Fe^{2+} species occurs as well. Therefore, we propose that two types of Fe^{2+} clusters are present in our samples: one formed with an oxygen vacancy ($\delta = 1.0$ mm/s, $\Delta = 0.9$ mm/s) and another type where beside the oxygen vacancy there is a Fe^{3+} ion as well ($\delta \cong 0.9$

mm/s, $\Delta \cong 2.3$ mm/s). Dézsi et al. [8] also observed two types of Fe^{2+} species in α-Al_2O_3 originally doped with ^{57}Co, the mother nuclide of the ^{57}Fe Mössbauer isotope. The isomer shifts (0.78 mm/s for both) were somewhat lower then the ones found by us, and the quadrupole splittings (2.7 mm/s and 1.6 mm/s) were significantly higher than ours. These authors suggested that the low isomer shift might be due to electron hopping between Fe^{2+} and Fe^{3+}. This may also be reasonable in our case when the co-existence of Fe^{2+} and Fe^{3+} is assumed in a cluster (δ= 0.85-0.91 mm/s). To explain the higher quadrupole splittings one has to take into account that, in the experiment of Dézsi et al., the original dopant is Co. This ion prefers lower coordination than Fe, thus its local environment must contain more oxygen vacancies on the average. This environment is preserved for iron within the 10^{-8}-10^{-6} s Mössbauer time window after the electron capture decay of ^{57}Co. It is reasonable to assume that the variation of the Mössbauer parameters of Fe^{2+} in different experiments is due to the different preparation conditions, which results in different vacancy distribution in one or another particular sample.

Irradiation of the samples (UV or X-ray) did not affect the Mössbauer spectra. Let us note that although, in general, paramagnetic relaxation makes it difficult to evaluate Mössbauer spectra because of the complicated line shape, one expects that in an intermediate relaxation state any perturbation of the Fe^{3+} ions (excitation, changing of the spin or valence state) should result in a dramatic change in the Mössbauer spectrum. We did not observe such change. This means that possible altered oxidation or excitation states of Fe are not involved in the long life time excited states (responsible for TL processes) of the doped Al_2O_3 lattice.

Diffuse reflection

Absorption spectra of samples prepared under oxygen or argon are identical (such as their Mössbauer spectra). Spectra of reduced ($Ar+H_2$) samples are quite different: peaks due to Fe^{2+} and oxygen vacancies can be observed (Fig. 2).

Absorption bands of iron in α-alumina can be classified as charge transfer, crystal field, exchange coupling or intensified crystal field transitions [11]. Charge transfer band of Fe^{3+} have very intense absorption peak at 38700 cm^{-1} [12] and could be readily observed in each sample containing Fe^{3+}. However, samples without any Fe (e.g. 500-2.5H_2-1450) have also a band around this wavelength (at 38200 cm^{-1}) but we believe that this band is due to F^+ center absorption since F^+ centers are known to be formed in alumina under reducing conditions [1]. In samples with 5000 ppm Fe^{3+}, a series of bands (around 22200, 25800, 26500 and 30200 cm^{-1}) can be observed which are due to magnetically coupled Fe^{3+} pairs [13]. Forbidden crystal field absorption of Fe^{3+} at 18200 cm^{-1} [14] appears weakly. In the 5000-5H_2-1450 sample an intense band appears at around 10700 cm^{-1}. This composite band is of Fe^{2+} crystal field transition [11, 15] This band is supposed to be intensified by lowered site symmetry that was shown by Mössbauer spectroscopy.

Absorption of the reduced samples decreases with increasing calcination temperature and hydrogen concentration, i.e. with smaller iron content. In these samples, the origin of the absorption peak at 22000 cm^{-1} and between 35000 and 25000 cm^{-1} is not clear but they must be related to Fe^{3+}.

Thermoluminescence

In comparison with the non-doped samples [2-4], iron doping has not introduced new TL peaks neither new emissions: we observed the same two glow peaks (at 200 and 350 °C) and the same emission spectra (Cr^{3+}). This means that iron ions are not trapping nor recombination sites as it was also demonstrated by Mössbauer spectroscopy. Furthermore, TL glow intensity is clearly related to optical absorption: samples with higher absorption (i.e. high iron concentration) show less intense TL (poison effect). However, samples with only 50 ppm Fe do not follow this simple rule: their TL properties are determined not by iron ions but other point defects.

4. CONCLUSION

The iron doped alumina sample heated in oxygen ambient contains isolated Fe^{3+} species substituting for Al^{3+} in six-fold coordination environment. The Mössbauer signal and optical absorption of this Fe^{3+} species depends on the average distance of Fe^{3+} ions from each other in the lattice, i.e. on their concentration. In case of low concentration, the otherwise paramagnetic Mössabuer doublets tend to show magnetic hyperfine splitting and exhibit complicated relaxational line shape. On the other hand, at high concentration, exchange coupled bands appear in the optical absorption spectra.

Upon reduction, oxygen vacancies form in the lattice, which accelerate diffusion of Fe and clusterization takes place. Clustered Fe^{3+} shows paramagnetic Mössbauer signal. Simultaneously, Fe^{3+} is

reduced, and markedly different Fe^{2+} species form depending on the type of species associated in the clusters (oxygen vacancies, Fe^{3+} or both). Finally, the formation of metallic iron presumes that large clusters are formed probably at grain boundaries and are reduced to volatile metallic iron which can evaporate from the sample at high temperature.

Acknowledgements - The authors wish to thank Mr. B. Guilhot, P. Grosseau and E. Papin (Ecole des Mines, St-Etienne, France) for the sample preparation facilities and for useful discussions. One of the authors (G.M.) gratefully acknowledges financial support received from the Ministry of Foreign Affairs of the French Republic in the form of a Graduate Research Fellowship. The Mössbauer measurements have been sponsored by OTKA T030835/1999.

REFERENCES

1. S.W.S. McKeever, M. Moscovitch and P. D. Townsend, Thermoluminescence Dosimetry Materials: Properties and Uses, Ch. 5, Nuclear Technology Publishing, Ashford, 1995
2. E. Papin, P. Grosseau, B. Guilhot, M. Benabdesselam, P. Iacconi and D. Lapraz, Influence of the calcining conditions on the thermoluminescence of pure and doped alumina powders, Radiat. Prot. Dosim. 65 (1996), 243-246.
3. E. Papin, P. Grosseau, B. Guilhot, M. Benabdesselam and P. Iacconi, Influence of point defects on the thermoluminescence of α-Al_2O_3, Radiat. Prot. Dosim. 84 (1999), 91-94.
4. E. Papin, Ph. D. Thesis, Ecole des Mines, St-Etienne, France, 1997.
5. A. S. Marfunin, Spectroscopy, Luminescence and Radiation Centers in Minerals, Ch. 1, Springer-Verlag, Berlin/Heidelberg, 1979
6. G. K. Wertheim and J. P. Remeika, Mössbauer effect hyprefine structure of trivalent Fe^{57} in corundum, Phys. Lett. 10 (1964), 14-15.
7. R.G. Burns and V.M. Burns, Optical and Mössbauer spectra of transition-metal-doped corundum and periclase, in: F. J. Berry and D. J. Vaughan (Eds), Advances in Ceramics. Vol. 10, Structure and Properties of MgO and Al_2O_3 Ceramics, Chapman and Hall, London/New York, 1985, p. 46-61.
8. I. Dézsi, I. Szucs, Cs. Fetzer, H. Pattyn, G. Langousche, H.D.. Pfannes, and R. Magalhaes-Paniago, Local Interactions of ^{57}Fe after electron capture of ^{57}Co implanted in α-Al_2O_3 and in α-Fe_2O_3, J. Phys.: Condens. Matter 12 (2000) 2291-96
9. J. Hess and A. Levy, Response of the Mössbauer spectrum of paramagnetic Fe^{3+} in Al_2O_3 to nuclear dipole fields, Phys. Rev. B 22 (1980), 5068-78.
10. L. Lévay, Y. Takashima, E. Kuramoto, J. Juhász, B. Lévay and A. Vértes, Studies of Fe_2O_3/ γ-Al_2O_3 surfaces by positron annihilation, Mössbauer spectroscopy and scanning electron microscopy, Mater. Sci. Forum 105-110 (1992), 1633-1636.
11. A. R. Moon and M. R. Phillips, Defect clustering and color in Fe,Ti: α-Al_2O_3, J. Am. Ceram. Soc. 77 (1994), 356-367.
12. H. H. Tippins, Charge-transfer spectra of transition-metal ions in corundum, Phys. Rev. B 1 (1970), 126-135.
13. J. J. Krebs and W. G. Maisch, Exchange effects in the optical-absorption spectrum of Fe^{3+} in Al_2O_3, Phys. Rev. B 4 (1971), 757-768.
14. D. S. McClure, Optical spectra of transition-metal ions in corundum, J. Chem. Phys. 36 (1962), 2757-2779.
15. G. Lehmann and H. Harder, Optical spectra of di- and trivalent iron in corundum, Am. Mineral. 55 (1970), 98-105.

sample notation	Fe (ppm)	calcination T (°C)	calcination atmosphere
γ-Al_2O_3	5000	600	air
5000-O_2-1450	5000	1450	O_2
5000-5H_2-1450	5000	1450	Ar + 5 % H_2
500-O_2-1450	500	1450	O_2
500-Ar-1450	500	1450	Ar
500-5H_2-1450	500	1450	Ar + 5 % H_2
50-O_2-1450	50	1450	O_2
50-Ar-1450	50	1450	Ar
50-5H_2-1450	50	1450	Ar + 5 % H_2
500-2.5H_2-1250	500	1250	Ar + 2.5 % H_2
500-2.5H_2-1350	500	1350	Ar + 2.5 % H_2
500-2.5H_2-1450	500	1450	Ar + 2.5 % H_2
500-1H_2-1350	500	1350	Ar + 1 % H_2
500-5H_2-1350	500	1350	Ar + 5 % H_2

Table 1: α-Al_2O_3:Fe powder samples and preparation conditions

sample	Ox.	I %	δ mm/s	Δ mm/s	Γ mm/s	HF kOe
γ-Al_2O_3	+3	100	0.27	1.05	0.94	-
5000-O_2-1450	+3	100	relaxation spectrum			
5000-5H_2-1450	+3	48	relaxation spectrum			
	+2	28	1.02	0.94	0.69	-
	+2	24	0.91	1.91	0.49	-
500-O_2-1450	+3	100	relaxationally broadened sextet			
500-Ar-1450	+3	100	relaxationally broadened sextet			
500-5H_2-1450	+2	100	1.00	0.58	0.26	-
50-O_2-1450	+3	100	weak magnetic sextet			
50-Ar-1450	+3	100	weak magnetic sextet			
50-5H_2-1450	no iron detected					
500-2.5H_2-1250	+3	96	0.33	0.87	0.56	-
	+2	4	0.90	2.41	0.50	-
500-2.5H_2-1350	+3	87	0.34	0.86	0.58	-
	+2	13	0.91	2.16	0.74	-
500-2.5H_2-1450	no iron detected					
500-1H_2-1350	+3	90	0.34	0.87	0.56	-
	+2	10	0.91	2.14	0.79	-
500-5H_2-1350	+3	54	0.35	0.85	0.59	-
	+2	15	0.79	2.18	1.15	-
	0	31	0.015	-	0.86	327

Table 2: Fe species and their Mössbauer parameters in α-Al_2O_3:Fe samples
(Ox.: oxidation state of the iron species, I: relative spectral intensity of the iron species, δ: isomer shift (relative to α-Fe), Δ: quadrupole splitting, Γ: line width at half maximum, HF: magnetic hyperfine field)

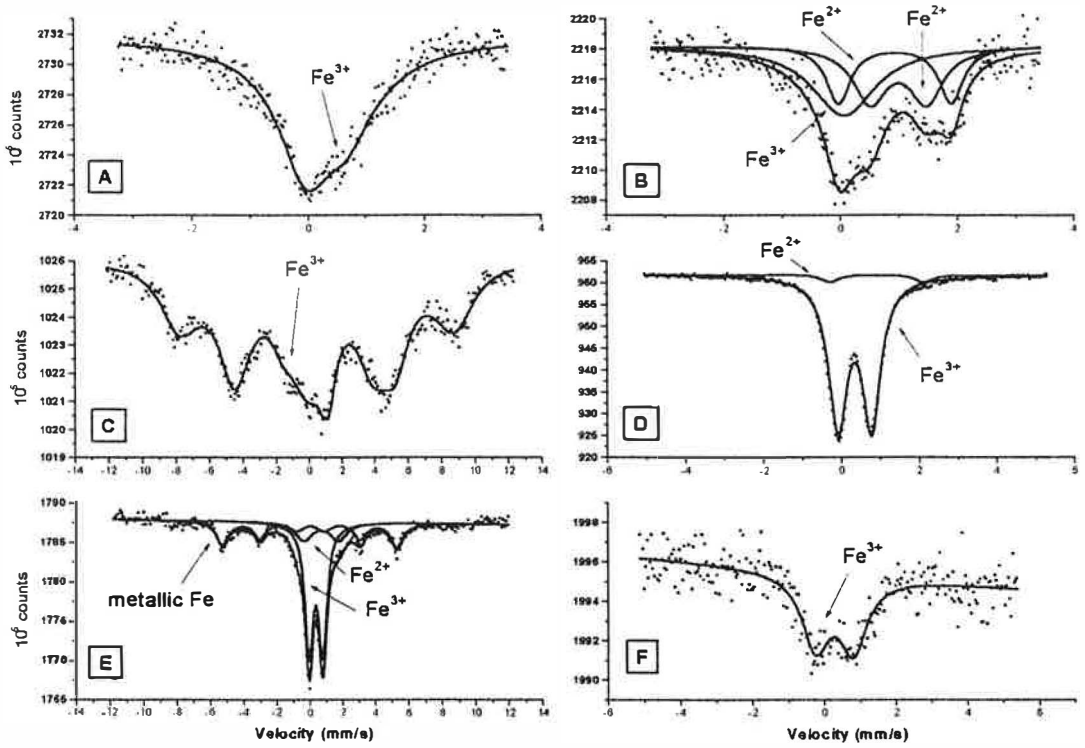

Figure 1: Room temperature Mössbauer spectra of some selected α-Al_2O_3:Fe powders. A: Sample 5000-O_2-1450; B: Sample 5000-5H_2-1450; C: Sample 500-O_2-1450; D: Sample 500-2.5H_2-1250; E: Sample 500-2.5H_2-1350; F: Sample γ–Al_2O_3 (See notation in Table 1)

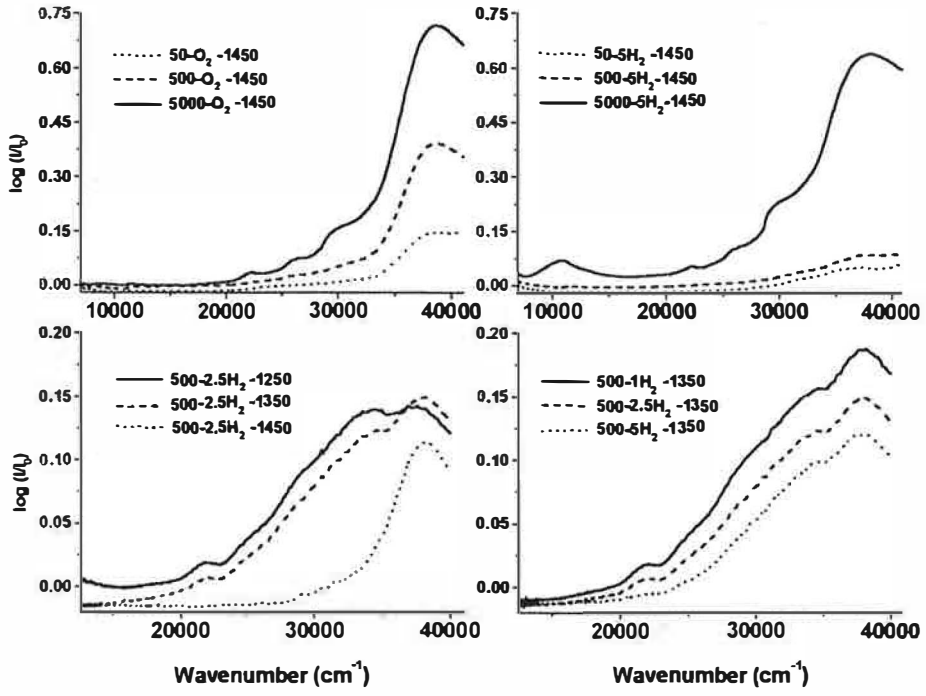

Figure 2: Room temperature optical (diffuse reflection) spectra of different α-Al_2O_3:Fe powders

REFERENCES BIBLIOGRAPHIQUES

IRODALMI HIVATKOZÁSOK

[ABR78] Abramov V.N., Ivanov B.G., Kuznetsov A.I., Meriloo I.A., Musatov M.I., **On the vacuum ultraviolet transparency of sapphire,** *Phys. Stat. Sol. (a) 48, 287-292 (1978)*

[ADD90] Addi D., **Réalisation d'un dispositif destiné à l'étude de l'émission exoélectronique thermostimulée entre 77 et 675 K. Caractérisation d'un phénomène de phototransfert dans l'alumine alpha,** *Thèse, Université Paul Sabatier de Toulouse, France (1990)*

[AGE99] Agersnap-Larsen N., Botter-Jensen L., McKeever S.W.S., **Thermally stimulated conductivity and thermoluminescence from Al_2O_3:C,** *Rad. Prot. Dosim. 84 (1-4), 87-90 (1999)*

[AGU88] Agullo-Lopez F., Catlow C.A., Townsend P.D., **Point defects in materials,** *Academic Press, London, England (1988)*

[AKS90A] Akselrod M.S., Kortov V.S., Kravetsky D.J., Gotlib V.I., **Highly sensitive thermoluminescence anion-defective α-Al_2O_3:C single crystal detectors,** *Radiat. Prot. Dosim. 32(1), 15-20 (1990)*

[AKS90B] Akselrod M.S., Kortov V.S., Kravetsky D.J., Gotlib V.I., **Highly sensitive thermoluminescence anion-defective α-Al_2O_3:C single crystal detectors,** *Radiat. Prot. Dosim. 33(1/4), 119-122 (1990)*

[AKS90C] Akselrod M.S., Kortov V.S., **Thermoluminescent and exoemission properties of new high-sensitivity TLD α-Al_2O_3:C crystals,** *Radiat. Prot. Dosim. 33(1/4), 123-126 (1990)*

[AKS91] Akselrod M.S., Kortov V.S., **Combined aluminium-oxide TSEE-TL detectors for skin dosimetry,** ***Rad. Prot. Dosim. 39(1/3), 135-138 (1991)***

[AKS93A] Akselrod M. S., Kortov V.S., Gorelova E.A., **Preparation and properties of α-Al_2O_3:C,** *Radiat. Prot. Dosim. 47 (1/4), 159-164 (1993)*

[AKS93B] Akselrod M.S., Gorelova E.A, **Deep traps in highly sensitive α-Al_2O_3: C TLD crystals,** *Nucl.Tracks Radiat.Meas. 21, 143-146 (1993)*

[AKS98] Akselrod M.S., Agersnap Larsen N., Whitley V., McKeever S.W.S., **Thermal quenching of F-center luminescence in Al_2O_3:C,** *J. Appl. Phys. 84(6), 3364-3373 (1998)*

[ALE89] Alessandri M.F., **Mise en évidence et étude d'un phototransfert de l'émission exoélectronique thermostimulée de l'alumine alpha,** *Thèse, Université Paul Sabatier de Toulouse, France (1989)*

[BAR65] Bartram R.H., Swenberg C.E., Fournier J.T., **Theory of trapped hole centers in aluminium oxide,** *Phys. Rev. 139(3A), A941-A951 (1965)*

[BEN96] Benabdesselam M., Iacconi P., Lapraz D., Petel M., Keller P., Portal G., **Qualification of specially prepared clothing material for gamma dosimetry. Application to neutron-photon radiation fields,** *Rad. Prot. Dosim. 66(1-4), 125-128 (1996)*

[BEN97] Benabdesselam M., Iacconi P., Lapraz D., Serbat A., Dhermain J., Laugier J., **Characterisation of clothing material for gamma dosimetry in mixed neutron-gamma fields,** *Rad. Prot. Dosim. 70(1-4), 461-465 (1997)*

[BER93] Bernache-Assollant D. (éditeur), **Chimie-physique du frittage,** *Hermes, Paris, France (1993)*

[BIG96] Bigarre J., **Effet des impuretés sur la charge d'espace dans l'alumine. Application au frottement,** *Thèse, Ecole Centrale de Lyon, France (1996)*

[BIN94] Bindi R., Lapraz D., Iacconi P., Boutayeb S., **Theoretical analysis of the simultaneous detection method of thermally stimulated conductivity (TSC) and luminescence (TSL) ; application to an α-Al_2O_3 monocrystal,** *J. Phys. D: Appl. Phys. 27, 2395-2400 (1994)*

[BIN97] Bindi R., Iacconi P., Lapraz D., Petel F., **The effective electron affinity estimation from the simultaneous detection of thermally stimulated luminescence and exoelectronic emission. Application to an α-alumina single crystal,** *J. Phys. D: Appl. Phys. 30, 137-143 (1997)*

[BLA90] Blasse G., Verweij J.W.M., **The luminescence of titanium in sapphire laser material,** *Mater. Chem. Phys. 26, 131-137 (1990)*

[BLU63] Blumberg W.E., Eisinger J., Geschwind S., **Cu^{3+} ion in corundum,** *Phys. Rev. 130(3), 900-909 (1963)*

[BOU93] Boutayeb S., **Conductibilité électrique thermostimulée de l'alumine alpha entre 77 et 900 K. Etude et caractérisation d'un phénomène**

photoinduit, *Thèse, Université Paul Sabatier de Toulouse, France (1993)*

[BRE80] Brewer J.D., Jeffries B.T., Summers G.P., **Low temperature fluorescence in sapphire,** *Phys. Rev. B 22(10), 4900-4906 (1980)*

[BRO92] Brousseau M., **Physique du solide,** *Masson, Paris, France (1992)*

[BRO99] Brozel M.R., **Identifying vacancies using positron annihilation,** *III-Vs Review 12(6), 24-27 (1999)*

[BUR84] Burns R.G., Burns V.M., **Optical and Mössbauer spectra of transition metal doped corundum and periclase,** *Adv. in Ceram. 10, 46-61 (1984)*

[CAT82] Catlow C.R.A., James R., Mackrodt W.C., Stewart R.F., **Defect energetics in α-Al_2O_3 and rutile TiO_2,** *Phys. Rev. B 25(2), 1006-1026 (1982)*

[CHA99] Chapouly R., Capdupuy C., Schvoerer M., Bechtel F., **Cathodoluminescence and crystal growth of sapphire,** *Phys. Stat. Sol. (a) 171, 613-621 (1999)*

[CHE81] Chen K., Kirsch Y., **Analysis of thermally stimulated processes,** *Pergamon Press, Oxford, England (1981)*

[COL96] Colyott L.E., Akselrod M.S., McKeever S.W.S., **Phototransferred thermoluminescence in α-Al_2O_3:C,** *Rad. Prot. Dosim. 65(1/4), 263-266 (1996)*

[CON78] Ecole d'été à Confolant - 1977, **Défauts ponctuels dans les solides,** *Les Editions de Physique, Orsay, France (1978)*

[COO78] Cooke D.W., Roberts H.E., Alexander C. Jr., **Thermoluminescence and emission spectra of UV-grade Al_2O_3 from 90 to 500K,** J. Appl. Phys. 49 (6), 3451-3457 (1978)

[COO81] Cooke D.W., Payne I.W., Santi R.S., **Low-temperature TL studies of Al_2O_3,** *J. Appl. Phys. 52(5), 3606-3610 (1981)*

[COO84] Cooke D.W., **Spectral emission from glow peaks in x-irradiated Al_2O_3,** *J. Appl. Phys. 55(9), 3437-3440 (1984)*

[COX71] Cox R.T., **Electron spin resonance studies of holes trapped at Mg^{2+}, Li^+ and cation vacancies in Al_2O_3,** *Solid State Comm. 9, 1989-1992 (1971)*

[COX72] Cox R.T., **Etude par résonance paramagnétique électronique des défauts ponctuels dans l'oxyde d'aluminium Al_2O_3,** *Thèse, Université Scientifique et Médicale de Grenoble, France (1972)*

[CRA82] Crawford J.H.Jr., **A review of neutron radiation damage on corundum crystals,** *J. Nucl. Mater. 108&109, 644-654 (1982)*

[DAS80] Das B.N., **Effect of transition metal impurities on the thermoluminescence of alumina,** *J. Mater. Sci. 15, 515-516 (1980)*

[DAV90] Daviller D., **Influence conjuguée du broyage et du dopage sur certaines propriétés physiques d'alumine monocristalline,** *Thèse, Ecole Nationale Supérieure des Mines de St-Etienne, France (1990)*

[DIE75] Dienes G.J., Welch D.O., Fischer C.R., Hatcher R.D., Lazareth O., Samberg M., **Shell model calculation of some point defect properties in α-Al_2O_3,** *Phys. Rev. B 11(8), 3060-3070 (1975)*

[DRA79] Draeger B.G. , Summers G.P., **Defects in unirradiated α-Al_2O_3,** *Phys. Rev. B 19(2), 1172-1177 (1979)*

[DUT75] Dutt B.V., Kröger F.A., **High temperature defect structure of iron doped α-alumina,** *J. Am. Ceram. Soc. 58(11/12), 474-476 (1975)*

[EMF96] Emfietzoglou D., Moscovitch M., **Phenomenological study of light induced effects in α-Al_2O_3:C,** *Rad. Prot. Dosim. 65(1/4), 259-262 (1996)*

[ENG80] Engstrom H., Bates J.B., Wang J.C., Abraham M.M., **Infrared spectra of hydrogen isotopes in α-Al_2O_3,** *Phys. Rev. B 21(4), 1520-1526 (1980)*

[EVA78] Evans B.D., Stapelbroek M., **Optical properties of the F^+ center in crystalline Al_2O_3,** *Phys. Rev. B 18(12), 7089-7098 (1978)*

[EVA80] Evans B.D., Stapelbroek M., **Optical vibronic absorption spectra in 14.8 MeV neutron irradiated sapphire,** *Solid State Comm. 3, 765-770 (1980)*

[EVA94a] Evans B.D., **Ubiquitous blue luminescence from undoped synthetic sapphires,** *J. Lumin. 60/61 620-626 (1994)*

[EVA94b] Evans B.D., Pogatshnik G.J., Chen Y., **Optical properties of lattice defects in α-Al_2O_3,** *Nucl. Instr. & Methods B 91, 258-262 (1994)*

[EVA95] Evans B.D., Cain L.S., **A cation vacancy center in cristalline Al_2O_3,** *Radiat. Effects & Defects in Solids 134, 329-332 (1995)*

[GAM64] Gamble F.T., Bartram R.H., Young C.G., Gilliam O.R., **Electron spin resonances in gamma ray irradiated aluminium oxide,** *Phys. Rev. 134(3A), A589-A595 (1964)*

[GAM65] Gamble F.T., Bartram R.H., Young C.G., Gilliam O.R., **Electron spin resonances in reactor irradiated aluminium oxide,** *Phys. Rev. 138(2A), A577-A583 (1965)*

[GES62] Geschwind S., Kislink P., Klein M.P., Remeika J.P., Wood D.L., **Sharp line fluorescence, electron paramagnetic resonance and thermoluminescence of Mn^{4+} in α-Al_2O_3,** *Phys. Rev. 126(5), 1684-1686 (1962)*

[GEU56] Geusic J.E., **Paramagnetic fine structure spectrum of Cr^{+++} in a single ruby crystal,** *Phys. Rev. 102(5), 1252-1253 (1956)*

[GOV75] Govinda S., **Coloration and luminescence in α-Al_2O_3 single crystals irradiated with x-rays at room temperature,** *Phys. Stat. Solidi (a) 32, K95-K100 (1975)*

[GOV76] Govinda S., **Coloration and luminescence in pure and chromium doped Al_2O_3 single crystals irradiated with x-rays at room temperature,** *Phys. Stat. Solidi (a) 37, 109-117 (1976)*

[GUI98A] Guissi S., **Modélisation des phénomènes thermostimulés. Validation par détection simultanée de la luminescence, de la conductivité électrique et de l'émission exoélectronique thermostimulées dans l'alumine alpha,** *Thèse, Université de Nice-Sophia Antipolis, France (1998)*

[GUI98B] Guissi S., Bindi R., Iacconi P., Jeambrun D., Lapraz D., **Theoretical model of thermally stimulated luminescence, conductivity and exoelectronic emission,** *J. Phys. D: Appl. Phys. 31, 137-145 (1998)*

[GUI99] Guissi S., Iacconi P., Bindi R., Lapraz D., **Characterisation and modelling of the 450 K TSL peak of alpha alumina by simultaneous analysis of TSL, TSC and TSEE,** *Rad. Prot. Dosim. 84(1-4), 247-251 (1999)*

[HEI84] Heinrich V.E., **Surface electronic structure of MgO and Al_2O_3 ceramics,** *Adv. in Ceram. 10, 205-216 (1984)*

[HOS64] Hoskins R.H., Soffer B.H., **Observation of Cr^{4+} in α-Al_2O_3,** *Phys. Rev. 133(A2), 490-493 (1964)*

[IAC86] Iacconi P., Lapraz D., Keller P., Portal G., Barthe J., **Photo induced thermoluminescence of x-irradiated α-Al_2O_3 dosimetric properties,** *Rad. Prot. Dosim. 17, 475-478 (1986)*

[IAC90] Iacconi P., Lapraz D., Alessandri-Fraccaro M.F., Addi D., **Phototransferred thermoluminescence and exoemission in alumine alpha,** *Rad. Prot. Dosim. 33(1/4), 127-130 (1990)*

[IAC93] Iacconi P., Petel F., Lapraz D., Bindi R., **Thermostimulated exoelectronic emission and thermoluminescence of various α-Al_2O_3 samples,** *Phys. Stat. Solidi (a) 139(2), 489-501 (1993)*

[IAC97] Iacconi P., **Méthodes d'étude physique des défauts ponctuels dans les solides,** *Cours de DEA de Génie des Procédés, Ecole des Mines, St-Etienne (1997)*

[JAC93] Jacobs P.W.M., Kotomin E.A., **Theory of point defects and vacancy motion in corundum crystals,** *J. Solid State Chem. 106, 27-34 (1993)*

[JAN83] Jansons J.L., Kulis P.A., Rachko Z.A., Springis M.J., Tale I.A., Valbis J.A., **Luminescence of Ga doped α-Al_2O_3 crystals,** *Phys. Stat. Sol. (b) 120, 511-518 (1983)*

[JAR96] Jardin C., Canut B, Ramos S.M.M., **The luminescence of sapphire subjected to the irradiation of energetic hydrogen and helium ions,** *J. Phys. D : Appl. Phys. 29, 2066-2070 (1996)*

[JEF81] Jeffries B.J., Brewer J.D., Summers G.P., **Photoconductivity and charge trapping in Al_2O_3,** *Phys. Rev. B 24(10), 6074-6082 (1981)*

[JOY69] Joyce R.R., Richards P.L., **Far infrared spectra of Al_2O_3 doped with Ti, V and Cr,** *Phys. Rev. 179(2), 375-380 (1969)*

[KAW78] Kawamura S., Royce B.S.H., **Thermally stimulated current studies of electron and hole traps in single crystal Al_2O_3,** *Phys. Stat. Sol. (a) 50, 669-677 (1978)*

[KIR81] Kirkegaard P., Eldrup M., Morgensen O.E., Pedersen N.J., , *Comput. Phys. Commun. 23, 307- (1981)*

[KIT74] Kitazawa K., Coble R.L., **Electrical conduction in single crystal and polycrystalline Al_2O_3 at high temperature,** *J. Am. Ceram. Soc. 57(6), 245-250 (1974)*

[KIT94] Kitis G., Papadopoulos J.G., Charalambous S., Tuyn J.W.N., **The influence of heating rate on the response and trapping parameters of α-Al_2O_3:C,** *Rad. Prot. Dosim. 55(4), 183-190 (1994)*

[KIT98] Kitis G., Gomez-Ros J.M., Tuyn J.W.N., **Thermoluminescence glow curve deconvolution for first, second and general orders of kinetics,** *J. Phys. D: Appl. Phys. 31, 2636-2641 (1998)*

[KLA80] Klaffky R.W., Rose B.H., Goland A.N., Dienes G.J., **Radiation induced conductivity of Al_2O_3: experiment and theory,** *Phys. Rev. B 21(8), 3610-3634 (1980)*

[KLE96] Klemic G.A., Azziz N., Marino S.A., **The neutron response of Al_2O_3:C, ^{7}LiF:Mg,Cu,P and ^{7}LiF:Mg,Ti TLDs,** *Rad. Prot. Dosim. 65(1-4), 221-226 (1996)*

[KLE96] Klemic G.A. et al.
State of art of environmental dosimetry: 11th international intercomparison and proposed performance tests
Rad. Prot. Dosim. 85(1-4), 201-206 (1999)

[KOK86] Kokta M.R., **Crystal growth and caracterisation of oxides host crystals for tunable lasers,** *Opt. Eng., SPIE Vol. 681, Laser and nonlinear optical materials 50-53 (1986)*

[KOR85] Kortov V.S., Bessonova T.S., Akselrod M.S., Milman I.I., **Hole-induced exoelectron emission and luminescence of corundum doped with Mg,** *Phys. Stat. Solidi (a) 87, 629-639 (1985)*

[KOR94] Kortov V.S., Milman I.I., Kirpa V.I., Lesz Ja., **Some features of α-Al_2O_3 dosimetric thermoluminescent crystals,** *Rad.Prot.Dosim. 55(4), 279-283 (1994)*

[KOR96A] Kortov V.S., Milman I.I., **Some new data on thermoluminescence properties of dosimetric α-Al_2O_3 crystals,** *Rad.Prot.Dosim. 65(1-4), 179-184 (1996)*

[KOR96B] Kortov V.S., Milman I.I., Kirpa V.I., Lesz Ja., **Thermal quenching of TL in α-Al_2O_3 dosimetric crystals,** *Rad.Prot.Dosim. 65(1-4), 255-258 (1996)*

[KOT95] Kotomin E.A., Stashans A., Kantorovitch L.N., Lifshitz A.I., Popov A.I., Tale I.A., Calais J.L., **Calculations of the geometry and optical properties of F_{Mg} centers and dimer (F_2 type) centers in corundum crystals,** *Phys. Rev. B 51(14), 8770-8778 (1995)*

[KRE71] Krebs J.J., Maisch W.G., **Exchange effects in the optical absorption spectrum of Fe^{3+} in Al_2O_3,** *Phys. Rev. B 4(3), 757-769 (1971)*

[KRI98A] Kristianpoller N., Rehavi A., Shmilevich A., Weiss D., Chen R., **Radiation effects in pure and doped Al_2O_3 crystals,** *Nucl. Instr. & Methods B 141, 343-346 (1998)*

[KRI98B] Kristianpoller N., Shmilevich A., Weiss D., Chen R., **Sensitization and desenzitization of the luminescence yield of α-Al_2O_3:C,** *Rad. Eff. & Def. in Solids 146, 237-241 (1998)*

[KRÖ83] Kröger F.A., **Oxidation-reduction and the major type of ionic disorder in α-Al_2O_3,** *J. Am. Ceram. Soc. 66(10), 730-732 (1983)*

[KUL79] Kulis P.A., Sringis M.J., Tale I.A., Valbis J.A., **Recombination luminescence in single crystal Al_2O_3,** *Phys. Stat. Solidi (a) 53, 113-119 (1979)*

[KUL80] Kulis P.A., Sringis M.J., Tale I.A., Valbis J.A., **On the mechanism of the recombination luminescence of single crystal Al_2O_3 with nonstoichiometric excess of aluminium,** *Phys. Stat. Solidi (a) 58, 225-229 (1980)*

[KUL81] Kulis P.A., Sringis M.J., Tale I.A., Vainer V.S., Valbis J.A., **Impurity associated colour centres in Mg and Ca doped in Al_2O_3 single crystals,** *Phys. Stat. Solidi (b) 104, 719-725 (1981)*

[KUL85] Kulagin N.A., Litvinov L.A., **The defects and spectral properties of sapphire grown by melting methods,** *Cryst. Res. Technol. 20(12), 1667-1672 (1985)*

[LAG98] Lagerlöf K.P.D., Grimes R.W., **The defect chemistry of sapphire (α-Al_2O_3),** *Acta Mater. 46(16), 5689-5700 (1998)*

[LAM60] Lambe J., Kikuchi C., **Spin resonance of V^{2+}, V^{3+}, V^{4+} in α-Al_2O_3,** *Phys. Rev. 118(1), 71-77 (1960)*

[LAP85] Lapraz D., Iacconi P., **Photo-induced thermoluminescence of X-irradiated α-Al_2O_3,** *Phys. Stat. Sol. (a) 87, K167-169 (1985)*

[LAP88] Lapraz D., Iacconi P., Sayadi Y., Keller P., Barthe J., Portal G., **Some thermoluminescence**

properties of an α-Al_2O_3 sample, *Phys. Stat. Sol. (a) 108, 783-794 (1988)*

[LAP90] Lapraz D., Iacconi P., Alessandri-Fraccaro M.F., Barthe J., Portal G., **Dosimetric properties of specially prepared clothing material,** *Rad. Prot. Dosim. 33(1/4), 131-134 (1990)*

[LAP91] Lapraz D., Iacconi P., Daviller D., Guilhot B., **Thermostimulated luminescence and fluorescence of α-Al_2O_3: Cr^{3+} samples (ruby),** *Phys. Stat. Solidi (a) 126, 521-531 (1991)*

[LAP93] Lapraz D., Boutayeb S., Iacconi P., Bindi R., Rostaing P., **Photoinduced thermostimulated electrical conductivity of an α-Al_2O_3 monocristal,** *Phys. Stat. Sol. (a) 136, 497-507 (1993)*

[LEE76] Lee K.H., Holmberg G.E., Crawford J.H.Jr., **Hole centers in γ-irradiated, oxidized Al_2O_3,** *Sol.Stat.Comm. 20, 183-185 (1976)*

[LEE77a] Lee K.H., Crawford J.H.Jr., **Electron centers in single-crystal Al_2O_3,** *Phys.Rev.B. 15(8), 4065-4070 (1977)*

[LEE77b] Lee K.H., Holmberg G.E., Crawford Jr.J.H., **Optical and ESR studies of hole centers in γ irradiated Al_2O_3,** *Physica Status Solidi (a) 39, 669-674 (1977)*

[LEE78] Lee K.H., Crawford J.H.Jr., **Additive coloration of sapphire,** *Appl. Phys. Lett. 33(4), 273-275 (1978)*

[LEE79] Lee K.H., Crawford J.H.Jr., **Luminescence of the F center in sapphire,** *Phys.Rev.B. 19(6), 3217-3221 (1979)*

[LEH70] Lehmann G., Harder H., **Optical spectra of di- and trivalent iron in corundum,** *Am. Mineral. 55, 98-105 (1970)*

[LIB98] Li Bin L., Da-Ling L., Chun-Xiang Z., Tie-Cheng L., **Defects in sapphire:Mn induced by neutron irradiation,** *Nucl. Instr. & Methods B 141(1-4), 450-454 (1998)*

[LOW60] Low W., Surs J.T., **Paramagnetic resonance spectra of manganese in corundum,** *Phys. Rev. 119, 132-133 (1960)*

[MAC84] Mackrodt W.C., **Calculated point defect formation, association and migration energies in MgO and α-Al_2O_3,** *Adv. in Ceram. 10, 62-78 (1984)*

[MAC92] Macalik B., Bausà L.E., Garcia S. J., Jaque F., Munoz Santiuste J.E., Vergara I., **Blue emission in Ti-sapphire laser crystals,** *Appl. Phys. B 55, 144-147 (1992)*

[MAR62] Marshall S.A., Kikuchi T.T., Reinberg A.R., **Paramagnetic resonance absorption of divalent nickel in α-Al_2O_3 single crystal,** *Phys. Rev. 125(2), 453-459 (1962)*

[MAR64] Maruyama T. Matsuda Y., **Color centers in γ - irradiated ruby,** *J. Phys. Soc. Jap. 19(7), 1096-1104 (1964)*

[MAR79] Marfunin A.S., **Spectroscopy, Luminescence and Radiation Centers in Minerals,** *Springer - Verlag, Berlin, DDR (1979)*

[MAR89] Mariani D.F., Castro M.J., **Thermoluminescent processes in Al_2O_3 x-irradiated at 80 K,** *J. Phys. Chem. Solids 50(2), 125-131 (1989)*

[MCC62] McClure D.S., **Optical spectra of transition - metal ions in corundum,** *J. Chem. Phys. 36(10), 2757-2779 (1962)*

[MCK85] McKeever S.W.S., **Thermoluminescence of solids,** *Cambridge University Press, Cambridge, England (1985)*

[MCK95] McKeever S.W.S., Moscovitch M., Townsend P.D., **Thermoluminescence dosimetry materials: properties and uses,** *Nuclear Technology Publishing, Ashford, England (1995)*

[MCK99] McKeever S.W.S., Akselrod M.S., Colyott L.E., Agersnap Larsen N., Polf J.C., Whitley V., **Characterisation of Al_2O_3 for use in thermally and optically stimulated luminescence dosimetry,** *Rad. Prot. Dosim. 84(1/4), 163-168 (1999)*

[MEH76] Mehta S.K., Sengupta S., **Gamma dosimetry with α-Al_2O_3 thermoluminescent phosphor,** *Phys. Med. Biol. 21(6), 955-964 (1976)*

[MEH79] Mehta S.K., Sengupta S., **Luminescence and colour centres in Al_2O_3:Si, Ti,** *Nucl. Instr. & Methods. 164, 349-354 (1979)*

[MEH82] Mehta S.K., Sengupta S., Oommen I.K., **Environmental dosimetry with Al_2O_3(Si, Ti) thermoluminescent phosphor,** *Nucl. Instr. & Methods. 197, 459-463 (1982)*

[MEY93] Meyn J.-P., Danger T., Petermann K., Huber G., **Spectroscopic characterization of V^{4+}**

doped Al_2O_3 and $YAlO_3$, *J. Lumin. 55(2), 55-62 (1993)*

[MIL98] Milman I.I., Kortov V.S., Nikiforov S.V., **An interactive process in the mechanism of the thermally stimulated luminescence of anion-defective α-Al_2O_3 crystals,** *Radiat. Meas. 29(3-4), 401-410 (1998)*

[MOH77] Mohapatra S.K., Kröger F.A., **Defect structure of α-alumina doped with titanium,** *J. Am. Ceram. Soc. 60(9/10), 381-387 (1977)*

[MOH78] Mohapatra S.K., Kröger F.A., **The dominant type of ionic disorder in α-Al_2O_3,** *J. Am. Ceram. Soc. 61(3/4), 106-109 (1978)*

[MOO91] Moon A.R. , Philips M.R., **Defect clustering in H,Ti: α-Al_2O_3,** *J. Phys.Chem.Solids 52, 1087 (1991)*

[MOO94] Moon A.R., Phillips M.R., **Defect clustering and color in Fe, Ti: α-Al_2O_3,** *J. Am. Ceram. Soc. 77(2), 356-367 (1994)*

[MUL66] Muller R., Gunthard H.H., **Spectroscopic study of the reduction of nickel and cobalt ions in sapphire,** *J. Chem. Phys. 44(1), 365-373 (1966)*

[NIK75] Niklas A., Sujak B., **Thermoluminescence of a ruby crystal colored by x-rays,** *Acta Phys. Polon. A 48(2), 291-305 (1975)*

[NIK00] Nikiforov S.V., Milman I.I., Kortov V.S., **Thermal and optical ionization of F centers in the luminescence mechanism of anion defective corundum crystals,** *Radiat. Meas. in press (2000)*

[NOV66] Novotny J., Spurny Z., **The effect of x-rays on ruby,** *Czech J. Phys. B 16, 119-124 (1966)*

[ORT68] Orton J.W., **Electron paramagnetic resonance,** *Hiffe Books Ltd., London, England (1968)*

[OSV80] Osvay M., Biro T., **Aluminium oxide in TL dosimetry,** *Nucl. Instr. & Methods 175, 60-61 (1980)*

[OSV90] Osvay M., Ranogajec-Komor M., Golder F., **Comparative PITL and PTTL investigations on TL detectors,** *Rad. Prot. Dosim. 33(1/4), 135-138 (1990)*

[OSV99] Osvay M., Ranogajec-Komor M., **LET dependence of high sensitivity TL dosemeters,** *Rad. Prot. Dosim. 84(1-4), 219-222 (1999)*

[PAP96] Papin E., Grosseau P., Guilhot B., Benabdesselam M., Iacconi P., Lapraz D., **Influence of the calcining conditions on the thermoluminescence of pure and doped α-alumina powders,** *Rad. Prot. Dosim. 65, 243-246 (1996)*

[PAP97] Papin E., **Influence des défauts ponctuels sur les propriétés dosimétriques et sur l'aptitude au frittage de l'alumine alpha,** *Thèse, Ecole Nationale Supérieure des Mines de St-Etienne, France (1997)*

[PAP99] Papin E., Grosseau P., Guilhot B., Benabdesselam M., Iacconi P., **Influence of point defects on the thermoluminescence of α-Al_2O_3: application to dosimetry,** *Rad. Prot. Dosim. 84(1-4), 91-94 (1999)*

[PEL94] Pells G.P., **Radiation demage effects in alumina,** *J. Am. Ceram. Soc. 77(2), 368-377 (1994)*

[PET90] Peto A., **Kinetic analysis of Al_2O_3:Mg,Y glow curves,** *Rad. Prot. Dosim. 33(1/4), 103-106 (1990)*

[PET94] Petel F., **Détection simultanée de l'émission exoélectronique et de la luminescence thermostimulées présentées par l'alumine alpha entre 77 et 650 K,** *Thèse, Université Paul Sabatier de Toulouse, France (1994)*

[PET96A] Peto A., Kelemen A., **Radioluminescence properties of α-Al_2O_3 TL dosemeters,** *Rad. Prot. Dosim. 65(1/4), 123-126 (1996)*

[PET96B] Petel F., Iacconi P., Bindi R., Lapraz D., Breuil P., **Simultaneous detection of thermostimulated luminescence and exoelectronic emission between 77 and 650 K Application to alpha alumina,** *Rad. Prot. Dosim. 65(1/4), 123-126 (1996)*

[PHI67] Philbrick C.R., Buckman W.G., Underwood N., **Ruby as a thermoluminescent radiation dosimeter,** *Health Phys. 13, 798-801 (1967)*

[POG87] Pogatshnik G.J., Chen Y., Evans B.D., **A model of lattice defects in sapphire,** *IEEE Trans. on Nucl. Sci. NS-34(6), 1709-1712 (1987)*

[POK94] Pokorny P., Ibarra A., **Impurity effects on the thermoluminescence of Al_2O_3,** *J. Appl. Phys. 75(2), 1088-1092 (1994)*

[POR78] Portal G., **Etude et développement de la dosimétrie par radiothermoluminescence,** *Thèse,*

Université Paul Sabatier de Toulouse, France (1978)

[POR80] Portal G., Lorrain S., Valladas G., **Very deep traps in Al_2O_3 and $CaSO_4$:Dy,** *Nucl. Instr. & Methods 175, 12-14 (1980)*

[PUJ80] Pujats A.V., Springis M.J., Valbis J.A., **On the nature of the violet luminescence in quenched α-Al_2O_3 single crystals,** *Phys. Stat. Solidi (a) 62, K85-K87 (1980)*

[RAN86] Ranogajec-Komor M., Osvay M., **Dosimetric characteristics of different TL phosphors,** *Rad. Prot. Dosim. 17(1-4), 379-384 (1986)*

[RAO79] Rao D.R., Das B.N., **On the stability of TL traps in alumina,** *J. Mater. Sci. 14, 19-24 (1979)*

[REG81] Regulla D.F., **Operational aspects, dans: Applied thermoluminescence dosimetry,** (editeurs : Oberhofer M., Scharmann A.) *A. HilgerLtd., Bristol, England*

[RIE57] Rieke J.K., Daniels F., **Thermoluminescence studies of aluminium oxide,** *J. Phys. Chem. 61, 629-633 (1957)*

[RUZ98] Ruza E., Reyher H.J., Trokss J., Wöhlecke M., **Optically detected magnetic resonance studied via the blue luminescence of Ti doped Al_2O_3,** *J. Phys. : Condens. Matter. 10, 4297-4306 (1998)*

[SAY88] Sayadi Y., **Etude et caractérisation d'un phénomène de thermoluminescence photoinduite dans l'alumine alpha: application à la dosimétrie des rayonnements ionisants,** *Thèse, Université Paul Sabatier de Toulouse, France (1988)*

[SPR84] Springis M.J., Valbis J.A., **Visible luminescence of colour centres in sapphire,** *Phys. Stat. Sol. (b) 123, 335-343 (1984)*

[SPR96] Springis M., Kulis P., Veispals A., Tale V., Tale I., **Origin of the 430 K TL peak in thermochemically reduced α-Al_2O_3,** *Rad. Prot. Dosim. 65(1/4), 231-234 (1996)*

[STA94] Stashans A., Kotomin E., Calais J.L., **Calculations of ground and excited states of F type centers in corundum crystals,** *Phys. Rev. B 49(21), 14854-14857 (1994)*

[SUM84a] Summers G.P., **Thermoluminescence in single crystal α-Al_2O_3,** *Radiat. Prot. Dosim. 8(1/2), 69-80 (1984)*

[SUM84b] Summers G.P., **Luminescence and photoconductivity in MgO and α-Al_2O_3 crystals,** *Advances in Ceramics 10, 25-45 (1984)*

[SÜV99] Süvegh K., Vértes A., Hyodo T., **Positronium as a sensitive detector of changes in molecular structure,** *Advances in Molecular Structure Research 5, 313-357 (1999)*

[TAL86] Tale I., Piters T.M., Barboza-Flores M., Perez-Salas R., Aceves R., Springis M., **Optical properties of complex anion vacancy centres and photo excited electronic processes in anion defective α-Al_2O_3,** *Rad. Prot. Dosim. 65(1/4), 235-238 (1996)*

[TIP70] Tippins H.H., **Charge transfer spectra of transition metal ions in corundum,** *Phys. Rev. B 1(1), 126-135 (1970)*

[TOL62] Tolstoi N.A., Shun-fu L., Lapidus M.E., **The luminescence kinetics of chromium luminors. III. Ruby,** *Opt. Spectr. (USSR) 13, 133-136 (1962)*

[TOW65] Townsend M.G., Hill F.O., **Tetravalent cobalt ion in Al_2O_3,** *Trans. Fraraday Soc. 61(12), 2597-2602 (1965)*

[TUR75] Turner T.J., Crawford J.H., **V centers in single crystal Al_2O_3,** *Solid State Commun. (a) 17, 167-169 (1975)*

[VAL99] Vallayer J., **Corrélation entre les propriétés optique, diélectrique et mécanique de l'alumine,** *Thèse, Ecole Centrale de Lyon, France (1999)*

[WAN83] Wang H.A., Lee C.H., Kröger F.A., Cox R.T., **Point defects in α-Al_2O_3:Mg studied by electrical conductivity, optical absorption and ESR,** *Phys. Rev. B 27(6), 3821-3841 (1983)*

[WEA67] Weast R.C. (editeur), **Handbook of Chemistry and Physics,** *The Chemical Rubber Co., Cleveland, USA (1967)*

[WHI00] Whitley V.H., McKeever S.W.S., **Photoionization of deep centers in Al_2O_3,** *J. Appl. Phys. 87(1), 249-256 (2000)*

[WON95A] Wong W.C., McClure D.S., Basun S.A., Kokta M.R., **Charge exchange processes in titanium doped sapphire crystals. I. Charge exchange energies and titanium bound exciton,** *Phys. Rev. B 51(9), 5682-5692 (1995)*

[WON95B] Wong W.C., McClure D.S., Basun S.A., Kokta M.R., **Charge exchange processes in titanium doped sapphire crystals. II. Charge transfer transition states, carrier trapping and detrapping,** *Phys. Rev. B 51(9), 5693-5698 (1995)*

[WYC65] Wyckoff R.W.G., **Crystal structures,** *John Wiley & Sons Inc. (1965)*

[YAM94] Yamaga M., Yosida T., Hara S., Kodama N., Henderson B., **Optical and electron spin resonance spectroscopy of Ti^{3+} and Ti^{4+} in Al_2O_3,** *J. Appl. Phys. 75(2), 1111-1117 (1994)*

[ZHA98] Zhang J., Li Bin L., Li Zhong L., Shi-Li J., Guang-Can W.,Yong L., Shou-Yong J., **Electron and neutron irradiation effects of in Al_2O_3:V,** *Nucl. Instr. & Methods B 141(1-4), 446-449 (1998)*

[ZIN73] Ziniker W.M., Rusin J.M., Stoebe T.G., **Thermoluminescence and activation energies in Al_2O_3, MgO and LiF (TLD-100),** *J. Mater. Sci. 8, 407-414 (1973)*